Thin Film Flow on Functional Surfaces: Stability and Morphology

GEORGE RICHARD DALY

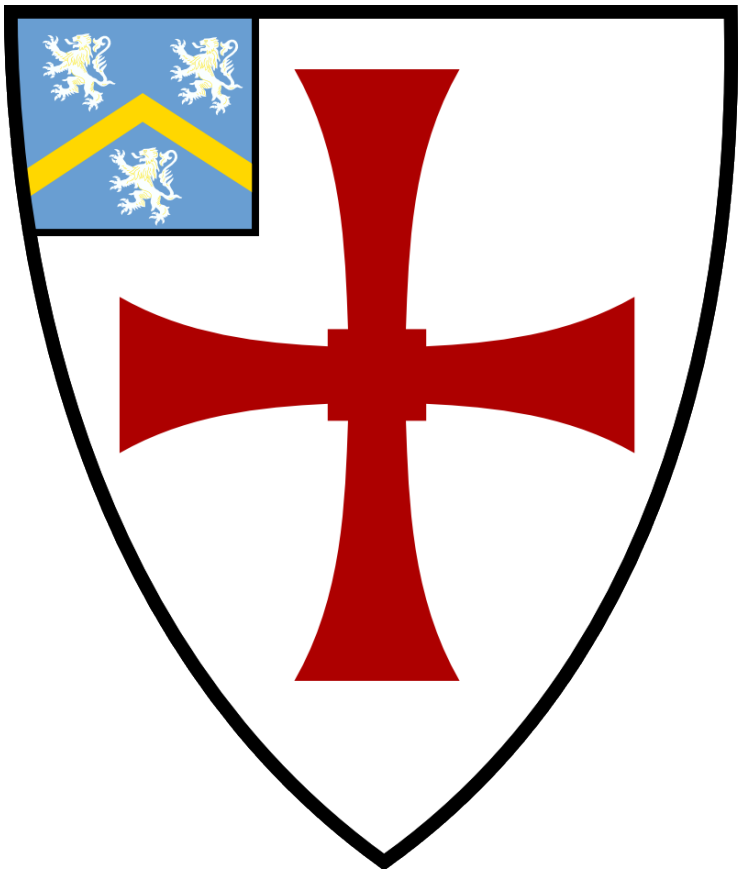

Thin Film Flow on Functional Surfaces: Stability and Morphology

by
George Richard Daly

Submitted in accordance with the requirements
for the degree of Doctor of Philosophy

University of Durham
Department of Engineering

April, 2022

"Sometimes one has to say difficult things, but one ought to say them as simply as one knows how."
– G.H. Hardy –

Abstract

This thesis explores the stability and morphology of gravity induced film flow down smoothly corrugated rigid substrate, uniformly heated/cooled from below. The problem of interest is complicated by the presence of a free-surface whose location is unknown *a priori*. This complication is overcome by reducing the governing equations of motion and energy to a manageable form within the framework of the well-known long-wave expansion, which exploits the disparity between the horizontal and vertical length scales in order to eliminate the depth-coordinate from the governing formulation. Two methods for implementing a long-wave expansion are considered, with each leading to an asymptotic model of reduced dimensionality. The first is a perturbation series of the fluid velocity and temperature with respect to a small parameter ϵ which represents the disparity between the horizontal and vertical length scales, the second is a power series expansion with respect to the vertical coordinate in which the series truncation is correlated to the number of degrees of freedom with respect to the horizontal coordinate.

A key feature of the power series method is proof that, for any asymptotic model to be able to accurately resolve the thermodynamics beyond the trivial case of 'a flat film flowing down a planar uniformly heated incline', the expansion of the fluid temperature must be quadratic to leading-order in the long-wave expansion. The ensuing analysis reveals why heat transfer models based on the Nusselt linear temperature distribution fail to converge outside of the long-wave limit and details how asymptotic models can be extended to higher-order. Superior predictions are obtained compared with earlier work and reinforced via a series of corresponding solutions to the full governing equations acquired using a purpose written finite element analogue, enabling comparisons of free-surface disturbance and temperature predictions to be made, as well as those of the streamline pattern and temperature contours inside the film. In particular, the free-surface temperature is captured extremely well at moderate Prandtl numbers for film flow down smoothly corrugated substrate.

Investigation of the stability characteristics of gravity-driven film flow is opened with the classical problem of a thin film flowing down an inclined plate and its associated hydrodynamic stability as described by the Orr-Sommerfeld equation, which reveals the asymptotic methods are not able to fully capture the thermo-capillary effect in the heated/cooled case. The stability problem is extended to film flow over non-planar substrate via Floquet theory, with the interaction between the substrate topography and thermo-capillarity investigated through a set of neutral stability curves. Although no

relevant experimental data is currently available for the heated film problem, existing numerical predictions and experimental data concerning the stability behaviour of isothermal film flow are taken as a reference point from which to explore the effect of both heating and cooling.

Publications

During the course of the research undertaken culminating in the presentation of this thesis, the following publications have appeared in the open literature:

G. R. Daly, P. H. Gaskell, and S. Veremieiev (2022). Gravity-driven film flow down a uniformly heated smoothly corrugated rigid substrate. *Journal of Fluid Mechanics*, 930: A23. doi:10.1017/jfm.2021.920

Declaration

The author confirms that the work submitted in this thesis is their own and that appropriate credit has been given when reference to the work of others has been made. No part of the thesis has been submitted elsewhere in respect of the award of any other degree or qualification.

Statement of Copyright

Acknowledgements

The author would first like to thank their supervisors, Professor Philip H. Gaskell and Dr. Sergii Veremieiev, for giving the author the opportunity to undertake this research and for their support thereafter. Secondly, the author would like to thank the Engineering and Physical Sciences Research Council (EPSRC) who granted funding to this work.

Mathematical Nomenclature

Symbol	Description	SI base units
∇	Differential operator, $\nabla = (\partial/\partial X, \partial/\partial Y, \partial/\partial Z)$	m^{-1}
$\int$	Integral sign	
$\cdot$	inner (scalar) product	
$\times$	cross (vector) product	
$\otimes$	outer (tensor) product	
$\mathbb{I}$	Identity Matrix	
$\mathbf{0}$	Zero vector	
$\lim_{x \to c} f(x)$	Limit of function $f(x)$ as the value of x approaches c	
X	X co-ordinate	m
Y	Y co-ordinate	m
Z	Z co-ordinate	m
T	Time	s
$\vec{\mathbf{U}}$	Flow vector, $\vec{\mathbf{U}} = (U, V, W)$	$m\ s^{-1}$
U	Flow velocity in the X-direction	$m\ s^{-1}$
V	Flow velocity in the Y-direction	$m\ s^{-1}$
W	Flow velocity in the Z-direction	$m\ s^{-1}$
Θ	Fluid temperature	K
Θ_a	Ambient temperature	K
Θ_S	Substrate temperature	K
P	Fluid pressure	$kg\ m^{-1}\ s^{-2}$
P_0	Ambient pressure	$kg\ m^{-1}\ s^{-2}$
S	Substrate height	m
H	Film thickness	m
F	Free-surface height	m
G	Surface-curvature pre-factor	
$\hat{\mathbf{T}}$	Stress tensor of the fluid	$kg\ m^{-1}\ s^{-2}$
$\hat{\mathbf{T}}_0$	Stress tensor of the ambient gas	$kg\ m^{-1}\ s^{-2}$

β	Inclination angle of the substrate	
$\bar{g}$	Acceleration due to gravity	$m\ s^{-2}$
ρ	Density of the fluid	$kg\ m^{-3}$
μ	Dynamic viscosity of the fluid	$kg\ m^{-1}\ s^{-1}$
ν	Kinematic viscosity of the fluid, $\nu = \mu/\rho$	$m^2\ s^{-1}$
σ	Surface tension along the free-surface	$kg\ s^{-2}$
σ_0	Surface tension at the ambient temperature – Θ_a	$kg\ s^{-2}$
$\frac{\partial\sigma}{\partial\Theta}$	Surface tension coefficient of proportionality with respect to the fluid temperature	K^{-1}
κ	Thermal conductivity of the fluid	$kg\ m\ s^{-3}\ K^{-1}$
c_P	Specific heat capacity of the fluid at constant pressure	$m^2\ s^{-2}\ K^{-1}$
α	Coefficient of heat transfer across the free-surface	$kg\ m\ s^{-3}\ K^{-1}$
H_0	Thickness of a Nusselt flat-film	m
U_0	Free-surface velocity of a Nusselt flat-film	$m\ s^{-1}$
$\mathcal{Q}_0$	Flow rate of a Nusselt flat-film	$m^2\ s^{-1}$
A	Amplitude of substrate topography	m
L	Wavelength of substrate topography	m
Θ_Δ	Temperature difference, $\Theta_\Delta = \Theta_s - \Theta_0$	K
L_c	Capillary length scale	m
L_ν	Viscous length scale	m
T_ν	Viscous time scale	s
ϵ	Shallowness parameter	
Re	Reynolds number	
Ca	Capillary number	
Ka	Kapitza number	
Ma	Marangoni number	
Pr	Prandtl number	
Pe	Péclet number	
Bi	Biot number	

Contents

Chapter 1

Introduction

1.1 Motivation

Thin film flows are ubiquitous in the formation of functional surfaces/barriers, while playing a key role as part of numerous manufacturing/conversion processes. In tandem, predicting their behaviour has motivated the work of experimentalists and modellers alike for decades. This remains true today, whether the objective is to produce defect free coated products as cheaply and as speedily as possible or to understand the source and means of suppressing free surface disturbances when trying to extend established stability envelops to bring down production costs, etc.

The focus of the present thesis is on the modelling of gravity-driven film flow down smoothly corrugated, uniformly heated/cooled, inclined surfaces; for the purpose of predicting their stability and morphology. Mathematical modelling of film flow is complicated by the presence of a free-surface which defines the material boundary between the liquid film and the ambient gas. Under certain conditions, this surface will become spontaneously disturbed by travelling waves even in the absence of wind; thus, film flow is a type of free-boundary problem in which an unknown function must be solved on an unknown domain. In consequence, models of reduced dimensionality which eliminate the depth coordinate from the equations, and with it the unbounded dimension, are popular within this field and many successful models describing the dynamics of wave-formation on isothermal falling films have been fabricated via a long-wave expansion. However, application of a long-wave expansion to the problem of heated film flow is less straight-forward; in the long-wave limit, the temperature inside the film is described by the Nusselt linear distribution, yet, for an infinitesimal but finite wave-number, a Robin boundary condition at the free-surface can only be satisfied by a non-linear temperature expansion – at first glance the two appear incompatible. The present thesis shows both these requirements can be met and that the derivation of a reduced asymptotic model which is consistent with the full governing equations outside the neighbourhood of the trivial case requires a quadratic temperature expansion to leading-order. This finding is of particular importance to heat transfer problems where accurately predicting the thermo-capillary stress across the free surface is critical to avoiding film rupture.

1.2 Falling Liquid Films

The study of wave formation on the surface of falling liquid films can be traced back to the pioneering work of Kapitza [1948] and the experiments he carried out with his son [Kapitza and Kapitza, 1949]. They revealed the parabolic velocity profile proposed by Nusselt [1916] for a steady laminar film of uniform thickness breaks down at a critical volumetric flux, whereupon travelling waves spontaneously manifest and propagate across the liquid free surface. At the time, the interplay between the volumetric flux $\mathcal{Q}$ and the kinematic viscosity of a fluid ν was understood to be a defining feature of fluid motion [Reynolds, 1883] – encapsulated by the eponymic Reynolds number:

$$Re = \frac{3\mathcal{Q}}{2\nu}, \tag{1.1}$$

however, preceding studies had principally focused on the transition of laminar flow to turbulence at high Reynolds number: plane Poiseuille flow becomes unstable at $Re \sim 2000$ [Reynolds, 1895]; open-channel flow down an inclined plane is ostensibly turbulent when $Re > 450$ [Hopf, 1910, Jeffreys, 1925, Cornish, 1934]. Evidence of an intermediate wavy regime in gravity-driven film flow, existing between the laminar and turbulent regions, emerged from chemical engineering where Nusselt's theory on laminar film dynamics was being applied to condensate films – see review by Badger and Monrad [1930]. Measurements of the average film thickness by Cooper et al. [1934] and Fallah et al. [1934] supported the foregoing theory; however, when Kirkbride [1934] measured the instantaneous thickness of a film flowing down the outside of a smooth vertical tube, the presence of ripples at $Re \geq 3$ caused his results to positively deviate from the theoretic values. These anomalous results were addressed by Friedman and Miller [1941] who concluded that wave motion in liquid films is a third type of flow existing between true laminar flow and turbulence; their measurements showed the velocity of the free surface increases in this region but the average film thickness-to-volumetric flux relationship of Nusselt is still obeyed. Naturally, succeeding studies sought to establish the characteristics of wavy film flow, chief of which was the apparent absence of waves on very thin films [Grimley, 1945, Dukler and Bergelin, 1952]; this phenomenon popularised the idea of a critical Reynolds number (Re_{crit}), the point at which waves/instabilities first form, however, empirical determination of Re_{crit} proved inconclusive.

The first theoretical study on the hydrodynamic stability of isothermal film flow down planar substrate was performed by Kapitza [1948]. His theory was built upon balancing the work done by gravity with the energy dissipation due to viscosity; this enabled him to obtain a family of steady solutions to undulatory film flow from which uniqueness was determined via an extremum principle and Re_{crit} predicted. In experiment, Kapitza and Kapitza [1949] employed synchronised vibrations to produce high quality standing images of travelling waves and pioneered the use of artificial perturbations to scrutinise the hydrodynamic stability. The Kapitzas describe two types of wave in their work: the first were regular and close to sinusoidal; whilst the second had large amplitudes, steep leading edges and were preceded by small, damped oscillations. Remarkably,

whilst Kapitza's theoretical predictions appeared to agree with experiment, his intuitive approach was flawed because minimising the viscous dissipation function (the extremum principle) would only work if the wave motion in film flow was an equilibrium state – it is not. Irregardless, Kapitza's contribution is lauded due to his descriptions of the physical mechanisms at work and his hypothesis that wavy film flow is characterised by the surface tension along the fluid-fluid interface.

The origin of instability in gravity-driven film flow was solved by Benjamin [1957] using a long-wave approximation – coetaneous experiments by Binnie [1957] had revealed the wave-length of disturbances to be much larger than the average film thickness, suggesting the stability threshold could be analysed in the limit of the wave-length going to infinity (or equivalently, the wave-number going to zero). Building upon an earlier erroneous attempt by Yih [1954], Benjamin solved the linear stability problem for the case of a neutrally stable disturbance (the boundary between stability and instability) with small wave-number and infinitesimal amplitude, and found the criteria for wave formation on the surface of gravity-driven film flow down inclined plane to be given by[1]:

$$Re_{crit} = \frac{5}{4}\cot\beta \tag{1.2}$$

where β is the inclination angle of the plane from the horizontal. Benjamin's result – equation (1.2) – showed uni-directional film flow down a vertical plate ($\beta = 90°$) is unstable for all finite Reynolds numbers irrespective of the surface tension of the fluid; the latter being true, surface tension does stabilise wave motion and thus characterises the range of wave-numbers which are unstable for $Re > Re_{crit}$. The apparent absence of waves at very low Reynolds numbers was attributed to the small amplification rate of instabilities in the neighbourhood just above Re_{crit} [Benjamin, 1957, Binnie, 1959]. Equation (1.2) was corroborated by Yih [1963] via a simpler method; moreover, Yih confirmed the primary stability of gravity-driven film flow to be governed by long surface waves, at least for large β, as both short surface waves and shear waves are highly damped by surface tension – Lin [1967] later showed this is true for all values of β, even in the absence of surface tension, and that shear waves only dominate when $Re \gg Re_{crit}$.

The success of the linearised theory [Benjamin, 1957, Yih, 1963] was followed by attempts to incorporate nonlinearity into the analysis; by all means, accounts of surface waves continuing to evolve well beyond their point of inception [Kapitza and Kapitza, 1949, Binnie, 1957, Tailby and Portalski, 1962] indicates a rich variety of wave dynamics in gravity-driven film flow which lie beyond the domain of linear stability analysis. Early attempts by Benney [1966a], Lin [1969], Gjevik [1970a,b], Lin [1970a] to study the weak nonlinearity of disturbances in gravity-driven film flow relied upon the Stuart-Landau equation [Landau, 1944, Stuart, 1958]; this equation can be written like so:

[1] In Benjamin's paper, the Reynolds number is defined by the mean flow velocity of a Nusselt laminar film – as oppose to its free-surface velocity; thus, Benjamin [1957] gives $Re = \mathcal{Q}/\nu$ and $Re_{crit} = \frac{5}{6}\cot\beta$.

$$\frac{d}{dt}|A|^2 = a|A|^2 + b|A|^4 + \mathcal{O}\left(|A|^6\right) \tag{1.3}$$

where $|A|$ is the amplitude is the disturbance (which is a function of time t), a is the growth rate of the disturbance obtained from the linear theory, and b is a constant which describes the non-linear development of the disturbance. Analyses based on the formalism of equation (1.3) are referred to as weakly nonlinear because there is only one term which accounts for the nonlinear evolution of instabilities.

Benney [1966a] conducted the first weak non-linear analysis of periodic waves using an evolution equation for the film thickness derived via a long-wave expansion; namely:

$$\frac{\partial h}{\partial t} + 2h^2\frac{\partial h}{\partial x} + \epsilon\frac{2}{3}\frac{\partial}{\partial x}\left[\left(\frac{4}{5}Reh^3 - \cot\beta\right)h^3\frac{\partial h}{\partial x} + \epsilon^2\frac{1}{2}\frac{h^3}{Ca}\frac{\partial^3 h}{\partial x^3}\right] + \mathcal{O}\left(\epsilon^2\right) = 0, \tag{1.4}$$

where h is the dimensionless film thickness, Ca is the Capillary number (defined in Chapter 2), and $\epsilon = H_0/L_0$ is the expansion parameter, with H_0 being the characteristic thickness of the film and L_0 being the characteristic wavelength of surface disturbances. In order to carry out an asymptotic expansion of the flow dynamics, Benney [1966a,b] imposed a shallow water condition, namely $\epsilon < 1$, based upon the characteristic film thickness being much smaller than the characteristic disturbance wavelength, $H_0 \ll L_0$. Equation (1.4) recovers Re_{crit} as per the linear theory; however, Benney omitted the effect of surface tension from his formulation ($Ca \to \infty$) and so it failed to predict the progression of instabilities to a steady, finite-amplitude stage as observed experimentally. Gjevik [1970a] rectified this shortcoming by moving surface tension ahead of its formal order in the long-wave expansion, $Ca \sim \mathcal{O}\left(\epsilon^2\right)$, leading to equation (1.4) as written; using this equation he showed steady finite-amplitude waves will form on the surface of a vertically falling film if the fluid possesses sufficiently strong surface tension. Parallel conclusions were drawn by: (i) Nakaya and Takaki [1967] who, in a similar vein, amended a power series approximation of the nonlinear equations by Mei [1966] to include surface tension; and (ii) Lin [1969] who used a closed-form solution for the nonlinear development of an initially infinitesimal periodic disturbance to show supercritically[2] stable wave motion is possible in a viscous film if the surface tension is non-zero. Lin's method was an adaption of the small-amplitude expansion approach developed by Stuart [1960], Reynolds and Potter [1967] to study weak nonlinearities in Couette/Poiseuille flow; with it, Lin showed subcritical instability in gravity-driven film flow down inclined plane to be impossible [Lin, 1970a] and that surfactants have no effect on the speed of instabilities [Lin, 1970b]. In fact, both Gjevik [1970a] and Lin [1971] found it is the inclusion of dispersion terms which is necessary to predict wave speeds which match experiment. The differences between the long-wave and small-amplitude expansions are discussed in

[2] A supercritical equilibrium occurs when the base flow is unstable to small disturbances but the linear growth rate is balanced by higher-order nonlinear terms, leading to a stable finite-amplitude disturbance.

Gjevik [1971]; the long-wave expansion was viewed as the most promising due to its simplicity [Krantz and Goren, 1970] and successive studies used it to investigate the weak nonlinearity of: three-dimensional disturbances [Roskes, 1970, Lin and Krishna, 1977], spatially-varying wave trains [Gjevik, 1970b], side-band instability [Lin, 1974, Krishna and Lin, 1977], and long waves on thin films with surface tension of order unity [Nakaya, 1975].

An important limitation of the Benney equation (1.4) is that it only converges to a valid solution when $Re \sim Re_{crit}$; a consequence of it being derived using a perturbation series [Alekseenko et al., 1985a]. Measurements of the primary instabilities of thin film flow down planar incline by Liu et al. [1993], which provided the first accurate experimental determination of the critical Reynolds number, confirm that the linear stability of the Benney equation is only valid close to Re_{crit}. And it was in a pivotal study by Pumir et al. [1983], which pointed out the quasi-stationary travelling waves propagating across the surface of falling liquid films equate to homoclinic trajectories in the theory of dynamical systems, that the Benney equation was found to exhibit catastrophic behaviour in fully nonlinear, finite-time simulations when $Re > Re_{crit}$ and the amplitude of the disturbance is large. Ruling out turbulence and film rupture, the authors attributed this catastrophic behaviour to a singularity in equation (1.4). Indeed, if the catastrophic behaviour was associated with dry patch formation then it would be preceded by a thinning of the film but the finite-time singularity of the Benney equation is only ever observed for thicker films. Furthermore, there has never been any experimental evidence to support that the finite-time blow-up of the Benney equation is in any way physical [Alekseenko et al., 1985a,b, Liu and Gollub, 1994] and the same catastrophic behaviour does not manifest in more elaborated models from which equation (1.4) can be derived, *e.g. the boundary layer equations* [Chang, 1994].

Interestingly, the Benney equation itself constitutes a generalisation of both the Kuromato-Sivashinsky (KS) and Korteweg–De Vries (KdV) equations: indeed, the KS equation is obtained from equation (1.4) by substituting $h = 1 + \hat{h}$, where $\hat{h} \ll 1$ is a small disturbance to the film thickness, and eliminating all but the lowest non-linearity in $\hat{h}$ [Panga and Balakotaiah, 2003]; meanwhile, the derivation of the KdV equation involves an amplitude expansion in combination with a long-wave expansion [Rosenau and Oron, 1992]. The KS equation was first used by Sivashinsky and Michelson [1980] to study irregular wavy flow in falling liquid films and with it they were able to show the phenomenon is not a result of random external factors but is instead an inherent property of the flow. Elsewhere, Hooper and Grimshaw [1985] recovered Yih's linear stability results from the KS equation, Hyman et al. [1986] found the same equation possesses the property of inertial manifolds[3], and Oron and Rosenau [1989a,b] introduced the regularised KS equation to model wave breaking and high-gradient zones. Numerical solutions to equation (1.4) by Joo et al. [1991a,b] put forward an argument that the existence of the Benney equation makes the KS equation redundant, along

[3]Inertial manifolds are finite-dimensional, smooth, invariant manifolds which describe the long-lasting behaviour of dissipative dynamical systems; and even for infinite-dimensional partial differential system, the inertial manifold is rigorously equivalent to the governing formalism.

with its regularised form, because the Benney equation is closer to the Navier-Stokes equations in the hierarchy of equations. However, Rosenau and Oron [1992] found the Benney equation is no more capable of modelling wave breaking than the KS equation, and they concluded that whilst the KS equation is more limited in scope than the Benney equation, it represents a much better balance between mathematical description and physics of problem. Indeed, the fact the KdV equation permits permanent solutions and is furthest from the Navier-Stokes equations in the hierarchy of equations, whereas the Benney and KS equations both exhibit finite-time divergence, implies the catastrophic behaviour of the Benney and KS equations is due to some mishandling of strong non-linear terms which are absent from the KdV equation [Takeshi, 1999]. In response, Takeshi [1999] proposed a regularisation procedure and derived a regularised Benney equation which behaves in a qualitatively plausible way far beyond the point of criticality. Ooshida's results predicted the existence of two distinct regimes in wavy film flow: the first is termed the drag-gravity regime and is very similar to the Nusselt parabolic velocity profile; whilst the second is coined the drag-inertia regime because it is characterised by the inertia effect. Traditional long-wave models, such as the Benney equation, successfully predict the drag-gravity regime but not the drag-inertia regime; Ooshida attributed the catastrophic behaviour of the Benney equation to its failure to describe the latter regime.

Whilst long-wave models are capable of describing the drag-gravity-regime, there is an alternative approach to modelling gravity-driven film flow which successfully describes the drag-inertia regime. Commonly known as the integral-boundary-layer (IBL) equations, this modelling approach utilises a two-equation depth-averaged model in terms of the flow rate and film thickness, derived on the assumption of a self-similar parabolic velocity profile through the film [Lee, 1969]. The IBL equations were popularised by Shkadov – see Shkadov [1967, 1968], Esmail and Shkadov [1971], Shkadov [1973, 1977], Demekhin and Shkadov [1979], Demekhin et al. [1983], Demekhin and Shkadov [1984], Bunov et al. [1984], Demekhin et al. [1985, 1987] – and in contrast to the Benney equation, they perform well at moderate Reynolds number but less so when $Re < 1$; in particular, their major flaw is a failure to recover the correct expression for Re_{crit} given by the linear theory [Demekhin et al., 1987]. In consequence, several studies had been dedicated to either extending the long-wave formalism to moderate Re [Nakoryakov and l. R. Shreiber, 1973, Rosenau and Oron, 1992, Takeshi, 1999] or finding a way to make the IBL equations reduce to the Benney equation in the limit of $Re \to 0$ [Alekseenko et al., 1985a,b]. Elsewhere, Roberts [1996] put forward a two-equation model of reduced dimensionality based on centre manifold theory; however, the derivation of the centre manifold model necessitates an unphysical perturbing of the governing equation set, whilst this perturbation is removed at the end of the derivation such that the model is an accurate description the original problem, modelling approaches which do not involve an unphysical perturbation have proved more popular in the research field.

The unification of Benney and IBL methodologies was brought about by Ruyer-Quil and Manneville [1998, 2000]; who addressed the flaw in the IBL equations by expanding Shkadov's self-similar parabolic profile to first-order in the long-wave expansion, leading

to the modified IBL equations which are able to recover the correct expression for Re_{crit} from the linear theory [Ruyer-Quil and Manneville, 1998]. Following this, Ruyer-Quil and Manneville [2000] presented an improved reduced asymptotic model based on a power series expansion of the fluid velocity with respect to the vertical coordinate; their approach resembles a long-wave expansion of the fluid velocity but in which the stream-wise flow rate is decoupled from the film thickness and introduced as it own degree of freedom with respect to time and the horizontal coordinate, leading to a two-equation model. Without explanation, Ruyer-Quil and Manneville [2000] noted that their reduced asymptotic model could be retrieved through a method of weighted residuals, in consequence, the modelling approach has become known as the weighted-integral-boundary-layer (WIBL) equations. In addition to accurately predicting Re_{crit}, the WIBL equations do not exhibit the catastrophic behaviour which plagues the Benney equation beyond Re_{crit} which has made them a popular choice with which to model wave formation in falling liquid films ever since. Further development of the WIBL methodology was carried out by: Ruyer-Quil and Manneville [2002] who examined the convergence of the simplified two-equation model and complete four-equation model, and also explained how a Galerkin method closes the power series expansion; whilst Scheid et al. [2006] who introduced a regularisation technique allowing for a two-equation WIBL model to be derived at second-order in the long-wave expansion which is more accurate than the simplified model but less robust than the complete model. Since the turn of the century, the WIBL methodology has certainly become the dominant modelling approach within the field of gravity-driven film flow: with it being extended to uniformly heated film flow by Ruyer-Quil et al. [2005], Scheid et al. [2005]; film flow down corrugated inclines by Oron and Henining [2008], Heining and Aksel [2009], D'Alessio et al. [2009]; and finally to heated, wavy inclines by D'Alessio et al. [2010].

1.3 Films Falling Over Non-Planar Inclines

The problem of isothermal film flow down non-planar substrate became of interest much later than its planar counterpart, with Tougou [1978] being the first to conduct a weak nonlinear analysis of film flow down a weakly wavy incline by incorporating the substrate profile into the KS equation. Tougou [1978] and Wang [1981] found Re_{crit} remains unchanged for small substrate waviness, and Wang [1984], Shetty and Cerro [1993] revealed the velocity profile through the film remains primarily parabolic provided the film thickness is sufficiently smaller than the amplitude of the substrate corrugations - a feature corroborated by experiment [Zhao and Cerro, 1992, Scholle et al., 2001a,b]. Creeping flow along an inclined periodic wall was explored by Pozrikidis [1988] using a boundary-integral formulation, who found the film dynamics remain a strong function of surface tension at very small flow rates, and drew an analogy between gravity-driven film flow and the flow of a liquid layer on a rotating disk (spin coating). Indeed, the flow fields in gravity-driven film flow and spin coating are similar enough that the same modelling techniques can be applied to either problem; the lubrication theory utilised by Stillwagon et al. [1987a,b], Stillwagon and Larson [1988, 1990, 1992], Peurrung and Graves

[1993] in their studies on spin coating is equivalent to a long-wave expansion of the fluid velocity for zero-Reynolds number flow.

In fact, all of the aforementioned works involving non-planar substrate are only applicable to zero-Reynolds number flow; howbeit, analysis by Wierschem et al. [2002] concludes that inertial effects can be neglected below the instability threshold for weak substrate undulations. First to consider inertia-dominated film flow over wavy substrate were Bontozoglou and Papapolymerou [1997] using an Orr-Sommerfeld formalism, they assumed the basic flow was given by the Nusselt parabolic velocity profile corresponding to a flat incline and thus their analysis is only valid for corrugation amplitudes which are significantly smaller than the film thickness; succeeding studies utilised the finite-element [Malamataris and Bontozoglou, 1999] and spectral [Bontozoglou, 2000] methods in their analysis. Subsequent work by Trifonov [1998], Wierschem et al. [2002, 2005] found that substrate corrugations lead to an increase in the mean thickness of the film and that the flow structure deviates significantly from the Nusselt parabolic velocity profile, particularly at point along the domain where the film is thickest. Accordingly, the validity of studies based on lubrication or perturbation theory are restricted to small substrate corrugations [Kalliadasis et al., 2000, Mazouchi and Homsy, 2001, Kalliadasis and Homsy, 2001, Scholle et al., 2001a,b, Trevelyan et al., 2002]. A key discovery was that substrate undulations of moderate steepness can actually delay the onset of surface instabilities when compared with their planar counterpart [Wierschem and Aksel, 2003, Wierschem et al., 2005]. Meanwhile, experiments by Wierschem et al. [2003] confirmed that flow separation can occur in film flow over corrugated substrate – at which point eddies form in the troughs of substrate corrugations. Further investigation on eddy formation and suppression [Wierschem et al., 2010] was undertaken both numerically and experimentally by Scholle et al. [2004] and Wierschem and Aksel [2004], respectively.

Documentation of a remarkable stabilisation of film flow over corrugated substrate at high Reynolds number [Vlachogiannis and Bontozoglou, 2002] initiated study on the interaction between inertia and substrate topography. Successive experiments [Argyriadi et al., 2006], theoretical analysis [Trifonov, 2007], and numerical solutions [Dávalos-Orozco, 2008] found substrate corrugations demonstrate a stabilising effect. Steady film flow over wavy substrate explored via finite-element simulations by Nguyen and Bontozoglou [2011] found a resonance between surface waves and the sinusoidal substrate, which was followed by the discovery of a short-wave instability in experiments by Cao et al. [2013]. Over time it was found substrate topography can both stabilise and destabilise gravity-driven film flow [Mogilevskiy and Shkadov, 2019]; the stabilisation effect being due to an increase in the film thickness whilst the destabilisation arises from resonant waves [Schörner et al., 2016]. Continuing research on the problem of film flow over corrugated substrate has revealed a rich variety of stability phenomena including: short-wave transitions and isles of stability [Trifonov, 2014b]; the combined effect of corrugation amplitude and wavelength on flow stabilisation [Schörner et al., 2015, 2016]; the transition from convective to absolute instability as the wall amplitude is increased [Tseluiko et al., 2013]; and culminating in the identification of six characteristic stability regimes for film flow over topography [Schörner and Aksel, 2018a, Schörner et al., 2018]

– for more information see review by Schörner and Aksel [2018b]. Recently, Veremieiev and Wacks [2019] have shown the qualitative stability behaviour caused by substrate topography can be captured by a WIBL model.

1.4 Heated Falling Films

The problem of film flow down uniformly heated substrate was initially studied by Bankoff [1971], Iyer and Kelly [1974], Lin [1975], Sreenivasan and Lin [1978], Goussis and Kelly [1985], Kelly et al. [1986], Goussis and Kelly [1990], Joo et al. [1991a]; however, it was Goussis and Kelly [1991] who performed the first rigorous stability analysis using the Orr-Sommerfeld equation and found that heated film flow plays host to two instability modes associated with thermo-capillarity: a long-wave variety linked to the hydrodynamic instability mode and a short-wave one. Goussis and Kelly [1991] derived a thermal analogy of equation (1.2) which details how the long-wave thermo-capillary mode modifies the stability criteria for gravity-driven film flow down uniformly heated inclines. Since then, the heated problem for both planar and corrugated substrate has received far less attention than its isothermal counterpart; nevertheless, over time the modelling techniques used to explore the isothermal problem have been extended to the heated problem [Oron and Rosenau, 1992]. Given the temperature distribution within "a flat-film flowing down a planar, uniformly heated incline" is linear, it has become commonplace to initiate a long-wave expansion with an assumed linear temperature dependence through the film, even though it is impossible for the latter to satisfy all of the required boundary conditions. Proceeding in this way, the *long-wave* thermo-capillary mode was explored by Kalliadasis et al. [2003b,a] using a mixed Shkadov-weighted-residual model; however, it fails to retrieve Re_{crit} for uniformly heated substrate. The WIBL model derived by Ruyer-Quil et al. [2005], using a self-similar linear temperature profile, overcame this problem, accurately predicting Re_{crit} [Scheid et al., 2005]; however, later studies have found models based on a self-similar linear temperature profile to be in accurate [Trevelyan et al., 2007]. Saprykin et al. [2007] were the first to consider the combined effect of topography and heating, employing a Benney-like long-wave expansion to model an evolving film on a horizontally aligned substrate; being later followed by Blyth and Bassom [2012]. Despite its known inaccuracy, a self-similar linear temperature profile has been further utilised in WIBL models investigating heated, wavy substrate [D'Alessio et al., 2010, Ogden et al., 2011]; studies involving temperature-dependent fluid properties [Dávalos-Orozco, 2012, Pascal et al., 2018]; and other heated film flow problems [Mukhopadhyay and Mukhopadhyay, 2020, Sterman-Cohen and Oron, 2020].

The problem of a linear temperature dependence is that it rapidly produces non-physical negative fluid temperatures in solitary wave simulations at moderate Péclet number; the fact most functional fluids exhibit large Péclet numbers underscores the importance of overcoming this barrier. Utilising a Galerkin projection of the energy equation, Trevelyan et al. [2007] showed the onset of negative temperature predictions can be stalled by a non-linear temperature dependence and eliminated entirely by modifying the weight functions; however, the latter predictions are only in qualitative agree-

ment with the full energy equation. Elsewhere, Chhay et al. [2015, 2017] were able to evade the negative predictions of a linear temperature dependence by interchanging asymptotically equivalent terms in their averaged energy equation; instead constraining the temperature to follow the flat-film solution at large Péclet number. Thompson et al. [2019] adopted a linear temperature profile satisfying the Dirichlet and Neumann conditions at the free-surface but not the substrate Dirichlet condition; in consequence, their "projection approach" is only consistent at moderate Péclet numbers close to a critical value. Some of the most promising came from Cellier and Ruyer-Quil [2020] who applied a relaxation to the linear temperature dependence which promotes the non-linear diffusion of heat inside the film. Proposing two models – a simpler single-variable one and a more complex two-variable one – they achieved good agreement with the full energy equation at moderate Péclet number, whilst concurrently delaying negative temperatures until large Péclet number. Building upon the modelling approach of Cellier and Ruyer-Quil [2020], Daly et al. [2022] put forward a three-equation model in which the energy residual was derived using a quadratic temperature ansatz; this model was shown to vastly out-perform previous models based upon a linear temperature ansatz. Furthermore, Daly et al. [2022] were able to show analytically why the leading temperature expansion needed to be non-linear and explain where the deficiency in the linear temperature ansatz arises from.

Unfortunately, experimental research on the problem of gravity-driven film flow uniformly heated from below has been practical non-existent; as a matter of fact, the author only knows of two experimental studies on this topic and both were published only within this past year, namely Collignon et al. [2021, 2022]. Whilst this welcome news, the present monograph does not make any comparison with these results because the boundary conditions behind the experimental setup and the present theory are not identical; accordingly, the general formulation of the problem outlined in chapter 2 would need to be modified in order to reflect the laboratory conditions which is beyond the time-frame of this research.

1.5 Thesis Outline

The thesis proceeds as follows: Chapter 2 includes a general formulation of the problem; the governing equations are first stated in terms of dimensional variables before being placed in dimensionless form. At the end of this chapter is a derivation of fluid pressure expression which is used to replace the fluid pressure in all of the asymptotic modelling approaches contained within this monograph. The asymptotic modelling approaches under consideration are laid out in chapter 3: first is a perturbation series expansion of the governing equation set, known more commonly as the Benney expansion [Benney, 1966a]; second is a power series expansion of the governing equation set, which is reduced to the modelling approach of Ruyer-Quil and Manneville [2000]. In each case, the modelling technique is scrutinised with the assumptions of the approach clearly stated; in this way, the strengths and weaknesses of both approaches is understood. Chapter 4 outlines the theory of linear stability analysis, which is used to explore the stability char-

acteristics of gravity-driven film flow, and contains a derivation of the Orr-Sommerfeld system of equations which governs the linear stability of the full governing equation set for the case of planar substrate. The numerical methods used to solve the governing equations, asymptotic models and Orr-Sommerfeld equation are introduced in chapter 5. The numerical solutions consist of: (i) steady-state solutions obtained through the finite element method for the governing equation set and the finite difference method for the asymptotic models; and (ii) linear stability results acquired through numerically solving an eigenvalue problem. The steady-state results are presented in chapter 6 and are separated into those concerning the isothermal and heated problem, respectively. The solutions obtained through linear stability analysis are displayed in chapter 7; the first set of results explore the stability of film flow down planar substrate such that the predictions of the asymptotic models can be compared against those of the Orr-Sommerfeld equation; this is followed by a set of results exploring the stability of film flow down corrugated substrate. Finally, the conclusions of this research and the recommendations for future work are laid out in chapter 8.

Chapter 2

General Formulation of the Problem

2.1 Problem schematic and co-ordinate system

The problem of interest is that of a gravity-driven layer of Newtonian fluid, with constant density ρ and dynamic viscosity μ, flowing over a uniformly heated, periodically corrugated rigid substrate inclined at an angle β to the horizontal, as illustrated schem-

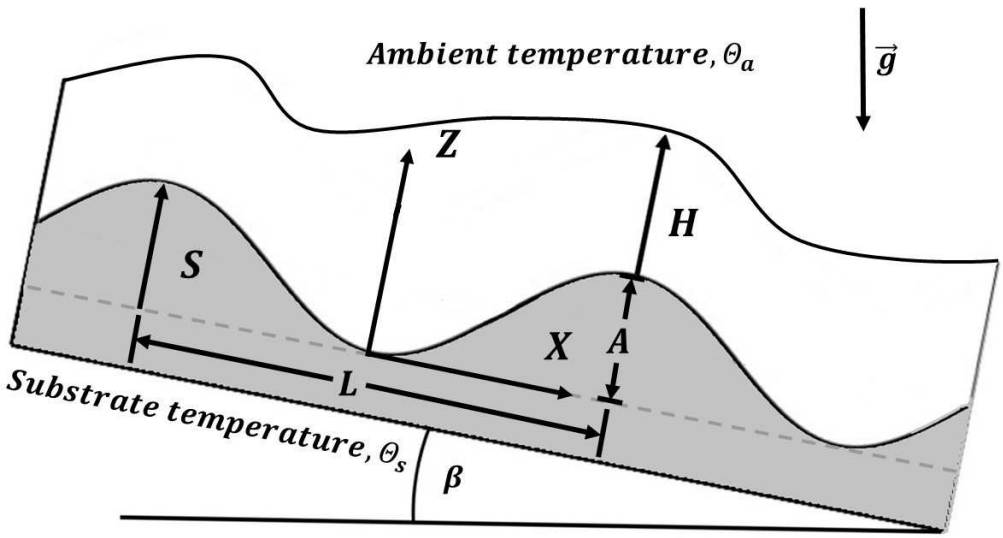

Figure 2.1: Schematic of film flow down a uniformly heated, wavy rigid substrate inclined at an angle β to the horizontal, showing the main geometrical features relative to the adopted co-ordinate system.

atically in figure 2.1. The kinematic viscosity of the fluid is defined by $\nu = \mu/\rho$ and is thus also a constant quantity.

At a time T, the corresponding Cartesian co-ordinate system is orientated such that the X-axis points along and down the inclined substrate, with the Z-axis normal to it. The substrate is considered to be infinite and invariant in the Y-direction, rendering the principal problem two-dimensional. The substrate profile, $S(X)$, is measured relative to the X-axis and given by:

$$S(X) = A\frac{\left[1 + \cos\left(\frac{2\pi X}{L_0}\right)\right]}{2}, \tag{2.1}$$

where A is the corrugation amplitude and L_0 its wavelength.

The film thickness, $H(X,T)$, at a downstream location X and time T, is the difference between the free-surface location, $Z = F(X,T)$, and the corrugation height, $Z = S(X)$. The temperature of the substrate, Θ_s, and that of the surrounding ambient gas, Θ_a, remain fixed and constant at all times with the difference between them defined as $\Theta_\Delta = \Theta_s - \Theta_a$.

2.2 Governing equations

2.2.1 Conservation of mass

The conservation of mass is described by the continuity equation:

$$\frac{\partial \rho}{\partial T} + \nabla \cdot \left(\rho \vec{\mathbf{U}}\right) = 0, \tag{2.2}$$

where $\vec{\mathbf{U}} = (U,V,W)$ is the flow vector, $\nabla = (\partial/\partial X, \partial/\partial Y, \partial/\partial Z)$ is the differential operator and $\cdot$ denotes the scalar product. Within the current work, the fluid density ρ is considered to remain constant, leading to the incompressible flow condition:

$$\nabla \cdot \vec{\mathbf{U}} = 0. \tag{2.3}$$

2.2.2 Conservation of momentum

The motion of the fluid is governed by the Navier-Stokes equations:

$$\rho\left(\frac{\partial \vec{\mathbf{U}}}{\partial T} + \left(\vec{\mathbf{U}} \cdot \nabla\right)\vec{\mathbf{U}}\right) = -\nabla P + \nabla \cdot \hat{\mathbf{T}} + \rho\vec{g}, \tag{2.4}$$

where P is the fluid pressure, $\vec{g} = (\bar{g}\sin\beta, 0, -\bar{g}\cos\beta)$ is the acceleration due to gravity,

and $\hat{\mathbf{T}} = \lambda\left(\nabla\cdot\vec{\mathbf{U}}\right)\mathbb{I} + \mu\left[\left(\nabla\otimes\vec{\mathbf{U}}\right) + \left(\nabla\otimes\vec{\mathbf{U}}\right)^T\right]$ is the Cauchy stress tensor in which: λ is the second viscosity coefficient, $\mathbb{I}$ is the identity matrix $\mathbb{I}$, $\otimes$ is the tensor product, and $(\nabla\otimes\vec{\mathbf{U}})^T$ is the transpose of $(\nabla\otimes\vec{\mathbf{U}})$. Within the current study, the fluid density and viscosity are both assumed to remain constant; thus, equation (2.4) simplifies to:

$$\rho\left(\frac{\partial\vec{\mathbf{U}}}{\partial T} + \left(\vec{\mathbf{U}}\cdot\nabla\right)\vec{\mathbf{U}}\right) = -\nabla P + \mu\nabla^2\vec{\mathbf{U}} + \rho\vec{g}. \tag{2.5}$$

2.2.3 Conservation of energy

The energy of the fluid (per unit mass), $\mathbf{E}$, is described by:

$$\rho\left(\frac{\partial\mathbf{E}}{\partial T} + \left(\vec{\mathbf{U}}\cdot\nabla\right)\mathbf{E}\right) = \rho\dot{Q} + \nabla\cdot\left(\kappa\nabla\Theta\right) + \rho\vec{\mathbf{U}}\cdot\vec{g} - \nabla\cdot\left(P\vec{\mathbf{U}}\right) + \nabla\cdot\left(\vec{\mathbf{U}}\cdot\hat{\mathbf{T}}\right), \tag{2.6}$$

where $\dot{Q}$ is the volumetric heating of the fluid per unit mass due the absorption or emission of thermal radiation, κ is the thermal conductivity of the fluid, and Θ is the fluid temperature. Equation (2.6) reduces to a *convection-diffusion* equation via a substitution of $\mathbf{E} = e + \frac{1}{2}\left|\vec{\mathbf{U}}\right|^2$ where $e = C_P\Theta$ is the internal energy of the fluid per unit mass, C_P is the specific heat capacity at constant pressure of a fluid element, and $\frac{1}{2}\left|\vec{\mathbf{U}}\right|^2$ is the kinetic energy per unit mass of the fluid; simplifying the resulting expression via equations (2.3,2.5) leads to:

$$\rho\left(\frac{\partial}{\partial T}\left(C_P\Theta\right) + \left(\vec{\mathbf{U}}\cdot\nabla\right)\left(C_P\Theta\right)\right) = \rho\dot{Q} + \nabla\cdot\left(\kappa\nabla\Theta\right) + \Phi, \tag{2.7}$$

where $\Phi = \left(\hat{\mathbf{T}}\cdot\nabla\right)\cdot\vec{\mathbf{U}}$ is the viscous dissipation function.

In the present analysis, there is no volumetric heating within the liquid layer, $\dot{Q} = 0$; the variation of the heat capacity C_P and thermal conductivity κ of the fluid due to temperature is neglected, instead these quantities are considered to be constants; and the heating due to viscous dissipation is assumed negligible compared to the external heating of the film, $\Phi \approx 0$. Consequently, equation (2.7) reduces to:

$$\rho C_P\left(\frac{\partial\Theta}{\partial T} + \left(\vec{\mathbf{U}}\cdot\nabla\right)\Theta\right) = \kappa\nabla^2\Theta. \tag{2.8}$$

2.3 Boundary conditions

The set of equations describing the dynamics of the film are completed by conditions at the boundaries of the domain, $\Omega = \{X\in[0,L], Y\in[-\infty,+\infty], Z\in[S(X),F(X,T)]\}$.

2.3.1 Periodic boundary conditions

The problem is considered periodic in the X-direction, thus:

$$X = X + L_0, \tag{2.9}$$

and invariant in the Y-direction; thus, $V = 0,\ \partial/\partial Y = 0\ \forall\,(X, Y, Z, T)$.

2.3.2 Substrate boundary conditions

At the non-porous substrate, $Z = S(X)$, two Dirichlet boundary conditions are imposed on the fluid velocity, namely:

$$U = 0, \qquad W = 0, \qquad at\ Z = S(X), \tag{2.10}$$

which correspond to a no-slip condition and no-penetration condition of the substrate. In addition, one Dirichlet condition is imposed on the fluid temperature:

$$\Theta = \Theta_S, \qquad at\ Z = S(X), \tag{2.11}$$

which states the fluid at the substrate is in thermal equilibrium with the substrate; the temperature of substrate is assumed to remain fixed, $\Theta_S = constant\ \forall\,(X, Y, T)$.

2.3.3 Free-surface boundary conditions

At the deformable free-surface, $Z = F(X, T)$, four conditions are required. The first is a kinematic condition which defines the free-surface as a material boundary, it reads:

$$\frac{\partial H}{\partial T} + U\frac{\partial F}{\partial X} = W. \qquad at\ Z = F(X, T), \tag{2.12}$$

Equation (2.12) is accompanied by two dynamic conditions describing the force balance at the free-surface. These conditions are derived from the stress balance equation:

$$\hat{n}\,(P_0 - P) + \hat{n}\cdot\hat{\mathbf{T}} - \hat{n}\cdot\hat{\mathbf{T}}_a = -\sigma\hat{n}\,(\nabla_S\cdot\hat{n}) + \nabla_S\sigma, \quad at\ Z = F(X, T), \tag{2.13}$$

where P_0 is the ambient pressure, $\hat{\mathbf{T}}_a$ is the Cauchy stress tensor of the ambient gas, $\hat{n}$ is the unit vector normal to the free-surface, σ is the surface tension of the fluid film,

and $\nabla_S = (\mathbb{I} - \hat{n} \otimes \hat{n}) \cdot \nabla$ is the surface gradient operator. The ambient gas is considered stationary at all times so no shearing of the free-surface occurs, $\hat{\mathbf{T}}_a \approx 0$; and the surface tension of the fluid film is assumed to vary with temperature in the following fashion:

$$\sigma = \sigma_0 \left[1 + (\Theta - \Theta_a) \left(\frac{\partial \sigma}{\partial \Theta} \right) \right], \tag{2.14}$$

where σ_0 is the value of the surface tension at Θ_a and $(\partial\sigma/\partial\Theta)$ is the surface tension gradient with respect to temperature which is taken to be a constant.

Equation (2.13) is a vector equation describing the stress balance along the free-surface; accordingly, the normal and tangential stress balance equations can be acquired by computing the scalar product $(\cdot)$ of equation (2.13) with the unit vectors normal, $\hat{n}$, and tangent, $\hat{t}_X$, to the free-surface, respectively. These unit vectors are given by:

$$\hat{n} = \frac{1}{\sqrt{1+G}} \left(-\frac{\partial F}{\partial X}, 0, 1 \right), \qquad \hat{t}_X = \frac{1}{\sqrt{1+G}} \left(1, 0, \frac{\partial F}{\partial X} \right), \tag{2.15}$$

which contain the surface curvature pre-factor, $G = (\partial F/\partial X)^2$. Computing the normal and tangential stress balance leads to:

$$P = P_0 - 2\mu \frac{(1-G)\frac{\partial U}{\partial X} + \frac{\partial F}{\partial X}\left(\frac{\partial W}{\partial X} + \frac{\partial U}{\partial X}\right)}{1+G} - \sigma \frac{\partial}{\partial X} \left[\frac{\frac{\partial F}{\partial X}}{\sqrt{1+G}} \right], \quad at\ Z = F(X,T), \tag{2.16}$$

$$\mu \left(\frac{\partial W}{\partial X} + \frac{\partial U}{\partial Z} \right) = 4\mu \frac{\frac{\partial F}{\partial X}\frac{\partial U}{\partial X}}{1-G} + \frac{\sqrt{1+G}}{1-G} \left(\frac{\partial \sigma}{\partial X} + \frac{\partial F}{\partial X}\frac{\partial \sigma}{\partial Z} \right). \quad at\ Z = F(X,T), \tag{2.17}$$

in which σ is given by equation (2.14).

The final condition describes the heat flux from the liquid film to the ambient gas. In the absence of radiative effects, this flux will be purely conductive and can be described by Newton's law of cooling; namely:

$$-\kappa \hat{n} \cdot \nabla \Theta = \alpha \left(\Theta - \Theta_a \right), \qquad at\ Z = F(X,T), \tag{2.18}$$

where α is the coefficient of heat transfer. Re-arranging equation (2.18) yields:

$$\frac{\partial \Theta}{\partial Z} = \frac{\partial F}{\partial X}\frac{\partial \Theta}{\partial X} - \frac{\alpha}{\kappa} \left(\Theta - \Theta_a \right) \sqrt{1+G}, \quad at\ Z = F(X,T), \tag{2.19}$$

2.4 Dimensionless equations

Equations (2.1 – 2.19) are non-dimensionalised using the following scalings:

$$\begin{array}{lll} X = L_0 x, & Y = L_0 y, & Z = H_0 z, \\ U = U_0 u, & V = U_0 v, & W = \frac{H_0 U_0}{L_0} w, \\ T = \frac{L_0}{U_0} t, & \Theta = \Theta_\Delta \theta + \Theta_a, & P = \frac{\mu U_0 L_0}{H_0^2} p, \\ S = H_0 s & H = H_0 h, & F = H_0 f, \end{array} \quad , \tag{2.20}$$

where lowercase letters represent the dimensionless variables.

The length scale in the Z-direction, H_0, corresponds to the thickness of a Nusselt laminar film; given by:

$$H_0 = \left(\frac{3\mu \mathcal{Q}_0}{\rho \bar{g} \sin\beta} \right)^{1/3}, \tag{2.21}$$

whilst the velocity scale is taken to be the free-surface velocity of a Nusselt laminar film, $U_0 = 3\mathcal{Q}_0/2H_0$; the two are linked through the volumetric flow rate per unit cross-sectional width of a Nusselt laminar film, $\mathcal{Q}_0$. A summary of Nusselt's theory of laminar film dynamics can be found in Appendix A. The characteristic length scale in the X-direction is taken to be the wavelength of the substrate corrugation, L_0, which is considered to be much larger than the Nusselt film thickness, *i.e.* $L_0 \gg H_0$.

Applying the scalings from equation (2.20) to equation (2.1) leads to the scaled substrate profile; which reads:

$$s(x) = \frac{A}{H_0} \frac{\left[1 + \cos\left(2\pi x\right)\right]}{2}. \tag{2.22}$$

Non-dimensionalising the continuity (2.3), Navier-Stokes (2.5) and convection-diffusion (2.8) equations yields the following dimensionless governing equations:

$$\frac{\partial u}{\partial x} + \frac{\partial w}{\partial z} = 0, \tag{2.23}$$

$$\epsilon Re \left[\frac{\partial u}{\partial t} + u\frac{\partial u}{\partial x} + w\frac{\partial u}{\partial z} \right] = -\frac{\partial p}{\partial x} + 2 + \epsilon^2 \frac{\partial^2 u}{\partial x^2} + \frac{\partial^2 u}{\partial z^2}, \tag{2.24}$$

$$\epsilon^3 Re \left[\frac{\partial w}{\partial t} + u\frac{\partial w}{\partial x} + w\frac{\partial w}{\partial z} \right] = -\frac{\partial p}{\partial z} - 2\epsilon \cot\beta + \epsilon^4 \frac{\partial^2 w}{\partial x^2} + \epsilon^2 \frac{\partial^2 w}{\partial z}, \tag{2.25}$$

$$\epsilon RePr \left[\frac{\partial \theta}{\partial t} + u\frac{\partial \theta}{\partial x} + w\frac{\partial \theta}{\partial z} \right] = \epsilon^2 \frac{\partial^2 \theta}{\partial x^2} + \frac{\partial^2 \theta}{\partial z^2}, \tag{2.26}$$

in which the following dimensionless groups are featured: the *shallowness parameter*, $\epsilon = H_0/L_0$; the Reynolds number, $Re = \rho U_0 H_0/\mu$; the Prandtl number, $Pr = \mu C_P/\kappa$.

Note the momentum equation in the y-direction has been excluded from equations (2.23 – 2.26) as the present analysis is restricted to just two-dimensions.

The dimensionless boundary conditions at the substrate, $z = s(x)$, read:

$$u|_{z=s} = w|_{z=s} = 0, \qquad \theta|_{z=s} = 1, \tag{2.27}$$

whilst those at the free-surface, $z = f(x,t)$, become:

$$w|_{z=f} = \frac{\partial h}{\partial t} + u|_{z=f}\frac{\partial f}{\partial x}, \tag{2.28}$$

$$p|_{z=f} = p_0 - 2\epsilon^2 \frac{\left(1-\epsilon^2 g\right)\frac{\partial u}{\partial x} + \frac{\partial f}{\partial x}\left[\epsilon^2\frac{\partial w}{\partial x} + \frac{\partial u}{\partial z}\right]}{1+\epsilon^2 g}\bigg|_{z=f} - \epsilon^3\frac{(1-Ma\vartheta)}{Ca}\frac{\partial}{\partial x}\left[\frac{\frac{\partial f}{\partial x}}{\sqrt{1+\epsilon^2 g}}\right], \tag{2.29}$$

$$\left[\epsilon^2\frac{\partial w}{\partial x} + \frac{\partial u}{\partial z}\right]\bigg|_{z=f} = 4\frac{\epsilon^2\frac{\partial f}{\partial x}\frac{\partial u}{\partial x}\Big|_{z=f}}{1-\epsilon^2 g} - \epsilon\frac{Ma}{Ca}\frac{\sqrt{1+\epsilon^2 g}}{1-\epsilon^2 g}\frac{\partial\vartheta}{\partial x}, \tag{2.30}$$

$$\frac{\partial\theta}{\partial z}\bigg|_{z=f} = \epsilon^2\frac{\partial f}{\partial x}\frac{\partial\theta}{\partial x}\bigg|_{z=f} - Bi\vartheta\sqrt{1+\epsilon^2 g}, \tag{2.31}$$

where p_0 is the dimensionless ambient pressure, $g = (\partial f/\partial x)^2$ is the dimensionless surface curvature pre-factor, $\vartheta = \theta|_{z=f}$ is the dimensionless temperature across the free-surface, $Ma = \Theta_\Delta\left(-\partial\sigma/\partial\Theta\right)$ is the Marangoni number, $Ca = \mu U_0/\sigma_0$ is the Capillary number, and $Bi = \alpha H_0/\kappa$ is the Biot number. Equation (2.30) has been simplified using the total derivative of the free-surface temperature; namely:

$$\frac{\partial\vartheta}{\partial x} = \frac{\partial\theta}{\partial x}\bigg|_{z=f} + \frac{\partial f}{\partial x}\frac{\partial\theta}{\partial z}\bigg|_{z=f} \tag{2.32}$$

The full dimensionless equation set for the two-dimensional problem – equations (2.22 – 2.31) – consists of four equations and seven boundary conditions; nevertheless, it is possible to reduce this number using algebra, allowing for the governing formalism to be expressed in terms of two governing equations and five boundary conditions.

2.5 Elimination of the vertical velocity

Re-arranging equation (2.23) yields an expression for the vertical velocity in terms of the stream-wise velocity; namely:

$$w = -\int_s^z \frac{\partial u}{\partial x}dz. \tag{2.33}$$

Equation (2.33) allows every occurrence of w in equations (2.23 – 2.31) to be expressed in terms of u, thus eliminating w and the need for the continuity equation (2.23).

2.6 Integral form of the kinematic condition

Substituting equation (2.33) into the kinematic condition – equation (2.28) – yields:

$$\frac{\partial h}{\partial t} + \int_s^f \frac{\partial u}{\partial x} dz + u|_{z=f} \frac{\partial f}{\partial x} - u|_{z=s} \frac{ds}{dx} = 0. \tag{2.34}$$

Simplifying equation (2.34) using the Leibniz integral rule and the definition of the stream-wise flow rate, where the latter is given by:

$$q = \int_s^f u \, dz, \tag{2.35}$$

leads to the *integral form of the kinematic condition* which reads:

$$\frac{\partial h}{\partial t} + \frac{\partial q}{\partial x} = 0, \tag{2.36}$$

and shows how the evolution of the film thickness is due to variations in the flow rate.

2.7 Derivation of the fluid pressure

An algebraic expression for the fluid pressure can be obtained by re-arranging equation (2.25) like so:

$$\frac{\partial p}{\partial z} = -2\epsilon \cot\beta + \epsilon^2 \frac{\partial}{\partial x}\left[\epsilon^2 \frac{\partial w}{\partial x} + \frac{\partial u}{\partial z}\right] + 2\epsilon^2 \frac{\partial^2 w}{\partial z^2} - \epsilon^3 Re\left[\frac{\partial w}{\partial t} + u\frac{\partial w}{\partial x} + w\frac{\partial w}{\partial z}\right], \tag{2.37}$$

and then integrating *with respect to* z between z and $z = f(x,t)$ to get:

$$\begin{aligned} p = p_0 + 2\epsilon \cot\beta \int_z^f dz - 2\epsilon^2 \frac{\partial u}{\partial x} + 2\epsilon^2 \left[1 - \frac{1-\epsilon^2 g}{1+\epsilon^2 g}\right] \frac{\partial u}{\partial x}\bigg|_{z=f} \\ -\epsilon^2 \int_z^f \frac{\partial}{\partial x}\left[\epsilon^2 \frac{\partial w}{\partial x} + \frac{\partial u}{\partial z}\right] dz + \epsilon^2 \frac{2}{1+\epsilon^2 g} \frac{\partial f}{\partial x}\left[\epsilon^2 \frac{\partial w}{\partial x} + \frac{\partial u}{\partial z}\right]\bigg|_{z=f} \\ +\epsilon^3 Re \int_z^f \left[\frac{\partial w}{\partial t} + u\frac{\partial w}{\partial x} + w\frac{\partial w}{\partial z}\right] dz - \epsilon^3 \frac{(1 - Ma\vartheta)}{Ca} \frac{\partial}{\partial x}\left[\frac{\frac{\partial f}{\partial x}}{\sqrt{1+\epsilon^2 g}}\right], \end{aligned} \tag{2.38}$$

where equation (2.33) has been utilised to replace $\partial w/\partial z$ by $-\partial u/\partial x$ and the upper limit

of integration has been given by the normal stress at the free-surface – equation (2.29). Expression (2.38) can be simplified, via the Leibniz integral rule, to:

$$\begin{aligned} p = p_0 + 2\epsilon \cot\beta \int_z^f dz - 2\epsilon^2 \frac{\partial u}{\partial x} + 2\epsilon^2 \frac{2\epsilon^2 g}{1+\epsilon^2 g} \frac{\partial u}{\partial x}\bigg|_{z=f} \\ -\epsilon^2 \frac{\partial}{\partial x} \int_z^f \left[\epsilon^2 \frac{\partial w}{\partial x} + \frac{\partial u}{\partial z} \right] dz - \epsilon^2 \frac{1-\epsilon^2 g}{1+\epsilon^2 g} \frac{\partial f}{\partial x} \left[\epsilon^2 \frac{\partial w}{\partial x} + \frac{\partial u}{\partial z} \right]\bigg|_{z=f} \\ +\epsilon^3 Re \int_z^f \left[\frac{\partial w}{\partial t} + u\frac{\partial w}{\partial x} + w\frac{\partial w}{\partial z} \right] dz - \epsilon^3 \frac{(1-Ma\vartheta)}{Ca} \frac{\partial}{\partial x} \left[\frac{\frac{\partial f}{\partial x}}{\sqrt{1+\epsilon^2 g}} \right]. \end{aligned} \tag{2.39}$$

A substitution of the shear stress boundary condition – equation (2.30) – and a factorisation of the capillary terms allows equation (2.39) to be reduced to:

$$\begin{aligned} p = p_0 + 2\epsilon (f - z) \cot\beta - \epsilon^2 \frac{\partial u}{\partial x} - \epsilon^2 \frac{\partial}{\partial x} \left(u|_{z=f} \right) - \epsilon^3 \frac{\partial}{\partial x} \left[\frac{(1-Ma\vartheta)}{Ca} \frac{\frac{\partial f}{\partial x}}{\sqrt{1+\epsilon^2 g}} \right] \\ +\epsilon^3 Re \int_z^f \left[\frac{\partial w}{\partial t} + u\frac{\partial w}{\partial x} + w\frac{\partial w}{\partial z} \right] dz - \epsilon^4 \frac{\partial}{\partial x} \int_z^f \frac{\partial w}{\partial x}\, dz, \end{aligned} \tag{2.40}$$

where $w = -\int_s^z (\partial u/\partial x)\, dz$. Herein, the fluid pressure is given by equation (2.40), thus eliminating the need for z-momentum equation (2.25).

2.8 Alternative forms of the shear stress and heat flux

A final modification to equations (2.23 – 2.31) is a re-writing of the shear stress and heat flux boundary conditions; equations (2.30 – 2.31) are replaced by:

$$\frac{\partial u}{\partial z}\bigg|_{z=f} = \frac{2\epsilon^2 \frac{\partial f}{\partial x} \frac{\partial}{\partial x} \left(u|_{z=f} \right)}{(1+\epsilon^2 g)} + \frac{\left(1-\epsilon^2 g\right)}{(1+\epsilon^2 g)} \frac{\epsilon^2 \left[\frac{\partial^2 q}{\partial x^2} - u|_{z=f} \frac{\partial^2 f}{\partial x^2} \right]}{(1+\epsilon^2 g)} - \frac{\epsilon \frac{Ma}{Ca} \frac{\partial \vartheta}{\partial x}}{\left[1+\epsilon^2 g\right]^{3/2}}, \tag{2.41}$$

$$\frac{\partial \theta}{\partial z}\bigg|_{z=f} = \frac{\epsilon^2 \frac{\partial f}{\partial x} \frac{\partial \vartheta}{\partial x}}{1+\epsilon^2 g} - \frac{Bi\vartheta}{\sqrt{1+\epsilon^2 g}}, \tag{2.42}$$

obtained using the total spatial derivatives along the free-surface, namely:

$$\frac{\partial \vartheta}{\partial x} = \frac{\partial \theta}{\partial x}\bigg|_{z=f} + \frac{\partial f}{\partial x} \frac{\partial \theta}{\partial z}\bigg|_{z=f}, \tag{2.43}$$

$$\frac{\partial}{\partial x} \left(u|_{z=f} \right) = \frac{\partial u}{\partial x}\bigg|_{z=f} + \frac{\partial f}{\partial x} \frac{\partial u}{\partial z}\bigg|_{z=f}, \tag{2.44}$$

$$\frac{\partial}{\partial x} \left(w|_{z=f} \right) = \frac{\partial w}{\partial x}\bigg|_{z=f} + \frac{\partial f}{\partial x} \frac{\partial w}{\partial z}\bigg|_{z=f}. \tag{2.45}$$

2.9 Compact equation set

Sections 2.5 – 2.8 detail how the full dimensionless equation set – equations (2.22 – 2.31) – can be reduced to just two governing equations – equations (2.24) and (2.26); and five boundary conditions – equations (2.27), (2.36) and (2.41 – 2.42); in which the substrate profile (s) is given by equation (2.22), the vertical velocity (w) is given by equation (2.33) and the fluid pressure (p) is given by equation (2.40). Importantly, the compact equation set – equations (2.24), (2.26), (2.27), (2.36) and (2.41 – 2.42) – is algebraically equivalent to the full dimensionless equation set and thus solutions sought to the former will be identical to those of the latter for a given parameter set; accordingly, the problem of two-dimensional gravity-driven film flow down uniformly heated, smoothly corrugated, inclined substrate is readily described by equations (2.22 – 2.31) or equivalently by equations (2.24), (2.26), (2.27), (2.36) and (2.41 – 2.42). The compact equation set is adopted in subsequent chapters as the elimination of the continuity and z-momentum equations and their associated variables from the governing formalism reduces the mathematical complexity of the problem and consequently eases the derivation of reduced asymptotic models.

Chapter 3

Methodology I: Mathematical Modelling

Even following an elimination of the vertical velocity and fluid pressure, see section 2.9, solving the full equation set (2.23 – 2.31) represents a daunting task due to the *a priori* unknown location of the free-surface, as the unknown domain must be solved for in addition to the unknown functions of the fluid velocity and temperature – this requires laborious numerical computation. However, if the flow is classifiable as a thin film, then the problem can be studied using models of reduced dimensionality which eliminate the z-dependence of the governing equations but still retain all the essential physics of the problem [Craster and Matar, 2009]. The most successful of these models are those based upon an asymptotic expansion of the fluid velocity and temperature [Benney, 1966a, Gjevik, 1970a, Ruyer-Quil and Manneville, 2000, Cellier and Ruyer-Quil, 2020]; such models consistently balance the interplay between competing physical mechanisms when surface instabilities form atop falling liquid films [Ruyer-Quil et al., 2005].

In the current chapter, two procedures for implementing an asymptotic expansion of the governing equations are laid out: (i) the first corresponds to the approach of Benney [1966a] which leads to a single evolution equation in terms of the film thickness; (ii) the second is the method of Ruyer-Quil and Manneville [2000] which yields a multi-variable model. The former is known to exhibit finite-time blow-up at moderate Reynold numbers far beyond the critical value at which surface instabilities first appear [Pumir et al., 1983]; this behaviour was shown to be unphysical by Salamon et al. [1994]. The latter approach does not suffer from this unrealistic behaviour and thus offers superior predictions beyond the point of criticality – the point at which instabilities first appear [Scheid et al., 2006]; nevertheless, research on film flow down heated inclines at large Péclet number has found the modelling approach of Ruyer-Quil and Manneville [2000] yields temperature predictions which lie outside of the physically permissible bounds set by the substrate temperature and the temperature of the ambient gas [Scheid et al., 2005] – the Péclet number is a dimensionless quantity expressed as the ratio of the advective and diffusive transport rates. Techniques to alleviate the unphysical thermodynamics of the aforementioned modelling approach have been put forward by Trevelyan et al. [2007],

Chhay et al. [2017], Thompson et al. [2019], Cellier and Ruyer-Quil [2020], Daly et al. [2022]; however, even the most advanced asymptotic methods still predict unphysical fluid temperatures [Cellier and Ruyer-Quil, 2020] and Chhay et al. [2017] have even gone as far as to suggest that the unphysical thermodynamic behaviour reported at large Péclet number is inevitably when employing models of reduced dimensionality.

The objective of the current work is therefore not to liberate the modelling approach of Ruyer-Quil and Manneville [2000] from its thermodynamic limitation – as such a goal may not be achievable; instead, the goal is to extend the validity of the approach to moderate Péclet number and develop a consistent asymptotic modelling approach with which to study gravity-driven film flow down heated inclined substrate. This is achieved by highlighting the constraints placed on the modelling approach by Ruyer-Quil and Manneville [2000], and identifying how these constraints can be relaxed in order to extend the validity of the modelling approach to new parameter spaces. To aid with this, the modelling approach of Benney [1966a] is outlined first in Section 3.3; this approach is known to be inconsistent, however, only in the present work is the source of this inconsistency clearly explained. The inconsistency of the Benney approach is rectified by relaxing the constraints on the asymptotic expansion of the fluid velocity and temperature in Section 3.4, and this course of action leads to the modelling approach of Ruyer-Quil and Manneville [2000]; accordingly, the modelling approach of Ruyer-Quil and Manneville [2000] is a generalisation of Benney's approach. The next step is then to seek a generalisation of the modelling approach of Ruyer-Quil and Manneville [2000] which is valid at moderate Péclet number; this is accomplished by formulating the modelling approach of Ruyer-Quil and Manneville [2000] as a special case of the Tau method – a technique for solving partial differential equations originally proposed by Lanczos [1938]. The advantage of casting the modelling approach of Ruyer-Quil and Manneville [2000] as a derivative of the Tau method is that doing so clearly highlights the unphysical constraint placed on the thermal analogy of the modelling approach by Ruyer-Quil et al. [2005], and explains why the leading approximation in the asymptotic expansion of the fluid temperature must be quadratic, even if the temperature field reduces to a linear distribution in the limit of the expansion parameter going to zero. This allows for: the derivation of a consistent first-order model in the long-wave expansion based upon the quadratic temperature approximation; an attempt to derive a consistent higher-order model; and the derivation of simplified higher-order models with which to study gravity-driven film flow down heated inclined substrate.

3.1 The Reduced Vertical Coordinate

To simplify and accelerate the algebra in the following chapter, it is beneficial to introduce the reduced vertical coordinate, given by:

$$\hat{z} = z - s(x). \tag{3.1}$$

Mapping the problem onto the domain of the reduced vertical coordinate, $\hat{z} \in [0, h]$, requires the following identities:

$$\frac{\partial}{\partial z} = \frac{\partial}{\partial \hat{z}}, \qquad \frac{\partial \hat{z}}{\partial x} = -\frac{ds}{dx}, \qquad \int_s^f dz = \int_0^h d\hat{z}. \tag{3.2}$$

Working in the terms of the reduced vertical coordinate means reducing the dimensionality of the problem now relies upon eliminating the $\hat{z}$-dependence from the governing equations; in any event, the set of equations recovered by each modelling approach is the same whether the derivation is carried out in terms of z or in terms of $\hat{z}$.

3.2 The long-wave expansion

The asymptotic expansion applied to the governing equations in the following sections is known within the literature as the long-wave expansion. The problem of gravity-driven film flow is well suited to mathematical modelling via a long-wave expansion due to: (a) the primary flow being governed by laminar friction [Benjamin, 1957]; and (b) the hydrodynamic instability being characterised by surface tension [Kapitza, 1948]. The former leads to a flow structure which is primarily uni-directional, whilst the latter ensures the disturbances to this structure typically have very long wavelengths as surface tension generates a damping force which is proportional to the curvature of the fluid-fluid interface, ergo, short waves producing large surface curvatures are strongly damped leading to long waves being the most unstable modes [Yih, 1963, Smith, 1990]. The wavelength of typical disturbances can be taken as the characteristic length scale in the x-direction, if there is no other obvious choice of length scale, and provided the disturbance wavelength is much larger than the thickness of the liquid film then one can say the film dynamics vary slowly in the x-direction and with respect to time as the most significant change in the flow structure occurs across the depth of the film in the z-direction; accordingly, derivatives of the fluid velocity and temperature *with respect to (w.r.t.)* x and t will be small quantities when compared against their corresponding derivatives *w.r.t.* z. The smallness of space-time derivatives in the present formulation is captured by the scaling parameter, $\epsilon = H_0/L_0$, which is called the *shallowness parameter*. The shallowness parameter represents the disparity between the characteristic length scale in the x-direction, L_0, and the mean thickness of the film, H_0. The long-wave expansion is applicable when the mean film thickness is much smaller than the characteristic length scale along the x-axis, *i.e.* $H_0 \ll L_0$, which leads one to write $\epsilon \ll 1$.

With $\epsilon \ll 1$, it is advantageous to seek a solution to the fluid velocity and temperature in the form of an asymptotic expansion *w.r.t.* the shallowness parameter, ϵ, like so:

$$(u, \theta) = (u_0, \theta_0) + \epsilon (u_1, \theta_1) + \epsilon^2 (u_2, \theta_2) + ... + \epsilon^n (u_n, \theta_n) + ... \tag{3.3}$$

where (u_n, θ_n) represents the n-th order contributions to the fluid velocity and temperature, respectively. Accordingly, an n-th order approximation of the film dynamics will require every contribution up to (u_n, θ_n) and will be valid provided $\epsilon \ll 1$.

In regard to the choice of scalings: (i) H_0 is taken to be the thickness of a Nusselt laminar film on the knowledge that the mean thickness of a wavy film remains close to this value; and (ii) the characteristic length scale in the x-direction, L_0, is taken to be the wavelength of the paramount disturbance: (a) in the case of planar substrate, this is the wavelength of the most unstable mode; (b) in the case of corrugated substrate, the substrate corrugation represents the chief disturbance and so its wavelength is used.

3.3 Perturbation Series

The first asymptotic modelling approach considered is that of Benney [1966a]. The strategy of this approach is to expand the problem with respect to the shallowness parameter, ϵ. This leads to an asymptotic expression for the stream-wise flow rate (q), in terms of the film thickness $h(x,t)$, which can then be substituted into the *integral form of the kinematic condition* – equation (2.36) – to obtain an evolution equation for the film thickness. The main appeal of this approach is that it leads to a single-equation model with which the film dynamics can be studied; however, its major limitation is the single-equation model quickly loses its validity beyond the point of criticality – the point at which surface instabilities first form atop falling liquid films [Benjamin, 1957]. Pumir et al. [1983] found the single-equation model returns singular solutions in time-dependent simulations and this behaviour was shown to be unphysical by Salamon et al. [1994] using finite-element analysis of the Navier-Stokes equations; accordingly, the single-equation model is said to be able to predict the onset of long waves but is incapable of modelling their evolution.

The asymptotic expression for the stream-wise flow rate, which is central to this approach, is retrieved via a perturbation series; this is to say, the flow rate (q) is expanded as a power series with respect to the shallowness parameter, like so:

$$q = q_0 + \epsilon q_1 + \epsilon^2 q_2 + \ldots \tag{3.4}$$

where q_0 is the exact solution for when $\epsilon = 0$, and $q_1, q_2, \ldots$ are perturbative corrections at first-order, second-order, etc. Since ϵ is just a surrogate for the smallness of (x,t)-derivatives, expansion (3.4) is analogous to a gradient expansion with respect to (x,t).

3.3.1 The Nusselt solution

The first step of the present approach is thus to solve exactly the equations when $\epsilon = 0$. The resultant equations describe the dynamics of *"a film of uniform thickness flowing down a planar incline"*; the scenario originally investigated by Nusselt [1916].

Setting $\epsilon = 0$ in equation set (2.23 – 2.31) with the vertical velocity and fluid pressure given by equations (2.33) and (2.40), respectively; and utilising $\hat{z} = z - s(x)$, leads to:

$$\frac{\partial^2 u}{\partial \hat{z}^2} = -2, \qquad u\big|_{\hat{z}=0} = 0, \qquad \left.\frac{\partial u}{\partial \hat{z}}\right|_{\hat{z}=h} = 0, \tag{3.5}$$

$$\frac{\partial^2 \theta}{\partial \hat{z}^2} = 0, \qquad \theta\big|_{\hat{z}=0} = 1, \qquad \left.\frac{\partial \theta}{\partial \hat{z}}\right|_{\hat{z}=h} = -\frac{Bi\vartheta}{\sqrt{1+\epsilon^2 g}}, \tag{3.6}$$

in which the effect of surface curvature is assumed to be of order unity, $\left(1 \pm \epsilon^2 g\right) \sim \mathcal{O}(1)$. Solving the above leads to the Nusselt velocity and temperature solutions; given by:

$$u_{\mathbb{N}} = \hat{z}\,(2h - \hat{z})\,, \qquad \theta_{\mathbb{N}} = 1 + \frac{(\vartheta_{\mathbb{N}} - 1)}{h}\hat{z}. \tag{3.7}$$

respectively; where $\vartheta_{\mathbb{N}} = 1\Big/\left(1 + Bih/\sqrt{1+\epsilon^2 g}\right)$ is the Nusselt free-surface temperature.

Equations (3.7) represent the film dynamics in the long-wave limit where the wavelengths of disturbances approach infinity; an important check of each model proposed in the present monograph is the recovery of these solutions in the limit of $\epsilon \to 0$.

3.3.2 The inviscid Burgers equation

Evaluating the definition of the flow rate – equation (2.35) – using the Nusselt parabolic velocity profile – equation (3.7) – finds the leading-order flow rate is equal to:

$$q_0 = \frac{2}{3}h^3. \tag{3.8}$$

Substituting equation (3.8) into the kinematic condition – equation (2.36) – yields an evolution equation for the film thickness in the case of $\epsilon = 0$; namely:

$$\frac{\partial h}{\partial t} + 2h^2\frac{\partial h}{\partial x} = 0, \tag{3.9}$$

which looks very similar to the inviscid Burgers' equation – the simplest equation describing nonlinear wave motion [Bateman, 1915, Burgers, 1948].

A solution to the equation (3.9) can be found through the method of characteristics; on the basis the solution lies on the characteristic curve $x = x(t)$, one can write:

$$\frac{dh}{dt} = \frac{\partial h}{\partial t} + \frac{dx}{dt}\frac{\partial h}{\partial x}. \tag{3.10}$$

Comparison of equations (3.9) and (3.10) leads to the characteristic equations $dh/dt = 0$ and $dx/dt = 2h^2$. The second equation describes the speed at which the solution $h(x,t)$ moves along the characteristic curve which, in practical terms, equates to the velocity at which long waves propagate across the free-surface; this turns out to be twice the local free-surface velocity as $u_{\mathbb{N}}|_{\hat{z}=h} = h^2$. Integrating the characteristic equations yields:

$$h(x,t) = const. \qquad x = \tau + 2h^2 t, \tag{3.11}$$

where τ is a constant of integration marking the point on the t-axis from where the

characteristic curve $x = x(t)$ originates. Equations (3.11) state the solution $h(x,t)$ must remain constant along the characteristic curve which means $x = x(t)$ is a straight line. Ergo, if the initial shape of the free-surface is given by $h(x,0) = 1 + \hat{h}(x)$, then the characteristic solution to equation (3.9) will take the form of:

$$h(x,t) = 1 + \hat{h}(\tau), \tag{3.12}$$

where $\tau = x - ct$ is the travelling coordinate and $c = 2h^2$ is the phase velocity of the disturbance, respectively. The solution given by equation (3.12) permits the propagation of travelling waves across the free-surface in the long-wave limit provided such waves possess infinitesimal amplitude, $\hat{h}(\tau) \to 0$; however, in the case of finite amplitude waves, the variation of the phase velocity across the domain eventually leads to shock-waves which occur when the characteristic curves intersect and the solution becomes multi-valued – this is illustrated by Figure 3.1 in which the characteristic curves are plotted for an initial disturbance of $\hat{h}(\tau) = \bar{h}\cos(2\pi\tau)$ where $\bar{h}$ is the amplitude of the disturbance and $t_b \approx 1/4\pi\bar{h}$ is the approximate time to intersect. This indicates a classical solution sought through the method of characteristics does not exist because equations (3.11) require $h(x,t)$ to only take a single and constant value along the trajectory of $x = \tau + ct$. Suffice to say, the analysis of equation (3.9) shows the leading-order flow rate alone is an incomplete and inadequate description of wave formation in gravity-driven film flow; in consequence, the perturbation series must be continued to higher-order in order to find additional terms which might moderate the phase velocity across the free-surface (analogous to how the diffusion terms dissipate shock in the viscous Burgers equation).

3.3.3 Benney equation

Extension of the perturbation series to higher-order follows a mechanistic procedure in which successive corrections to the velocity and temperature seek to reconcile the exact solution for $\epsilon = 0$ – given by equations (3.7) – with the full equation set (2.23 – 2.31). Expanding the fluid velocity and temperature as power series with respect to ϵ, like so:

$$(u,\theta) = (u_0,\theta_0) + \epsilon\,(u_1,\theta_1) + \epsilon^2\,(u_2,\theta_2) + \ldots \tag{3.13}$$

and substituting into equations (2.24, 2.26 – 2.27, 2.41 – 2.42) allows each governing equation and boundary condition to be written in the following form:

$$\mathbb{B}_0(x,\hat{z},t) + \epsilon\mathbb{B}_1(x,\hat{z},t) + \epsilon^2\mathbb{B}_2(x,\hat{z},t) + \ldots = 0, \tag{3.14}$$

such that $\mathbb{B}_n$ represents the collection of terms which make up the nth-order contribution

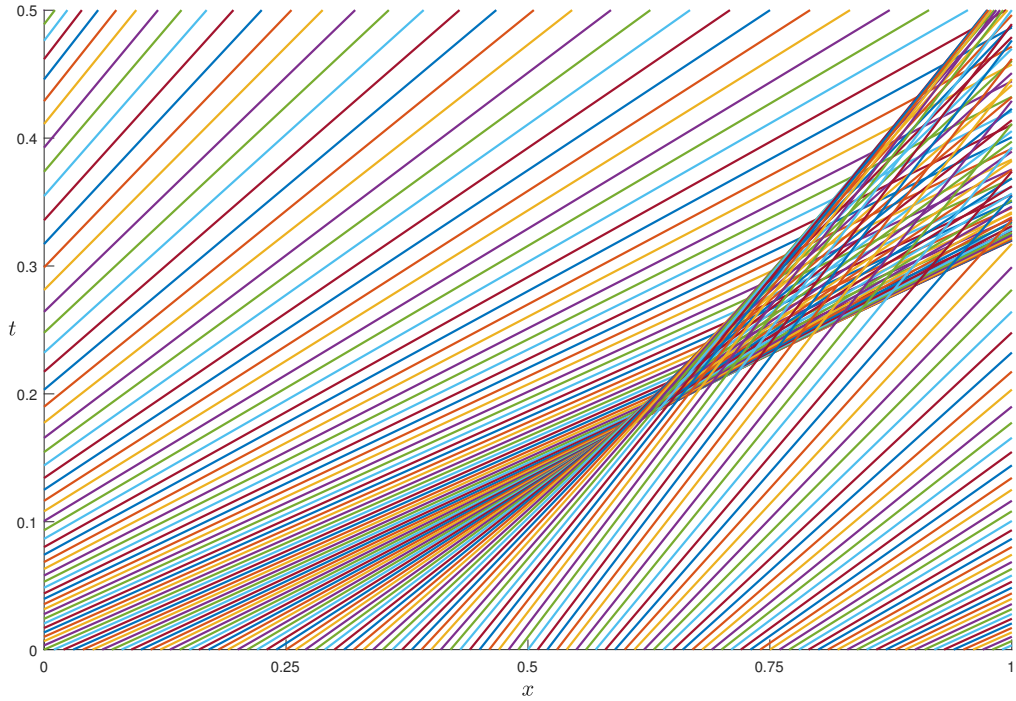

Figure 3.1: Characteristics curves of equation (3.9) corresponding to an initial disturbance given by $h = 1 + \bar{h}\cos(2\pi\tau)$ with $\bar{h} = 1/2$. It can be seen the characteristic curves intersect at about $t_b \approx 1/\left(4\pi\bar{h}\right)$, signalling that a classical solution does not exist.

to the equation under consideration. Letting $(u_0, \theta_0) = (u_{\mathbb{N}}, \theta_{\mathbb{N}})$ in equation (3.14) yields $\mathbb{B}_0 = 0$; the perturbative expansions for the fluid velocity and temperature – equation (3.13) – must therefore correspond to the expressions for (u_n, θ_n) which yield $\mathbb{B}_n = 0$ $\forall n$. In this way, the governing equations are satisfied even when $\epsilon > 0$ because the perturbative expansions guarantee the coefficients of ϵ^n will vanish in equation (3.14).

Ergo, extension of the perturbation series to higher-order relies upon solving a set of recursive equations defined by $\mathbb{B}_n = 0$ for $0 \leq n \leq N$. To reiterate, equations (3.5 – 3.6) correspond to $\mathbb{B}_0 = 0$ and so $(u_0, \theta_0) = (u_{\mathbb{N}}, \theta_{\mathbb{N}})$ with the latter given by equations (3.7). The next set of equations are the first-order contributions, $\mathbb{B}_1 = 0$; which read:

$$\frac{\partial^2 u_1}{\partial \hat{z}^2} = Re\left[\frac{\partial u_0}{\partial t} + u_0\frac{\partial u_0}{\partial x} + w_1\frac{\partial u_0}{\partial \hat{z}}\right] + 2\frac{\partial f}{\partial x}\cot\beta - \frac{\partial^2}{\partial x^2}\left[\frac{(1 - Ma\vartheta_0)}{\epsilon^{-2}Ca}\frac{\frac{\partial f}{\partial x}}{\sqrt{1+\epsilon^2 g}}\right], \quad (3.15)$$

$$\left.\frac{\partial u_1}{\partial \hat{z}}\right|_{\hat{z}=h} = -\frac{\frac{Ma}{Ca}\frac{\partial \vartheta_0}{\partial x}}{[1+\epsilon^2 g]^{3/2}}, \qquad u|_{\hat{z}=0} = 0, \quad (3.16)$$

$$\frac{\partial^2 \theta_1}{\partial \hat{z}^2} = RePr\left[\frac{\partial \theta_0}{\partial t} + u_0\frac{\partial \theta_0}{\partial x} + w_1\frac{\partial \theta_0}{\partial \hat{z}}\right], \qquad \left.\frac{\partial \theta_1}{\partial \hat{z}}\right|_{\hat{z}=h} = -\frac{Bi\vartheta_1}{\sqrt{1+\epsilon^2 g}}, \qquad \theta_1|_{\hat{z}=0} = 0, \quad (3.17)$$

where $w_{n+1} = -\int_0^{\hat{z}} (\partial u_n/\partial x)\, d\hat{z}$ and $\vartheta_n = \theta_n|_{\hat{z}=h}$. The effect of surface curvature is assumed to be of order unity in equations (3.15 – 3.17) – as it was in equations (3.7); one could expand these non-linear terms using Newton's generalised binomial theorem, however, Section 3.4 explains why expanding the fluid velocity and temperature *w.r.t.* ϵ is a flawed approach to modelling film flow and so expanding the surface curvature terms *w.r.t.* powers of ϵ is in fact unnecessary. Following Gjevik [1970a], the term describing the Laplace pressure along the free-surface has been brought ahead of its formal order in equation (3.15) on the account that letting the length scale, L_0, equal the capillary length along the surface of a laminar film, namely $L_c = \sqrt{\sigma_0/\rho\bar{g}\sin\beta}$, leads to $Ca = \epsilon^2/2$; this indicates that surface tension will likely play a key role in the film dynamics whenever the free-surface becomes curved, $\partial f/\partial x \neq 0$, therefore, it is appropriate to include its effect in the perturbation expansion at the earliest convenience.

With expressions for (u_0, θ_0) given by equations (3.7), closed-form solutions to (u_1, θ_1) are readily obtained from equations (3.15 – 3.17), these read:

$$\begin{aligned} u_1 = &-\frac{Re}{3}\left(\frac{\partial h}{\partial t}\left(3h^2 - \hat{z}^2\right) + \frac{h}{2}\frac{\partial h}{\partial x}\left(4h^3 - \hat{z}^3\right)\right)\hat{z} - \frac{Ma}{Ca}\frac{\frac{\partial \vartheta_0}{\partial x}}{\left[1+\epsilon^2 g\right]^{3/2}}\hat{z} \\ &-\left(\frac{\partial f}{\partial x}\cot\beta - \frac{1}{2}\frac{\partial^2}{\partial x^2}\left[\frac{(1 - Ma\vartheta_0)}{\epsilon^{-2}Ca}\frac{\frac{\partial f}{\partial x}}{\sqrt{1+\epsilon^2 g}}\right]\right)\hat{z}\left(2h - \hat{z}\right), \end{aligned} \tag{3.18}$$

$$\begin{aligned} \theta_1 = -\frac{\epsilon RePr}{2}\Bigg(&\frac{\left(3 - 2Bih\vartheta_0 - \frac{\hat{z}^2}{h^2}\right)}{3}\left(h\frac{\partial \vartheta_0}{\partial t} - (\vartheta_0 - 1)\frac{\partial h}{\partial t}\right) \\ &+\frac{\left(25 - 18Bih\vartheta_0 - 10\frac{\hat{z}^3}{h^3} + 3\frac{\hat{z}^4}{h^4}\right)h^3}{30}\frac{\partial \vartheta_0}{\partial x} \\ &-\frac{(\vartheta_0 - 1)\left(15 - 11Bih\vartheta_0 - 5\frac{\hat{z}^3}{h^3} + \frac{\hat{z}^4}{h^4}\right)h^2}{10}\frac{\partial h}{\partial x}\Bigg)\hat{z}, \end{aligned} \tag{3.19}$$

in which $\vartheta_0 = 1\big/\left(1 + Bih/\sqrt{1+\epsilon^2 g}\right)$, and the temporal derivative of $h(x,t)$ has been approximated to first-order in the long-wave expansion by re-arranging the integral form of the kinematic condition – equation (2.36) – and substituting in the leading-order flow rate – equation (3.8) – to obtain $\partial h/\partial t = -\partial q_0/\partial x + \mathcal{O}(\epsilon) = -2h^2\partial h/\partial x + \mathcal{O}(\epsilon)$. Whilst the error associated with approximating $\partial h/\partial t$ in this way is of first-order, $\sim \mathcal{O}(\epsilon)$, the overall error incurred is only of second-order, $\sim \mathcal{O}\left(\epsilon^2\right)$, because the temporal derivative of $h(x,t)$ is a first-order term and so its first-order error is of second-order *w.r.t.* the long-wave expansion.

Substituting u_1 from equation (3.18) into the definition of the flow rate – equation (2.35) – yields the first-order contribution to the flow rate in terms of the film thickness; simplifying through $\partial h/\partial t = -2h^2\partial h/\partial x$, the substitution yields:

$$q_1 = \frac{h^3}{3}\frac{\partial^2}{\partial x^2}\left[\frac{\frac{(1-Ma\vartheta_0)}{\epsilon^{-2}Ca}\frac{\partial f}{\partial x}}{\sqrt{1+\epsilon^2 g}}\right] - \frac{2h^3}{3}\frac{\partial f}{\partial x}\cot\beta + Re\frac{8h^6}{15}\frac{\partial h}{\partial x} - \frac{\frac{Ma}{Ca}\frac{h^2}{2}\frac{\partial \vartheta_0}{\partial x}}{\left[1+\epsilon^2 g\right]^{3/2}}, \tag{3.20}$$

A first-order equation describing the evolution of the film is recovered by substituting the flow rate contributions $q = q_0 + \epsilon q_1$ into the *integral form of the kinematic condition* – equation (2.36); this leads to the following mathematical model:

$$\frac{\partial h}{\partial t} + \frac{\partial}{\partial x}\left[\left(1 - \epsilon\frac{\partial f}{\partial x}\cot\beta + \frac{1}{2}\epsilon\frac{\partial^2}{\partial x^2}\left[\frac{(1-Ma\vartheta_0)}{\epsilon^{-2}Ca}\frac{\frac{\partial f}{\partial x}}{\sqrt{1+\epsilon^2 g}}\right]\right)\frac{2h^3}{3} + \epsilon Re\frac{8h^6}{15}\frac{\partial h}{\partial x} - \epsilon\frac{\frac{Ma}{Ca}\frac{h^2}{2}\frac{\partial \vartheta_0}{\partial x}}{\left[1+\epsilon^2 g\right]^{3/2}}\right] + \mathcal{O}\left(\epsilon^2\right) = 0, \tag{3.21}$$

where $\vartheta_0 = 1\big/\left(1 + Bih/\sqrt{1+\epsilon^2 g}\right)$, and $\mathcal{O}\left(\epsilon^2\right)$ denotes the order of the expected error. Equation (3.21) is called the Benney equation (BE) to first-order in homage to Benney [1966a] who initiated this approach, however, it was Gjevik [1970a] who first included the capillary pressure term ahead of its formal order by assuming a scaling of $Ca \sim \mathcal{O}\left(\epsilon^2\right)$ – justified above – and was therefore the first to derive it in its current form; some of the solutions to equation (3.21) are scrutinised in later Chapters.

3.3.4 Regularised Benney equation

Fully non-linear analysis of the Benney equation (3.21) undertaken by Pumir et al. [1983] found "the numerical results lose any connection with the partial differential equation" when the initial disturbance amplitude is too large or when the Reynolds number (Re) is greater than a certain value which is related to the critical value above which single-hump solitary waves cease to exist. In either case, periodic solutions to equation (3.21) remain finite but are characterised by large derivatives which are in contradiction to the long-wave expansion and lead to significant variation between each spatial step and cause the film thickness $h(x,t)$ to reach zero somewhere along the domain [Pumir et al., 1983]; through analysis of Lyapunov numbers Pumir et al. [1983] showed that this is not due to turbulence, and that increasing the resolution of the numerical scheme has no effect on this phenomenon, signalling that this catastrophic behaviour is thereby a property of equation (3.21). Numerical analysis of the full Navier-Stokes equations by Salamon et al. [1994] using the finite element method confirmed that the numerical results to the Benney equation diverge from the true Navier-Stokes solution when the amplitude of surface disturbances is sufficiently large and that this convergence problem is not overcome by extending the expansion to second-order, $\sim \mathcal{O}\left(\epsilon^2\right)$. Howbeit, the catastrophic behaviour associated with the divergence of equation (3.21) may be avoided through use of a regularisation procedure; the resulting regularised Benney equation

behaves in a plausible beyond the point of criticality, however, it is only qualitatively accurate with the Navier-Stokes solution [Takeshi, 1999]. The regularisation procedure is known as the Padé approximation and it gives the best rationale approximation of a function at any given order [Baker and Graves-Morris, 1996].

In the perturbation approach, the flow dynamics are described by a power series expansion of the flow rate with respect to the shallowness parameter, $q = q_0 + \epsilon q_1 + \epsilon^2 q_2 + ...$, which has a radius of convergence about $\epsilon = 0$. Unfortunately, as discussed above, this power series is known to diverge in finite-time simulations once the Reynolds number surpasses a critical value as the derivatives of the film thickness become unacceptably large which causes the film thickness to reach zero somewhere along the domain [Pumir et al., 1983]. The Padé approximation improves the radius of convergence by recasting the power series as a ratio of two polynomials; which will be represented presently by:

$$q = \hat{L}^{-1} r = \left(\hat{L}_0 + \epsilon \hat{L}_1 + ... + \epsilon^m \hat{L}_m \right)^{-1} \left(r_0 + \epsilon r_1 + ... + \epsilon^n r_n \right), \tag{3.22}$$

where r and $\hat{L}$ are referred to as the regularised flow rate and regularisation operator, respectively (this choice of naming will become clear in time).

The core idea behind the Padé approximant is that if a function has a pole (or a zero) at a particular point then approximating the function as a rational function allows the singularity (or its reciprocal) to be well-represented at that particular point; this is not the case if the function is approximated as a power series expansion [Baker and Graves-Morris, 1996]. The aforementioned issue with the perturbation approach is that, at a finite value of ϵ, equation (3.21) returns a solution to $h(x,t)$ which possesses a zero, $h \to 0$, and this behaviour is not observed in the corresponding solution to the full Navier-Stokes equations [Pumir et al., 1983, Salamon et al., 1994]; ergo, the catastrophic behaviour is a property of the Benney equation and not of the physical system. With this in mind, the application of the Padé approximation to the Benney equation (3.21) is not about correctly modelling the zero (or pole) but rather about eliminating it from the perturbative expansion. This is the rationale of equation (3.22) in which the zero associated with the flow rate expansion of q will be eliminated by ensuring there is a pole associated with $\hat{L}$, i.e. $\hat{L} \to \infty$ as $q \to 0$; this means the power series of r will be a well-behaved expansion which possesses no zeros or poles, and that a model based upon the power series of r will not suffer from the same catastrophic behaviour which plagues the Benney equation. An expression for the expansion of r is easily found through $r = \hat{L} q$ and, as already mentioned, this allows for the catastrophic behaviour of the Benney equation to be circumnavigated by basing the derivation of the evolution equation for the film thickness upon the expansion of the regularised flow rate, $r = r_0 + \epsilon r_1 + ...$, which does not possess any zeros or poles. Put more simply, the idea if for $\hat{L}$ to act as an operator which maps the power series expansion of q onto the regularised flow rate r in such a way that the latter does not exhibit any singular behaviour because the singularity in $\hat{L}$ cancels with the zero in q. The first step is to assign an appropriate form to the regularisation operator, $\hat{L}$; on the account that the long-wave expansion

is essentially a power series with respect to the streamwise differential operator, $\partial/\partial x$, Takeshi [1999] proposed $\hat{L}$ should take the form:

$$\hat{L} = 1 + \epsilon A^{(1)} \frac{\partial}{\partial x} + \epsilon^2 A^{(2)} \frac{\partial^2}{\partial x^2} + ... + \epsilon^m A^{(m)} \frac{\partial^m}{\partial x^m}, \tag{3.23}$$

in which $A^{(m)}$ are unknown coefficients which may depend on $h(x,t)$ but which must be independent of ϵ and so cannot contain the spatial derivatives of any quantities. Since the coefficients $A^{(m)}$ may vary with (x,t), this means the present technique is not strictly a Padé approximation but nevertheless follows the same principle.

With the form of $\hat{L}$ given by equation (3.23), it is clear $r_0 = q_0$ by design and that the other contributions to the regularised flow rate can be found through:

$$r_n = q_n + \sum_{m=1}^{n} A^{(m)} \frac{\partial^m q_{n-m}}{\partial x^m}, \qquad n \geq 1. \tag{3.24}$$

Following Takeshi [1999], the power series expansion of the regularised flow rate is only sought to first-order, $r = r_0 + \epsilon r_1 = q_0 + \epsilon r_1$; there is in fact little purpose to seeking a higher-order expansion because the singularity in the Benney equation is not a pole (or zero) [Takeshi, 1999]. The regularisation procedure relies upon the singularity being a pole (or zero) because then its reciprocal is a zero (or pole) and can be used to cancel out the singularity [Conway, 1978]; if the singlarity is not a pole (or zero), the it can only ever be partially cancelled out by regularisation [Conway, 1995] which means extending the regularised formulation to higher-order does not yield any additional benefits. The first-order regularised flow rate contribution, r_1, can be determined by considering the first two conditions given by equation (3.24) with $r_n = 0$ for $n \geq 2$; namely:

$$r_1 = q_1 + A^{(1)} \frac{\partial q_0}{\partial x}, \qquad 0 = q_2 + A^{(1)} \frac{\partial q_1}{\partial x} + A^{(2)} \frac{\partial^2 q_0}{\partial x^2}, \tag{3.25}$$

Higher-order contributions to the flow rate (q_n) are found by extending the perturbation series to higher-order – see section (3.3.3). This makes $A^{(1)}$ and $A^{(2)}$ the unknown quantities and the task is to find expressions for these quantities which satisfy equation $(3.25b)$; the resulting expression for $A^{(1)}$ can then be used to compute r_1. In order to make analytical progress whilst keeping $A^{(m)}$ independent of ϵ, it is necessary to discard all nonlinear differential terms in equation $(3.25b)$ along with the substrate gradient.

According to the perturbation series – see section (3.3.3); q_2 is given by:

$$
\begin{aligned}
q_2 = &\left[\frac{1016}{315}\left(\frac{\partial h}{\partial x}\right)^2 + \frac{32h}{63}\frac{\partial^2 h}{\partial x^2}\right] Re^2 h^9 - \frac{h^3}{3}\frac{\partial^2}{\partial x^2}\left[\frac{\frac{Ma\vartheta_1}{\epsilon^{-2}Ca}\frac{\partial f}{\partial x}}{\sqrt{1+\epsilon^2 g}}\right] \\
&- \left[\frac{32}{15}\left(\frac{\partial h}{\partial x}\right)^2 + \frac{16}{15}\frac{\partial h}{\partial x}\frac{ds}{dx} + \frac{40h}{63}\frac{\partial^2 h}{\partial x^2} + \frac{32h}{315}\frac{d^2 s}{dx^2}\right] Reh^6 \cot\beta \\
&+ \left[\frac{8h^2}{15}\frac{\partial h}{\partial x}\frac{\partial^2}{\partial x^2}\left[\frac{(1-Ma\vartheta_0)}{\epsilon^{-2}Ca}\frac{\frac{\partial f}{\partial x}}{\sqrt{1+\epsilon^2 g}}\right] + \frac{16h^3}{315}\frac{\partial^3}{\partial x^3}\left[\frac{(1-Ma\vartheta_0)}{\epsilon^{-2}Ca}\frac{\frac{\partial f}{\partial x}}{\sqrt{1+\epsilon^2 g}}\right]\right. \\
&- \frac{2h}{15}\frac{\partial^3}{\partial x^2 \partial t}\left[\frac{(1-Ma\vartheta_0)}{\epsilon^{-2}Ca}\frac{\frac{\partial f}{\partial x}}{\sqrt{1+\epsilon^2 g}}\right] - \frac{4h}{15}\frac{\partial h}{\partial x}\frac{\frac{Ma}{Ca}\frac{\partial \vartheta_0}{\partial x}}{\sqrt{1+\epsilon^2 g}\,[1-\epsilon^2 g]} \\
&\left.+ \frac{5}{24}\frac{\partial}{\partial t}\left[\frac{\frac{Ma}{Ca}\frac{\partial \vartheta_0}{\partial x}}{\sqrt{1+\epsilon^2 g}\,[1-\epsilon^2 g]}\right] - \frac{7h^2}{120}\frac{\partial}{\partial x}\left[\frac{\frac{Ma}{Ca}\frac{\partial \vartheta_0}{\partial x}}{\sqrt{1+\epsilon^2 g}\,[1-\epsilon^2 g]}\right]\right] Reh^4 \\
&+ \left[\frac{2\frac{\partial f}{\partial x}\frac{\partial}{\partial x}\left(h^2\right)}{(1+\epsilon^2 g)} + \frac{\left(1+\epsilon^2 g\right)}{(1-\epsilon^2 g)}\frac{\left[\frac{2}{3}\frac{\partial^2}{\partial x^2}\left(h^3\right) - h^2\frac{\partial^2 f}{\partial x^2}\right]}{(1+\epsilon^2 g)} - \frac{\frac{Ma}{Ca}\frac{\partial \vartheta_1}{\partial x}}{\left[1+\epsilon^2 g\right]^{3/2}}\right]\frac{h^2}{2} \\
&+ \frac{2}{3}h^3\left[\left(\frac{\partial h}{\partial x}\right)^2 - 4\frac{\partial h}{\partial x}\frac{ds}{dx} - 2\left(\frac{ds}{dx}\right)^2\right] + \frac{h^4}{2}\left[3\frac{\partial^2 h}{\partial x^2} - \frac{d^2 s}{dx^2}\right], \\
\approx &\left(2h^4 + \frac{8Reh^7\left(4Reh^3 - 5\cot\beta\right)}{63} + \frac{19}{40}\frac{MaReBi}{Ca}h^6\vartheta_0^2\right)\frac{\partial^2 h}{\partial x^2} \\
&- \frac{h^3}{3}\frac{Ma\vartheta_1}{\epsilon^{-2}Ca}\frac{\partial^3 h}{\partial x^3} + \frac{20h^7}{63}\frac{(1-Ma\vartheta_0)}{\epsilon^{-2}Ca}\frac{\partial^4 h}{\partial x^4} - \frac{h^2}{2}\frac{Ma}{Ca}\frac{\partial \vartheta_1}{\partial x},
\end{aligned}
\tag{3.26}
$$

which contains ϑ_1; the first-order correction to the free-surface temperature is given by:

$$
\begin{aligned}
\vartheta_1 &= \frac{RePrh\left(Bih\vartheta_0 - 1\right)\left(20\left(h\frac{\partial \vartheta_0}{\partial t} - \left(\vartheta_0 - 1\right)\frac{\partial h}{\partial t}\right) + 18h^3\frac{\partial \vartheta_0}{\partial x} - 33h^2\left(\vartheta_0 - 1\right)\frac{\partial h}{\partial x}\right)}{60} \\
&\approx \frac{RePrh^3\left(Bih\vartheta_0 - 1\right)\left(22Bih\vartheta_0^2 + 7\vartheta_0 - 7\right)}{60}\frac{\partial h}{\partial x}.
\end{aligned}
\tag{3.27}
$$

With the expansion of the flow rate given by equations (3.8, 3.20, 3.26), it is possible to find $\{A^{(1)}, A^{(2)}\}$ which satisfy the linearised forms of equations (3.25) – noting that r_1 is still unknown. Presently, the first two regularisation coefficients are defined like so:

$$
A^{(1)} = -\frac{20}{21}Reh^4, \tag{3.28}
$$

$$
A^{(2)} = -h^2 + \frac{ReBih^4\vartheta_0^2}{1680}\frac{Ma}{Ca} + \frac{RePrh^3}{240}\frac{Ma}{Ca}\left(22Bih\vartheta_0^2 + 7\vartheta_0 - 7\right)\left(Bih\vartheta_0 - 1\right), \tag{3.29}
$$

however, it is important to note that equations (3.29) are not unique because $\{A^{(1)}, A^{(2)}\}$ can be defined differently and still satisfy the linearised forms of equations (3.25) [Takeshi, 1999]. The present choice of $\{A^{(1)}, A^{(2)}\}$ leads to the following first-order contribution to the regularised flow rate; namely:

$$r_1 = \frac{h^3}{3}\frac{\partial^2}{\partial x^2}\left[\frac{\frac{(1-Ma\vartheta_0)}{\epsilon^{-2}Ca}\frac{\partial f}{\partial x}}{\sqrt{1+\epsilon^2 g}}\right] - \frac{2h^3}{3}\frac{\partial f}{\partial x}\cot\beta - Re\frac{48h^6}{35}\frac{\partial h}{\partial x} - \frac{\frac{Ma}{Ca}\frac{h^2}{2}\frac{\partial \vartheta_0}{\partial x}}{\sqrt{1+\epsilon^2 g}\left[1-\epsilon^2 g\right]}. \tag{3.30}$$

As stated above, the suspicion is that the flow rate expansion contains a singularity, however, mapping the flow rate expansion onto the regularised flow rate expansion, through the operator $\hat{L}$, allows for this singularity can be cancelled out by its reciprocal. Ergo, to derive an evolution equation for the film thickness based on the regularised flow rate, one simply applies the regularisation operator, $\hat{L} = 1 + \epsilon A^{(1)}\partial/\partial x + \epsilon^2 A^{(2)}\partial^2/\partial x^2$, to the kinematic condition – equation (2.36) – like so:

$$\hat{L}\left[\frac{\partial h}{\partial t} + \frac{\partial q}{\partial x}\right] = \frac{\partial h}{\partial t} + \epsilon\frac{\partial}{\partial x}\left[A^{(1)}\frac{\partial h}{\partial t}\right] + \epsilon^2\frac{\partial}{\partial x}\left[A^{(2)}\frac{\partial^2 h}{\partial x \partial t}\right] + \frac{\partial r}{\partial x} = 0. \tag{3.31}$$

Accordingly, the regularised Benney equation (RBE) at first-order is given by:

$$\begin{aligned}
&\frac{\partial h}{\partial t} - \epsilon\frac{4Re}{21}\frac{\partial^2}{\partial x \partial t}\left[h^5\right] - \epsilon^2\frac{\partial}{\partial x}\left[h^2\frac{\partial^2 h}{\partial x \partial t}\right] + \epsilon^2\frac{ReBi}{1680}\frac{Ma}{Ca}\frac{\partial}{\partial x}\left[h^4\vartheta_0^2\frac{\partial^2 h}{\partial x \partial t}\right] \\
&\quad + \epsilon^2\frac{RePr}{240}\frac{Ma}{Ca}\frac{\partial}{\partial x}\left[h^3\left(22Bih\vartheta_0^2 + 7\vartheta_0 - 7\right)\left(Bih\vartheta_0 - 1\right)\frac{\partial^2 h}{\partial x \partial t}\right] \\
&\quad + \frac{\partial}{\partial x}\left[\left(1 - \epsilon\frac{\partial f}{\partial x}\cot\beta + \frac{1}{2}\epsilon^3\frac{\partial^2}{\partial x^2}\left[\frac{(1-Ma\vartheta_0)}{Ca}\frac{\frac{\partial f}{\partial x}}{\sqrt{1+\epsilon^2 g}}\right]\right)\frac{2h^3}{3}\right. \\
&\quad \left. - \epsilon Re\frac{48h^6}{35}\frac{\partial h}{\partial x} - \epsilon\frac{Ma}{Ca}\frac{\frac{h^2}{2}\frac{\partial \vartheta_0}{\partial x}}{\left[1+\epsilon^2 g\right]^{3/2}}\right] + \mathcal{O}\left(\epsilon^2\right) = 0.
\end{aligned} \tag{3.32}$$

The regularisation procedure will be tested by comparing equation (3.32) with the original Benney equation (3.21).

3.4 Power Series Method

The second asymptotic modelling considered is that of Ruyer-Quil and Manneville [2000]. An alternative approach to modelling gravity-driven film flow is necessitated by the poor performance of the Benney-style models obtained from a perturbation expansion of the full equation set (2.23 – 2.31) with respect to ϵ – see section 3.3. This poor performance is due to the fact that making the coefficients of ϵ^n vanish from all the governing equations and boundary conditions except the kinematic condition is not just overly stringent but actually inconsistent; indeed, this can be proved through *reductio ad absurdum.*

Consider how the perturbation approach expands the fluid velocity and temperature as a power series with respect to the shallowness parameter, namely:

$$(u, \theta) = (u_0, \theta_0) + \epsilon\,(u_1, \theta_1) + \epsilon^2\,(u_2, \theta_2) + \ldots \tag{3.33}$$

The above expansion can only be performed on the grounds that the nth-order components of the velocity and temperature are independent of the expansion parameter, which is to say $u_n \neq u_n(\epsilon)$ and $\theta_n \neq \theta_n(\epsilon)$. Instead, computing the perturbative expansions finds the nth-order components to be functions of the film thickness, $u_n = u_n(h)$ and $\theta_n = \theta_n(h)$, and substituting these expansions into the kinematic condition – equation (2.36) – yields an evolution equation for the thickness of the film – equation (3.21). However, the solution to the evolution equation depends upon the shallowness parameter which means the film thickness is a function of ϵ; herein lies the contradiction, the perturbative expansions lead to $u_n = u_n(h) = u_n(\epsilon)$ and $\theta_n = \theta_n(h) = \theta_n(\epsilon)$ but the original expansion was performed on the premise that $u_n \neq u_n(\epsilon)$ and $\theta_n \neq \theta_n(\epsilon)$. Ergo, the perturbative approach to modelling film flow is shown to be inconsistent.

The inconsistency of basing the perturbation series on the parameter ϵ thereby warrants a different approach to modelling gravity-driven film flow. Since expanding the fluid velocity and temperature as power series with respect to ϵ is unsound, it is necessary to let a different variable serve as the formal expansion parameter. The rationale of the long-wave expansion is that gradients are small in the x-direction and with respect to time – see section 3.2; this implies the gradients in the $\hat{z}$-direction are large by comparison. Furthermore, equations (3.7), which were derived on the assumption of the (x, t)-derivatives belonging to the flow velocity and fluid temperature being negligible, *i.e.* $\epsilon = 0$, show that $\hat{z}$-derivatives exist even when (x, t)-derivatives do not – as differentiating equations (3.7) *w.r.t.* $\hat{z}$ shows that $\partial/\partial\hat{z}\,(u, \theta) > 0$ provided that $(h, \vartheta) > 0$. On this account, it is justifiable to expand the fluid velocity and temperature as power series with respect to the reduced vertical coordinate like so:

$$(u, \theta) = (a_0, b_0) + (a_1, b_1)\,\hat{z} + (a_2, b_2)\,\hat{z}^2 + \ldots \tag{3.34}$$

where $\{a_j, b_j\}$ represent unknown expansion coefficients which are functions of (x, t).

Equation (3.34) is equivalent to expanding (u, θ) as power series with respect to the vertical coordinate z and centring the expansions about the substrate location $s(x)$; in any event, the key assumption of equation (3.34) is that the fluid velocity and temperature are both infinitely differentiable functions with respect to the vertical coordinate.

Substituting expansions (3.34) into the x-momentum (2.24) and energy (2.26) equations converts each into a sum of the powers of $\hat{z}$; represented mathematically by:

$$\mathbb{M}_0(x,t) + \mathbb{M}_1(x,t)\hat{z} + \mathbb{M}_2(x,t)\hat{z}^2 + ... = 0, \tag{3.35}$$

$$\mathbb{E}_0(x,t) + \mathbb{E}_1(x,t)\hat{z} + \mathbb{E}_2(x,t)\hat{z}^2 + ... = 0, \tag{3.36}$$

in which $\{\mathbb{M}_i, \mathbb{E}_i\}$ are referred to as the momentum and energy residuals, respectively, and depend upon $\{a_j, b_j\}$. Despite having expanded the fluid velocity and temperature with respect to the reduced vertical coordinate $\hat{z}$, satisfying equations (3.35 – 3.36) relies upon analysing the (x,t)-dependence of the residuals, $\{\mathbb{M}_i, \mathbb{E}_i\}$. This is because the governing equations (2.24, 2.26) need to be satisfied across the domain of $\hat{z} \in [0, h]$; therefore, equations (3.35 – 3.36) must equate to zero for any arbitrary value of $\hat{z}$ and this can only be guaranteed by having the residuals vanish, $\mathbb{M}_i = \mathbb{E}_i = 0 \ \forall i$. In other words, the monomials of $\hat{z}$ form the mathematical basis upon which a solution is sought and $\{\mathbb{M}_i, \mathbb{E}_i\}$ represent the linearly independent components of the governing equations which must be self-cancelling. A solution is then recovered by finding the $\{a_j, b_j\}$ which satisfy the residual conditions, $\mathbb{M}_i = \mathbb{E}_i = 0 \ \forall i$, subject to the boundary conditions (2.27, 2.36, 2.41 – 2.42); a reduction in dimensionality is achieved because the residual equations and boundary conditions are all purely functions of (x,t).

This technique is called the power series method to solving differential equations. It is most commonly used to solve linear ordinary differential equations and frequently the differential equation in question can only be solved approximately as a truncation of the power series is necessary to limit the number of residual equations to a finite, manageable amount. The added difficulty of applying the method to a nonlinear differential system – equations (2.24, 2.26) – is that whilst all of the resulting residual equations are independent of the vertical coordinate, they are still nonlinear partial differential equation with respect to (x,t). With this in mind, the objective of the present modelling approach is not to solve the governing equations via a power series, only to reduce the dimensionality of the problem, via a truncated power series, in order to arrive at a set of asymptotically equivalent equations which are independent of the vertical coordinate.

3.4.1 The Tau method

Equations (2.24, 2.26) are assumed to be infinitely differentiable and so a truncation of the power series is necessary to restrict the number of degrees of freedom to a finite, manageable amount. In this way, one can view the modelling approach of Ruyer-Quil and Manneville [2000] as a derivative of the Tau method proposed by Lanczos [1938]. Lanczos noted that approximating the solution to a differential equation through a

truncated series is equivalent to solving exactly a perturbed form of the same differential equation. It is a more robust method of approximation because the perturbations which allow the series solution to satisfy the differential system exactly double as an error measurement on the approximation. For this reason, it is advantageous to follow the Tau method and then simplify to the approach of Ruyer-Quil and Manneville [2000].

For the sake of coherence, the full equation set is re-stated before proceeding forward. With the fluid pressure given by equation (2.40); equations (2.24 – 2.26) become:

$$\begin{aligned}\frac{\partial^2 u}{\partial \hat{z}^2} =& -2\left(1-\epsilon\frac{\partial f}{\partial x}\cot\beta\right)+\epsilon Re\left(\frac{\partial u}{\partial t}+u\frac{\partial u}{\partial x}+w\frac{\partial u}{\partial \hat{z}}\right)-2\epsilon^2\frac{\partial^2 u}{\partial x^2}-\epsilon^2\frac{\partial^2}{\partial x^2}\Big[\,u|_{\hat{z}=h}\,\Big] \\ &+\epsilon^3 Re\frac{\partial}{\partial x}\int_{\hat{z}}^{h}\left(\frac{\partial w}{\partial t}+u\frac{\partial w}{\partial x}+w\frac{\partial w}{\partial \hat{z}}\right)d\hat{z}-\epsilon^3\frac{\partial^2}{\partial x^2}\left[\frac{\frac{(1-Ma\vartheta)}{Ca}\frac{\partial f}{\partial x}}{\sqrt{1+\epsilon^2 g}}\right]-\epsilon^4\frac{\partial^2}{\partial x^2}\int_{\hat{z}}^{h}\frac{\partial w}{\partial x}\,d\hat{z},\end{aligned} \tag{3.37}$$

$$\frac{\partial^2\theta}{\partial \hat{z}^2} =\epsilon RePr\left(\frac{\partial\theta}{\partial t}+u\frac{\partial\theta}{\partial x}+w\frac{\partial\theta}{\partial \hat{z}}\right)-\epsilon^2\frac{\partial^2\theta}{\partial x^2}. \tag{3.38}$$

in which the vertical flow velocity is given by $w = -\int_0^{\hat{z}}(\partial u/\partial x)\,d\hat{z}$.

Equations (3.37 – 3.38) are subject to the following boundary conditions:

$$u|_{\hat{z}=0} = 0, \qquad \theta|_{\hat{z}=0} = 1, \tag{3.39}$$

$$\left.\frac{\partial u}{\partial \hat{z}}\right|_{\hat{z}=h} = \frac{2\epsilon^2\frac{\partial f}{\partial x}\frac{\partial}{\partial x}\left(u|_{\hat{z}=h}\right)}{(1+\epsilon^2 g)}+\frac{\left(1-\epsilon^2 g\right)}{(1+\epsilon^2 g)}\frac{\epsilon^2\left[\frac{\partial^2 q}{\partial x^2}-u|_{\hat{z}=h}\frac{\partial^2 f}{\partial x^2}\right]}{(1+\epsilon^2 g)}-\frac{\epsilon\frac{Ma}{Ca}\frac{\partial\vartheta}{\partial x}}{\left[1+\epsilon^2 g\right]^{3/2}}, \tag{3.40}$$

$$\left.\frac{\partial\theta}{\partial \hat{z}}\right|_{\hat{z}=h} = \frac{\epsilon^2\frac{\partial f}{\partial x}\frac{\partial\vartheta}{\partial x}}{1+\epsilon^2 g}-\frac{Bi\vartheta}{\sqrt{1+\epsilon^2 g}}, \tag{3.41}$$

$$\frac{\partial h}{\partial t}+\frac{\partial q}{\partial x} = 0, \tag{3.42}$$

which contain the stream-wise flow rate, $q = \int_0^h (u)\,d\hat{z}$, the free-surface velocity, $u|_{\hat{z}=h}$, the free-surface temperature, $\vartheta = \theta|_{\hat{z}=h}$, and the surface curvature pre-factor, $g = (\partial f/\partial x)^2$.

The power series method relies upon gradients in the $\hat{z}$-direction being smooth for all finites values of ϵ as this allows for the fluid velocity and temperature to be expanded as power series in $\hat{z}$. Following the Tau method, these power series are truncated at the Nth degree so the residual equations (3.35 – 3.36) permit a closed-form solution; accordingly, the power series are specified by the following finite sums:

$$u = \sum_{j=0}^{N} a_j(x,t)\hat{z}^j, \qquad \theta = \sum_{j=0}^{N} b_j(x,t)\hat{z}^j, \tag{3.43}$$

in which the unknown expansion coefficients $\{a_j, b_j\}$ are functions of (x,t).

The objective of any power series method is to find the expressions for $\{a_j, b_j\}$ which satisfy equations (3.37 – 3.42); these expressions can then be substituted back into expansions (3.43) to find approximate solutions to the fluid velocity and temperature. The expressions for $\{a_0, b_0\}$ are readily found from substituting expansions (3.43) into the substrate boundary conditions (3.39); doing so finds:

$$a_0 = 0, \qquad\qquad b_0 = 1. \tag{3.44}$$

The expressions for $\{a_0, b_0\}$ are unaffected by the degree of truncation, N, which means they can always be given by equations (3.44) – provided there is no alteration to the substrate boundary conditions or a change in the mathematical basis of the approach. Finding the expressions for $\{a_j, b_j\}$ corresponding to $j \geq 1$ is significantly more involved due to the nonlinear behaviour of these expansion coefficients; nevertheless, substituting expansions (3.43) into equations (3.37 – 3.38) and equating the coefficients of $\hat{z}^i$ to zero, $\{\mathbb{M}_i, \mathbb{E}_i\} = 0$ for $1 \leq i \leq N-2$ in equations (3.35 – 3.36), yields a pair of recurrence relations for the expansion coefficients $\{a_j, b_j\}$ corresponding to $3 \leq j \leq N$; namely:

$$a_j = \frac{\mathbb{M}^*_{j-2}\left(\{a_i\}\right)}{|\ell_s|^4 j\,(j-1)}, \qquad\qquad b_j = \frac{\mathbb{E}^*_{j-2}\left(\{a_i, b_i\}\right)}{|\ell_s|^2 j\,(j-1)}, \tag{3.45}$$

in which $i < j$, $\{\mathbb{M}^*_i, \mathbb{E}^*_i\} = \{\mathbb{M}_i, \mathbb{E}_i\} + |\ell_s|^2\,(i+2)\,(i+1)\,\{|\ell_s|^2 a_{i+2}, b_{i+2}\}$ are functions containing the partial derivatives of $\{a_i, b_i\}$ – found in Appendix B; and $|\ell_s| = \sqrt{1+\epsilon^2(ds/dx)^2}$ is the dimensionless length of an infinitesimal segment of the substrate corrugation.

The recurrence relations (3.45) state that, for $j \geq 3$, a_j is a function of $\{a_i\}$ and b_j is a function of $\{a_i, b_i\}$ where $i < j$. This means the expansion coefficients $\{a_j, b_j\}$ corresponding to $3 \leq j \leq N$ can all be expressed entirely in terms of the partial derivatives of $\{a_0, a_1, a_2, b_0, b_1, b_2\}$ by recursively substituting $\{a_i\}$ into a_j and $\{a_i, b_i\}$ into b_j. Of course, $\{a_0, b_0\}$ are given by equations (3.44) and are constant which means their partial derivatives vanish; consequently, $\{a_j, b_j\}$ for $3 \leq j \leq N$ can be expressed purely in terms of the partial derivatives of $\{a_1, a_2, b_1, b_2\}$. The evolutions of $\{a_1, a_2, b_1, b_2\}$ would then be described by the following partial differential equations: (i) the shear stress boundary condition (3.40); (ii) the heat flux boundary condition (3.41); (iii) $\mathbb{M}_0 = 0$ from equation (3.35) which is equivalent to an evaluation of the momentum equation (3.37) at $\hat{z} = 0$; and (iv) $\mathbb{E}_0 = 0$ from equation (3.36) which is equivalent to an evaluation of the energy equation (3.38) at $\hat{z} = 0$. These four equations are coupled to the *integral form of the kinematic condition* – equation (3.42); leading to five partial differential equations in terms of $\{h, a_1, a_2, b_1, b_2\}$. Having said that, because there are no heat sources/sinks inside the film, b_2 can be expressed in terms of b_1 by re-arranging $\mathbb{E}_0 = 0$ like so:

$$b_2 = \epsilon^2 \frac{\frac{\partial b_1}{\partial x}\frac{ds}{dx} + \frac{b_1}{2}\frac{d^2 s}{dx^2}}{|\ell_s|^2}. \tag{3.46}$$

Equation (3.46) additionally demonstrates how the quadratic component of the temperature distribution vanishes when the substrate is flat, *i.e.* $ds/dx = 0$.

Accordingly, the equation set (3.37 – 3.42) is reduced to four partial differential equations in terms of $\{h, a_1, a_2, b_1\}$ which are asymptotically equivalent to the full equation set (2.23 – 2.31)) and can be derived from:

$$\frac{\partial h}{\partial t} + \frac{\partial q}{\partial x} = 0, \tag{3.47}$$

$$\left.\frac{\partial u}{\partial \hat{z}}\right|_{\hat{z}=h} = \frac{2\epsilon^2 \frac{\partial f}{\partial x}\frac{\partial}{\partial x}\left(u|_{\hat{z}=h}\right)}{(1+\epsilon^2 g)} + \frac{\left(1-\epsilon^2 g\right)}{(1+\epsilon^2 g)}\frac{\epsilon^2\left[\frac{\partial^2 q}{\partial x^2} - u|_{\hat{z}=h}\frac{\partial^2 f}{\partial x^2}\right]}{(1+\epsilon^2 g)} - \frac{\epsilon\frac{Ma}{Ca}\frac{\partial \vartheta}{\partial x}}{\left[1+\epsilon^2 g\right]^{3/2}}, \tag{3.48}$$

$$\left.\frac{\partial \theta}{\partial \hat{z}}\right|_{\hat{z}=h} = \frac{\epsilon^2 \frac{\partial f}{\partial x}\frac{\partial \vartheta}{\partial x}}{1+\epsilon^2 g} - \frac{Bi\vartheta}{\sqrt{1+\epsilon^2 g}}, \tag{3.49}$$

$$\begin{aligned}\left.\frac{\partial^2 u}{\partial \hat{z}^2}\right|_{\hat{z}=0} &= -2\left(1-\epsilon\frac{\partial f}{\partial x}\cot\beta\right) - \epsilon^2\frac{\partial^2}{\partial x^2}\left[\,u|_{\hat{z}=h}\,\right] - \epsilon^3\frac{\partial^2}{\partial x^2}\left[\frac{\frac{(1-Ma\vartheta)}{Ca}\frac{\partial f}{\partial x}}{\sqrt{1+\epsilon^2 g}}\right] \\ &\quad - \left[2\epsilon^2\frac{\partial^2 u}{\partial x^2} - \epsilon^3 Re\frac{\partial}{\partial x}\int_{\hat{z}}^{h}\left(\frac{\partial w}{\partial t} + u\frac{\partial w}{\partial x} + w\frac{\partial w}{\partial \hat{z}}\right)d\hat{z} + \epsilon^4\frac{\partial^2}{\partial x^2}\int_{\hat{z}}^{h}\frac{\partial w}{\partial x}\,d\hat{z}\right]\Bigg|_{\hat{z}=0},\end{aligned} \tag{3.50}$$

in which (u, θ) are given by expansions (3.43); the stream-wise flow rate and free-surface temperature are defined by $q = \int_0^h (u)\,d\hat{z}$ and $\vartheta = \theta|_{\hat{z}=h}$, respectively; $\{a_0, b_0\}$ are given by equations (3.44); $\{a_j, b_j\}$ for $j \geq 3$ are eliminated via the recurrence relations (3.45); and b_2 is removed through expression (3.46).

To close off the Tau method, the equation set (3.37 – 3.42) must be perturbed so that the truncated series solutions become exact solutions of the differential system. Only the momentum (3.37) and energy (3.38) equations require perturbation terms because the error associated with the truncated series solution stems directly from the residuals $\{\mathbb{M}_i, \mathbb{E}_i\}$ lying in the range of $N-1 \leq i \leq 2N+2$. These residuals represent the unbounded components of the truncated series solutions because they only receive contributions from the nonlinear terms located on the right hand-sides of equations (3.37 – 3.38). These unbounded residuals can be eliminated by adding identical terms to the left hand-sides of equations (3.37 – 3.38); these added terms are assigned the form of $\tau_i^{\mathbb{M}}\hat{z}^i$ in the momentum equation (3.37) and $\tau_i^{\mathbb{E}}\hat{z}^i$ in the energy equation (3.38). The quantities $\{\tau_i^{\mathbb{M}}, \tau_i^{\mathbb{E}}\}$ are called the tau coefficients and they are given presently by:

$$\tau_j^{\mathbb{M}} = \mathbb{M}_j^*\left(\{a_i\}\right), \qquad \tau_j^{\mathbb{E}} = \mathbb{E}_j^*\left(\{a_i, b_i\}\right), \tag{3.51}$$

for $N-1 \leq j \leq 2N+2$ where $j+2 > i \leq N$ and $\{\mathbb{M}_j^*, \mathbb{E}_j^*\}$ are given in Appendix B.

The magnitude of the tau coefficients measure of the error incurred by the Tau method. On this knowledge, solutions to the asymptotically equivalent formulations of

equations (3.47 – 3.50) are sought on the principle that $\{\tau_j^{\mathbb{M}}, \tau_j^{\mathbb{E}}\}$ are minimised. Ergo, the approximate solutions to the fluid velocity and temperature are good if the values of $\{\tau_j^{\mathbb{M}}, \tau_j^{\mathbb{E}}\}$ are close to zero because then the perturbed equations are not too dissimilar from the original system; however, if any of the values of $\{\tau_j^{\mathbb{M}}, \tau_j^{\mathbb{E}}\}$ are large then the approximation is poor and the degree of truncation (N) must be increased to find a more robust solution.

3.4.2 Reduction of the Tau method to a long-wave expansion

As stated at the start of section 3.4.1, the complexity of the full equation set (3.37 – 3.42) necessitates a truncation of the velocity and temperature power series (3.43); otherwise, the derivation of the asymptotically equivalent equations would involve a infinite number of steps. This leads to the Tau method whose validity is checked through a minimisation of the tau coefficients, whilst this makes the modelling approach robust, it significantly increases the computational cost because the method of solution must minimise the tau coefficients (3.51) in addition to solving the asymptotically equivalent formulations of equations (3.47 – 3.50). This is made worse by the terrible scaling between the degree of truncation (N) and the number of tau coefficients required: for a truncation of degree N, the method of solution must minimise $N+4$ tau coefficients for the velocity and $N+2$ tau coefficients for the temperature. It would therefore be convenient to simplify the Tau method and adopt a modelling approach which has no need of the tau coefficients.

As a matter of fact, simplification of the Tau method in the manner prescribed above is readily forthcoming. Recall that the tau coefficients are a measure of the discrepancy between the approximate and exact solutions to the differential system of interest; in the ideal scenario, all the tau coefficients would be equal to zero and the approximate solution sought via the Tau method would be indistinguishable from the quixotic exact solution of the untarnished differential system. The simplification therefore is to assume the ideal scenario and work backwards from this assumption to find the conditions under which the associated asymptotically equivalent equations constitute a valid description of the film dynamics. From equations (3.51), it is seen the tau coefficients will vanish when:

$$\mathbb{M}_j^* \left(\{a_i\}\right) = 0, \qquad \mathbb{E}_j^* \left(\{a_i, b_i\}\right) = 0, \tag{3.52}$$

where $N - 1 \leq j \leq 2N + 2$, $j + 2 > i \leq N$ and $\{\mathbb{M}_j^*, \mathbb{E}_j^*\}$ are found in Appendix B; consequently, the task turns to finding the conditions under which $\{\mathbb{M}_j^*, \mathbb{E}_j^*\}$ vanish. The expressions for $\{\mathbb{M}_j^*, \mathbb{E}_j^*\}$ in Appendix B correspond to gravity-driven film flow over corrugated substrate; in the case of planar substrate $(ds/dx = 0)$, they simplify to:

$$\mathbb{M}_j^*\left(\{a_i\}\right) = \epsilon Re\left\{\frac{\partial a_j}{\partial t} + \sum_{i=1}^{j-1}\frac{(j-2i+1)}{(j-i+1)}a_i\frac{\partial a_{j-i}}{\partial x}\right\} - \epsilon^2\frac{\partial^2 a_j}{\partial x^2} - \frac{\epsilon^4}{j\,(j-1)}\frac{\partial^4 a_{j-2}}{\partial x^4}$$
$$+ \frac{\epsilon^3 Re}{j\,(j-1)}\left\{\frac{\partial^3 a_{j-2}}{\partial x^2\partial t} + \sum_{i=1}^{j-3}\frac{(j-1)}{(j-i-1)}\left(a_i\frac{\partial^3 a_{j-i-2}}{\partial x^3} - \frac{\partial^2 a_i}{\partial x^2}\frac{\partial a_{j-i-2}}{\partial x}\right)\right\}, \quad (3.53)$$

$$\mathbb{E}_j^*\left(\{a_i, b_i\}\right) = \epsilon RePr\left\{\frac{\partial b_j}{\partial t} + \sum_{i=1}^{j}\left(a_i\frac{\partial b_{j-i}}{\partial x} - \frac{(j-i)}{(i+1)}b_{j-i}\frac{\partial a_i}{\partial x}\right)\right\} - \epsilon^2\frac{\partial^2 b_j}{\partial x^2}, \quad (3.54)$$

where $j \geq 1$; note however, that the vertical inertia ($\epsilon^3 Re$) and vertical viscosity (ϵ^4) terms only appear in equation (3.53) when $j \geq 3$. Equations (3.53 – 3.54) show the functions $\{\mathbb{M}_j^*, \mathbb{E}_j^*\}$ are wholly dependent upon the partial derivatives of $\{a_i, b_i\}$ with respect to (x,t) corresponding to $i \leq j$; this means $\{\mathbb{M}_j^*, \mathbb{E}_j^*\}$ will disappear whenever the partial derivatives which they depend upon are vanishingly small. Which is to say, the asymptotically equivalent equations derived via the Tau method constitute a valid description of the film dynamics when there exists a subset of gradients with respect to time and in the x-direction which are negligible – the size of this subset is inversely proportional to the degree of truncation (N). The strategy to simplifying the Tau method is therefore to identify and pre-emptively eliminate these negligible partial derivatives so that the tau coefficients are met automatically; this can be achieved through a long-wave expansion.

Gravity-driven film flow is well-suited to a long-wave (or gradient) expansion because higher-order derivatives of (u,θ) with respect to (x,t) are often inconsequential to the film dynamics and so it is permissible to neglect such derivatives from the power series expansions of the fluid velocity and temperature – see section 3.2. Substituting equations (3.53 – 3.54) into the recurrence relations (3.45), with $ds/dx = 0$, yields the expressions:

$$a_j = \frac{\epsilon Re\left\{\frac{\partial a_{j-2}}{\partial t} + \sum_{i=1}^{j-3}\frac{(j-2i-1)}{(j-i-1)}a_i\frac{\partial a_{j-i-2}}{\partial x}\right\} - \epsilon^2\frac{\partial^2 a_{j-2}}{\partial x^2}}{j\,(j-1)},$$
$$+ \frac{\epsilon^3 Re\left\{\frac{\partial^3 a_{j-2}}{\partial x^2\partial t} + \sum_{i=1}^{j-5}\frac{(j-3)}{(j-i-3)}\left(a_i\frac{\partial^3 a_{j-i-4}}{\partial x^3} - \frac{\partial^2 a_i}{\partial x^2}\frac{\partial a_{j-i-4}}{\partial x}\right)\right\} - \epsilon^4\frac{\partial^4 a_{j-4}}{\partial x^4}}{j\,(j-1)\,(j-2)\,(j-3)}, \quad (3.55)$$

$$b_j = \frac{\epsilon RePr\left\{\frac{\partial b_{j-2}}{\partial t} + \sum_{i=1}^{j-2}\left(a_i\frac{\partial b_{j-i-2}}{\partial x} - \frac{(j-i-2)}{(i+1)}b_{j-i-2}\frac{\partial a_i}{\partial x}\right)\right\} - \epsilon^2\frac{\partial^2 b_{j-2}}{\partial x^2}}{j\,(j-1)}, \quad (3.56)$$

for $j \geq 3$. Equations (3.55 – 3.56) illustrate how the successive contributions to the velocity and temperature power series depend upon the partial derivatives of the preceding contributions; this means the successive contributions must coincide with the higher-order derivatives of (u,θ) with respect to (x,t) and belong to higher-orders of the long-wave expansion. The tau coefficients can thereby be dispelled by truncating the

fluid velocity and temperature power series (3.43) with respect to the (x,t)-derivatives of (u,θ); in this way, the asymptotically equivalent equations will be valid as long as the neglected higher-order derivatives of (u,θ) remain negligible.

A long-wave expansion of the fluid velocity and temperature is accomplished by expressing the power series (3.43) in terms of $\{a_1,a_2,b_1,b_2\}$; this is because these quantities are all of order unity, and so their nth-order derivatives will be of nth-order in the long-wave expansion. The shallowness parameter ϵ is used to represent the smallness of such derivatives; in this way, ϵ acts as a surrogate expansion parameter and its powers denote the order of any term in the long-wave expansion. The coefficients $\{a_1,a_2,b_1\}$ are said to of order unity because they each remain finite as $\epsilon\to 0$ – see equations (3.7); in contrast, b_2 tends to zero as $\epsilon\to 0$ but, because it is not explicitly a function of ϵ, it is treated as being of order unity. From equations (3.55 – 3.56), it can be seen all of the expansion coefficients $\{a_j,b_j\}$ corresponding to $j\geq 3$ are functions of ϵ which signifies they all must be of at least first-order in the long-wave expansion. To determine the exact order of any given $\{a_j,b_j\}$ one needs to find the power of ϵ^n which the expansion coefficient in question is proportional to; this is done by expressing the right hand-sides of equations (3.55 – 3.56) in terms of $\{a_0,a_1,b_1,b_2\}$. This leads to the following proportionality relation:

$$\{a_j,b_j\}\propto\epsilon^{\lceil\frac{j-2}{4}\rceil}, \tag{3.57}$$

where $\lceil\frac{j-2}{4}\rceil$ denotes the ceiling function which outputs the smallest integer greater than or equal to the input. Equation (3.57) arises from the proportionality relationship between the laminar viscosity/conduction terms and the nonlinear inertia/convection terms in the momentum (3.37) and energy (3.38) equations, respectively; namely:

$$\frac{\partial^2 u}{\partial\hat{z}^2}\propto\epsilon Re\left(u\frac{\partial u}{\partial x}+w\frac{\partial u}{\partial\hat{z}}\right),\qquad\qquad\frac{\partial^2\theta}{\partial\hat{z}^2}\propto\epsilon RePr\left(u\frac{\partial\theta}{\partial x}+w\frac{\partial\theta}{\partial\hat{z}}\right). \tag{3.58}$$

The laminar viscosity/conduction terms on the left hand-side decrease the polynomial degree by two with respect to $\hat{z}$ whilst the inertia/convection terms on the right hand-side increase the polynomial degree by two with respect to $\hat{z}$ and one with respect to ϵ. The two sides are proportional and so the following expression must be satisfied:

$$\epsilon^m\hat{z}^{j_m-2}=\epsilon^{n+1}\hat{z}^{j_n+2}, \tag{3.59}$$

which requires $m=n+1$ and $j_m-2=j_n+2$; this leads to the following recurrence relation, $j_{n+1}=j_n+4$, where j_n is the polynomial degree of the nth-order truncation with respect to $\hat{z}$. Expanding this recurrence relation then finds $j_n=j_0+4n$ where $j_0=2$ is the polynomial degree of the leading-order truncation with respect to $\hat{z}$. Therefore, an alternative way to state equation (3.57) would be to say "an approximation of the

fluid velocity and temperature to nth-order in the long-wave expansion requires power series which contain all the expansion coefficients $\{a_j, b_j\}$ up to $j \geq 4n + 2$".

The long-wave expansion offers an efficient way to truncate the power series and eliminate the need for the tau coefficients; instead, the validity of the resulting nth-order asymptotically equivalent equations can be checked through comparison with those asymptotically equivalent equations corresponding to the next order in the long-wave expansion – agreement would indicate the higher-order derivatives contained in the latter are negligible. Strictly speaking, an nth-order truncation of the fluid velocity and temperature power series (3.43) would retain all the derivatives of $\{a_1, a_2, b_1, b_2\}$ up to nth-order; however, as will be shown in subsequent chapters, it is permissible to relax this requirement. In closing, the key distinction between the Tau method and the long-wave expansion is in how they limit the degrees of freedom in order to find an approximate solution: the Tau method restricts the degrees of freedom with respect to $\hat{z}$ whereas the long-wave expansion restricts the degrees of freedom with respect to x; in either case, limiting the degrees of freedom in one direction involuntarily leads to a limiting of the degrees of freedom in the other.

3.4.3 Reduced asymptotic model

The analysis in section 3.4.2 demonstrates how switching from a truncation of the power series with respect to the powers of $\hat{z}$ to a truncation with respect to the (x,t)-derivatives of (u,θ) leads to a simplification of the Tau method (which is itself a curtailment of the generalised power series methodology) by dispelling with the need for the tau coefficients. The current section demonstrates how the asymptotically equivalent equations of the Tau method – see section 3.4.1 – can be systematically transformed into a series of reduced asymptotic models. Naturally, the starting point of this transformation is the asymptotically equivalent equations of the Tau method – see section 3.4.1 – which are derived from:

$$\frac{\partial h}{\partial t} + \frac{\partial q}{\partial x} = 0, \tag{3.60}$$

$$\left.\frac{\partial u}{\partial \hat{z}}\right|_{\hat{z}=h} = \frac{2\epsilon^2 \frac{\partial f}{\partial x}\frac{\partial}{\partial x}\left(u|_{\hat{z}=h}\right)}{(1+\epsilon^2 g)} + \frac{\left(1-\epsilon^2 g\right)}{(1+\epsilon^2 g)}\frac{\epsilon^2\left[\frac{\partial^2 q}{\partial x^2} - u|_{\hat{z}=h}\frac{\partial^2 f}{\partial x^2}\right]}{(1+\epsilon^2 g)} - \frac{\epsilon\frac{Ma}{Ca}\frac{\partial \vartheta}{\partial x}}{\left[1+\epsilon^2 g\right]^{3/2}}, \tag{3.61}$$

$$\left.\frac{\partial \theta}{\partial \hat{z}}\right|_{\hat{z}=h} = \frac{\epsilon^2 \frac{\partial f}{\partial x}\frac{\partial \vartheta}{\partial x}}{1+\epsilon^2 g} - \frac{Bi\vartheta}{\sqrt{1+\epsilon^2 g}}, \tag{3.62}$$

$$\begin{aligned}\left.\frac{\partial^2 u}{\partial \hat{z}^2}\right|_{\hat{z}=0} &= -2\left(1-\epsilon\frac{\partial f}{\partial x}\cot\beta\right) - \epsilon^2\frac{\partial^2}{\partial x^2}\left[\,u|_{\hat{z}=h}\,\right] - \epsilon^3\frac{\partial^2}{\partial x^2}\left[\frac{\frac{(1-Ma\vartheta)}{Ca}\frac{\partial f}{\partial x}}{\sqrt{1+\epsilon^2 g}}\right] \\ &\quad - \left[2\epsilon^2\frac{\partial^2 u}{\partial x^2} - \epsilon^3 Re\frac{\partial}{\partial x}\int_{\hat{z}}^{h}\left(\frac{\partial w}{\partial t} + u\frac{\partial w}{\partial x} + w\frac{\partial w}{\partial \hat{z}}\right)d\hat{z} + \epsilon^4\frac{\partial^2}{\partial x^2}\int_{\hat{z}}^{h}\frac{\partial w}{\partial x}\;d\hat{z}\right]\Bigg|_{\hat{z}=0},\end{aligned} \tag{3.63}$$

where $q = \int_0^h u\,d\hat{z}$ is the stream-wise flow rate, $u|_{\hat{z}=h}$ is the free-surface flow velocity, and $\vartheta = \theta|_{\hat{z}=h}$ is the free-surface temperature. For clarity, the flow velocity in x-direction (u) and fluid temperature (θ) are given by power series with respect to $\hat{z}$; namely:

$$u = \sum_{j=1}^{N} a_j(x,t)\hat{z}^j, \qquad\qquad \theta = 1 + \sum_{j=1}^{N} b_j(x,t)\hat{z}^j, \tag{3.64}$$

respectively; where $\{a_j, b_j\}$ are expansion coefficients which are functions of (x,t). An expansion for the vertical flow velocity is found through $w = -\int_0^{\hat{z}}(\partial u/\partial x)\,d\hat{z}$ like so:

$$w = \sum_{j=1}^{N}\left(a_j\frac{ds}{dx}\hat{z}^j - \frac{\partial a_j}{\partial x}\frac{\hat{z}^{j+1}}{(j+1)}\right), \tag{3.65}$$

in which $a_0 = 0$ is known from equations (3.44) and $a_j = 0$ for $j > N$ by result of the power series being truncated. The truncation of the power series is determined with reference to a long-wave expansion; it was found in section 3.4.2 that an expansion of the fluid

velocity and temperature with respect to the (x,t)-derivatives of (u,θ) to nth-order in the long-wave expansion requires all $\{a_j, b_j\}$ up to $j \geq 4n+2$. Accordingly, the degree of truncation (N) at nth-order in the long-wave expansion equates to:

$$N = 4n+2, \qquad at \qquad \sim \mathcal{O}\left(\epsilon^n\right). \tag{3.66}$$

Note that equation (3.66) gives the maximum degree of truncation for the fluid velocity and temperature power series at nth-order; only terms of order unity in equations (3.60 – 3.63) need to approximated to the maximum degree. In contrast, higher-order terms in equations (3.60 – 3.63) must be approximated to lesser degrees; this is because approximating any higher-order term to the maximum degree will generate terms which are of beyond nth-order. It is important to state that the derivation of a set of nth-order asymptotically equivalent equations and the elimination of the tau coefficients relies on the assumption that (x,t)-derivatives belonging to beyond nth-order are negligible to the problem of interest; retaining any of these derivatives in a reduced asymptotic model would imbalance the long-wave expansion and introduce unbounded elements to the asymptotically equivalent equations. Accordingly, an nth-order approximation of a mth-order term must be done using a power series truncated at the Mth degree where $M = 4(n-m)+2$. In this way, the resulting asymptotically equivalent equations will only contain: first-order (x,t)-derivatives of (u,θ) at first-order; first- and second-order (x,t)-derivatives of (u,θ) at second-order; etc.

Finally, the derivation of any reduced asymptotic model requires the recurrence relations for $\{a_j, b_j\}$ corresponding to $j \geq 3$ which are given by:

$$
\begin{aligned}
a_j = & \frac{\epsilon Re\left\{\frac{\partial a_{j-2}}{\partial t} + \sum_{i=1}^{j-3} \frac{(j-2i-1)}{(j-i-1)} a_i \frac{\partial a_{j-i-2}}{\partial x}\right\} - \epsilon^2 \frac{\partial^2 a_{j-2}}{\partial x^2}}{|\ell_s|^2 j\,(j-1)} + \frac{\epsilon^2\left\{2\frac{\partial a_{j-1}}{\partial x}\frac{ds}{dx} + a_{j-1}\frac{d^2s}{dx^2}\right\}}{|\ell_s|^2 j} \\
& + \frac{\epsilon^3 Re \frac{\partial^3 a_{j-4}}{\partial x^2 \partial t}}{|\ell_s|^4 j\,(j-1)\,(j-2)\,(j-3)} + \frac{\epsilon^3 Re \sum_{i=1}^{j-5}\left\{\frac{1}{(j-i-3)}\left(a_i \frac{\partial^3 a_{j-i-4}}{\partial x^3} - \frac{\partial a_{j-i-4}}{\partial x}\frac{\partial^2 a_i}{\partial x^2}\right)\right\}}{|\ell_s|^4 j\,(j-1)\,(j-2)} \\
& - \frac{\epsilon^3 Re\left\{2\frac{\partial^2 a_{j-3}}{\partial x \partial t}\frac{ds}{dx} + \frac{\partial a_{j-3}}{\partial t}\frac{d^2s}{dx^2}\right\}}{|\ell_s|^4 j\,(j-1)\,(j-2)} + \frac{\epsilon^3 Re \sum_{i=1}^{j-3}\left\{a_i a_{j-i-2}\frac{ds}{dx}\frac{d^2s}{dx^2} - \frac{2a_{j-i-3}}{(i+1)}\frac{\partial^2 a_i}{\partial x^2}\frac{ds}{dx}\right\}}{|\ell_s|^4 j\,(j-1)} \\
& - \frac{\epsilon^3 Re \sum_{i=1}^{j-4}\left\{\frac{1}{(j-i-2)}\left(2i\frac{\partial a_i}{\partial x}\frac{ds}{dx} + (3j-4i-6)\,a_i\frac{d^2s}{dx^2}\right)\frac{\partial a_{j-i-3}}{\partial x} + a_i a_{j-i-3}\frac{d^3s}{dx^3}\right\}}{|\ell_s|^4 j\,(j-1)\,(j-2)} \\
& - \frac{\epsilon^4 \frac{\partial^4 a_{j-4}}{\partial x^4}}{|\ell_s|^4 j\,(j-1)\,(j-2)\,(j-3)} + \frac{\epsilon^4\left\{4\frac{\partial^3 a_{j-3}}{\partial x^3}\frac{ds}{dx} + 6\frac{\partial^2 a_{j-3}}{\partial x^2}\frac{d^2s}{dx^2} + 4\frac{\partial a_{j-3}}{\partial x}\frac{d^3s}{dx^3} + a_{j-3}\frac{d^4s}{dx^4}\right\}}{|\ell_s|^4 j\,(j-1)\,(j-2)} \\
& - \frac{\epsilon^4\left\{5\frac{\partial^2 a_{j-2}}{\partial x^2}\left(\frac{ds}{dx}\right)^2 + 12\frac{\partial a_{j-2}}{\partial x}\frac{ds}{dx}\frac{d^2s}{dx^2} + 3a_{j-2}\left(\frac{d^2s}{dx^2}\right)^2 + 4a_{j-2}\frac{ds}{dx}\frac{d^3s}{dx^3}\right\}}{|\ell_s|^4 j\,(j-1)} \\
& + \frac{\epsilon^4\left\{2\frac{\partial a_{j-1}}{\partial x}\frac{ds}{dx} + 5a_{j-1}\frac{d^2s}{dx^2}\right\}\left(\frac{ds}{dx}\right)^2}{|\ell_s|^4 j}
\end{aligned}
\tag{3.67}
$$

$$
\begin{aligned}
b_j = & \frac{\epsilon RePr\left\{\frac{\partial b_{j-2}}{\partial t} + \sum_{i=1}^{j-3}\left(a_i\frac{\partial b_{j-i-2}}{\partial x} - \frac{(j-i-2)}{(i+1)}b_{j-i-2}\frac{\partial a_i}{\partial x}\right)\right\} - \epsilon^2\frac{\partial^2 b_{j-2}}{\partial x^2}}{|\ell_s|^2 j\,(j-1)} \\
& + \frac{\epsilon^2\left\{2\frac{\partial b_{j-1}}{\partial x}\frac{ds}{dx} + b_{j-1}\frac{d^2s}{dx^2}\right\}}{|\ell_s|^2 j},
\end{aligned}
\tag{3.68}
$$

where $|\ell_s| = \sqrt{1+\epsilon^2(ds/dx)^2}$ is the dimensionless length of an infinitesimal segment of the substrate corrugation (or substrate curvature). In addition, an expression for b_2 is found by evaluating the energy equation at the substrate; this yields:

$$
b_2 = \frac{\epsilon^2\left\{\frac{\partial b_1}{\partial x}\frac{ds}{dx} + \frac{b_1}{2}\frac{d^2s}{dx^2}\right\}}{|\ell_s|^2}. \tag{3.69}
$$

First-order reduced asymptotic model

At first-order, $\sim \mathcal{O}(\epsilon)$, the degree of truncation is $N = 6$; substituting expansions (3.64 – 3.65) into equations (3.60 – 3.63) and writing out the recurrence relations (3.67 – 3.68), discarding all terms of second-order or higher in the process[1], yields:

[1]The capillary term from equation (3.63) is retained at first-order even though it is of higher-order.

$$a_2 = \frac{\epsilon\frac{\partial f}{\partial x}\cot\beta - 1 - \frac{\epsilon^3}{2}\frac{\partial^2}{\partial x^2}\left[\frac{\frac{1-Ma\vartheta}{Ca}\frac{\partial f}{\partial x}}{\sqrt{1+\epsilon^2 g}}\right]}{|\ell_s|^4}, \quad b_2 = 0, \tag{3.70}$$

$$a_3 = \frac{\epsilon Re\frac{\partial a_1}{\partial t}}{6|\ell_s|^2}, \qquad b_3 = \frac{\epsilon RePr\frac{\partial b_1}{\partial t}}{6|\ell_s|^2}, \tag{3.71}$$

$$a_4 = \frac{\epsilon Re\left\{\frac{\partial a_2}{\partial t} + \frac{a_1}{2}\frac{\partial a_1}{\partial x}\right\}}{12|\ell_s|^2}, \qquad b_4 = \frac{\epsilon RePr\left\{\frac{\partial b_2}{\partial t} + a_1\frac{\partial b_1}{\partial x} - \frac{b_1}{2}\frac{\partial a_1}{\partial x}\right\}}{12|\ell_s|^2}, \tag{3.72}$$

$$a_5 = \frac{\epsilon Re\left\{\frac{2a_1}{3}\frac{\partial a_2}{\partial x}\right\}}{20|\ell_s|^2}, \qquad b_5 = \frac{\epsilon RePr\left\{a_1\frac{\partial b_2}{\partial x} + a_2\frac{\partial b_1}{\partial x} - b_2\frac{\partial a_1}{\partial x} - \frac{b_1}{3}\frac{\partial a_2}{\partial x}\right\}}{20|\ell_s|^2}, \tag{3.73}$$

$$a_6 = \frac{\epsilon Re\left\{\frac{a_2}{3}\frac{\partial a_2}{\partial x}\right\}}{30|\ell_s|^2}, \qquad b_6 = \frac{\epsilon RePr\left\{a_2\frac{\partial b_2}{\partial x} - \frac{2b_2}{3}\frac{\partial a_2}{\partial x}\right\}}{30|\ell_s|^2}, \tag{3.74}$$

which describe the asymptotic behaviour of $\{a_j, b_j\}$ corresponding to $j \geq 2$ at first-order; whilst the boundary conditions at the free-surface (3.60 – 3.62) read:

$$\frac{\partial h}{\partial t} + \frac{\partial q}{\partial x} = 0, \qquad \frac{1}{h}\sum_{j=1}^{6} jh^j a_j = \frac{-\epsilon\frac{Ma}{Ca}\frac{\partial\vartheta}{\partial x}}{[1+\epsilon^2 g]^{3/2}}, \qquad \frac{1}{h}\sum_{j=1}^{6} jh^j b_j = \frac{-Bi\vartheta}{\sqrt{1+\epsilon^2 g}}. \tag{3.75}$$

At this point, one might be tempted to try substituting expressions (3.70 – 3.74) into equations (3.75) in order arrive at three evolution equations in terms of (h, a_1, b_1); however, such action would be foolhardy and completely disregard the intricacy and limitations of a long-wave expansion. Consider how expressions (3.70 – 3.74) would look within the framework of the Tau method – see section 3.4.1; the key difference is that they would contain the derivatives of $\{a_j, b_j\}$ with respect to (x, t) for $3 \leq j \leq 6$, which would make these quantities degrees of freedom with respect to (x, t) in their own right, howbeit, in a limited capacity because they are the degrees of freedom appearing in the tau coefficients and must therefore be minimised to ensure the validity of the approximate solution. Nevertheless, it indicates that the derivatives of $\{a_j, b_j\}$ corresponding to $3 \leq j \leq 6$ influence those of $\{a_1, a_2, b_1, b_2\}$ in Tau method; when recasting the power series method to work within the framework of a long-wave expansion, this detail is not lost and it actually betrays the fact that terms belonging to different orders of the long-wave expansion are linearly dependent upon one another. This explains why modelling the film dynamics via a perturbation series is unsound (section 3.3) because doing so erroneously assumes that terms of different orders in the long-wave expansion are linearly independent; recall that the present power series method was initiated upon the realisation that ϵ cannot serve as the formal expansion parameter of any asymptotic modelling approach – see discussion at the start of section 3.4.

The fact that powers of ϵ are linearly dependent leads to an interesting consequence, which is that whilst the asymptotic expressions in equations (3.70 – 3.74) provide adequate descriptions for the expansion coefficients $\{a_j, b_j\}$ corresponding to $2 \leq j \leq 6$ at first-order, the same expressions do not offer accurate descriptions for the derivatives of these quantities. To understand why this is the case, one must appreciate that, as functions of (x,t), the expansion coefficients $\{a_j, b_j\}$ are subject to a long-wave expansion in the exact same fashion as the fluid velocity and temperature are; one can thus write $\{a_j, b_j\} = \{a_{j_0}, b_{j_0}\} + \epsilon\{a_{j_1}, b_{j_1}\} + \epsilon^2\{a_{j_2}, b_{j_2}\} + ...$ To this effect, equations (3.70 – 3.74) represent asymptotically equivalent expressions for $\{a_j, b_j\} = \{a_{j_0}, b_{j_0}\} + \epsilon\{a_{j_1}, b_{j_1}\} + \mathcal{O}\left(\epsilon^2\right)$. However, an asymptotic expression for the derivative of any $\{a_j, b_j\}$ must only take into consideration the (x,t)-dependence of the leading-order component, $\{a_{j_0}, b_{j_0}\}$. In the case of $\{a_2, b_2\}$ – equations (3.70); one might naively try to obtain $\{a_{2_0}, b_{2_0}\}$ by writing:

$$a_{2_0} + \epsilon a_{2_1} = \frac{-1 + \epsilon \frac{\partial f}{\partial x} \cot\beta - \frac{\epsilon^3}{2} \frac{\partial^2}{\partial x^2} \left[\frac{\frac{1 - Ma\vartheta}{Ca} \frac{\partial f}{\partial x}}{\sqrt{1+\epsilon^2 g}} \right]}{|\ell_s|^4}, \qquad b_{2_0} + \epsilon b_{2_1} = 0, \tag{3.76}$$

and then solving for $\{a_{2_0}, b_{2_0}\}$ by isolating the powers of ϵ; but this would completely neglect the fact that powers of ϵ are linearly dependent. As a matter of fact, trying to solve for $\{a_{2_0}, b_{2_0}\}$ in equations (3.76) by isolating the powers of ϵ is futile and leads one to the inviscid Burgers equation which was considered in section 3.3.2. Instead, asymptotically equivalent expressions for the derivatives of $\{a_1, a_2, b_1, b_2\}$ at first-order in the long-wave expansion must be found through an equivalence principle.

It can be clearly seen from equations (3.75) that (h, q, ϑ) are all degrees of freedom with respect to (x,t) at first-order; this implies the derivatives of $\{a_1, a_2, b_1, b_2\}$ must be asymptotically equivalent to the derivatives of (h, q, ϑ) in some fashion. Accordingly, the task is find the relationships linking $\{a_1, a_2, b_1, b_2\}$ to (h, q, ϑ); this is achieved by substituting the power series (3.64) into the definitions of the stream-wise flow rate and free-surface temperature which yields the following expressions:

$$q = \sum_{j=1}^{N} \frac{h^{j+1}}{(j+1)} a_j, \qquad \vartheta = 1 + \sum_{j=1}^{N} h^j b_j. \tag{3.77}$$

Expanding equations (3.77), and the shear stress and heat flux boundary conditions (3.75), leads to a set of simultaneous equations in terms of $\{a_j, b_j\}$ for $j \leq 6$; namely:

$$q = \frac{h^2}{2} a_1 + \frac{h^3}{3} a_2 + \frac{h^4}{4} a_3 + \frac{h^5}{5} a_4 + \frac{h^6}{6} a_5 + \frac{h^7}{7} a_6 + \mathcal{O}\left(\epsilon^2\right), \tag{3.78}$$

$$\frac{-\epsilon \frac{Ma}{Ca} \frac{\partial \vartheta}{\partial x}}{\left[1 + \epsilon^2 g\right]^{3/2}} = a_1 + 2h a_2 + 3h^2 a_3 + 4h^3 a_4 + 5h^4 a_5 + 6h^5 a_6 + \mathcal{O}\left(\epsilon^2\right), \tag{3.79}$$

$$\vartheta = 1 + hb_1 + h^2 b_2 + h^3 b_3 + h^4 b_4 + h^5 b_5 + h^6 b_6 + \mathcal{O}\left(\epsilon^2\right), \tag{3.80}$$

$$\frac{-Bi\vartheta}{\sqrt{1+\epsilon^2 g}} = b_1 + 2hb_2 + 3h^2 b_3 + 4h^3 b_4 + 5h^4 b_5 + 6h^5 b_6 + \mathcal{O}\left(\epsilon^2\right). \tag{3.81}$$

where $g = (\partial f/\partial x)^2$. Asymptotic expressions for $\{a_1, a_2, b_1, b_2\}$ can therefore be obtained by manipulating equations (3.78 – 3.81) in order to acquire the following expressions:

$$a_1 = \frac{3q}{h^2} + \frac{\sum_{j=3}^{6} \frac{(j+3)(j-2)}{(j+1)} h^j a_j - \tau_1}{2h}, \qquad b_1 = \frac{\left(1 + \vartheta_{\mathbb{N}}^{-1}\right)\vartheta - 2}{h} + \frac{1}{h}\sum_{j=3}^{6}(j-2)\,h^j b_j, \tag{3.82}$$

$$a_2 = \frac{-3q}{2h^3} + \frac{3\tau_1 - 3\sum_{j=3}^{6} \frac{(j+2)(j-1)}{(j+1)} h^j a_j}{4h^2}, \quad b_2 = \frac{1 - \vartheta_{\mathbb{N}}^{-1}\vartheta}{h^2} - \frac{1}{h^2}\sum_{j=3}^{6}(j-1)\,h^j b_j, \tag{3.83}$$

where $\tau_1/h = -(\epsilon Ma/Ca)(\partial\vartheta/\partial x)/[1+\epsilon^2 g]^{3/2}$ is the shear stress at the free-surface and $\vartheta_{\mathbb{N}} = 1/(1 + Bih/\sqrt{1+\epsilon^2 g})$ is the Nusselt free-surface temperature. In the framework of a long-wave expansion: the film thickness, stream-wise flow rate, and free-surface temperature are all quantities of order unity, $(h, q, \vartheta) \sim \mathcal{O}(1)$; in contrast, the expansion coefficients $\{a_j, b_j\}$ corresponding to $j \geq 3$ are all of at least first-order, $\sim \mathcal{O}(\epsilon)$. On this knowledge, asymptotically equivalent expressions for the derivatives of $\{a_1, a_2, b_1, b_2\}$ are obtained by differentiating equations (3.82 – 3.83) with respect to (x, t); this yields:

$$\frac{\partial a_1}{\partial r_i} = \frac{3}{h^2}\frac{\partial q}{\partial r_i} - \frac{6q}{h^3}\frac{\partial h}{\partial r_i} + \mathcal{O}\left(\epsilon^2\right), \qquad \frac{\partial b_1}{\partial r_i} = \frac{\left(1+\vartheta_{\mathbb{N}}^{-1}\right)}{h}\frac{\partial \vartheta}{\partial r_i} - \frac{2\,(\vartheta - 1)}{h^2}\frac{\partial h}{\partial r_i} + \mathcal{O}\left(\epsilon^2\right), \tag{3.84}$$

$$\frac{\partial a_2}{\partial r_i} = \frac{9q}{2h^4}\frac{\partial h}{\partial r_i} - \frac{3}{2h^3}\frac{\partial q}{\partial r_i} + \mathcal{O}\left(\epsilon^2\right), \quad \frac{\partial b_2}{\partial r_i} = \frac{\left(1+\vartheta_{\mathbb{N}}^{-1}\right)\vartheta - 2}{h^3}\frac{\partial h}{\partial r_i} - \frac{\vartheta_{\mathbb{N}}^{-1}}{h^2}\frac{\partial \vartheta}{\partial r_i} + \mathcal{O}\left(\epsilon^2\right), \tag{3.85}$$

for $(r_1, r_2) = (x, t)$, respectively. With expressions for the derivatives of $\{a_1, a_2, b_1, b_2\}$, a reduced asymptotic model can be derived by replacing $\{a_j, b_j\}$ for $j \geq 2$ in the boundary conditions at the free-surface – equations (3.75) – with their asymptotically equivalent expressions from equation (3.70 – 3.73) and $\{a_1, b_1\}$ with their expressions in equations (3.82); the derivatives of $\{a_1, a_2, b_1, b_2\}$ are then given by equations (3.84 – 3.85). This leads to the first-order reduced asymptotic model in terms of (h, q, ϑ), which reads:

$$\frac{\partial h}{\partial t}+\frac{\partial q}{\partial x}=0, \tag{3.86}$$

$$\frac{\epsilon Re}{|\ell_s|^2}\left(\frac{\partial q}{\partial t}-\frac{9q^2}{7h^2}\frac{\partial h}{\partial x}+\frac{17q}{7h}\frac{\partial q}{\partial x}\right)+\frac{\epsilon\frac{5}{4}\frac{Ma}{Ca}\frac{\partial\vartheta}{\partial x}}{[1+\epsilon^2 g]^{3/2}}$$
$$+\epsilon\frac{5h}{3}\frac{\cot\beta}{|\ell_s|^4}\frac{\partial f}{\partial x}-\epsilon^3\frac{5h}{6\,|\ell_s|^4}\frac{\partial^2}{\partial x^2}\left[\frac{(1-Ma\vartheta)\,\frac{\partial f}{\partial x}}{Ca\sqrt{1+\epsilon^2 g}}\right]+\frac{5q}{2h^2}-\frac{5h}{3}+\mathcal{O}\left(\epsilon^2\right)=0, \tag{3.87}$$

$$\frac{\epsilon RePr}{|\ell_s|^2}\left(\frac{\partial\vartheta}{\partial t}+\frac{(27\vartheta_{\mathbb{N}}+6)}{(4\vartheta_{\mathbb{N}}+1)}\frac{q}{5h}\frac{\partial\vartheta}{\partial x}+\frac{(17\vartheta_{\mathbb{N}}-11)}{(4\vartheta_{\mathbb{N}}+1)}\frac{\vartheta}{10h}\frac{\partial q}{\partial x}\right.$$
$$\left.-\frac{\vartheta_{\mathbb{N}}}{(4\vartheta_{\mathbb{N}}+1)}\frac{3}{5h}\frac{\partial q}{\partial x}-\frac{(\vartheta_{\mathbb{N}}-1)}{(4\vartheta_{\mathbb{N}}+1)}\frac{6q\vartheta}{5h^2}\frac{\partial h}{\partial x}\right)+\frac{12}{h^2}\frac{(\vartheta-\vartheta_{\mathbb{N}})}{(4\vartheta_{\mathbb{N}}+1)}+\mathcal{O}\left(\epsilon^2\right)=0, \tag{3.88}$$

in which $h(x,t)$ is the film thickness, $q(x,t)=\int_0^h u\;d\hat{z}$ is the stream-wise flow rate, $\vartheta(x,t)=\theta|_{\hat{z}=h}$ is the free-surface temperature; with the free-surface curvature pre-factor given by $g=(\partial f/\partial x)^2$; the substrate curvature given by $|\ell_s|=\sqrt{1+\epsilon^2(ds/dx)}$; and the Nusselt free-surface temperature given by $\vartheta_{\mathbb{N}}=1/(1+Bih/\sqrt{1+\epsilon^2 g})$.

Equations (3.86 – 3.88) constitute the first-order reduced asymptotic model (or first-order RAM for short), and a thermal analogy of the first-order isothermal model derived in Ruyer-Quil and Manneville [2000]. In that original paper, it was noted the exact same set of equations could be retrieved from a method of weighted residuals using a self-similar-style velocity profile. It is important to recognise that neither the velocity or temperature distributions in gravity-driven film flow are self-similar; indeed, the derivation process above shows that these distributions require corrections at first-order and beyond. Nevertheless, it is possible to arrive at equations (3.86 – 3.88) via a weighted-residual technique in which the fluid velocity and temperature expansions would appear to be self-similar. The self-similar-esque profiles required for a weighted-residual derivation are obtained by replacing $\{a_1,a_2,b_1,b_2\}$ with their expressions from equations (3.82 – 3.83) and then truncating the power series at $\sim\mathcal{O}(1)$; this yields:

$$u=\frac{3q}{2h^3}\left(2h\hat{z}-\hat{z}^2\right)+\mathcal{O}(\epsilon), \qquad \tilde{w}_u=2h\hat{z}-\hat{z}^2, \tag{3.89}$$

$$\theta=1+\frac{(\vartheta-1)}{h}\hat{z}+\frac{\left(\frac{\vartheta-\vartheta_{\mathbb{N}}}{\vartheta_{\mathbb{N}}}\right)}{h^2}\left(h\hat{z}-\hat{z}^2\right)+\mathcal{O}(\epsilon), \qquad \tilde{w}_\theta=\hat{z}, \tag{3.90}$$

where $(\tilde{w}_u,\tilde{w}_\theta)$ correspond to the weight functions needed for a weighted-residual derivation of equations (3.86 – 3.88). The weighted residual derivation can be accomplished by: (i) multiplying the momentum (3.37) and energy (3.38) equations by $\tilde{w}_u$ and $\tilde{w}_\theta$, (ii) replacing (u,θ) with their self-similar-esque expressions from equations (3.89 – 3.90), and (iii) then integrating the momentum and energy equations between $\hat{z}=0$ and $\hat{z}=h$.

Since the weighted-residual derivation uses the same self-similar-style velocity profile as the depth-averaged approach of Shkadov [1967] which yields the integral-boundary-layer (IBL) equations, the present modelling approach has become popularly known as the weighted-integral-boundary-layer (WIBL) equations, and its ease of derivation via a weighted-residual technique has certainly helped popularise its use within the field. Howbeit, the weighted-residual technique has also turned out to be the bane of the modelling approach by virtue of the fact that it is a simplification of the full power series method. As a result, a lot of the mathematical rigour and justification of the power series method is lost when employing the weighted-residual derivation of the model, and this has meant the modelling approach has rarely been extended to higher-order or to include other effects such as heating in a rigorous fashion; this is partly because the ambiguity of the weighted-residual derivation has allowed many misconceptions to persist within the research field, such as: *treating powers of ϵ as being linearly independent, assuming the velocity/temperature profiles to be self-similar, depth-averaging the governing equations.* This is why the models considered presently are referred to as reduced asymptotic models (RAM) in order to distinguish that they have been derived via the power series method rather than a weighted-residual technique.

The best example of the weighted-residual technique corrupting the present modelling approach would be the extension of the methodology to the case of heated film flow where the self-similar velocity/temperature hypothesis has led to many reduced asymptotic models which are based on a temperature expansion which is linear to leading-order. This reason for this is because the temperature distribution becomes linear with respect to $\hat{z}$ in the long-wave limit, $\epsilon \to 0$; as can be seen by the Nusselt linear temperature distribution in equations (3.7). However, models based on a linear temperature approximation are only valid in a narrow neighbourhood close to the Nusselt solution and are known to rapidly predict unphysical negative free-surface temperatures at moderate Reynolds numbers. The problem with a linear temperature approximation is that it only affords the fluid temperature one degree of freedom with respect to (x,t) at first-order; however, the fluid temperature actually possesses two degrees of freedom with respect to (x,t) at first-order, these are the inter-facial temperature (ϑ) and the heat flux through the free-surface $(\partial\theta/\partial\hat{z}|_{\hat{z}=h})$. To be able to capture the evolution of both these quantities at first-order, the temperature expansion must be comprised of two expansion coefficients $\{b_j\}$ which are functions of (x,t) – this can only happen if it is afforded two degrees of freedom with respect to $\hat{z}$ at leading-order. Indeed, the only reason why the energy equation can be expressed as a single evolution equation (3.88) at first-order is because the heat flux through the free-surface is linearly dependent upon the free-surface temperature, *i.e.* $\partial\theta/\partial\hat{z}|_{\hat{z}=h} = -Bi\vartheta$. The degrees of freedom of the fluid temperature at first-order can be seen very clearly from self-similar-style expression given in (3.90); the first term corresponds to the scaled substrate temperature, the second term describes how the temperature deviates from the substrate temperature, and the final term accounts for how the temperature is affected by fluctuations in the heat flux passing through the free-surface. The linear temperature approximation forgoes the final term of equation (3.90) which restricts the validity of the resultant reduced

asymptotic model to problems in which the heat flux through the free-surface is not a function of (x, t); problematically, because the heat flux is linearly dependent upon the free-surface temperature, such scenarios only occur when either the Biot number (Bi) is vanishingly small or when the free-surface temperature is not a function of (x, t) – these scenarios only occur in the long-wave limit $(\epsilon \to 0)$ or in the case of isothermal film flow $(Bi = 0)$. Thus, a reduced asymptotic model based on a linear temperature approximation is only valid for heated film flow when $\epsilon \to 0$.

Second-order reduced asymptotic model

Given that the first-order evolution equations (3.86 – 3.88) can be obtained through a weighted-residual technique, Ruyer-Quil and Manneville [2000] opted to extend the evolutions to second-order in the long-wave expansion via a method of weighted residuals. However, as explained in the section above on the first-order reduced asymptotic model, the weighted-residual technique is an ambiguous method of derivation which is not always suitably rigorous; on this account, the derivation of the second-order model is derived using the same power series method as was used for the first-order model.

Having said that, several insights can be taken from the first-order model which will help speed the derivation process and make the modelling more accessible to others. First, the process of finding the derivatives of $\{a_1, a_2, b_1, b_2\}$ in terms of (h, q, ϑ) is no different to seeking a variable transformation in which the expansion coefficients are exchanged with the stream-wise flow rate (q), the shear stress at the free-surface (τ_1), the free-surface temperature (ϑ), and finally the heat flux through the free-surface $(-Bi\vartheta)$. There is no reason why this variable transformation cannot be carried out at the start of the derivation process, so that the derivatives of each $\{a_j, b_j\}$ corresponding to a degree of freedom of the nth-order system can be defined beforehand in terms of a set of new reduced variables, *e.g. the stream-wise flow rate* (q). Second, it is obvious that each new reduced variable will require its own evolution equation; however, if the definition of each new reduced variable is chosen to be a linear equation in terms of the expansion coefficients $\{a_j, b_j\}$, then the required evolution equation can be easily obtained from the definition of the variable itself. This is because expressions for each of the expansion coefficients $\{a_j, b_j\}$ are offered by: the recurrence relations (3.67 – 3.68) for $\{a_j, b_j\}$ corresponding to $j \geq 3$; the evaluations of the momentum and energy equations at the substrate $(\hat{z} = 0)$ for $\{a_2, b_2\}$; the shear stress and heat flux boundary conditions at the free-surface for $\{a_1, b_1\}$; and equations (3.44) give $\{a_0, b_0\}$. Ergo, the derivation of a second-order model can be accomplished in the following steps: (i) define a set of new reduced variables which each depend linearly on $\{a_j, b_j\}$; (ii) substitute the expressions for $\{a_j, b_j\}$ from the recurrence relations, etc. into the definitions of the new reduced variables; (iii) replace the derivatives of $\{a_j, b_j\}$ in the resulting equations with asymptotically equivalent expressions in terms of the new reduced variables.

The first step is therefore to define a new set of reduced variables which will replace the expansion coefficients $\{a_j, b_j\}$ and represent the degrees of freedom in the second-order reduced asymptotic model. As explained in section 3.4.2, extension of the

asymptotically equivalent equations to second-order in the long-wave expansion requires all the expansion coefficients $\{a_j, b_j\}$ up to $j \leq 10$; furthermore, the derivatives of the expansion coefficients $\{a_j, b_j\}$ corresponding to $j \leq 6$ must be retained; ergo, the second-order reduced asymptotic model possesses thirteen degrees of freedom[2]: six for the flow velocity, six for the fluid temperature, and lastly, the film thickness. The degrees of freedom for the flow velocity and fluid temperature, respectively, are chosen using the following definitions:

$$q = \int_0^h u \, d\hat{z}, \qquad \bar{\theta} = \frac{1}{h}\int_0^h \theta \, d\hat{z}, \tag{3.91}$$

$$\upsilon = u|_{\hat{z}=h}, \qquad \vartheta = \theta|_{\hat{z}=h}, \tag{3.92}$$

$$\tau_1 = h\frac{\partial u}{\partial \hat{z}}\bigg|_{\hat{z}=h}, \qquad \phi_1 = h\frac{\partial \theta}{\partial \hat{z}}\bigg|_{\hat{z}=h}, \tag{3.93}$$

$$\tau_2 = h^2\frac{\partial^2 u}{\partial \hat{z}^2}\bigg|_{\hat{z}=h}, \qquad \phi_2 = h^2\frac{\partial^2 \theta}{\partial \hat{z}^2}\bigg|_{\hat{z}=h}, \tag{3.94}$$

$$\tau_3 = h^3\frac{\partial^3 u}{\partial \hat{z}^3}\bigg|_{\hat{z}=h}, \qquad \phi_3 = h^3\frac{\partial^3 \theta}{\partial \hat{z}^3}\bigg|_{\hat{z}=h}, \tag{3.95}$$

$$\tau_4 = h^4\frac{\partial^4 u}{\partial \hat{z}^4}\bigg|_{\hat{z}=h}, \qquad \phi_4 = h^4\frac{\partial^4 \theta}{\partial \hat{z}^4}\bigg|_{\hat{z}=h}, \tag{3.96}$$

where the stream-wise flow rate (q), the free-surface velocity (υ) and the free-surface temperature (ϑ) have all been chosen because they appear explicitly in the boundary conditions; the mean fluid temperature ($\bar{\theta}$) has been introduced since it is a physical quantity which is relevant to the problem; the shear stress (τ_1) and heat flux (ϕ_1) at the free-surface have both been converted from boundary conditions into their respective degrees of freedom – they have also been multiplied by the film thickness so that they respectively possess the dimension of velocity and temperature; the additional degrees of freedom then correspond to the evaluations of the momentum (3.37) and energy (3.38) equations at the free-surface (τ_2, ϕ_2), respectively, along with the evaluations of the derivatives of these equations with respect to $\hat{z}$ at the free-surface, which are represented by (τ_2, τ_3, τ_4) for the momentum equation and(ϕ_2, ϕ_3, ϕ_4) for the energy equation.

By manipulating equations (3.91 – 3.96), expressions for $\{a_j, b_j\}$ corresponding to $1 \leq j \leq 6$ can be found in terms of $(h, q, \upsilon, \tau_1, \tau_2, \tau_3, \tau_4)$ and $(\bar{\theta}, \vartheta, \phi_1, \phi_2, \phi_3, \phi_4)$ like so:

[2]It might be possible to express the second-order reduced asymptotic model in terms of less than six variables; however, this can be checked after the derivation by seeing if any of the second-order evolution equations are linearly dependent upon one another.

$$a_1 = \frac{3q}{h^2} - \frac{30}{h}\left(\upsilon - \frac{3q}{2h}\right) + \frac{10}{h}\tau_1 - \frac{2}{h}\left(\tau_2 + \frac{3q}{h}\right) + \frac{1}{4h}\tau_3 - \frac{1}{60h}\tau_4 + \mathcal{O}\left(\epsilon^2\right), \tag{3.97}$$

$$a_2 = -\frac{3q}{2h^3} + \frac{165}{h^2}\left(\upsilon - \frac{3q}{2h}\right) - \frac{60}{h^2}\tau_1 + \frac{13}{h^2}\left(\tau_2 + \frac{3q}{h}\right) - \frac{7}{4h^2}\tau_3 + \frac{1}{8h^2}\tau_4 + \mathcal{O}\left(\epsilon^2\right), \tag{3.98}$$

$$a_3 = -\frac{340}{h^3}\left(\upsilon - \frac{3q}{2h}\right) + \frac{130}{h^3}\tau_1 - \frac{30}{h^3}\left(\tau_2 + \frac{3q}{h}\right) + \frac{13}{3h^3}\tau_3 - \frac{1}{3h^3}\tau_4 + \mathcal{O}\left(\epsilon^2\right), \tag{3.99}$$

$$a_4 = \frac{345}{h^4}\left(\upsilon - \frac{3q}{2h}\right) - \frac{135}{h^4}\tau_1 + \frac{65}{2h^4}\left(\tau_2 + \frac{3q}{h}\right) - \frac{5}{h^4}\tau_3 + \frac{5}{12h^4}\tau_4 + \mathcal{O}\left(\epsilon^2\right), \tag{3.100}$$

$$a_5 = -\frac{174}{h^5}\left(\upsilon - \frac{3q}{2h}\right) + \frac{69}{h^5}\tau_1 - \frac{17}{h^5}\left(\tau_2 + \frac{3q}{h}\right) + \frac{11}{4h^5}\tau_3 - \frac{1}{4h^5}\tau_4 + \mathcal{O}\left(\epsilon^2\right), \tag{3.101}$$

$$a_6 = \frac{35}{h^6}\left(\upsilon - \frac{3q}{2h}\right) - \frac{14}{h^6}\tau_1 + \frac{7}{2h^6}\left(\tau_2 + \frac{3q}{h}\right) - \frac{7}{12h^6}\tau_3 + \frac{7}{120h^6}\tau_4 + \mathcal{O}\left(\epsilon^2\right), \tag{3.102}$$

for the velocity coefficients, and for the temperature coefficients:

$$b_1 = \frac{2\left(\vartheta - 1\right) - \phi_1}{h} + \frac{42}{h}\left(\bar{\theta} - \frac{2 + 4\vartheta - \phi_1}{6}\right) - \frac{2}{h}\left(\phi_2 + 2\left(\vartheta - 1 - \phi_1\right)\right) + \frac{\phi_3}{4h} - \frac{\phi_4}{60h} + \mathcal{O}\left(\epsilon^2\right), \tag{3.103}$$

$$b_2 = \frac{\phi_1 - \left(\vartheta - 1\right)}{h^2} - \frac{210}{h^2}\left(\bar{\theta} - \frac{2 + 4\vartheta - \phi_1}{6}\right) + \frac{13}{h^2}\left(\phi_2 + 2\left(\vartheta - 1 - \phi_1\right)\right) - \frac{7\phi_3}{4h^2} + \frac{\phi_4}{8h^2} + \mathcal{O}\left(\epsilon^2\right), \tag{3.104}$$

$$b_3 = \frac{420}{h^3}\left(\bar{\theta} - \frac{2 + 4\vartheta - \phi_1}{6}\right) - \frac{30}{h^3}\left(\phi_2 + 2\left(\vartheta - 1 - \phi_1\right)\right) + \frac{13\phi_3}{3h^3} - \frac{\phi_4}{3h^3} + \mathcal{O}\left(\epsilon^2\right), \tag{3.105}$$

$$b_4 = \frac{420}{h^4}\left(\frac{2 + 4\vartheta - \phi_1}{6} - \bar{\theta}\right) + \frac{65}{2h^4}\left(\phi_2 + 2\left(\vartheta - 1 - \phi_1\right)\right) - \frac{5\phi_3}{h^4} + \frac{5\phi_4}{12h^4} + \mathcal{O}\left(\epsilon^2\right), \tag{3.106}$$

$$b_5 = \frac{210}{h^5}\left(\bar{\theta} - \frac{2 + 4\vartheta - \phi_1}{6}\right) - \frac{17}{h^5}\left(\phi_2 + 2\left(\vartheta - 1 - \phi_1\right)\right) + \frac{11\phi_3}{4h^5} - \frac{\phi_4}{4h^5} + \mathcal{O}\left(\epsilon^2\right), \tag{3.107}$$

$$b_6 = \frac{42}{h^6}\left(\frac{2 + 4\vartheta - \phi_1}{6} - \bar{\theta}\right) + \frac{7}{2h^6}\left(\phi_2 + 2\left(\vartheta - 1 - \phi_1\right)\right) - \frac{7\phi_3}{12h^6} + \frac{7\phi_4}{120h^6} + \mathcal{O}\left(\epsilon^2\right). \tag{3.108}$$

Equations (3.97 – 3.102) thus allow for the derivatives of $\{a_j, b_j\}$ to be found in terms of $(h, q, \upsilon, \tau_1, \tau_2, \tau_3, \tau_4)$ and $(\bar{\theta}, \vartheta, \phi_1, \phi_2, \phi_3, \phi_4)$, respectively. Note that the reason why the free-surface velocity (υ) and second shear stress gradient (τ_2) are bracketed together with the stream-wise flow rate (q) in equations (3.97 – 3.102) is because whilst these quantities are of order unity, they can be described exclusively in terms of the (h, q) in the long-wave limit; in fact, it is only at second-order in the long-wave expansion that the free-surface velocity (υ) and second shear gradient (τ_2) become decoupled from the stream-wise flow rate (q) and require their own degrees of freedom. The bracketed terms therefore represent the difference between the value of the quantity in question at

second-order and the value of the quantity predicted by its long-wave limit relationship with the flow rate; whilst the individual quantity and the flow rate may both be of order unity, the difference between them is of first-order with respect to the long-wave expansion and in this way, it can be said the expansion coefficients $\{a_j\}$ corresponding to $3 \leq j \leq 6$ are comprised entirely of first-order contributions. In the same fashion, the mean temperature ($\bar{\theta}$) and second heat flux gradient (ϕ_2) have been bracketed with the free-surface temperature (ϑ) and heat flux (ϕ_1) in equations (3.103 – 3.108).

In addition to offering the derivatives of $\{a_j, b_j\}$ in terms of the reduced variables; equations (3.97 – 3.108) allow for the velocity and temperature expansions to be split into their leading and first-order parts, $u = u_0 + \epsilon u_1 + \mathcal{O}(\epsilon^2)$ and $\theta = \theta_0 + \epsilon\theta_1 + \mathcal{O}(\epsilon^2)$, with:

$$u_0 = \frac{3q}{2h^3}\left(2h\hat{z} - \hat{z}^2\right), \tag{3.109}$$

$$\begin{aligned} u_1 = &-\frac{\tilde{\upsilon}}{h^6}\left(30h^5\hat{z} - 165h^4\hat{z}^2 + 340h^3\hat{z}^3 - 345h^2\hat{z}^2 + 174h\hat{z}^5 - 35\hat{z}^6\right) \\ &+ \frac{\tilde{\tau}_1}{h^6}\left(10h^5\hat{z} - 60h^4\hat{z}^2 + 130h^3\hat{z}^3 - 135h^2\hat{z}^2 + 69h\hat{z}^5 - 14\hat{z}^6\right) \\ &- \frac{\tilde{\tau}_2}{h^6}\left(2h^5\hat{z} - 13h^4\hat{z}^2 + 30h^3\hat{z}^3 - \frac{65}{2}h^2\hat{z}^2 + 17h\hat{z}^5 - \frac{7}{2}\hat{z}^6\right) \\ &+ \frac{\tilde{\tau}_3}{h^6}\left(\frac{h^5}{4}\hat{z} - \frac{7}{4}h^4\hat{z}^2 + \frac{13}{3}h^3\hat{z}^3 - 5h^2\hat{z}^2 + \frac{11}{4}h\hat{z}^5 - \frac{7}{12}\hat{z}^6\right) \\ &- \frac{\tilde{\tau}_4}{h^6}\left(\frac{h^5}{60}\hat{z} - \frac{h^4}{8}\hat{z}^2 + \frac{h^3}{3}\hat{z}^3 - \frac{5h^2}{12}\hat{z}^2 + \frac{h}{4}\hat{z}^5 - \frac{7}{120}\hat{z}^6\right), \end{aligned} \tag{3.110}$$

$$\theta_0 = 1 + \frac{(\vartheta - 1)}{h}\hat{z} + \frac{(\vartheta - 1 - \phi_1)}{h^2}\left(h\hat{z} - \hat{z}^2\right), \tag{3.111}$$

$$\begin{aligned} \theta_1 = &\frac{42\tilde{\theta}}{h^6}\left(h^5\hat{z} - 5h^4\hat{z}^2 + 10h^3\hat{z}^3 - 10h^2\hat{z}^2 + 5h\hat{z}^5 - \hat{z}^6\right) \\ &- \frac{\tilde{\phi}_2}{h^6}\left(2h^5\hat{z} - 13h^4\hat{z}^2 + 30h^3\hat{z}^3 - \frac{65}{2}h^2\hat{z}^2 + 17h\hat{z}^5 - \frac{7}{2}\hat{z}^6\right) \\ &+ \frac{\tilde{\phi}_3}{h^6}\left(\frac{h^5}{4}\hat{z} - \frac{7}{4}h^4\hat{z}^2 + \frac{13}{3}h^3\hat{z}^3 - 5h^2\hat{z}^2 + \frac{11}{4}h\hat{z}^5 - \frac{7}{12}\hat{z}^6\right) \\ &- \frac{\tilde{\phi}_4}{h^6}\left(\frac{h^5}{60}\hat{z} - \frac{h^4}{8}\hat{z}^2 + \frac{h^3}{3}\hat{z}^3 - \frac{5h^2}{12}\hat{z}^2 + \frac{h}{4}\hat{z}^5 - \frac{7}{120}\hat{z}^6\right). \end{aligned} \tag{3.112}$$

in which $\epsilon\tilde{\upsilon} = (\upsilon - 3q/2h)$, $\epsilon\tilde{\tau}_1 = \tau_1$, $\epsilon\tilde{\tau}_2 = (\tau_2 + 3q/h)$, $\epsilon\tilde{\tau}_3 = \tau_3$, $\epsilon\tilde{\tau}_4 = \tau_4$; and then $\epsilon\tilde{\theta} = \bar{\theta} - (2 + 4\vartheta - \phi_1)/6$, $\epsilon\tilde{\phi}_2 = \phi_2 + 2(\vartheta - 1 - \phi_1)$, $\epsilon\tilde{\phi}_3 = \phi_3$, $\epsilon\tilde{\phi}_4 = \phi_4$.

The decomposition of the velocity and temperature expansions into their leading and first-order components in equations (3.109 – 3.112), respectively, highlights an important feature which is that certain the higher-order terms, namely $\{\tilde{\upsilon}, \tilde{\tau}_2, \tilde{\theta}, \tilde{\phi}_2\}$, only arise when dynamics of two leading-order quantities diverge from some mutual relationship.

The second step in the derivation of a second-order model is to substitute the recurrence relationships into the definitions of new reduced variables (3.91 – 3.96); the

recurrence relations are stated at the beginning of this section, having originally been obtained in section 3.4.1 by substituting the power series for the flow velocity and fluid temperature into the governing equations (3.37 – 3.41) and isolating the powers of $\hat{z}$. At second-order, the recurrence relations for velocity coefficients $\{a_j\}$ are given by:

$$a_1 = \frac{2\epsilon^2 \frac{\partial f}{\partial x}\frac{\partial \upsilon}{\partial x}}{(1+\epsilon^2 g)} + \frac{\left(1-\epsilon^2 g\right)}{(1+\epsilon^2 g)}\frac{\epsilon^2\left[\frac{\partial^2 q}{\partial x^2} - \upsilon\frac{\partial^2 f}{\partial x^2}\right]}{(1+\epsilon^2 g)} - \frac{\epsilon\frac{Ma}{Ca}\frac{\partial \vartheta}{\partial x}}{[1+\epsilon^2 g]^{3/2}} - \frac{1}{h}\sum_{j=2}^{10} j h^j a_j, \tag{3.113}$$

$$a_2 = \frac{\epsilon\frac{\partial f}{\partial x}\cot\beta - 1 - \frac{\epsilon^3}{2}\frac{\partial^2}{\partial x^2}\left[\frac{\frac{1-Ma\vartheta}{Ca}\frac{\partial f}{\partial x}}{\sqrt{1+\epsilon^2 g}}\right] - \frac{\epsilon^2}{2}\frac{\partial^2 \upsilon}{\partial x^2} + \epsilon^2\left\{2\frac{ds}{dx}\frac{\partial a_1}{\partial x} + \frac{a_1}{2}\frac{d^2 s}{dx^2}\right\}}{|\ell_s|^4}, \tag{3.114}$$

$$a_3 = \frac{\epsilon Re\frac{\partial a_1}{\partial t} - \epsilon^2\frac{\partial^2 a_1}{\partial x^2}}{6|\ell_s|^2} + \frac{\epsilon^2\left\{2\frac{\partial a_2}{\partial x}\frac{ds}{dx} + a_2\frac{d^2 s}{dx^2}\right\}}{3|\ell_s|^2}, \tag{3.115}$$

$$a_4 = \frac{\epsilon Re\left\{\frac{\partial a_2}{\partial t} + \frac{a_1}{2}\frac{\partial a_1}{\partial x}\right\} - \epsilon^2\frac{\partial^2 a_2}{\partial x^2}}{12|\ell_s|^2}, \tag{3.116}$$

$$a_5 = \frac{\epsilon Re\left\{\frac{\partial a_3}{\partial t} + \frac{2a_1}{3}\frac{\partial a_2}{\partial x}\right\}}{20|\ell_s|^2}, \tag{3.117}$$

$$a_6 = \frac{\epsilon Re\left\{\frac{\partial a_4}{\partial t} + \frac{3a_1}{4}\frac{\partial a_3}{\partial x} + \frac{a_2}{3}\frac{\partial a_2}{\partial x} - \frac{a_3}{2}\frac{\partial a_1}{\partial x}\right\}}{30|\ell_s|^2}, \tag{3.118}$$

$$a_7 = \frac{\epsilon Re\left\{\frac{\partial a_5}{\partial t} + \frac{4a_1}{5}\frac{\partial a_4}{\partial x} + \frac{a_2}{2}\frac{\partial a_3}{\partial x} - a_4\frac{\partial a_1}{\partial x}\right\}}{42|\ell_s|^2}, \tag{3.119}$$

$$a_8 = \frac{\epsilon Re\left\{\frac{\partial a_6}{\partial t} + \frac{5a_1}{6}\frac{\partial a_5}{\partial x} + \frac{8a_2}{5}\frac{\partial a_4}{\partial x} - \frac{a_4}{3}\frac{\partial a_2}{\partial x} - \frac{3a_5}{2}\frac{\partial a_1}{\partial x}\right\}}{56|\ell_s|^2}, \tag{3.120}$$

$$a_9 = \frac{\epsilon Re\left\{\frac{6a_1}{7}\frac{\partial a_6}{\partial x} + \frac{2a_2}{3}\frac{\partial a_5}{\partial x} - \frac{2a_5}{3}\frac{\partial a_2}{\partial x} - 2a_6\frac{\partial a_1}{\partial x}\right\}}{72|\ell_s|^2}, \tag{3.121}$$

$$a_{10} = \frac{\epsilon Re\left\{\frac{5a_2}{7}\frac{\partial a_6}{\partial x} - a_6\frac{\partial a_2}{\partial x}\right\}}{90|\ell_s|^2}. \tag{3.122}$$

Ergo, the evolution equations describing the fluid momentum can be obtained by substituting the recurrence relations (3.113 – 3.122) into the definitions of $(q, \upsilon, \tau_1, \tau_2, \tau_3, \tau_4)$ given by equations (3.91 – 3.96) and then replacing the derivatives of $\{a_j\}$ in these equations with asymptotically equivalent expressions in terms of $(q, \upsilon, \tau_1, \tau_2, \tau_3, \tau_4)$ ascertained by differentiating equations (3.97 – 3.102) with respect to (x, t) and discarding terms which belong to beyond second-order.

In the exact same fashion, the evolution equations describing the fluid temperature can be obtained by substituting the recurrence relations for the temperature coefficients $\{b_j\}$ into the definitions of $(\vartheta, \bar{\theta}, \phi_1, \phi_2, \phi_3, \phi_4)$ given by equations (3.91 – 3.96) and then replacing the derivatives of $\{a_j, b_j\}$ in these equations with asymptotically equivalent expressions in terms of $(q, \upsilon, \tau_1, \tau_2, \tau_3, \tau_4)$ and $(\vartheta, \bar{\theta}, \phi_1, \phi_2, \phi_3, \phi_4)$, respectively. At

second-order, the recurrence relations for the temperature coefficients $\{b_j\}$ are given by:

$$b_1 = \frac{\epsilon^2 \frac{\partial f}{\partial x}\frac{\partial \vartheta}{\partial x}}{1+\epsilon^2 g} - \frac{Bi\vartheta}{\sqrt{1+\epsilon^2 g}} - \frac{1}{h}\sum_{j=2}^{10} j h^j b_j, \tag{3.123}$$

$$b_2 = \frac{\epsilon^2 \left\{ \frac{\partial b_1}{\partial x}\frac{ds}{dx} + \frac{b_1}{2}\frac{d^2 s}{dx^2} \right\}}{|\ell_s|^2}. \tag{3.124}$$

$$b_3 = \frac{\epsilon RePr \frac{\partial b_1}{\partial t}}{6|\ell_s|^2}, \tag{3.125}$$

$$b_4 = \frac{\epsilon RePr \left\{ \frac{\partial b_2}{\partial t} + a_1 \frac{\partial b_1}{\partial x} - \frac{b_1}{2}\frac{\partial a_1}{\partial x} \right\}}{12|\ell_s|^2}, \tag{3.126}$$

$$b_5 = \frac{\epsilon RePr \left\{ \frac{\partial b_3}{\partial t} + a_1 \frac{\partial b_2}{\partial x} + a_2 \frac{\partial b_1}{\partial x} - b_2 \frac{\partial a_1}{\partial x} - \frac{b_1}{3}\frac{\partial a_2}{\partial x} \right\}}{20|\ell_s|^2}, \tag{3.127}$$

$$b_6 = \frac{\epsilon RePr \left\{ \frac{\partial b_4}{\partial t} + a_1 \frac{\partial b_3}{\partial x} + a_2 \frac{\partial b_2}{\partial x} + a_3 \frac{\partial b_1}{\partial x} - \frac{b_1}{4}\frac{\partial a_3}{\partial x} - \frac{2b_2}{3}\frac{\partial a_2}{\partial x} - \frac{3b_3}{2}\frac{\partial a_1}{\partial x} \right\}}{30|\ell_s|^2}, \tag{3.128}$$

$$\begin{aligned} b_7 = {} & \frac{\epsilon RePr \left\{ \frac{\partial b_5}{\partial t} + a_1 \frac{\partial b_4}{\partial x} + a_2 \frac{\partial b_3}{\partial x} + a_3 \frac{\partial b_2}{\partial x} + a_4 \frac{\partial b_1}{\partial x} \right\}}{42|\ell_s|^2} \\ & + \frac{\epsilon RePr \left\{ -\frac{b_1}{5}\frac{\partial a_4}{\partial x} - \frac{b_2}{2}\frac{\partial a_3}{\partial x} - b_3 \frac{\partial a_2}{\partial x} - 2b_4 \frac{\partial a_1}{\partial x} \right\}}{42|\ell_s|^2}, \end{aligned} \tag{3.129}$$

$$\begin{aligned} b_8 = {} & \frac{\epsilon RePr \left\{ \frac{\partial b_6}{\partial t} + a_1 \frac{\partial b_5}{\partial x} + a_2 \frac{\partial b_4}{\partial x} + a_4 \frac{\partial b_2}{\partial x} + a_5 \frac{\partial b_1}{\partial x} \right\}}{56|\ell_s|^2} \\ & + \frac{\epsilon RePr \left\{ -\frac{b_1}{6}\frac{\partial a_5}{\partial x} - \frac{2b_2}{5}\frac{\partial a_4}{\partial x} - \frac{4b_4}{3}\frac{\partial a_2}{\partial x} - \frac{5b_5}{2}\frac{\partial a_1}{\partial x} \right\}}{56|\ell_s|^2}, \end{aligned} \tag{3.130}$$

$$b_9 = \frac{\epsilon RePr \left\{ a_1 \frac{\partial b_6}{\partial x} + a_2 \frac{\partial b_5}{\partial x} + a_5 \frac{\partial b_2}{\partial x} + a_6 \frac{\partial b_1}{\partial x} - \frac{b_1}{7}\frac{\partial a_6}{\partial x} - \frac{b_2}{3}\frac{\partial a_5}{\partial x} - \frac{5b_5}{3}\frac{\partial a_2}{\partial x} - 3b_6 \frac{\partial a_1}{\partial x} \right\}}{72|\ell_s|^2}, \tag{3.131}$$

$$b_{10} = \frac{\epsilon RePr \left\{ a_2 \frac{\partial b_6}{\partial x} + a_6 \frac{\partial b_2}{\partial x} - \frac{2b_2}{7}\frac{\partial a_6}{\partial x} - 2b_6 \frac{\partial a_2}{\partial x} \right\}}{90|\ell_s|^2}. \tag{3.132}$$

This procedure to obtaining the evolution equations for the reduced variables is very similar to the derivation process used by Cellier and Ruyer-Quil [2020] in which an evolution equation for the free-surface temperature (ϑ) is acquired by solving for the corrections to a self-similar-style temperature profile and then demanding the corrections satisfy the definition of the free-surface temperature. In fact, one will obtain the same evolution equation for the free-surface temperature whether the present derivation process is used or the one from Cellier and Ruyer-Quil [2020]; this is because the only difference here is that the corrections are solved prior to the variable transformation, in the latter derivation process, the opposite is true. To derive the evolution equations in the style of Cellier and Ruyer-Quil [2020] one would: (i) substitute $u = u_0 + \epsilon u_1 + \epsilon^2 u_2$

into the momentum equation and shear stress boundary conditions with u_0 given by equation (3.109) and u_1 given by equation (3.110), solve for u_2, and then substitute $u = u_0 + \epsilon u_1 + \epsilon^2 u_2$ into the definitions (3.91 – 3.96) to obtain a set of evolution equations for the momentum. and (ii) substitute $\theta = \theta_0 + \epsilon\theta_1 + \epsilon^2\theta_2$ into the energy equation and heat flux boundary conditions with θ_0 given by equation (3.111) and θ_1 given by equation (3.112), solve for θ_2, and then substitute $\theta = \theta_0 + \epsilon\theta_1 + \epsilon^2\theta_2$ into the definitions (3.91 – 3.96) to obtain a set of evolution equations for the temperature.

One can actually borrow a clever technique from Cellier and Ruyer-Quil [2020] which is to utilise the fact that the evaluation of the energy equation at the free-surface can be written in the following form:

$$\left.\frac{\partial^2\theta}{\partial\hat{z}^2}\right|_{\hat{z}=h} = \frac{\epsilon RePr\left\{\frac{\partial\vartheta}{\partial t} + \upsilon\frac{\partial\vartheta}{\partial x}\right\} - \epsilon^2\left\{\frac{\partial^2\vartheta}{\partial x^2} - 2\frac{\partial f}{\partial x}\frac{\partial}{\partial x}\left[\left.\frac{\partial\theta}{\partial\hat{z}}\right|_{\hat{z}=h}\right] - \left.\frac{\partial^2 f}{\partial x^2}\frac{\partial\theta}{\partial\hat{z}}\right|_{\hat{z}=h}\right\}}{(1+\epsilon^2 g)}, \tag{3.133}$$

and thus be used in place of the evolution equation obtained from substituting the corrections into the definition of ϕ_2; the two equations are asymptotically equivalent in the long-wave limit but the equation (3.133) is acquired through algebra alone and will therefore be superior because it retains the character of a strong form equation. As a matter of fact, the evolutions equations acquired from the definitions of (τ_1, τ_2, τ_3) and (ϕ_2, ϕ_3, ϕ_4) can all be replaced by equations acquired through algebra alone. This is accomplished using the following algebraic identities:

$$\begin{aligned}
\frac{\partial^2}{\partial x^2}\left[\left.\frac{\partial^n u}{\partial\hat{z}^n}\right|_{\hat{z}=h}\right] &= \left.\frac{\partial^{n+2}u}{\partial x^2\partial\hat{z}^n}\right|_{\hat{z}=h} + 2\frac{\partial f}{\partial x}\frac{\partial}{\partial x}\left[\left.\frac{\partial^{n+1}u}{\partial\hat{z}^{n+1}}\right|_{\hat{z}=h}\right] + \left.\frac{\partial^2 f}{\partial x^2}\frac{\partial^{n+1}u}{\partial\hat{z}^{n+1}}\right|_{\hat{z}=h} - g\left.\frac{\partial^{n+2}u}{\partial\hat{z}^{n+2}}\right|_{\hat{z}=h}, \\
\frac{\partial}{\partial t}\left[\left.\frac{\partial^n u}{\partial\hat{z}^n}\right|_{\hat{z}=h}\right] + \upsilon\frac{\partial}{\partial x}\left[\left.\frac{\partial^n u}{\partial\hat{z}^n}\right|_{\hat{z}=h}\right] &= \left.\frac{\partial^{n+1}u}{\partial\hat{z}^n\partial t}\right|_{\hat{z}=h} + \upsilon\left.\frac{\partial^{n+1}u}{\partial x\partial\hat{z}^n}\right|_{\hat{z}=h} + w|_{\hat{z}=h}\left.\frac{\partial^{n+1}u}{\partial\hat{z}^{n+1}}\right|_{\hat{z}=h}, \qquad (3.134) \\
\frac{\partial^2}{\partial x^2}\left[\left.\frac{\partial^n u}{\partial\hat{z}^n}\right|_{\hat{z}=h}\right] &= \left.\frac{\partial^{n+2}\theta}{\partial x^2\partial\hat{z}^n}\right|_{\hat{z}=h} + 2\frac{\partial f}{\partial x}\frac{\partial}{\partial x}\left[\left.\frac{\partial^{n+1}\theta}{\partial\hat{z}^{n+1}}\right|_{\hat{z}=h}\right] + \left.\frac{\partial^2 f}{\partial x^2}\frac{\partial^{n+1}\theta}{\partial\hat{z}^{n+1}}\right|_{\hat{z}=h} - g\left.\frac{\partial^{n+2}\theta}{\partial\hat{z}^{n+2}}\right|_{\hat{z}=h}, \\
\frac{\partial}{\partial t}\left[\left.\frac{\partial^n \theta}{\partial\hat{z}^n}\right|_{\hat{z}=h}\right] + \upsilon\frac{\partial}{\partial x}\left[\left.\frac{\partial^n \theta}{\partial\hat{z}^n}\right|_{\hat{z}=h}\right] &= \left.\frac{\partial^{n+1}\theta}{\partial\hat{z}^n\partial t}\right|_{\hat{z}=h} + \upsilon\left.\frac{\partial^{n+1}\theta}{\partial x\partial\hat{z}^n}\right|_{\hat{z}=h} + w|_{\hat{z}=h}\left.\frac{\partial^{n+1}\theta}{\partial\hat{z}^{n+1}}\right|_{\hat{z}=h}. \qquad (3.135)
\end{aligned}$$

In this way, the only evolutions equations which need to be derived using the recurrence relations are those obtained from the definitions of the flow rate (q), free-surface velocity (υ), free-surface temperature (ϑ), and mean temperature $(\bar{\theta})$ – the rest can be replaced by expressions akin to equation (3.133).

To this effect, the second-order reduced asymptotic model is comprised of: the *integral form of the kinematic condition* – equation (3.42):

$$\frac{\partial h}{\partial t} + \frac{\partial q}{\partial x} = 0, \tag{3.136}$$

four asymptotically equivalent evolution equations which serve to satisfy the definitions of $(q, \upsilon, \vartheta, \bar{\theta})$:

$$
\begin{aligned}
&q - \frac{2h^3}{3} + \epsilon\frac{2h^3}{3}\frac{\partial f}{\partial x}\cot\beta + \frac{\epsilon\frac{h^2}{2}\frac{Ma}{Ca}\frac{\partial\vartheta}{\partial x}}{\left[1+\epsilon^2 g\right]^{3/2}} + \epsilon Re\left\{\frac{5h^2}{24}\frac{\partial q}{\partial t} + \frac{59q^2}{308}\frac{\partial h}{\partial x} - \frac{5681hq}{18480}\frac{\partial q}{\partial x}\right\}\\
&- \epsilon^3\frac{h^3}{3}\frac{\partial^2}{\partial x^2}\left[\frac{\frac{1-Ma\vartheta}{Ca}\frac{\partial f}{\partial x}}{\sqrt{1+\epsilon^2 g}}\right] + \epsilon^2\left\{\frac{23hq}{40}\frac{\partial^2 h}{\partial x^2} + \frac{23h}{20}\frac{\partial h}{\partial x}\frac{\partial q}{\partial x} - \frac{2h^2}{5}\frac{\partial^2 q}{\partial x^2} - \frac{21q}{20}\left(\frac{\partial h}{\partial x}\right)^2\right.\\
&\left. - \frac{q}{4}\frac{\partial h}{\partial x}\frac{ds}{dx} + \frac{3h}{4}\frac{\partial q}{\partial x}\frac{ds}{dx} + \frac{3hq}{8}\frac{d^2 s}{dx^2} - \frac{h^3}{3}\frac{\partial^2\upsilon}{\partial x^2} - \frac{h^2}{2}\frac{2\frac{\partial f}{\partial x}\frac{\partial\upsilon}{\partial x} + \frac{\left(1-\epsilon^2 g\right)}{\left(1+\epsilon^2 g\right)}\left(\frac{\partial^2 q}{\partial x^2} - \upsilon\frac{\partial^2 f}{\partial x^2}\right)}{\left(1+\epsilon^2 g\right)}\right\}\\
&+ \epsilon Reh^2\left\{\frac{5h}{36}\frac{\partial\upsilon}{\partial t} - \frac{5h}{144}\frac{\partial\tau_1}{\partial t} + \frac{h}{180}\frac{\partial\tau_2}{\partial t} - \frac{h}{1728}\frac{\partial\tau_3}{\partial t} + \frac{h}{30240}\frac{\partial\tau_4}{\partial t} + \frac{167q}{440}\frac{\partial\upsilon}{\partial x} - \frac{31q}{352}\frac{\partial\tau_1}{\partial x}\right.\\
&+ \frac{41q}{3080}\frac{\partial\tau_2}{\partial x} - \frac{7q}{5280}\frac{\partial\tau_3}{\partial x} + \frac{9q}{123200}\frac{\partial\tau_4}{\partial x} - \left(\frac{167\upsilon}{1320} - \frac{31\tau_1}{1056} + \frac{41\tau_2}{9240} - \frac{7\tau_3}{15840}\right.\\
&\left.\left. + \frac{3\tau_4}{123200}\right)\frac{q}{h}\frac{\partial h}{\partial x} + \left(\frac{131\upsilon}{330} - \frac{23\tau_1}{264} + \frac{29\tau_2}{2310} - \frac{19\tau_3}{15840} + \frac{53\tau_4}{831600}\right)\frac{\partial q}{\partial x}\right\} = 0,
\end{aligned}
\tag{3.137}
$$

$$
\begin{aligned}
&\upsilon - h^2 + \epsilon h^2\frac{\partial f}{\partial x}\cot\beta + \frac{\epsilon h\frac{Ma}{Ca}\frac{\partial\vartheta}{\partial x}}{\left[1+\epsilon^2 g\right]^{3/2}} + \epsilon Re\left\{\frac{h}{4}\frac{\partial q}{\partial t} + \frac{17q^2}{40h}\frac{\partial h}{\partial x} - \frac{3q}{5}\frac{\partial q}{\partial x}\right\}\\
&- \epsilon^3\frac{h^2}{2}\frac{\partial^2}{\partial x^2}\left[\frac{\frac{1-Ma\vartheta}{Ca}\frac{\partial f}{\partial x}}{\sqrt{1+\epsilon^2 g}}\right] + \epsilon^2\left\{\frac{7q}{8}\frac{\partial^2 h}{\partial x^2} + \frac{7}{4}\frac{\partial h}{\partial x}\frac{\partial q}{\partial x} - \frac{5h}{8}\frac{\partial^2 q}{\partial x^2} - \frac{3q}{2h}\left(\frac{\partial h}{\partial x}\right)^2 + \frac{\partial q}{\partial x}\frac{ds}{dx}\right.\\
&\left. + \frac{q}{2}\frac{d^2 s}{dx^2} - \frac{h^2}{2}\frac{\partial^2\upsilon}{\partial x^2} - h\frac{2\frac{\partial f}{\partial x}\frac{\partial\upsilon}{\partial x} + \frac{\left(1-\epsilon^2 g\right)}{\left(1+\epsilon^2 g\right)}\left(\frac{\partial^2 q}{\partial x^2} - \upsilon\frac{\partial^2 f}{\partial x^2}\right)}{\left(1+\epsilon^2 g\right)}\right\} + \epsilon Re\left\{\frac{15h^2}{56}\frac{\partial\upsilon}{\partial t} - \frac{5h^2}{84}\frac{\partial\tau_1}{\partial t}\right.\\
&+ \frac{h^2}{112}\frac{\partial\tau_2}{\partial t} - \frac{h^2}{1120}\frac{\partial\tau_3}{\partial t} + \frac{h^2}{20160}\frac{\partial\tau_4}{\partial t} + \frac{205hq}{336}\frac{\partial\upsilon}{\partial x} - \frac{11hq}{84}\frac{\partial\tau_1}{\partial x} + \frac{191hq}{10080}\frac{\partial\tau_2}{\partial x}\\
&- \frac{37hq}{20160}\frac{\partial\tau_3}{\partial x} + \frac{hq}{10080}\frac{\partial\tau_4}{\partial x} + \left(-\frac{31\upsilon}{112} + \frac{47\tau_1}{840} - \frac{79\tau_2}{10080} + \frac{\tau_3}{1344} - \frac{\tau_4}{25200}\right)q\frac{\partial h}{\partial x}\\
&\left. + \left(\frac{211\upsilon}{336} - \frac{13\tau_1}{105} + \frac{169\tau_2}{10080} - \frac{31\tau_3}{20160} + \frac{\tau_4}{12600}\right)h\frac{\partial q}{\partial x}\right\} = 0,
\end{aligned}
\tag{3.138}
$$

$$\vartheta-1+\frac{Bih\vartheta}{\sqrt{1+\epsilon^2 g}}+\epsilon RePr\Bigg\{\frac{15h^2}{56}\frac{\partial\vartheta}{\partial t}+\frac{h^2}{4}\frac{\partial\bar{\theta}}{\partial t}-\frac{5h^2}{84}\frac{\partial\phi_1}{\partial t}+\frac{h^2}{112}\frac{\partial\phi_2}{\partial t}-\frac{h^2}{1120}\frac{\partial\phi_3}{\partial t}$$
$$+\frac{h^2}{20160}\frac{\partial\phi_4}{\partial t}+\frac{hq}{5}\frac{\partial\bar{\theta}}{\partial x}+\frac{3hq}{224}\frac{\partial\phi_2}{\partial x}-\frac{13hq}{10080}\frac{\partial\phi_3}{\partial x}+\frac{hq}{14400}\frac{\partial\phi_4}{\partial x}+\Bigg(\frac{h^2}{9}\frac{\partial\upsilon}{\partial x}-\frac{h^2}{40}\frac{\partial\tau_1}{\partial x}$$
$$+\frac{h^2}{270}\frac{\partial\tau_2}{\partial x}-\frac{11h^2}{30240}\frac{\partial\tau_3}{\partial x}+\frac{h^2}{50400}\frac{\partial\tau_4}{\partial x}\Bigg)(\vartheta-1)+\Bigg(\frac{h^2}{56}\frac{\partial\upsilon}{\partial x}+\frac{h^2}{5040}\frac{\partial\tau_1}{\partial x}-\frac{h^2}{3024}\frac{\partial\tau_2}{\partial x}$$
$$+\frac{h^2}{20160}\frac{\partial\tau_3}{\partial x}-\frac{h^2}{302400}\frac{\partial\tau_4}{\partial x}\Bigg)\phi_1-\Bigg(\frac{73}{1680}\frac{q}{h}+\frac{19\upsilon}{504}-\frac{4\tau_1}{315}+\frac{11\tau_2}{5040}-\frac{\tau_3}{4320}+\frac{\tau_4}{75600}\Bigg)h^2\frac{\partial\phi_1}{\partial x}$$
$$+\Bigg(\frac{3}{112}\frac{q}{h}+\frac{149\upsilon}{504}-\frac{157\tau_1}{2520}+\frac{\tau_2}{112}-\frac{13\tau_3}{15120}+\frac{\tau_4}{21600}\Bigg)h^2\frac{\partial\vartheta}{\partial x}+\Bigg(\frac{\upsilon}{9}-\frac{\tau_1}{40}+\frac{\tau_2}{270}$$
$$-\frac{11\tau_3}{30240}+\frac{\tau_4}{50400}\Bigg)h\left(\vartheta-1\right)\frac{\partial h}{\partial x}+\Bigg(\frac{\upsilon}{56}+\frac{\tau_1}{5040}-\frac{\tau_2}{3024}+\frac{\tau_3}{20160}-\frac{\tau_4}{302400}\Bigg)h\phi_1\frac{\partial h}{\partial x}$$
$$+\Bigg(\frac{41}{252}+\frac{73\vartheta}{2520}-\frac{23\bar{\theta}}{120}-\frac{293\phi_1}{5040}+\frac{17\phi_2}{5040}-\frac{\phi_3}{4032}+\frac{\phi_4}{100800}\Bigg)h\frac{\partial q}{\partial x}\Bigg\}+\epsilon^2\Bigg\{-\frac{h\frac{\partial f}{\partial x}\frac{\partial\vartheta}{\partial x}}{1+\epsilon^2 g}$$
$$-\frac{5h^2}{12}\frac{\partial^2\vartheta}{\partial x^2}+\frac{h}{3}\frac{\partial h}{\partial x}\frac{\partial\vartheta}{\partial x}+\frac{2h}{3}\frac{ds}{dx}\frac{\partial\vartheta}{\partial x}+\frac{h^2}{12}\frac{\partial^2\phi_1}{\partial x^2}+\frac{h}{3}\frac{\partial f}{\partial x}\frac{\partial\phi_1}{\partial x}\frac{\vartheta-1+\phi_1}{6}h\frac{\partial^2 h}{\partial x^2}$$
$$+\frac{2\left(\vartheta-1\right)-5\phi_1}{3}\frac{\partial h}{\partial x}\frac{ds}{dx}+\frac{2\left(\vartheta-1\right)+\phi_1}{6}h\frac{d^2 s}{dx^2}+\frac{\left(\vartheta-1\right)-5\phi_1}{6}\left(\frac{\partial h}{\partial x}\right)^2\Bigg\}=0, \tag{3.139}$$

$$\bar{\theta}-1+\frac{1}{2}\frac{Bih\vartheta}{\sqrt{1+\epsilon^2 g}}+\epsilon RePr\Bigg\{\frac{5h^2}{36}\frac{\partial\vartheta}{\partial t}+\frac{5h^2}{24}\frac{\partial\bar{\theta}}{\partial t}-\frac{5h^2}{144}\frac{\partial\phi_1}{\partial t}+\frac{h^2}{180}\frac{\partial\phi_2}{\partial t}-\frac{h^2}{1728}\frac{\partial\phi_3}{\partial t}$$
$$+\frac{h^2}{30240}\frac{\partial\phi_4}{\partial t}+\frac{71hq}{440}\frac{\partial\bar{\theta}}{\partial x}+\frac{41hq}{4620}\frac{\partial\phi_2}{\partial x}-\frac{7hq}{7920}\frac{\partial\phi_3}{\partial x}+\frac{3hq}{61600}\frac{\partial\phi_4}{\partial x}+\Bigg(\frac{167h^2}{1980}\frac{\partial\upsilon}{\partial x}-\frac{31h^2}{1584}\frac{\partial\tau_1}{\partial x}$$
$$+\frac{41h^2}{13860}\frac{\partial\tau_2}{\partial x}-\frac{7h^2}{23760}\frac{\partial\tau_3}{\partial x}+\frac{h^2}{61600}\frac{\partial\tau_4}{\partial x}\Bigg)(\vartheta-1)+\Bigg(\frac{439h^2}{55440}\frac{\partial\upsilon}{\partial x}+\frac{17h^2}{18480}\frac{\partial\tau_1}{\partial x}-\frac{23h^2}{66528}\frac{\partial\tau_2}{\partial x}$$
$$+\frac{31h^2}{665280}\frac{\partial\tau_3}{\partial x}-\frac{h^2}{332640}\frac{\partial\tau_4}{\partial x}\Bigg)\phi_1-\Bigg(\frac{587}{18480}\frac{q}{h}+\frac{1157\upsilon}{55440}-\frac{443\tau_1}{55440}+\frac{23\tau_2}{15840}-\frac{53\tau_3}{332640}$$
$$+\frac{31\tau_4}{3326400}\Bigg)h^2\frac{\partial\phi_1}{\partial x}+\Bigg(\frac{41}{2310}\frac{q}{h}+\frac{167\upsilon}{990}-\frac{31\tau_1}{792}+\frac{41\tau_2}{6930}-\frac{7\tau_3}{11880}+\frac{\tau_4}{30800}\Bigg)h^2\frac{\partial\vartheta}{\partial x}$$
$$+\Bigg(\frac{167\upsilon}{1980}-\frac{31\tau_1}{1584}+\frac{41\tau_2}{13860}-\frac{7\tau_3}{23760}+\frac{\tau_4}{61600}\Bigg)h\left(\vartheta-1\right)\frac{\partial h}{\partial x}+\Bigg(\frac{439\upsilon}{55440}+\frac{17\tau_1}{18480}$$
$$-\frac{23\tau_2}{66528}+\frac{31\tau_3}{665280}-\frac{\tau_4}{332640}\Bigg)h\phi_1\frac{\partial h}{\partial x}+\Bigg(\frac{17}{140}+\frac{81\vartheta}{3080}-\frac{13\bar{\theta}}{88}-\frac{2291\phi_1}{55440}+\frac{17\phi_2}{4620}$$
$$-\frac{\phi_3}{3168}+\frac{\phi_4}{66528}\Bigg)h\frac{\partial q}{\partial x}\Bigg\}+\epsilon^2\Bigg\{-\frac{\frac{h}{2}\frac{\partial f}{\partial x}\frac{\partial\vartheta}{\partial x}}{1+\epsilon^2 g}\frac{14\left(\vartheta-1\right)+11\phi_1}{120}h\frac{\partial^2 h}{\partial x^2}+\frac{\left(\vartheta-1\right)-3\phi_1}{3}\frac{\partial h}{\partial x}\frac{ds}{dx}$$
$$+\frac{3\left(\vartheta-1\right)+\phi_1}{12}h\frac{d^2 s}{dx^2}-\frac{4h^2}{15}\frac{\partial^2\vartheta}{\partial x^2}+\frac{4\left(\vartheta-1\right)-29\phi_1}{60}\left(\frac{\partial h}{\partial x}\right)^2+\frac{7h}{30}\frac{\partial h}{\partial x}\frac{\partial\vartheta}{\partial x}$$
$$+\frac{h}{2}\frac{ds}{dx}\frac{\partial\vartheta}{\partial x}+\frac{7h^2}{120}\frac{\partial^2\phi_1}{\partial x^2}+\frac{11h}{60}\frac{\partial h}{\partial x}\frac{\partial\phi_1}{\partial x}+\frac{h}{6}\frac{ds}{dx}\frac{\partial\phi_1}{\partial x}\Bigg\}=0, \tag{3.140}$$

which are coupled to the shear stress and heat flux conditions, plus the evaluations of the momentum and energy equations at the free-surface and their $\hat{z}$-gradients; namely:

$$\tau_1 + \frac{\epsilon h \frac{Ma}{Ca}\frac{\partial \vartheta}{\partial x}}{[1+\epsilon^2 g]^{3/2}} - \epsilon^2 h\left\{\frac{2\frac{\partial f}{\partial x}\frac{\partial \upsilon}{\partial x}}{(1+\epsilon^2 g)} + \frac{(1-\epsilon^2 g)}{(1+\epsilon^2 g)}\frac{\left(\frac{\partial^2 q}{\partial x^2} - \upsilon\frac{\partial^2 f}{\partial x^2}\right)}{(1+\epsilon^2 g)}\right\} = 0, \tag{3.141}$$

$$\tau_2 + 2h^2 - 2\epsilon h^2\frac{\partial f}{\partial x}\cot\beta - \epsilon Re h^2\left\{\frac{\partial \upsilon}{\partial t} + \upsilon\frac{\partial \upsilon}{\partial x}\right\} + \epsilon^2\left\{3\frac{\partial^2 \upsilon}{\partial x^2} - 4\frac{\partial f}{\partial x}\frac{\partial}{\partial x}\left(\frac{\tau_1}{h}\right) - 2\frac{\tau_1}{h}\frac{\partial^2 f}{\partial x^2}\right\} + \epsilon^3 h^2\frac{\partial^2}{\partial x^2}\left[\frac{\frac{1-Ma\vartheta}{Ca}\frac{\partial f}{\partial x}}{\sqrt{1+\epsilon^2 g}}\right] = 0, \tag{3.142}$$

$$\tau_n - \epsilon Re h^n\left\{\frac{\partial}{\partial t}\left[\frac{\tau_{n-2}}{h^{n-2}}\right] + \upsilon\frac{\partial}{\partial x}\left[\frac{\tau_{n-2}}{h^{n-2}}\right]\right\} + \epsilon^2\left\{2\frac{\partial^2}{\partial x^2}\left[\frac{\tau_{n-2}}{h^{n-2}}\right] - 4\frac{\partial f}{\partial x}\frac{\partial}{\partial x}\left[\frac{\tau_{n-1}}{h^{n-1}}\right] - 2\frac{\tau_{n-1}}{h^{n-1}}\frac{\partial^2 f}{\partial x^2}\right\} = 0, \tag{3.143}$$

$$\phi_1 + \frac{Bih\vartheta}{\sqrt{1+\epsilon^2 g}} - \frac{\epsilon^2 h\frac{\partial f}{\partial x}\frac{\partial \vartheta}{\partial x}}{(1+\epsilon^2 g)} = 0, \tag{3.144}$$

$$\phi_2 - \epsilon RePr h^2\left\{\frac{\partial \vartheta}{\partial t} + \upsilon\frac{\partial \vartheta}{\partial x}\right\} + \epsilon^2 h^2\left\{\frac{\partial^2 \vartheta}{\partial x^2} - 2\frac{\partial f}{\partial x}\frac{\partial}{\partial x}\left[\frac{\phi_1}{h}\right] - \frac{\phi_1}{h}\frac{\partial^2 f}{\partial x^2}\right\} = 0, \tag{3.145}$$

$$\phi_n - \epsilon RePr h^n\left\{\frac{\partial}{\partial t}\left[\frac{\phi_{n-2}}{h^{n-2}}\right] + \upsilon\frac{\partial}{\partial x}\left[\frac{\phi_{n-2}}{h^{n-2}}\right]\right\} + \epsilon^2 h^n\left\{\frac{\partial^2}{\partial x^2}\left(\frac{\phi_{n-2}}{h^{n-2}}\right) - 2\frac{\partial f}{\partial x}\frac{\partial}{\partial x}\left(\frac{\phi_{n-1}}{h^{n-1}}\right) - \frac{\phi_{n-1}}{h^{n-1}}\frac{\partial^2 f}{\partial x^2}\right\} = 0, \tag{3.146}$$

for $n = 3, 4$.

Equations (3.136 – 3.146) form the complete reduced asymptotic model at second-order in the long-wave expansion and represent a significant increase in complexity when compared to the first-order equations (3.86 – 3.88). Of particular concern, is the appearance of multiple partial derivatives with respect to time in equations (3.137 – 3.140) which suggests additional manipulation of the equations would be necessary if one desired to use the equations in time-dependent analysis; fortunately, only the steady-state behaviour and linear stability of equations above are considered in the present monograph. Unfortunately, it will be shown the present formulation of the complete second-order model is poorly behaved and fails to offer accurate predictions of the film dynamics; in fact, the complete second-order model derived here is only accurate for the case of planar substrate $s(x) = 0$ and in the limit of $\epsilon \to 0$ as its steady solutions diverge from corresponding solutions to the full equation set (2.23 – 2.31 when $\epsilon \neq 0$ and $s(x) \neq 0$. This poor behaviour stems from the introduction of new degrees of freedom; the new degrees of freedom introduce second-order terms which are in linear combination with the existing leading- and first-order terms, therefore, the anticipation is that these second-order terms will become negligible when the square of the shallowness parameter is vanishingly small, *i.e.* $\epsilon^2 \sim 0$, and in such cases the accuracy of the lower-order model should be recovered by the higher-order model. Unfortunately, this is not the case as

the lower-order model is seen to outperform the higher-order model in Chapter 6; this clearly indicates that the second-order terms are not becoming negligible as anticipated and hints that there must be a flaw in the derivation procedure presented currently, ergo, extension of the modelling approach to second-order for the problem of gravity-driven film flow down uniformly heated, smoothly corrugated substrate remains as incomplete. Nevertheless, a viable approach to modelling the film dynamics is to simplify equations (3.136 – 3.146) by assuming the new degrees of freedom introduced at second-order are still described in terms of their behaviour at first-order; namely:

$$\lim_{\epsilon\to 0} \upsilon = \frac{3q}{2h}, \qquad \lim_{\epsilon\to 0} \tau_2 = -\frac{3q}{h}, \qquad \lim_{\epsilon\to 0} \bar{\theta} = \frac{2 + 4\vartheta + Bih\vartheta}{6}, \tag{3.147}$$

$$\lim_{\epsilon\to 0} \phi_1 = -Bih\vartheta, \qquad \lim_{\epsilon\to 0} \phi_2 = 2 - 2\left(1 + Bih\right)\vartheta, \qquad \lim_{\epsilon\to 0} \left(\tau_1, \tau_3, \tau_4, \phi_3, \phi_4\right) = 0, \tag{3.148}$$

which allows for the second-order model to be expressed as three equations in terms of three variables (h, q, ϑ), and re-introduces significant stiffness into the reduced asymptotic model. Alternatively, one could selectively eliminate the degrees of freedom depending upon the specifications of the problem using the limiting behaviours in equations (3.147 – 3.148); in this way, one would arrive at an asymptotic model similar in structure to Cellier and Ruyer-Quil [2020] who compared a single-variable heat transfer model in terms of (ϑ) against a two-variable model in terms of (ϑ, ϕ_2). However, a legitimate critique of the work done by Cellier and Ruyer-Quil [2020] is that in obtaining their single-variable model they assumed $\lim_{\epsilon\to 0} \phi_2 = 0$, however, whilst ϕ_2 does tend to zero in the long-wave limit, its algebraic form remains non-trivial as long as $Bi > 0$ and this must be reflected in the modelling. In consequence, Cellier and Ruyer-Quil [2020] placed an unnecessary constraint on their single-variable model which in turn will have hampered its performance, suggesting the introduction of their second temperature variable, ϕ_2, led to a much greater improvement in performance than it actually does. As a matter of fact, if one takes the two-variable self-similar-style temperature profile from Cellier and Ruyer-Quil [2020] and allows ϕ_2 to be described by the limiting behaviour given in equation (3.148), then they will recover the quadratic self-similar temperature profile located in equation (3.90) and which was first seen in Daly et al. [2022].

Higher-order and simplified models

Due to the poor performance of the complete second-order model derived presently, no complete model is derived beyond second order in the long-wave expansion; instead, only simplified higher-order models are considered beyond second order in which the higher-order terms, such as those corresponding to the vertical inertia and vertical viscous dissipation, are only ever approximated to the lowest degree using (u_0, θ_0) – equations (3.89 – 3.90). In any simplified model, the dynamics of $\{\upsilon, \tau_1, \tau_2, \tau_3, \tau_4, \bar{\theta}, \phi_1, \phi_2, \phi_3, \phi_4\}$ are assumed to follow their long-wave behaviour given by equations (3.147 – 3.148). In any event, it would be useful to establish a labelling system for the reduced asymptotic

models under consideration which vary both in their long-wave order but also in their complexity with respect to the $\hat{z}$-coordinate. Accordingly, each model derived following the modelling approach laid out in this section is referred to as a reduced asymptotic model (or RAM for short) and is said to be of nth-order in the long-wave expansion where n corresponds to the highest order derivative with respect (x, t) contained within the model, whilst the complexity of each model corresponds to the number of degrees of freedom with respect to $\hat{z}$ that it possesses. Ergo, equations (3.136 – 3.146) would be referred to as a second-order reduced asymptotic model of degree six, or $RAM[\epsilon^2/\hat{z}^6]$ for short, since all the expansion coefficients corresponding up to $\hat{z}^6$ are functions of (x, t). Meanwhile, a fourth-order reduced asymptotic model of degree two; namely:

$$\frac{\partial h}{\partial t}+\frac{\partial q}{\partial x}=0, \tag{3.149}$$

$$\epsilon Re\left[\frac{\partial q}{\partial t}-\frac{9}{7}\frac{q^2}{h^2}\frac{\partial h}{\partial x}+\frac{17}{7}\frac{q}{h}\frac{\partial q}{\partial x}\right]+\epsilon^3 Re\Bigg[\frac{29}{56}\frac{\partial q}{\partial t}\left(\frac{\partial h}{\partial x}\right)^2+\frac{107h}{336}\frac{\partial q}{\partial t}\frac{\partial^2 h}{\partial x^2}+\frac{73q^2}{128}\frac{d^3 s}{dx^3}$$
$$+\frac{29}{32}\left(\frac{\partial q}{\partial x}\right)^2\frac{ds}{dx}+\frac{509}{672}\left(\frac{\partial q}{\partial x}\right)^2\frac{\partial h}{\partial x}-\frac{187q}{1344}\frac{\partial^2 q}{\partial x^2}\frac{\partial h}{\partial x}+\frac{277q}{128}\frac{\partial q}{\partial x}\frac{d^2 s}{dx^2}-\frac{15q}{64}\frac{\partial^2 q}{\partial x^2}\frac{ds}{dx}$$
$$+\frac{163q^2}{448h}\frac{\partial^2 h}{\partial x^2}\frac{ds}{dx}-\frac{185q^2}{896h}\frac{\partial h}{\partial x}\frac{d^2 s}{dx^2}+\frac{9q^2}{7h}\frac{d^2 s}{dx^2}\frac{ds}{dx}-\frac{11h^2}{56}\frac{\partial^3 q}{\partial x^2\partial t}+\frac{17q}{7h}\frac{\partial q}{\partial x}\left(\frac{ds}{dx}\right)^2$$
$$+\frac{1205q^2}{2688}\frac{\partial^3 h}{\partial x^3}-\frac{601hq}{1008}\frac{\partial^3 q}{\partial x^3}-\frac{683h}{1008}\frac{\partial^2 q}{\partial x^2}\frac{\partial q}{\partial x}+\frac{297q}{224h}\frac{\partial q}{\partial x}\frac{\partial h}{\partial x}\frac{ds}{dx}+\frac{4633q}{2688}\frac{\partial q}{\partial x}\frac{\partial^2 h}{\partial x^2}$$
$$-\frac{555q^2}{896h}\frac{\partial^2 h}{\partial x^2}\frac{\partial h}{\partial x}+\frac{11}{8}\frac{\partial q}{\partial t}\frac{\partial h}{\partial x}\frac{ds}{dx}+\frac{\partial q}{\partial t}\left(\frac{ds}{dx}\right)^2+\frac{5h}{12}\frac{\partial q}{\partial t}\frac{d^2 s}{dx^2}+\frac{115q^2}{672h^2}\left(\frac{\partial h}{\partial x}\right)^3$$
$$-\frac{11h}{56}\frac{\partial^2 q}{\partial x\partial t}\frac{\partial h}{\partial x}-\frac{163q^2}{224h^2}\left(\frac{\partial h}{\partial x}\right)^2\frac{ds}{dx}-\frac{253q}{672h}\frac{\partial q}{\partial x}\left(\frac{\partial h}{\partial x}\right)^2-\frac{9q^2}{7h^2}\frac{\partial h}{\partial x}\left(\frac{ds}{dx}\right)^2\Bigg]$$
$$+\epsilon^4\Bigg[\frac{15}{4h}\frac{\partial q}{\partial x}\left(\frac{ds}{dx}\right)^3+\frac{5q}{2h^2}\left(\frac{ds}{dx}\right)^4-\frac{30q}{7h^2}\left(\frac{\partial h}{\partial x}\right)^4+\frac{61}{14h}\frac{\partial q}{\partial x}\left(\frac{\partial h}{\partial x}\right)^3-\frac{q}{4}\frac{\partial h}{\partial x}\frac{d^3 s}{dx^3}$$
$$-7\frac{\partial q}{\partial x}\frac{d^2 s}{dx^2}\frac{ds}{dx}-\frac{q}{4}\frac{\partial^3 h}{\partial x^3}\frac{ds}{dx}-\frac{5h}{3}\frac{\partial^2 q}{\partial x^2}\frac{d^2 s}{dx^2}+\frac{49q}{4h}\frac{\partial h}{\partial x}\frac{d^2 s}{dx^2}\frac{ds}{dx}-\frac{107qh}{336}\frac{\partial^4 h}{\partial x^4}$$
$$-\frac{5qh}{12}\frac{d^4 s}{dx^4}-\frac{5h}{3}\frac{\partial q}{\partial x}\frac{d^3 s}{dx^3}+\frac{113q}{28h}\frac{\partial^2 h}{\partial x^2}\left(\frac{\partial h}{\partial x}\right)^2+\frac{19q}{4h}\left(\frac{\partial h}{\partial x}\right)^2\frac{d^2 s}{dx^2}-\frac{23}{4}\frac{\partial^2 q}{\partial x^2}\frac{\partial h}{\partial x}\frac{ds}{dx}$$
$$+\frac{3q}{7}\frac{\partial^3 h}{\partial x^3}\frac{\partial h}{\partial x}+\frac{45q}{8h}\frac{d^2 s}{dx^2}\left(\frac{ds}{dx}\right)^2+\frac{7q}{8}\frac{\partial^2 h}{\partial x^2}\frac{d^2 s}{dx^2}-\frac{107h}{84}\frac{\partial q}{\partial x}\frac{\partial^3 h}{\partial x^3}-\frac{19}{4}\frac{\partial^2 q}{\partial x^2}\left(\frac{ds}{dx}\right)^2$$
$$-\frac{13}{7}\frac{\partial^2 q}{\partial x^2}\left(\frac{\partial h}{\partial x}\right)^2+\frac{12q}{h}\frac{\partial^2 h}{\partial x^2}\frac{\partial h}{\partial x}\frac{ds}{dx}+\frac{29}{2h}\frac{\partial q}{\partial x}\left(\frac{\partial h}{\partial x}\right)^2\frac{ds}{dx}-\frac{53q}{4h^2}\left(\frac{\partial h}{\partial x}\right)^2\left(\frac{ds}{dx}\right)^2$$
$$+\frac{53q}{56}\left(\frac{\partial^2 h}{\partial x^2}\right)^2-\frac{q}{2}\left(\frac{d^2 s}{dx^2}\right)^2-\frac{17}{14}\frac{\partial q}{\partial x}\frac{\partial^2 h}{\partial x^2}\frac{\partial h}{\partial x}+\frac{11h}{28}\frac{\partial^3 q}{\partial x^3}\frac{\partial h}{\partial x}-\frac{14q}{h^2}\left(\frac{\partial h}{\partial x}\right)^3\frac{ds}{dx}$$
$$-\frac{13}{4}\frac{\partial q}{\partial x}\frac{\partial h}{\partial x}\frac{d^2 s}{dx^2}-\frac{3q}{2}\frac{d^3 s}{dx^3}\frac{ds}{dx}-\frac{181h}{168}\frac{\partial^2 q}{\partial x^2}\frac{\partial^2 h}{\partial x^2}+\frac{59}{4h}\frac{\partial q}{\partial x}\frac{\partial h}{\partial x}\left(\frac{ds}{dx}\right)^2+\frac{11h^2}{56}\frac{\partial^4 q}{\partial x^4}$$
$$-\frac{13}{4}\frac{\partial q}{\partial x}\frac{\partial^2 h}{\partial x^2}\frac{ds}{dx}+\frac{59q}{8h}\frac{\partial^2 h}{\partial x^2}\left(\frac{ds}{dx}\right)^2-\frac{5q}{4h^2}\frac{\partial h}{\partial x}\left(\frac{ds}{dx}\right)^3\Bigg]+\frac{\epsilon\frac{5}{4}\frac{Ma}{Ca}\frac{\partial\vartheta}{\partial x}}{[1+\epsilon^2 g]^{3/2}}$$
$$+\epsilon^2\Bigg[\frac{5q}{h^2}\left(\frac{ds}{dx}\right)^2+\frac{15q}{8h}\frac{d^2 s}{dx^2}+\frac{15}{4h}\frac{\partial q}{\partial x}\frac{ds}{dx}+\frac{33}{4h}\frac{\partial q}{\partial x}\frac{\partial h}{\partial x}-\frac{31q}{4h^2}\left(\frac{\partial h}{\partial x}\right)^2+\frac{33q}{8h}\frac{\partial^2 h}{\partial x^2}$$
$$-\frac{13}{4}\frac{\partial^2 q}{\partial x^2}-\frac{5q}{4h^2}\frac{\partial h}{\partial x}\frac{ds}{dx}-\frac{15}{4}\frac{\frac{\partial f}{\partial x}\frac{\partial}{\partial x}\left[\frac{q}{h}\right]}{1+\epsilon^2 g}-\frac{15}{8}\frac{1-\epsilon^2 g}{1+\epsilon^2 g}\frac{\frac{2}{3}\frac{\partial^2 q}{\partial x^2}-\frac{q}{h}\frac{\partial^2 f}{\partial x^2}}{1+\epsilon^2 g}\Bigg]$$
$$+\epsilon\frac{5h}{3}\frac{\partial f}{\partial x}\cot\beta+\frac{5q}{2h^2}-\frac{5h}{3}-\epsilon^3\frac{5h}{6}\frac{\partial^2}{\partial x^2}\left[\frac{(1-Ma\vartheta)}{Ca}\frac{\frac{\partial f}{\partial x}}{\sqrt{1+\epsilon^2 g}}\right]=0, \tag{3.150}$$

$$
\begin{aligned}
\epsilon RePr\Bigg[& \frac{Bih}{\sqrt{1+\epsilon^2 g}}\left(\frac{1}{5}\frac{\partial\vartheta}{\partial t}-\frac{11}{50}\frac{\vartheta}{h}\frac{\partial q}{\partial x}+\frac{6}{25}\frac{q\vartheta}{h^2}\frac{\partial h}{\partial x}+\frac{6}{25}\frac{q}{h}\frac{\partial\vartheta}{\partial x}\right)+\frac{3}{25}\frac{(\vartheta-1)}{h}\frac{\partial q}{\partial x} \\
& +\frac{33}{25}\frac{q}{h}\frac{\partial\vartheta}{\partial x}+\frac{\partial\vartheta}{\partial t}\Bigg]+\frac{\epsilon^3 RePrBih\vartheta}{\left[1+\epsilon^2 g\right]^{3/2}}\frac{\partial f}{\partial x}\Bigg[\frac{1}{5}\frac{\partial^2 q}{\partial x^2}-\frac{6}{5}\frac{q}{h}\frac{\partial^2 f}{\partial x^2}\Bigg] \\
+\epsilon^2\Bigg[& \frac{4\left(\vartheta-1\right)}{5h}\frac{d^2 s}{dx^2}+\frac{12\left(\vartheta-1\right)}{5h^2}\left(\frac{ds}{dx}\right)^2+\frac{2\left(\vartheta-1\right)}{5h^2}\left(\frac{\partial h}{\partial x}\right)^2+\frac{2\left(\vartheta-1\right)}{5h}\frac{\partial^2 h}{\partial x^2} \\
& +\frac{8\left(\vartheta-1\right)}{5h^2}\frac{\partial h}{\partial x}\frac{ds}{dx}+\frac{\partial^2\vartheta}{\partial x^2}+\frac{8}{5h}\frac{\partial\vartheta}{\partial x}\frac{ds}{dx}+\frac{4}{5h}\frac{\partial h}{\partial x}\frac{\partial\vartheta}{\partial x}-\frac{12}{5h}\frac{\frac{\partial f}{\partial x}\frac{\partial\vartheta}{\partial x}}{1+\epsilon^2 g}\Bigg] \\
+\epsilon^2\frac{Bi}{\sqrt{1+\epsilon^2 g}}\Bigg[& \frac{6\vartheta}{5h}\left(\frac{\partial h}{\partial x}\right)^2+\frac{16\vartheta}{5h}\frac{\partial h}{\partial x}\frac{ds}{dx}+\frac{12\vartheta}{5h}\left(\frac{ds}{dx}\right)^2-\frac{3\vartheta}{5}\frac{\partial^2 h}{\partial x^2}-\frac{2\vartheta}{5}\frac{d^2 s}{dx^2} \\
& -\frac{6}{5}\frac{\partial h}{\partial x}\frac{\partial\vartheta}{\partial x}-\frac{4}{5}\frac{\partial\vartheta}{\partial x}\frac{ds}{dx}-\frac{h}{5}\frac{\partial^2\vartheta}{\partial x^2}\Bigg]+\epsilon^4\frac{Bi}{\left[1+\epsilon^2 g\right]^{3/2}}\Bigg[\frac{h\vartheta}{5}\frac{\partial f}{\partial x}\frac{\partial^3 f}{\partial x^3} \\
& +\frac{6\vartheta}{5}\left(\frac{\partial h}{\partial x}\right)^2\frac{\partial^2 f}{\partial x^2}+2\vartheta\frac{\partial h}{\partial x}\frac{ds}{dx}\frac{\partial^2 f}{\partial x^2}+\frac{4\vartheta}{5}\left(\frac{ds}{dx}\right)^2\frac{\partial^2 f}{\partial x^2}+\frac{2h}{5}\frac{\partial f}{\partial x}\frac{\partial^2 f}{\partial x^2}\frac{\partial\vartheta}{\partial x}\Bigg] \\
+\epsilon^4\frac{2Bih\vartheta}{5}\frac{1-\epsilon^2 g}{\left[1+\epsilon^2 g\right]^{5/2}}\left(\frac{\partial^2 f}{\partial x^2}\right)^2+\frac{12}{5h^2}\Bigg[& \vartheta-1+\frac{Bih\vartheta}{\sqrt{1+\epsilon^2 g}}\Bigg]=0, \qquad (3.151)
\end{aligned}
$$

is referred to as $RAM[\epsilon^4/\hat{z}^2]$. From equations (3.149 – 3.151), one can obtain $RAM[\epsilon^n/\hat{z}^2]$ for $n \leq 4$ by discarding all terms sharing a factor of ϵ^m where $m > n$ – the only exception is the capillary pressure term which is retained in all RAM formalisms because this term plays a key role in stabilising the liquid film and its algebraic form is independent of the number of degrees of freedom afforded to the velocity field with respect to $\hat{z}$, thus its inclusion ahead of its formal order does not negatively impact the asymptotic behaviour of the RAM formulation.

Unless specified otherwise, every reduced asymptotic model considered in the subsequent chapters will be referred to using this naming convention.

Chapter 4

Methodology II: Linear Stability Analysis

In the present thesis, the stability of the gravity-driven film flow is studied using linear stability analysis. As implied by the name, the linearised theory only takes into account the linear time evolution of the system of interest; this is achieved by considering a small time-dependent perturbation $\hat{h}$ to a stationary solution of the system and only retaining linear terms in $\hat{h}$. In this way, the evolution of $\hat{h}$ is described by:

$$\frac{d\hat{h}}{dt} = a\hat{h} + \mathcal{O}\left(\hat{h}^2\right), \tag{4.1}$$

where a is a constant *w.r.t.* $\hat{h}$; note however, that the above linear description of the film's evolution is only strictly valid for infinitesimal disturbances, $\hat{h} \ll 1$. Howbeit, the Hartman-Grobman theorem asserts the linear evolution of a disturbance is sufficient to describe the qualitative behaviour of a dynamical system in the neighbourhood of a hyperbolic equilibrium point; a hyperbolic equilibrium point is a stationary solution for which $\Re(a) \neq 0$ in equation (4.1), where $\Re(a)$ denotes the real part of a. When $\Re(a) = 0$, the evolution of the system is described by non-linear terms in equation (4.1).

To begin, the classical hydrodynamic stability problem of a gravity-driven film flowing down a inclined, uniformly heated plane is set out according to the linearised theory of Orr [1907a,b], Sommerfeld [1908], such that the linear stability of the complete governing equation set (2.23 – 2.31) can be determined for the special case of $s(x) = 0$ $\forall x$. The Orr-Sommerfeld theory establishes a benchmark from which the quantitative accuracy of linear stability results obtained from the Benney equation and reduced asymptotic models can be measured. The linear stability analysis of the asymptotic models is then extended to smoothly corrugated substrate via Floquet theory [Floquet, 1883] – see Glendinning [1994], Chicone [1999]. In practice, the key difference between the linearised theory of Orr [1907a,b], Sommerfeld [1908] and Floquet theory is in how the disturbance to the equilibrium state is modelled: in the former, the disturbance

takes the form of a single plane wave whereas in Floquet theory, the disturbance is expanded as a Fourier series so that the different harmonics of the disturbance are taken into account.

4.1 The Orr-Sommerfeld equation

The hydrodynamic stability of a *"gravity-driven film flowing down an inclined plane"* is described by the Orr-Sommerfeld equation. The Orr-Sommerfeld system corresponding to the problem of heated gravity-driven film flow is derived by considering an infinitesimal disturbance to the laminar Nusselt velocity and temperature distributions, namely:

$$\left.\begin{aligned} u &= u_{\mathbb{N}}|_{h=1} + \frac{\partial\hat{\psi}}{\partial\hat{z}}, & w &= -\frac{\partial\hat{\psi}}{\partial x}, \\ \theta &= \theta_{\mathbb{N}}|_{h=1} + \hat{\theta}, & h &= 1+\hat{h}, \end{aligned}\right\} \tag{4.2}$$

where $(u_{\mathbb{N}}, \theta_{\mathbb{N}})$ correspond to the Nusselt solutions given by expressions (3.7), $\hat{\psi}$ is the perturbation stream-function satisfying the continuity equation (2.23), $\hat{\theta}$ is the perturbation to the temperature field, and $\hat{h}$ is the perturbation to the film thickness.

Perturbations to the laminar Nusselt flow are described via a separation of variables:

$$\hat{\psi} = \breve{\psi}(\hat{z})e^{i(2\pi Qx-\omega t)}, \qquad \hat{\theta} = \breve{\theta}(\hat{z})e^{i(2\pi Qx-\omega t)}, \qquad \hat{h} = \breve{h}e^{i(2\pi Qx-\omega t)}, \tag{4.3}$$

where Q is the wave-number and ω is angular frequency of the disturbance, respectively.

The Orr-Sommerfeld equation is obtained by substituting the fluid pressure – equation (2.40) – and expressions (4.2 – 4.3) into the x-momentum equation (2.24) and differentiating once *w.r.t.* $\hat{z}$ with $s(x) = 0\ \forall x$; the equation is then linearised by discarding all non-linear terms in $\left(\breve{\psi}, \breve{\theta}, \breve{h}\right)$. The linearised energy equation is acquired by substituting expressions (4.2 – 4.3) into the *convection-diffusion* equation (2.26), and discarding all non-linear terms in (ψ, θ). The resulting linearised equations read:

$$\frac{\partial^4\breve{\psi}}{\partial\hat{z}^4} - 2\tilde{Q}^2\frac{\partial^2\breve{\psi}}{\partial\hat{z}^2} + \tilde{Q}^4\breve{\psi} = i\tilde{Q}Re\left[(u_{\mathbb{N}}-c)\left(\frac{\partial^2\breve{\psi}}{\partial\hat{z}^2} - \tilde{Q}^2\breve{\psi}\right) + 2\breve{\psi}\right], \tag{4.4}$$

$$\frac{\partial^2\breve{\theta}}{\partial\hat{z}^2} - \tilde{Q}^2\breve{\theta} = i\tilde{Q}RePr\left[(u_{\mathbb{N}}-c)\,\breve{\theta} - \frac{\breve{\psi}}{1+Bi}\right]. \tag{4.5}$$

where $\tilde{Q} = 2\epsilon\pi Q$ is the reduced wave-number and $c = \omega/(2\pi Q)$ is the phase velocity. Boundary conditions which accompany equations (4.4 – 4.5) are obtained by substituting expressions (4.2 – 4.3) into equations (2.27), (2.36) and (2.41 – 2.42) – note that $h = 1+\hat{h}$; and discarding all non-linear terms in $\left(\breve{\psi}, \breve{\theta}, \breve{h}\right)$. The linearised boundary conditions read:

$$\breve{\psi}\big|_{\hat{z}=0} = 0, \qquad \left.\frac{\partial\breve{\psi}}{\partial\hat{z}}\right|_{\hat{z}=0} = 0, \qquad \breve{\psi}\big|_{\hat{z}=h} = (c-1)\,\breve{h}, \tag{4.6}$$

$$\left.\frac{\partial^2\breve{\psi}}{\partial\hat{z}^2}\right|_{\hat{z}=h} = 2\breve{h} - \tilde{Q}^2\,\breve{\psi}\big|_{\hat{z}=h} + i\tilde{Q}\frac{Ma}{CaBi}\left.\frac{\partial\breve{\theta}}{\partial\hat{z}}\right|_{\hat{z}=h}, \tag{4.7}$$

$$\breve{\theta}\big|_{\hat{z}=0} = 0, \qquad \left.\frac{\partial\breve{\theta}}{\partial\hat{z}}\right|_{\hat{z}=h} = Bi\left[\frac{Bi\breve{h}}{1+Bi} - \breve{\theta}\big|_{\hat{z}=h}\right]. \tag{4.8}$$

The final boundary condition is acquired by substituting the fluid pressure – equation (2.40) – and expressions (4.2 – 4.3) into the x-momentum equation – equation (2.24) – and evaluating at $\hat{z} = h$; discarding all non-linear terms in $\left(\breve{\psi}, \breve{\theta}, \breve{h}\right)$ then yields:

$$\left.\frac{\partial^3\breve{\psi}}{\partial\hat{z}^3}\right|_{\hat{z}=h} = 3\tilde{Q}^2\left.\frac{\partial\breve{\psi}}{\partial\hat{z}}\right|_{\hat{z}=h} + i\tilde{Q}\left[Re\,(1-c)\left.\frac{\partial\breve{\psi}}{\partial\hat{z}}\right|_{\hat{z}=h} + \left(2\cot\beta + \tilde{Q}^2\frac{1-\frac{Ma}{1+Bi}}{Ca}\right)\breve{h}\right]. \tag{4.9}$$

Equations (4.4 – 4.9) represent an eigenvalue problem in c describing one-dimensional disturbances to laminar Nusselt flow; the method of solutions with which these eigenvalues can be found are laid out in the next chapter. Formulating the Orr-Sommerfeld system as an eigenvalue problem with respect to c corresponds to studying the temporal linear stability of gravity-driven film flow with the wave-number Q being wholly real and the angular frequency ω being complex, $\omega = \Re(\omega) + i\Im(\omega)$ where $i = \sqrt{-1}$ is the imaginary unity. The flow is considered: (i) stable when c possesses a negative imaginary part; (ii) unstable when any c possesses a positive imaginary part; and (iii) neutrally stable when any c is wholly real and every other c possesses a negative imaginary part. It is the final case which of the main interest as finding the conditions under which the flow is neutrally stable allows for one to define a boundary between stability and instability. An alternative way to find this boundary is to study the spatial linear stability in which $Q \in \mathbb{C}$ and $\omega \in \mathbb{R}$; however, this would lead to a polynomial eigenvalue in Q and since, at neutral stability, the dominant eigenvalue possesses both $Q \in \mathbb{R}$ and $\omega \in \mathbb{R}$, it does not matter whether the boundary is found through a temporal or a spatial analysis as the two converge will converge at said boundary.

The solutions to the Orr-Sommerfeld system – equations (4.4 – 4.9) – provide a benchmark for the special case of film flow down a uniformly heated, inclined plane, *i.e.* $s(x) = 0 \forall x$, which with the accuracy of the linear stability results obtained from the Benney equation and reduced asymptotic models can be compared and quantified.

4.2 Floquet Theory

The stability of film flow down smoothly corrugated substrate is explored using the Floquet approach of Trifonov [2014a,b]; extended to the thermal problem here and

applied exclusively to the asymptotic models derived in chapter 3. Floquet theory is used to study the linear stability of film flow over corrugated substrate because the domain is periodic with respect to the x-coordinate – see section 2.2; from Floquet's theorem, it can then be stated that if the steady-state flow and temperature profiles are periodic functions with a minimum period corresponding to the substrate wavelength, L_0, then the stability of these solutions can be analysed through a sum of Floquet harmonics.

The strategy of the Floquet approach is thereby very similar to the linearised theory utilised in section 4.1 with the system of interest being perturbed and linearised with respect to its respective degrees of freedom; however, in the Floquet approach, the perturbations to the steady-state system correspond to a sum of harmonics and are each represented by a Fourier series. For a three-equation model expressed in terms of (h, q, ϑ), perturbations are introduced for each degree of freedom; namely:

$$h = h_s(x) + \hat{h}(x,t), \qquad q = q_s(x) + \hat{q}(x,t), \qquad \vartheta = \vartheta_s(x) + \hat{\vartheta}(x,t), \tag{4.10}$$

where (h_s, q_s, ϑ_s) are the steady-state solutions to the system of interest, and $(\hat{h}, \hat{q}, \hat{\vartheta})$ are an infinitesimal perturbation to this equilibrium state. Substituting the perturbations into the three-equation model and discarding all non-linear terms in $(\hat{h}, \hat{q}, \hat{\vartheta})$ yields:

$$\frac{\partial \hat{h}}{\partial t} + \frac{\partial \hat{q}}{\partial x} = 0, \tag{4.11}$$

$$\sum_{k=0}^{k=2} \alpha_k(x) \frac{\partial^{k+1} \hat{q}}{\partial x^k \partial t} + \sum_{k=0}^{k=4} \left[\beta_k(x) \frac{\partial^k \hat{h}}{\partial x^k} + \gamma_k(x) \frac{\partial^k \hat{q}}{\partial x^k} + \xi_k(x) \frac{\partial^k \hat{\vartheta}}{\partial x^k} \right] = 0, \tag{4.12}$$

$$\zeta_0(x) \frac{\partial \hat{\vartheta}}{\partial t} + \sum_{k=0}^{k=2} \left[\eta_k(x) \frac{\partial^k \hat{h}}{\partial x^k} + \mu_k(x) \frac{\partial^k \hat{q}}{\partial x} + \nu_k(x) \frac{\partial^k \hat{\vartheta}}{\partial x^k} \right] = 0, \tag{4.13}$$

where $\{\alpha_k, \beta_k, \gamma_k, \xi_k, \zeta_k, \eta_k, \mu_k, \nu_k\}$ are linearised periodic coefficients comprised of the steady-state solutions (h_s, q_s, ϑ_s). The disturbances $(\hat{h}, \hat{q}, \hat{\vartheta})$ are then modelled by a sum of Floquet wave harmonics, which take the form of a Fourier series; namely:

$$\hat{h} = \sum_{m=-\mathcal{F}}^{m=\mathcal{F}} \breve{h}_m e^{i(2\pi(Q+m)x - \omega t)}, \tag{4.14}$$

$$\hat{q} = \sum_{m=-\mathcal{F}}^{m=\mathcal{F}} \breve{q}_m e^{i(2\pi(Q+m)x - \omega t)}, \tag{4.15}$$

$$\hat{\vartheta} = \sum_{m=-\mathcal{F}}^{m=\mathcal{F}} \breve{\vartheta}_m e^{i(2\pi(Q+m)x - \omega t)}, \tag{4.16}$$

where $Q \in [0, 1]$ is the Floquet parameter (i.e. wave-number), ω is the angular frequency,

$\mathcal{F} \in \mathbb{Z}$ is the number of Floquet harmonics, and $(\breve{h}_m, \breve{q}_m, \breve{\vartheta}_m)$ are the disturbance amplitudes. Substituting expressions (4.14 – 4.16) into equations (4.11 – 4.13) and then applying a Fourier transform to each linearised equation, $\mathrm{f}(x)$, like so:

$$\mathrm{F} = \int_0^1 \mathrm{f}(x) e^{-2\pi i n x} dx \qquad for \quad n = -\mathcal{F}, ..., \mathcal{F}, \tag{4.17}$$

separates the linearised stability problem into its constitute harmonic components. Focusing on the temporal stability, $Q \in \mathbb{R}$ and $\omega \in \mathbb{C}$; the harmonic components then form a generalised eigenvalue problem $(\mathbf{A} - c\mathbf{B})\,\hat{x} = 0$ in which the phase velocity $c = \omega / (2\pi Q)$ serves as the eigenvalue, thus $c \in \mathbb{C}$, and the disturbance amplitudes $(\breve{h}_m, \breve{q}_m, \breve{\vartheta}_m)$ constitute the eigenvector. The matrix $(\mathbf{A} - c\mathbf{B})$ is a $3(2\mathcal{F}+1)$-square matrix with row entries given by the following expressions:

$$\sum_{m=-\mathcal{F}}^{m=\mathcal{F}} \delta_{m,n} \left[-c\breve{h}_m + \left(1 + \frac{m}{Q}\right) \breve{q}_m \right] = 0, \tag{4.18}$$

$$\sum_{m=-\mathcal{F}}^{m=\mathcal{F}} \sum_{k=0}^{k=4} (2\pi i\,(Q+m))^k \left[\hat{\beta}_{k,n-m} \breve{h}_m + \left(\hat{\gamma}_{k,n-m} - c\,(2\pi i Q)\,\hat{\alpha}_{k,n-m} \right) \breve{q}_m + \hat{\xi}_{k,n-m} \breve{\vartheta}_m \right] = 0, \tag{4.19}$$

$$\sum_{m=-\mathcal{F}}^{m=\mathcal{F}} \sum_{k=0}^{k=2} (2\pi i\,(Q+m))^k \left[\hat{\eta}_{k,n-m} \breve{h}_m + \hat{\mu}_{k,n-m} \breve{q}_m + \left(\hat{\nu}_{k,n-m} - c\,(2\pi i Q)\,\hat{\zeta}_{k,n-m} \right) \breve{\vartheta}_m \right] = 0, \tag{4.20}$$

for $n = -\mathcal{F}, ..., \mathcal{F}$; where $\delta_{m,n}$ is the Kronecker-delta function which equals one if $m = n$ and zero otherwise, meanwhile $\hat{\varphi}_{k,n-m} = \int_0^1 \varphi_k(x) e^{-2\pi i (n-m) x} dx$ are the Fourier expansion coefficients arising from the linearised periodic coefficients, $\varphi_k(x)$. In the work reported here, the eigenvalues to the linearised stability problem were found numerically using Matlab's built-in subroutine *eig* and the stability was determined from the eigenvalue c possessing the largest positive imaginary part, *i.e. the eigenvalue with the largest growth rate is the most unstable and therefore dominates the stability*; if there are no eigenvalues possessing a positive imaginary part then the film is considered stable. Neutral stability is defined as when instabilities neither grow nor decay in an exponential fashion; this ensues when the eigenvalue of the most unstable mode is wholly real.

When performing the analysis, it is sufficient to consider only half the interval of the Floquet parameter (i.e. wave-number), $Q \in \left[0, \frac{1}{2}\right]$. This is because the symmetry and periodicity of the eigenvalues, $c_n(-Q) = c_n^*(Q)$ and $c_n(Q+1) = c_n(Q)$ respectively; lead to, $c_n\left(\frac{1}{2} + Q\right) = c_n^*\left(\frac{1}{2} - Q\right)$.

The Floquet theory outlined above is easily extended to the other asymptotic models considered in this thesis by introducing or eliminating the necessary degrees of freedom

to/from equations (4.10, 4.14 – 4.16). For an asymptotic model possessing n degrees of freedom, the generalised eigenvalue problem with consist of a $n\,(2\mathcal{F}+1)$-square matrix; and when only a single Floquet harmonic is considered, $\mathcal{F} = 0$, the stability analysis reduces to the Orr-Sommerfeld theory outlined in section 4.1.

4.3 Squire's theorem and non-linear stability

In the present thesis, the stability of gravity-driven film flow is analysed exclusively within a two-dimensional framework; this is inspired by Squire's theorem which states that one-dimensional surface instabilities are the most unstable modes in the context of (parallel) shear flows and thus define the flow stability. The same is assumed to be true here for gravity-driven film flow, however, it is important to highlight that Squire's theorem is not applicable to problems involving thermo-capillarity as the Marngoni effect may cause two-dimensional surface instabilities to appear ahead of one-dimensional ones [Scheid et al., 2008]. Nonetheless, Squire's theorem is imprecisely upheld on the grounds that: (i) for most fluids, the Marangoni number (Ma) is a small quantity because the rate-of-change of surface tension *w.r.t.* temperature is small and thus one-dimensional surface instabilities arising from the hydrodynamic instability mode remain dominant [Kalliadasis et al., 2003b]; and (ii) there is a significant lack of experimental data available for the heated film problem and so the validation of any asymptotic model relies primarily upon comparison with benchmark numerical solutions, to this effect, restricting the analysis to two-dimensions provides an efficient way to test the quantitative accuracy of the asymptotic model in question.

Another constraint on the stability analysis performed presently, is that it is restricted exclusively to the linear stability of liquid film flow. Fortunately, the Hartman-Grobman theorem asserts that scrutinising the linear stability of the steady-state solutions is sufficient to determine whether the flow is stable or unstable, $\Im(c) < 0$ or $\Im(c) > 0$, respectively; however, in the case of neutral stability, the linear theory only confirms that there is no disturbance which will grow in an exponential fashion, it does not take into account the non-linear evolution of instabilities and thereby cannot confirm that there are in fact no unstable modes. Indeed, in order to determine the stability characteristics of the film at neutral stability, one would need to study the non-linear evolution of disturbance either through the Stuart-Landau equation, travelling wave solutions, or full time-dependent simulations. All of these tasks are beyond the scope of the present study but are raised here to clarify that linear stability analysis only begins to scratch the surface of the wave dynamics at play in gravity-driven liquid film flow.

Chapter 5

Methodology III: Methods of Solution

The following chapter outlines the analytic and numeric schemes used to obtain solutions to the full equation set (2.23 – 2.31), the asymptotic models derived in chapter 3 and the Orr-Sommerfeld equation laid out in chapter 4.

5.1 Steady-state solutions to the Navier-Stokes and energy equations via a finite-element method

In order to validate the steady-state solutions for film flow over smoothly corrugated, uniformly heated substrate obtained from the asymptotic models derived in Chapter 3, the corresponding steady-state solutions to the full equation set (2.23 – 2.31) were obtained using a purpose-built finite element formulation capable of locating the *a priori* free-surface position. In the finite element method, the unknown fields describing the fluid velocity, temperature, pressure and grid coordinates are expanded in terms of a set of basis functions; namely:

$$\mathbf{u} = \sum_{i=1}^{N_i} \mathbf{u}_i \gamma_i, \qquad \theta = \sum_{i=1}^{N_i} \theta_i \gamma_i, \qquad p = \sum_{j=1}^{N_j} p_j \lambda_j, \qquad \mathbf{r} = \sum_{i=1}^{N_i} \mathbf{r}_i \gamma_i, \tag{5.1}$$

where $\mathbf{u} = (u, v, w)$ and $\mathbf{r} = (x, y, z)$; with $\mathbf{u}_i$, θ_i, p_j and $\mathbf{r}$ being unknown nodal values of the fluid velocity, temperature, pressure and coordinate fields, respectively; $\{N_i, N_j\}$ being the total number of nodes for the $\mathbf{u}/\theta/\mathbf{r}$ and p fields, respectively; and $\{\gamma_i, \lambda_j\}$ being the set of basis functions for the $\mathbf{u}/\theta/\mathbf{r}$ and p fields, respectively. The solutions to $(\mathbf{u}, \theta, p, \mathbf{r})$ were sought on an unstructured triangular mesh using a 'mixed-interpolation' formalism in which linear basis (interpolation) functions were used for the pressure field, and quadratic basis (interpolation) functions were used for the velocity, temperature and mesh coordinate fields – explaining why N_i and N_j are separate quantities. In contrast to

an 'equal-order-interpolation', a 'mixed-interpolation' must satisfy the Ladyzhenskaya-Babuška-Brezzi (LBB) condition which gives the criteria for when the discretisation is stable and ensures the pressure field is not polluted by spurious non-physical oscillations.

The strong form equations (2.23 – 2.31) are transformed into a set of weak form equation via a Bubnov-Galerkin weighted-residual formalism, which assumes the weight functions in the weighted-residual procedure are the same as the basis (interpolation) functions used to discretise the velocity, temperature, pressure and coordinate fields. Ergo, the momentum equation is converted into a discrete system of algebraic equations by multiplying it by the set of basis functions $\{\gamma_i\}$ and integrating each over the domain Ω; the resulting equations are placed into a divergence form using the continuity equation (2.23), the boundary conditions (2.27 – 2.31), and the volume and surface divergence theorems; the last two allow for the order of the spatial derivatives to be lowered in the weak form equations; namely:

$$\begin{aligned} 0 &= \int_{\Omega} \left\{ Re\left(\mathbf{u}\cdot\nabla\mathbf{u}\right) - \nabla\hat{\tau} - \vec{\mathbf{g}} \right\} \gamma_i d\Omega, \\ &= \int_{\Omega} \left\{ \left[\tau - Re\left(\mathbf{u}\otimes\mathbf{u}\right) \right] \nabla\gamma_i - \vec{\mathbf{g}}\gamma_i \right\} d\Omega + \int_{S} \left(\frac{1 - Ma\vartheta}{Ca} \right) \nabla_s \gamma_i dS, \end{aligned} \tag{5.2}$$

where $\hat{\tau} = -p\mathbb{I} + \left(\nabla\times\mathbf{u}\right) + \left(\nabla\times\mathbf{u}\right)^T$ is the Cauchy stress tensor, $\vec{\mathbf{g}} = 2\left(-1, 0, \cot\beta\right)$ is the acceleration due to gravity, $\otimes$ denotes the outer (tensor) product, $\nabla_s = \left(\mathbb{I} - \hat{n}\otimes\hat{n}\right)\cdot\nabla$ is the surface gradient operator, and dS denotes the surface integral.

In a similar fashion, the continuity and convection-diffusion equations are discretised via the Bubnov-Galerkin method like so:

$$0 = \int_{\Omega} \nabla\cdot\mathbf{u}\lambda_j d\Omega, \tag{5.3}$$

$$\begin{aligned} 0 &= \int_{\Omega} \left\{ RePr\left(\mathbf{u}\cdot\nabla\theta\right) - \nabla^2\theta \right\} \gamma_i d\Omega, \\ &= \int_{\Omega} \left\{ \left[\nabla\theta - RePr\left(\mathbf{u}\theta\right) \right] \right\} \nabla\gamma_i d\Omega + Bi \int_{S} \vartheta\gamma_i dS, \end{aligned} \tag{5.4}$$

and finally, the kinematic boundary condition; namely:

$$0 = \int_{S} \left(\hat{n}\cdot\mathbf{u}\right) \gamma_S dS \tag{5.5}$$

for each node belonging to the $\mathbf{u}/\theta/\mathbf{r}$ field which lies on the free-surface; ergo, $\{\gamma_S\}$ represents the set of basis functions corresponding to the nodes which lie on the free-surface and $N_s < N_i$ is the total number of nodes which lie on the free-surface.

The discrete system is completed via the spine method, which relates the positions of the mesh nodes, $\mathbf{r}_i$, to a set of free-surface parameters which are called spinal distances,

$\{h_S\}$, and whose values determine how the mesh adapts in response to the deformable free boundary at the surface of the liquid layer – for further details see Gaskell et al. [2004], Scholle et al. [2008], Veremieiev et al. [2015]. The relation is thus:

$$\mathbf{r}_i = \Delta_{i,S}\left(\mathbf{r}_S^b + h_S d_S\right) = \mathbf{r}_i^b + \Delta_{i,S} h_S \mathbf{d}_S, \tag{5.6}$$

where $\Delta_{i,S}$ is the Boolean matrix, whilst $\mathbf{r}_S^b$ and $\mathbf{d}_S$ are fixed base nodes and direction vectors of the spines, respectively – these direction vectors always lie normal to the x-axis. Every moving mesh node $\mathbf{r}_i$ is made to lie on a spine and as a result possesses an associated fixed base node, $\mathbf{r}_i^b = \Delta_{i,S}\mathbf{r}_S^b$, and direction vector, $\mathbf{d}_i = \Delta_{i,S}\mathbf{S}$, whose length will be less than the displacement between the spine's free-surface node and its base node. The Boolean matrix, $\Delta_{i,S}$, is defined as:

$$\Delta i, S = \begin{cases} 1, & \text{if the global node } i \text{ lies on the spine } k, \\ 0, & \text{otherwise.} \end{cases}$$

The no-slip and constant substrate temperature boundary conditions were incorporated into the weak form equations explicitly by replacing the corresponding weighted residual equations with the values given by equations (2.27). The system of discrete equations was linearised via the Newton-Raphson method with Jacobian matrices evaluated analytically and solved using a parallel multi-frontal method available in the MUMPS library. With the Jacobians calculated analytically, only two or three Newton-Raphson iterations were typically needed to reduce the norm of the residual equation below 10^{-6}; the number of elements in the unstructured triangular mesh was increased systematically until the maximum difference between the free-surface profile prediction on consecutive meshes was less than 0.05%. The distribution of nodes in the irregular finite element grid was heavily concentrated close to the corrugated substrate and at the free-surface, as these locations represent contain the most sophisticated dynamics. For more information on the finite-element analogue used in the present study, see Veremieiev [2011].

5.2 Steady-state solutions to the asymptotic models via a finite difference scheme

Steady-state solutions for the problem of film flow over smoothly corrugated substrate were acquired via a finite difference scheme from the asymptotic models derived in chapter 3. The procedure is simple because the degrees of freedom of the respective asymptotic models are only functions of (x, t) and in the steady-state problem, this reduces to just being functions of x because $\partial/\partial t \to 0$; ergo, each asymptotic model needs only be solved with respect to the single independent variable x.

Accordingly, the spatial domain of the problem, $x \in [0, 1]$, is discretised into a finite number of points, N_x, such that the value of a given degree of freedom, $\varphi(x)$, at the ith

discrete point on the spatial domain is denoted by φ_i. For each point on the discrete spatial domain, x_i, there will be a corresponding equation obtained by substituting $\varphi(x_i) = \varphi_i$ into the asymptotic model under consideration. The derivatives of a given degree of freedom, φ, with respect to x at the ith point on the spatial domain are then computed through a central difference scheme with second-order accuracy; namely:

$$\frac{\partial \varphi_i}{\partial x} = \frac{\varphi_{i+1} - \varphi_{i-1}}{2\Delta x} + \mathcal{O}\left(\Delta x^2\right), \tag{5.7}$$

$$\frac{\partial^2 \varphi_i}{\partial x^2} = \frac{\varphi_{i+2} - 2\varphi_i + \varphi_{i-2}}{\Delta x^2} + \mathcal{O}\left(\Delta x^2\right), \tag{5.8}$$

$$\frac{\partial^3 \varphi_i}{\partial x^3} = \frac{\varphi_{i+2} - 2\varphi_{i+1} + 2\varphi_{i-1} - \varphi_{i-2}}{2\Delta x^3} + \mathcal{O}\left(\Delta x^2\right), \tag{5.9}$$

$$\frac{\partial^4 \varphi_i}{\partial x^4} = \frac{\varphi_{i+2} - 4\varphi_{i+1} + 6\varphi_i - 4\varphi_{i-1} + \varphi_{i-2}}{\Delta x^4} + \mathcal{O}\left(\Delta x^2\right), \tag{5.10}$$

where $\Delta x = 1/N_x$ is the size of one spatial step. Note that the problem is considered periodic with respect to the x-domain; ergo, $\varphi_{N_x+1} = \varphi_1$, $\varphi_{(-1)} = \varphi_{N_x-1}$, etc.

To illustrate this process, the Benney equation (3.21) which possesses only one degree of freedom – the film thickness, $h(x,t)$ – would be written in discrete form like so:

$$2h_i^2 \frac{\partial h_i}{\partial x} + \epsilon \Bigg\{ Re \left(\frac{8h_i^6}{15} \frac{\partial^2 h_i}{\partial x^2} + \frac{16h_i^5}{5} \left(\frac{\partial h_i}{\partial x} \right)^2 \right) - 2h_i^2 \left(\frac{\partial h_i}{\partial x} \frac{\partial f_i}{\partial x} + \frac{h_i}{3} \frac{\partial^2 f_i}{\partial x^2} \right) \cot \beta$$
$$- h_i \frac{Ma}{Ca} \left(\frac{\partial h_i}{\partial x} \frac{\partial \vartheta_0}{\partial x} + \frac{h_i}{2} \frac{\partial^2 \vartheta_0}{\partial x^2} \right) \Bigg\} + \mathcal{O}\left(\epsilon^2\right) = 0, \tag{5.11}$$

if surface curvature, $g = 0$, and higher-order terms, $\sim \mathcal{O}\left(\epsilon^3\right)$, are neglected; to this effect, $\vartheta_0 = 1/(1 + Bih_i)$. Equation (5.11) would thereby be responsible for governing the dynamics of the film at the ith point on the spatial domain; ergo, for a spatial domain consisting of N_x discrete points, one will have N_x discrete equations in terms of $\{h_i\}$ which can be solved numerically. In the present study, the system of discrete equations corresponding to the asymptotic models derived via the procedures laid out in chapter 3 were solved using Matlab's built-in *fsolve* subroutine.

In the case of the mutil-variable reduced asymptotic models – see section 3.4.3; each degree of freedom must be discretised just as the film thickness is the Benney equation. The only exception is the stream-wise flow rate (q) which can be seen to be constant in the steady-state problem as equation (2.36) gives $\partial q/\partial x = 0$. Accordingly, the steady flow rate (q_s) must be replaced by an appropriate expression in the steady-state problem which is constant across the entire spatial domain; a suitable expression for q_s is offered by the long-wave flow rate solution which states $q = \frac{2}{3}h^3$ as $\epsilon \to 0$. From the long-wave flow rate solution one can either: (i) assume the steady flow rate remains

the same as the long-wave value which leads to $q = \frac{2}{3}$; or (ii) assume the steady flow rate become a function of the mean film thickness which leads to $q = \frac{2}{3}\bar{h}^3$ where $\bar{h} = \int_0^1 h dx = (1/N_x)\sum_{i=0}^{N_x} h_i$ is the mean thickness of the film. Indeed, the mean thickness of a film flowing over corrugated substrate is typically larger than the Nusselt laminar film thickness, *i.e.* $\bar{h} > 1$ which might suggest the steady flow rate increases in the presence of substrate corrugations; however, the non-steady flow rate is known to decrease in the presence of surface instabilities, and this could also be the case for the steady flow rate in film flow over corrugated substrate. In any event, the solutions arising from each assumption are compared in chapter 6.

5.3 Solutions to the Orr-Sommerfeld equation

Validation of the linear stability results obtained from the asymptotic models for the case of planar substrate ($s(x) = 0\ \forall x$) is achieved through comparison with the corresponding solutions belonging to the Orr-Sommerfeld equation set – derived in chapter 4. As stated in chapter 4, one-dimensional surface waves constitute the most unstable modes in isothermal film flow down planar substrate [Kelly et al., 1986], the same is true for heated film flow provided the temperature difference between the substrate and ambient air remains reasonably small, $\Theta_\Delta \leq 100K$ [Kalliadasis et al., 2003a]. Under this conjecture, it can be said that the Orr-Sommerfeld system of equations governs the hydrodynamic stability of a gravity-driven liquid film flowing down a planar uniformly heated incline.

In the current section, the Orr-Sommerfeld system of equations is recast like so:

$$\frac{i}{Re}\frac{\partial^4\breve{\psi}}{\partial\hat{z}^4} + \left(u_{\mathbb{N}}\tilde{Q} - \frac{2i\tilde{Q}^2}{Re}\right)\frac{\partial^2\breve{\psi}}{\partial\hat{z}^2} + \left(2\tilde{Q} - u_{\mathbb{N}}\tilde{Q}^3 + \frac{i\tilde{Q}^4}{Re}\right)\breve{\psi} = c\tilde{Q}\left(\frac{\partial^2\breve{\psi}}{\partial\hat{z}^2} - \tilde{Q}^2\breve{\psi}\right), \quad (5.12)$$

$$\frac{i}{RePr}\frac{\partial^2\breve{\theta}}{\partial\hat{z}^2} + \left(u_{\mathbb{N}}\tilde{Q} - \frac{i\tilde{Q}^2}{RePr}\right)\breve{\theta} - \frac{\tilde{Q}}{1+Bi}\breve{\psi} = c\tilde{Q}\breve{\theta}. \quad (5.13)$$

$$\breve{\psi}\big|_{\hat{z}=0} = 0, \qquad \left.\frac{\partial\breve{\psi}}{\partial\hat{z}}\right|_{\hat{z}=0} = 0, \qquad \breve{\theta}\big|_{\hat{z}=0} = 0, \qquad \breve{\psi}\big|_{\hat{z}=h} + \breve{h} = c\breve{h}, \quad (5.14)$$

$$\left.\frac{\partial^2\breve{\psi}}{\partial\hat{z}^2}\right|_{\hat{z}=h} + \tilde{Q}^2\breve{\psi}\big|_{\hat{z}=h} - i\tilde{Q}\frac{Ma}{CaBi}\left.\frac{\partial\breve{\theta}}{\partial\hat{z}}\right|_{\hat{z}=h} - 2\breve{h} = 0, \quad Bi\breve{\theta}\big|_{\hat{z}=h} + \left.\frac{\partial\breve{\theta}}{\partial\hat{z}}\right|_{\hat{z}=h} - \frac{Bi^2\breve{h}}{1+Bi} = 0, \quad (5.15)$$

$$\frac{i}{Re}\left.\frac{\partial^3\breve{\psi}}{\partial\hat{z}^3}\right|_{\hat{z}=h} + \left(\tilde{Q} - \frac{3i\tilde{Q}^2}{Re}\right)\left.\frac{\partial\breve{\psi}}{\partial\hat{z}}\right|_{\hat{z}=h} + \left(\frac{2\cot\beta}{Re} + \frac{1 - \frac{Ma}{1+Bi}}{CaRe}\tilde{Q}^2\right)\tilde{Q}\breve{h} = c\tilde{Q}\left.\frac{\partial\breve{\psi}}{\partial\hat{z}}\right|_{\hat{z}=h}. \quad (5.16)$$

so that the phase velocity c only appears on the right hand-side in the equations above; $(\breve{\psi}, \breve{\theta})$ represent the disturbances to the Nusselt stream-function and temperature distributions, respectively; meanwhile, $\breve{h}$ is the amplitude of the surface disturbance and $\tilde{Q} = 2\pi\epsilon Q$ is the reduced wave-number of the surface disturbance.

Solutions to the Orr-Sommerfeld system of equations (5.12 – 5.16) are sought by expanding the perturbation stream-function ($\breve{\psi}$) and temperature ($\breve{\theta}$) distributions via

two methods: (i) a perturbation series expansion; and (ii) a polynomial expansion. Two varieties of polynomial expansion are used to solve the Orr-Sommerfeld system; the first is a power series in $\hat{z}$, whilst the second utilises the Chebyshev polynomials ($\mathcal{T}_n$).

5.3.1 Perturbation series

An asymptotic solution to the Orr-Sommerfeld equations can be found using perturbation theory [Yih, 1963]. Within this framework: the perturbation stream-function ($\breve{\psi}$) and temperature ($\breve{\theta}$), along with the phase velocity (c) are expanded with respect to the reduced wave-number ($\tilde{Q}$) in the following fashion:

$$\left(\breve{\psi}, \breve{\theta}, c\right) = \left(\breve{\psi}_0, \breve{\theta}_0, c_0\right) + \tilde{Q}\left(\breve{\psi}_1, \breve{\theta}_1, c_1\right) + \tilde{Q}^2\left(\breve{\psi}_2, \breve{\theta}_2, c_2\right) + ... \tag{5.17}$$

where $\{\breve{\psi}_0, \breve{\theta}_0, c_0\}$ are the exact solutions to the Orr-Sommerfeld problem in the long wave limit, whilst $\{\breve{\psi}_n, \breve{\theta}_n, c_n\}$ for $n > 1$ are perturbations to the exact solutions. In this way, the perturbation approach solves the Orr-Sommerfeld equation by assuming the powers of $\tilde{Q}$ to be linearly independent, analogous to how the perturbation series of Benney [1966a] outlined in section 3.3 assumes the powers of ϵ to be linearly independent. As matter of fact, linearising the Benney equation (3.21) with respect to an infinitesimal disturbance leads to the asymptotic solution recovered here; this is because the present approach is invariant with respect to the order of perturbation and linearisation.

The exact solutions $\{\breve{\psi}_0, \breve{\theta}_0, c_0\}$ are found by substituting expressions (5.17) into equations (5.12 – 5.16) and allowing the reduced wave-number to go to zero, $\tilde{Q} \to 0$. This leads to a algebraically solvable problem in $\{\breve{\psi}_0, \breve{\theta}_0, c_0\}$ which reads:

$$\frac{\partial^4 \breve{\psi}_0}{\partial \hat{z}^4} = 0, \qquad \breve{\psi}_0\big|_{\hat{z}=0} = 0, \qquad \left.\frac{\partial \breve{\psi}_0}{\partial \hat{z}}\right|_{\hat{z}=0} = 0, \tag{5.18}$$

$$\left.\frac{\partial^2 \breve{\psi}_0}{\partial \hat{z}^2}\right|_{\hat{z}=1} = 2\breve{h}, \qquad \left.\frac{\partial^3 \breve{\psi}_0}{\partial \hat{z}^3}\right|_{\hat{z}=1} = 0, \qquad \breve{\psi}_0\big|_{\hat{z}=1} = (c_0 - 1)\,\breve{h}, \tag{5.19}$$

$$\frac{\partial^2 \breve{\theta}_0}{\partial \hat{z}^2} = 0, \qquad \breve{\theta}_0\big|_{\hat{z}=0} = 0, \qquad \left.\frac{\partial \breve{\theta}_0}{\partial \hat{z}}\right|_{\hat{z}=1} = \frac{Bi^2\breve{h}}{1+Bi} - Bi\breve{\theta}_0\big|_{\hat{z}=1}. \tag{5.20}$$

Equations (5.18 – 5.20) are satisfied (in the long-wave limit) by the exact solutions:

$$\breve{\psi}_0 = \breve{h}\hat{z}^2, \qquad \breve{\theta}_0 = \frac{Bi^2\breve{h}}{(1+Bi)^2}\hat{z}, \qquad c_0 = 2, \tag{5.21}$$

which are valid for any specified value of the disturbance amplitude, $\breve{h}$.

With $\{\breve{\psi}_0, \breve{\theta}_0, c_0\}$ given by expressions (5.21), the first-order perturbations $\{\breve{\psi}_1, \breve{\theta}_1, c_1\}$ are found from terms which share $\tilde{Q}$ as a common factor; namely:

$$\frac{\partial^4 \breve{\psi}_1}{\partial \hat{z}^4} = iRe\left(c_0 - u_{\mathbb{N}}\right)\frac{\partial^2 \breve{\psi}_0}{\partial \hat{z}^2} + 2iRe\breve{\psi}_0, \tag{5.22}$$

$$\frac{\partial^2 \breve{\theta}_1}{\partial \hat{z}^2} = iRePr\left(c - u_{\mathbb{N}}\right)\breve{\theta}_0 + \frac{iRePr}{(1+Bi)}\breve{\psi}_0, \tag{5.23}$$

$$\breve{\psi}_1\big|_{\hat{z}=0} = 0, \qquad \left.\frac{\partial \breve{\psi}_1}{\partial \hat{z}}\right|_{\hat{z}=0} = 0, \qquad \left.\frac{\partial^2 \breve{\psi}_1}{\partial \hat{z}^2}\right|_{\hat{z}=1} = -\,i\frac{Ma}{CaBi}\left.\frac{\partial \breve{\theta}_0}{\partial \hat{z}}\right|_{\hat{z}=1}, \tag{5.24}$$

$$\left.\frac{\partial^3 \breve{\psi}_1}{\partial \hat{z}^3}\right|_{\hat{z}=1} = iRe\left(1 - c_0\right)\left.\frac{\partial \breve{\psi}_0}{\partial \hat{z}}\right|_{\hat{z}=1} + 2i\cot\beta\breve{h}, \qquad \breve{\psi}_1\big|_{\hat{z}=1} = c_1\bar{h}, \tag{5.25}$$

$$\breve{\theta}_1\big|_{\hat{z}=0} = 0, \qquad \left.\frac{\partial \breve{\theta}_1}{\partial \hat{z}}\right|_{\hat{z}=1} = -\,Bi\breve{\theta}_1\big|_{\hat{z}=1}. \tag{5.26}$$

Solving for the first-order perturbations $\{\breve{\psi}_1, \breve{\theta}_1, c_1\}$ yields:

$$\breve{\psi}_1 = i\breve{h}\left[Re\left(\frac{40 - 15\hat{z}^2 + 2\hat{z}^3}{60}\right) - \left(3 - \hat{z}\right)\frac{\cot\beta}{3} + \frac{1}{2}\frac{Ma}{Ca}\frac{Bi}{\left(1+Bi\right)^2}\right]\hat{z}^2, \tag{5.27}$$

$$\bar{\theta}_1 = \frac{i\breve{h}RePr}{\left(1+Bi\right)^3}\left[\frac{4 - \hat{z}^3}{12} + Bi\left(\frac{5 - 2\hat{z}^3}{12}\right) + Bi^2\left(\frac{40 - 20\hat{z}^2 + 5\hat{z}^3 - 3\hat{z}^4}{60}\right) + Bi^3\left(\frac{13 - 20\hat{z}^2 + 10\hat{z}^3 - 3\hat{z}^4}{60}\right)\right]\hat{z}, \tag{5.28}$$

$$c_1 = i\left(\frac{8}{15}Re - \frac{2}{3}\cot\beta + \frac{1}{2}\frac{Ma}{Ca}\frac{Bi}{\left(1+Bi\right)^2}\right). \tag{5.29}$$

Equations (5.27 – 5.29) give the imaginary parts of the perturbation stream-function ($\breve{\psi}$), perturbation temperature ($\breve{\theta}$), and phase velocity (c) which are linear in $\tilde{Q}$, and thus represent the first-order approximation of the linear growth rates of $(\breve{\psi}, \breve{\theta}, c)$. As stated in chapter 4, neutral stability ensues when the phase velocity is wholly real which correlates to setting $c_1 = 0$ in equation (5.29); this returns the condition for when 'a flat-film flowing down a planar, uniformly heated incline' is neutrally stable; namely:

$$Re - \frac{5}{4}\cot\beta + \frac{15}{16}\frac{Ma}{Ca}\frac{Bi}{\left(1+Bi\right)^2} = 0, \tag{5.30}$$

equivalent to the expression obtained by Goussis and Kelly [1991] – who were the first to recover equation (5.30).

The perturbation series can be extended to higher-order using the same mechanistic procedure with which it was extended to first-order; however, the perturbation series'

presumption that powers of $\tilde{Q}$ are linearly independent severely limits its validity to the problem of neutral stability in the long-wave limit, $\tilde{Q} \to 0$. This is because the perturbation series for the phase velocity is acquired on the condition that the coefficients of $\tilde{Q}^n$ vanish; under this condition, the phase velocity expansion, namely $c = c_0 + c_1\tilde{Q}$, constructed from equations (5.21, 5.29), is only valid when $c_1 = 0$. This restricts the perturbation approach to the long-wave neutral stability because: (i) $\Im(c) \neq 0$ for stable and unstable disturbances; and (ii) $\Im(c) \neq c_1$ at finite wave-numbers, $\tilde{Q} > 0$, as the imaginary part of the phase velocity will be comprised of higher powers of $\tilde{Q}$. To extend the analysis to large wave-number, one must allow for the coefficients $\tilde{Q}^n$ to be linearly dependent; this is achieved through a polynomial expansion of $(\breve{\psi}, \breve{\theta})$ with respect to $\hat{z}$.

5.3.2 Polynomial expansion: Power series

Kelvin [1887] was the first to show linearised problems, such as the Orr-Sommerfeld equation, could be approximated through a power series expansion; and this was the approach adopted by Benjamin [1957] to analyse wave formation on falling liquid films. Equations (5.12 – 5.16) are placed in the same coordinate system as Benjamin [1957] through a variable transformation of $\hat{z} = 1 - \chi$, with $\chi \in [0, 1]$. The perturbation streamfunction and temperature are then expanded as power series with respect to χ like so:

$$\breve{\psi} = \sum_{n=0}^{N+4} A_n \chi^n, \qquad \breve{\theta} = \sum_{n=0}^{N+4} B_n \chi^n, \tag{5.31}$$

where $\{A_n, B_n\}$ are the unknown expansion coefficients of the streamfunction and temperature perturbations, respectively; and N represents the number of true degrees of freedom in each expansion. Within the monomial basis of χ, the Nusselt parabolic velocity profile becomes Poiseuille flow for the interval of $\chi \in [0, 1]$; namely:

$$u_{\mathbf{N}} = 1 - \chi^2. \tag{5.32}$$

Replacing $\{\breve{\psi}, \breve{\theta}\}$ in equations (5.12 – 5.16) with expressions (5.31) results in a generalised eigenvalue problem, $(\mathbf{A} - c\mathbf{B})\,\hat{x} = 0$, for the eigenvector $\hat{x} = \left\{A_0, ..., A_{N+4}, B_0, ..., B_{N+4}, \breve{h}\right\}$ and eigenvalue c; where $(\mathbf{A} - c\mathbf{B})$ is a $(2N + 9)$ square matrix. The first $2\,(N + 1)$ rows of $(\mathbf{A} - c\mathbf{B})$ are given by recurrence relations arising from the requirement that the coefficients of χ^n must vanish in equations (5.12 – 5.13); namely:

$$\frac{i\,(n+4)\,(n+3)\,(n+2)\,(n+1)}{Re}A_{n+4} + (n+2)\,(n+1)\left((1-c) - \frac{2i\tilde{Q}}{Re}\right)\tilde{Q}A_{n+2}$$
$$-\left((n+1)\,(n-2) + \tilde{Q}^2\,(1-c) - \frac{i\tilde{Q}^3}{Re}\right)\tilde{Q}A_n + \tilde{Q}^3 A_{n-2} = 0, \quad (5.33)$$

$$\frac{i\,(n+2)\,(n+1)}{RePr}B_{n+2} + \left((1-c) - \frac{i\tilde{Q}}{RePr}\right)\tilde{Q}B_n - \tilde{Q}B_{n-2} - \frac{\tilde{Q}}{1+Bi}A_n = 0, \quad (5.34)$$

which correspond to the coefficients of χ^n for $0 \le n \le N$. The bottom seven rows of $(\mathbf{A} - c\mathbf{B})$ then correspond to the seven boundary conditions (5.14 – 5.16).

The generalised eigenvalue problem $(\mathbf{A} - c\mathbf{B})\,\hat{x} = 0$ was then solved numerically using Matlab's built-in *eig* subroutine which yielded $(2N + 9)$ eigenvalues and associated eigenvectors. Following the Tau method – see section 3.4.1; evaluating equations (5.33 – 5.34) for $N < n \le N + 4$ whilst replacing the right hand-side of each equation with an undefined constant C_n^τ, yields eight tau conditions from which the error of each eigenvalue can be computed [Lanczos, 1938]. These conditions are critical to solving the linear stability problem because whilst the generalised eigenvalue problem $(\mathbf{A} - c\mathbf{B})\,\hat{x} = 0$ possesses $(2N + 9)$ eigenvalues, not all of these eigenvalues are true solutions of the linear problem as they either lack physical or mathematical justification; the function of the tau conditions is to eliminate those eigenvalues lacking mathematical justification. The error of a particular eigenvalue c was found by substituting the eigenvalue c and it associated eigenvector $\hat{x}$ into the eight tau conditions which returned the value of each undefined constant C_n^τ – the norm of these constants was then defined to be the error of the approximation. Eigenvalues whose error was greater than a tolerance of 10^{-6} were eliminated from the solution, this consistently left three eigenvalues corresponding to the long-wave, thermo-capillary and upstream modes [Kalliadasis et al., 2003b]. The upstream mode can be eliminated upon the knowledge that wave formation in gravity-driven film flow down inclined plane is a type of convective instability, rather than a type of absolute instability, and that surface disturbances are universally swept downstream by the primary flow and never propagate upstream. Out of the long-wave and thermo-capillary modes, the one with the largest growth rate defines the stability.

One consideration the reader must take into account is that the eigenvalue problem $(\mathbf{A} - c\mathbf{B})\,\hat{x} = 0$ is ill-posed because the matrix $\mathbf{B}$ is singular; a consequence of c not appearing in all of the boundary conditions. In the present study, Matlab's build-in *eig* subroutine was able to handle the singularity in the eigenvalue problem without issue. Nevertheless, it is useful to know how the singularity can be overcome; one strategy is to reduce the rank of the generalised eigenvalue problem until the matrix $\mathbf{B}$ is no longer singular. This can be achieved by re-arranging the kinematic condition – equation $(5.14d)$ – to find an expression for the amplitude of the surface disturbance like so:

$$\breve{h} = \frac{A_0}{(c-1)} = \frac{-A_0}{(1-c)}. \quad (5.35)$$

Expression (5.35) eliminates the kinematic condition from the eigenvalue problem and thus reduces the matrix rank by one. More importantly, its substitution introduces the eigenvalue c into the shear stress and heat flux boundary conditions at the free-surface, eliminating the singularity from these rows; however, the substitution also makes the normal stress quadratic in c, resulting in the quadratic eigenvalue problem, $\left(\mathbf{A} - c\mathbf{B} - c^2\mathbf{C}\right)\hat{x} = 0$. Nevertheless, a quadratic eigenvalue problem can easily be transformed into a generalised eigenvalue problem through linearisation; this involves introducing a set of supplementary equations which take the forms of $\hat{A}_n = cA_n$ and $\hat{B}_n = c\hat{B}_n$ where $\{\hat{A}_n, \hat{B}_n\}$ are supplementary variables. The supplementary equations and variables allow for the quadratic terms with respect to c in the quadratic eigenvalue problem with the eigenvector $\hat{x} = \left\{A_0, ..., A_{N+4}, B_0, ..., B_{N+4}, \breve{h}\right\}$, to be expressed as linear terms with respect to c in a generalised eigenvalue problem with the eigenvector $\hat{x} = \left\{A_0, ..., A_{N+4}, \hat{A}_0, ...\hat{A}_{N+4}, B_0, ..., B_{N+4}, \hat{B}_0, ..., \hat{B}_{N+4}\right\}$. Inevitably, the linearisation of the quadratic eigenvalue problem increases the rank of eigenvalue matrix, but it does allow for the problem to be handled using standard eigenvalue techniques.

Even after eliminating the disturbance amplitude ($\breve{h}$) and linearising the quadratic eigenvalue problem, matrix $\mathbf{B}$ is still singular because the substrate boundary conditions do not contain the eigenvalue c and thus possesses three empty rows. A matrix $\mathbf{B}$ which possesses m empty rows, it is said to have m infinite eigenvalues. The eigenvalues are referred to as being infinite because they are undefined and their values are unbounded; moreover, if one considers the inverse eigenvalue problem of $\left(c^{-1}\mathbf{A} - \mathbf{B}\right)\hat{x} = 0$, one will find that the reciprocal of these eigenvalues must tend to zero in order for the eigenvalue problem to be satisfied which implies the actual eigenvalues must tend to infinite. One could try to use extensive algebra to try and reduce the problem to the point at which it is well-posed; however, an easier approach is to "map the infinite eigenvalues to specified points on the complex plane". The issue surrounding the infinite eigenvalues is that they are undefined, and so mapping the infinite eigenvalues to specified points on the complex plane is simply defining what values the eigenvalues should take. Accordingly, one can make the eigenvalue problem well-posed by introducing artificial entries to the empty rows of $\mathbf{B}$; in this way, the set of infinite eigenvalues are replaced by a set of artificial eigenvalues. Since the set of artificial eigenvalues is defined prior to solving the eigenvalue problem, these artificial can be easily removed from the set of eigenvalues after the problem has been solved. To ease with the removal of the artificial eigenvalues, it is good practice to assign them values in the complex plane which lie far away from the expected eigenvalues of the problem; in the present problem, the infinite eigenvalues were mapped to points on the complex plane corresponding to strongly stable modes, $\Im(c) \ll 0$, this ensured the artificial eigenvalues did not pollute the linear stability results where it is the eigenvalue with the largest imaginary part which defines the stability.

Unfortunately, even after "mapping the infinite eigenvalues to specified points in the complex plane", the power series formulation of the eigenvalue problem remains singular for the problem of gravity-driven film flow down planar, uniformly heated inclines; this is a result of one of the rows in matrix $\mathbf{B}$ being linearly dependent upon the others. The

culprit turns out to be the heat flux boundary condition (5.16) and so the singularity is only present in the heated problem. As mentioned above, Matlab's *eig* subroutine is able to handle the power series formulation without issue; be that as it may, one can develop a more robust method of solution which does not possess a singularity in the heat flux boundary condition by switching from a power series expansion in χ to an expansion of the perturbation stream-function and temperature in terms of Chebyshev polynomials.

5.3.3 Polynomial expansion: Chebyshev polynomials of the first kind

The chief advantage to seeking an expansion of the perturbation stream-function ($\breve{\psi}$) and temperature ($\breve{\theta}$) in terms of Chebyshev polynomials is it guarantees the heat flux boundary condition is linearly independent of the other weak form equations; this allows for matrix $\mathbf{B}$ to be made non-singular, ensuring the eigenvalue problem is well-posed. More specifically, the perturbation stream-function ($\breve{\psi}$) and temperature ($\breve{\theta}$) are expanded in terms of the Chebyshev polynomials of the first kind like so:

$$\breve{\psi} = \sum_{n=0}^{N+4} A_n \mathcal{T}_n, \qquad \breve{\theta} = \sum_{n=0}^{N+4} B_n \mathcal{T}_n, \tag{5.36}$$

where $\mathcal{T}_n$ are the Chebyshev polynomials of the first kind and are given by the expression $\mathcal{T}_n(\cos\alpha) = \cos(n\alpha)$, and N is number of degrees of freedom belonging to the expansions. Utilising the transformation $\xi = \cos\alpha$, the Chebyshev polynomials can be written as:

$$\mathcal{T}_0(\xi) = 1, \qquad \mathcal{T}_1(\xi) = \xi, \qquad \mathcal{T}_n(\xi) = 2\xi\mathcal{T}_{n-1}(\xi) - \mathcal{T}_{n-2}(\xi). \tag{5.37}$$

where $\xi \in [-1, +1]$ and $\xi = 2\hat{z} - 1$. The Nusselt parabolic velocity profile can be expressed in the Chebyshev basis via the coordinate transformation $\hat{z} = (\xi + 1)/2$; leading to:

$$u_{\mathbb{N}} = \frac{5}{8}\mathcal{T}_0(\xi) + \frac{1}{2}\mathcal{T}_1(\xi) - \frac{1}{8}\mathcal{T}_2(\xi). \tag{5.38}$$

Substituting (5.36) into equations (5.12 – 5.16) leads to a system of $(2N + 9)$ weak form equations in terms of $\{A_n, B_n, c, \breve{h}\}$ corresponding to the vanishing coefficients of $\mathcal{T}(\xi)$ and eight tau conditions measuring the error of the approximation. The weak form equations form a $(2N + 9)$ square matrix which can be handled as a generalised eigenvalue problem in c, namely $(\mathbf{A} - c\mathbf{B})\,\hat{x} = 0$ where $\hat{x} = \left\{A_0, ..., A_{N+4}, B_0, ..., B_{N+4}, \breve{h}\right\}$ – this approach is identical to one used for the power series expansion in section 5.3.2, the only difference is the matrix entries differ due to the change of basis.

Constructing the matrix $(\mathbf{A} - c\mathbf{B})$ for the Chebyshev basis can be accelerated through knowledge of the properties belonging to the Chebyshev polynomials of the first kind. To start, the product of any two Chebyshev polynomials satisfies the relationship:

$$\mathcal{T}_m(\xi)\mathcal{T}_n(\xi) = \frac{1}{2}\left(\mathcal{T}_{m+n}(\xi) + \mathcal{T}_{|m-n|}(\xi)\right), \qquad \forall m, n \leq 0. \tag{5.39}$$

From equation (5.39), one finds the product of the Nusselt parabolic velocity profile – equation (5.38) – with any Chebyshev polynomial, $\mathcal{T}_n(\xi)$, is given by:

$$u_{\mathbb{N}}\mathcal{T}_n = \frac{5}{8}\mathcal{T}_n + \frac{1}{4}\left(\mathcal{T}_{n+1} + \mathcal{T}_{|n-1|}\right) - \frac{1}{16}\left(\mathcal{T}_{n+2} + \mathcal{T}_{|n-2|}\right). \tag{5.40}$$

Differentiating the Chebyshev polynomials in their trigonometric form, one can show:

$$\frac{\partial}{\partial\xi}\Big[\mathcal{T}_n(\xi)\Big] = \begin{cases} 2n \sum\limits_{k=0}^{|\frac{n}{2}-1|} \mathcal{T}_{2k+1}(\xi) & \text{if n even,} \\ 2n \sum\limits_{k=1}^{|\frac{n-1}{2}|} \mathcal{T}_{2k}(\xi) + n\mathcal{T}_0(\xi) & \text{if n odd,} \end{cases}$$

for $n \geq 2$, which can be used to compute the derivatives in the Orr-Sommerfeld equation set – note that the coordinate transformation yields $\partial/\partial\hat{z} = 2\partial/\partial\xi$.

Finally, the symmetry of the Chebyshev basis gives $\mathcal{T}_n(\pm x) = (\pm 1)^n\mathcal{T}_n(x)$ which means evaluating the Chebyshev polynomials at the substrate ($\xi = -1$) and free-surface ($\xi = 1$) boundaries correlates to computing $\mathcal{T}_n(\pm 1) = (\pm 1)^n$. Utilising the properties of the Chebyshev polynomials, one can recast the Orr-Sommerfeld system of equations in martix form with respect to the Chebyshev basis like so:

$$\left[\mathbf{D}^4 - \left(i\tilde{Q}Re\mathbf{U} + 2\tilde{Q}^2\right)\mathbf{D}^2 + \left(i\tilde{Q}Re\left(\mathbf{U}\tilde{Q}^2 - 2\right) + \tilde{Q}^4\right)\mathbb{I}\right]\breve{\Psi} = \left[ci\tilde{Q}Re\left(\tilde{Q}^2\mathbb{I} - \mathbf{D}^2\right)\right]\breve{\Psi}, \tag{5.41}$$

$$\left[\mathbf{D}^2 - i\tilde{Q}RePr\mathbf{U} - \tilde{Q}^2\mathbb{I}\right]\breve{\Theta} + \left[\frac{i\tilde{Q}RePr}{1+Bi}\mathbb{I}\right]\breve{\Psi} = \left[-ci\tilde{Q}RePr\mathbb{I}\right]\breve{\Theta}, \tag{5.42}$$

in which $\mathbb{I}$ is the identity matrix, $\breve{\Psi} = (A_0, ..., A_{N+4})^T$ is the vector of the perturbation stream-function, and $\breve{\Theta} = (B_0, ..., B_{N+4})^T$ is the vector of the perturbation temperature. The differentiation matrix ($\mathbf{D}$) is given by:

$$\mathbf{D} = \begin{pmatrix} 0 & 1 & 0 & 3 & 0 & 5 & 0 & 7 & \cdots \\ 0 & 0 & 4 & 0 & 8 & 0 & 12 & 0 & \cdots \\ 0 & 0 & 0 & 6 & 0 & 10 & 0 & 14 & \cdots \\ 0 & 0 & 0 & 0 & 8 & 0 & 12 & 0 & \cdots \\ \vdots & \vdots & \vdots & \vdots & \vdots & \vdots & \vdots & \vdots & \ddots \end{pmatrix} \tag{5.43}$$

where the entry to ith row and jth column of $\mathbf{D}$ are computed via:

$$\begin{aligned} \mathbf{D}_{0,2j-1} &= 2j-1, && \text{for} \quad j \geq 1, \\ \mathbf{D}_{i,i+2j-1} &= 2(i+2j-1), && \text{for} \quad i \geq 1, j \geq 1, \end{aligned} \tag{5.44}$$

in which the leftmost column and top row of $\mathbf{D}$ correspond to $j = 0$ and $i = 0$, respectively. The second-, third-, and fourth-order differentiation matrices are acquired by putting $\mathbf{D}$ to the powers of two, three and four, respectively.

The Nusselt parabolic velocity profile ($\mathbf{U}$) is expressed in matrix form like so:

$$\mathbf{U} = \frac{5}{8}\begin{pmatrix} 1 & 0 & 0 & \cdots \\ 0 & 1 & 0 & \cdots \\ 0 & 0 & 1 & \cdots \\ \vdots & \vdots & \vdots & \ddots \end{pmatrix} + \frac{1}{4}\begin{pmatrix} 0 & a & 0 & \cdots \\ 1 & 0 & 1 & \cdots \\ 0 & 1 & 0 & \cdots \\ \vdots & \vdots & \vdots & \ddots \end{pmatrix} - \frac{1}{16}\begin{pmatrix} 0 & 0 & b & \cdots \\ c & 0 & 0 & \cdots \\ 1 & 0 & 0 & \cdots \\ \vdots & \vdots & \vdots & \ddots \end{pmatrix} \tag{5.45}$$

where $a = b = 2$ and $c = 1$ – these entries arise from the symmetry $\mathcal{T}_n(\xi) = \mathcal{T}_{|-n|}(\xi)$. Conveniently, the matrices making up the Nusselt parabolic velocity profile in the Chebyshev basis can be expressed in terms of shift matrices; in this way, the entries to the ith row and jth column of the Nusselt parabolic velocity matrix can be computed via:

$$\mathbf{U}_{i,j} = \frac{5}{8}\delta_{i,j} + \frac{1}{4}\left(\delta_{i+1,j} + \delta_{i,j+1} + \delta_{i,0}\delta_{1,j}\right) - \frac{1}{16}\left(\delta_{i+1,j}^2 + \delta_{i,j+1}^2 + \delta_{i,0}\delta_{2,j} + \delta_{i,1}\delta_{0,j}\right). \tag{5.46}$$

The accompanying boundary conditions to equations (5.41 – 5.42) are given by:

$$\mathbb{I}\cdot\mathbf{t}(-1)\breve{\Psi} = 0, \qquad \mathbf{D}\cdot\mathbf{t}(-1)\breve{\Psi} = 0, \qquad \mathbb{I}\cdot\mathbf{t}(+1)\breve{\Psi} + \breve{h} = c\breve{h}, \tag{5.47}$$

$$\left[\mathbf{D}^2 + \tilde{Q}^2\mathbf{I}\right]\cdot\mathbf{t}(+1)\breve{\Psi} - i\tilde{Q}\frac{Ma}{CaBi}\mathbf{D}\cdot\mathbf{t}(+1)\breve{\Theta} - 2\breve{h} = 0, \tag{5.48}$$

$$\left[\mathbf{D}^3 - \left(i\tilde{Q}Re + 3\tilde{Q}^2\right)\mathbf{D}\right]\cdot\mathbf{t}(+1)\breve{\Psi} - i\tilde{Q}\left(2\cot\beta + \tilde{Q}^2\frac{1 - Ma + Bi}{Ca(1+Bi)}\right)\breve{h} = -ci\tilde{Q}Re\mathbf{D}\cdot\mathbf{t}(+1)\breve{\Psi}, \tag{5.49}$$

$$\mathbf{I}\cdot\mathbf{t}(-1)\breve{\Theta} = 0, \qquad \left[\mathbf{D} + Bi\mathbb{I}\right]\cdot\mathbf{t}(+1)\breve{\Theta} + \frac{Bi^2}{1+Bi}\breve{h} = 0, \tag{5.50}$$

where the entries to the vector $\mathbf{t}(\xi)$ are given by $\mathbf{t}_i(\pm 1) = (\pm 1)^i$ and correspond to the evaluations of the Chebyshev polynomials (T_n) at $\xi = \pm 1$. These boundary conditions form the bottom seven rows of the eigenvalue matrix; since the eigenvalue c does not appear in each of these boundary condition this results in a set of undefined eigenvalues.

These undefined singularities were mapped to specified points on the complex plane in order to make the eigenvalue problem well-posed – see section 5.3.2.

From equations (5.41 – 5.42, 5.47 – 5.48), one can construct the eigenvalue problem $(\mathbf{A} - c\mathbf{B})\,\hat{x} = 0$ in which the eigenvector is given by $\hat{x} = \left(\breve{\Psi}, \breve{\Theta}, \breve{h}\right)^T$. The generalised eigenvalue problem was then solved using Matlab's built-in *eig* subroutine, after which spurious eigenvalues were eliminated if the norm of their tau coefficients did not lie within a tolerance of 10^{-6}.

5.3.4 Orr-Sommerfeld: Finite difference scheme

Restricted to the isothermal problem of gravity-driven film flow down planar incline, one may also solve the Orr-Sommerfeld system of equations by discretising the perturbation stream-function over the spatial domain of $\hat{z} \in [0, 1]$ and then approximating its derivatives via a central difference scheme with second-order accuracy; namely:

$$\frac{\partial \breve{\psi}_i}{\partial \hat{z}} = \frac{\breve{\psi}_{i+1} - \breve{\psi}_{i-1}}{2\Delta\hat{z}} + \mathcal{O}\left(\Delta\hat{z}^2\right), \tag{5.51}$$

$$\frac{\partial^2 \breve{\psi}_i}{\partial \hat{z}^2} = \frac{\breve{\psi}_{i+2} - 2\breve{\psi}_i + \breve{\psi}_{i-2}}{\Delta\hat{z}^2} + \mathcal{O}\left(\Delta\hat{z}^2\right), \tag{5.52}$$

$$\frac{\partial^3 \breve{\psi}_i}{\partial \hat{z}^3} = \frac{\breve{\psi}_{i+2} - 2\breve{\psi}_{i+1} + 2\breve{\psi}_{i-1} - \breve{\psi}_{i-2}}{2\Delta\hat{z}^3} + \mathcal{O}\left(\Delta\hat{z}^2\right), \tag{5.53}$$

$$\frac{\partial^4 \breve{\psi}_i}{\partial \hat{z}^4} = \frac{\breve{\psi}_{i+2} - 4\breve{\psi}_{i+1} + 6\breve{\psi}_i - 4\breve{\psi}_{i-1} + \breve{\psi}_{i-2}}{\Delta\hat{z}^4} + \mathcal{O}\left(\Delta\hat{z}^2\right), \tag{5.54}$$

where $\Delta\hat{z} = 1/N_{\hat{z}}$ denotes the spatial step size along the $\hat{z}$-domain with $N_{\hat{z}}$ being the number of discrete points along the $\hat{z}$-domain.

The only consideration one must make is that near the boundaries of the $\hat{z}$-domain, the central difference scheme includes quantities of the perturbation stream-function which lie outside of the $\hat{z}$-domain. Fortunately, these quantities can be eliminated by rearranging the discretised boundary conditions like so:

$$\breve{\psi}_0 = 0, \qquad \breve{\psi}_{(-1)} = \breve{\psi}_1, \qquad \breve{\psi}_{N_{\hat{z}}} = (c-1)\,\breve{h}, \tag{5.55}$$

$$\breve{\psi}_{N_{\hat{z}}+1} = \Delta\hat{z}^2\left(2\breve{h} - \tilde{Q}^2\breve{\psi}_{N_{\hat{z}}}\right) + 2\breve{\psi}_{N_{\hat{z}}} - \breve{\psi}_{N_{\hat{z}}-1}, \tag{5.56}$$

$$\begin{aligned}\breve{\psi}_{N_{\hat{z}}+2} = {} & \left[2 + \Delta\hat{z}^2(3\tilde{Q}^2 - i\tilde{Q}Re(c-1))\right]\left(\breve{\psi}_{N_{\hat{z}}+1} - \breve{\psi}_{N_{\hat{z}}-1}\right) \\ & + 2\Delta\hat{z}^3 i\tilde{Q}\left[2\cot\beta + \frac{\tilde{Q}^2}{Ca}\right]\breve{h} + \breve{\psi}_{N_{\hat{z}}-2}.\end{aligned} \tag{5.57}$$

In this way, the Orr-Sommerfeld system of equations can be discretised and made to form a generalised eigenvalue problem $(\mathbf{A} - c\mathbf{B})\,\hat{x} = 0$ for the eigenvector $\hat{x} = \left\{\breve{\psi}_1, .., \breve{\psi}_{N_{\hat{z}}}, \breve{h}\right\}$, which was solved using Matlab's *eig* subroutine.

5.4 Overview of Methodologies

Method of Solution	Domain Geometry	Interpolation Method	Coefficients of ϵ^n vanish	Variable Transformation
Steady-State Solutions				
Finite-Element Method [Veremieiev, 2011]	Unstructured Triangular Grid	Spline	No	No
Reduced Asymptotic Model (RAM)	z-axis: Continuous x-axis: Discrete	Polynomial Linear	No	Yes
Perturbation Series [Benney, 1966a]	z-axis: Continuous x-axis: Discrete	Polynomial Linear	Yes	Yes
Orr-Sommerfeld Theory (Flat Plate)				
Central Difference (Isothermal Case)	z-axis: Discrete	Linear	No	No
Power Series [Benjamin, 1957]	z-axis: Continuous	Polynomial	No	No
Perturbation Series [Yih, 1963]	z-axis: Continuous	Polynomial	Yes	No
Chebyshev Polynomials [Goussis and Kelly, 1991]	z-axis: Continuous	Polynomial	No	No
Floquet Theory (Corrugated Substrate)				
Reduced Asymptotic Model (RAM)	$\hat{z}$-axis: Continuous x-axis: Fourier series	Polynomial Sinusoidal	No	Yes
Perturbation Series [Benney, 1966a]	$\hat{z}$-axis: Continuous x-axis: Fourier series	Polynomial Sinusoidal	Yes	Yes

Table 5.1: Comparative overview of the different methods of solutions.

Chapter 6

Results I: Steady-State

A collection of steady-state solutions for two-dimensional gravity-driven film flow down inclined substrate are presented in this chapter; subdivided into those concerning the isothermal flow case ($Ma = 0$) and those relating to the thermal problem ($Ma \neq 0$). The present analysis on the steady-state problem is carried out within the frame of reference of the substrate and is almost universally restricted to gravity-driven film flow over smoothly corrugated, uniformly heated inclined substrate as the steady-state solutions to problem of film flow down planar, uniformly heated inclined substrate correspond exactly with the Nusselt solutions, which were found analytically in section 3.3.1. For the case of isothermal film flow, extensive comparison is made with experimental and numerical data available from the research literature; however, the same cannot be said of the thermal problem as there is a significant lack of steady-state solutions when both substrate corrugations and heating are considered in tandem. Accordingly, the steady-state solutions relating to the thermal problem are chiefly those acquired from the full equation set (2.23 – 2.31) via the purpose-built finite-element method, outlined in section 5.1, and from the asymptotic models derived in chapter 3 via a finite difference scheme – see section 5.2. The solutions to the full equation set (2.23 – 2.31) obtained via the finite-element method are identified as *N-SE* subsequently. Whilst the solutions to the asymptotic models are labelled according to their naming conventions laid out in Chapter 3: the Benney equation and its regularised form are abbreviated to BE and RBE, respectively; meanwhile, each reduced asymptotic model (RAM) is referred to as $RAM[\epsilon^n/\hat{z}^m]$ where n denotes its long-wave order and m signals how many degrees of freedom it possesses with respect to the $\hat{z}$-coordinate.

The heated problem involves eight parameters: ϵ, Re, Ca, β, A/H_0, Pr, Ma and Bi. However, the Capillary number, Ca, is not independent of the Reynolds number, Re, and so it is switched for the Kapitza number, Ka, which is purely a function of the fluid properties. Furthermore, since the substrate amplitude, A/H_0, and *shallowness parameter*, ϵ, are both characterised by the Nusselt film thickness, H_0, they can be redefined in terms of the more tangible substrate wavelength, L_0, and capillary length, L_c, leading to a substrate amplitude, $A/L = \epsilon \cdot A/H_0$, and scaled wavelength, L/L_c. The Kapitza number and scaled wavelength are given by:

$$Ka = \left(\frac{\rho\sigma_0^3}{g\mu^4}\right)^{1/11} = \left(\frac{\sin\beta Re^2}{2Ca^3}\right)^{1/11}, \quad L/L_c = \frac{L}{\sqrt{\sigma_0/\rho g}} = \frac{\sqrt{2Ca/\sin\beta}}{\epsilon}, \tag{6.1}$$

respectively.

6.1 Isothermal case

Figure 6.1 shows the free-surface profile predictions obtained from a reduced asymptotic model (RAM) possessing two degrees of freedom with respect to the $\hat{z}$-coordinate at various orders of the long-wave expansion; these predictions are compared against both *N-SE* solutions and experimental data collected by Schörner et al. [2016]. The results first serve to validate the *N-SE* solutions which are in excellent agreement with the experimental measurements of Schörner et al. [2016]; indeed, the only perceptible discrepancy at this resolution appears for large substrate amplitude $A/L = 0/4$ in figures 6.1(d,h) where the *N-SE* solutions can be seen to over-estimate the thickness of the film across the entire domain. In contrast, the *N-SE* solutions actually under-estimate the film thickness for film flow down planar substrate by around 2% on average, however, at the current resolution, this difference is imperceivable in figures 6.1(a,e). One might be tempted to attribute the 2% mean discrepancy between the $NS-E$ solutions and experimental data for the case of $A/L = 0.0$ to errors arising from either the experimental measurements or digitisation of the published data but such errors should be evenly distributed about the true experimental value and as such should have a little-to-no effect upon the mean experimental value. Furthermore, experiments carried out by Liu et al. [1993] found the measured free-surface velocity of a laminar film is $5-10\%$ larger than the corresponding theoretical value predicted by Nusselt's theory, suggesting that physical liquid films are consistently thicker than their theoretic counterparts for the case of $A/L = 0.0$. Turning attention to the performance of the reduced asymptotic model $RAM[\epsilon^n/\hat{z}^2]$ for $n = 1, 2, 3, 4$, it can be seen that all of the reduced asymptotic models agree perfectly with the *N-SE* solutions for the case of $A/L = 0.0$ as this scenario is analogous to the long-wave limit and thus the dynamics of steady film flow down planar substrate are given by the Nusselt solution – see section 3.3.1. The introduction of substrate topography precipitates a divergence in the free-surface profile predictions of $RAM[\epsilon^n/\hat{z}^2]$ corresponding to $n = 1, 2, 3, 4$: even at moderately small substrate amplitude $A/L = 0.1$, the first-order model ($n = 1$) produces unsatisfactory results with this approximation severely over-estimating the hydraulic jump caused by the stream-wise velocity slowing in the region above the corrugation trough; the inclusion of viscous dissipation at second-order ($n = 2$) couples the fluid pressure to the variation of the stream-wise velocity across the x-domain and thus does much to remedy the deficiency of the first-order model, be that as it may, the second-order approximation still diverges from the corresponding *N-SE* solution even for small substrate amplitude ($A/L = 0.1$); indeed, it is only when the RAM formulation is taken to third- ($n = 3$) and fourth-order

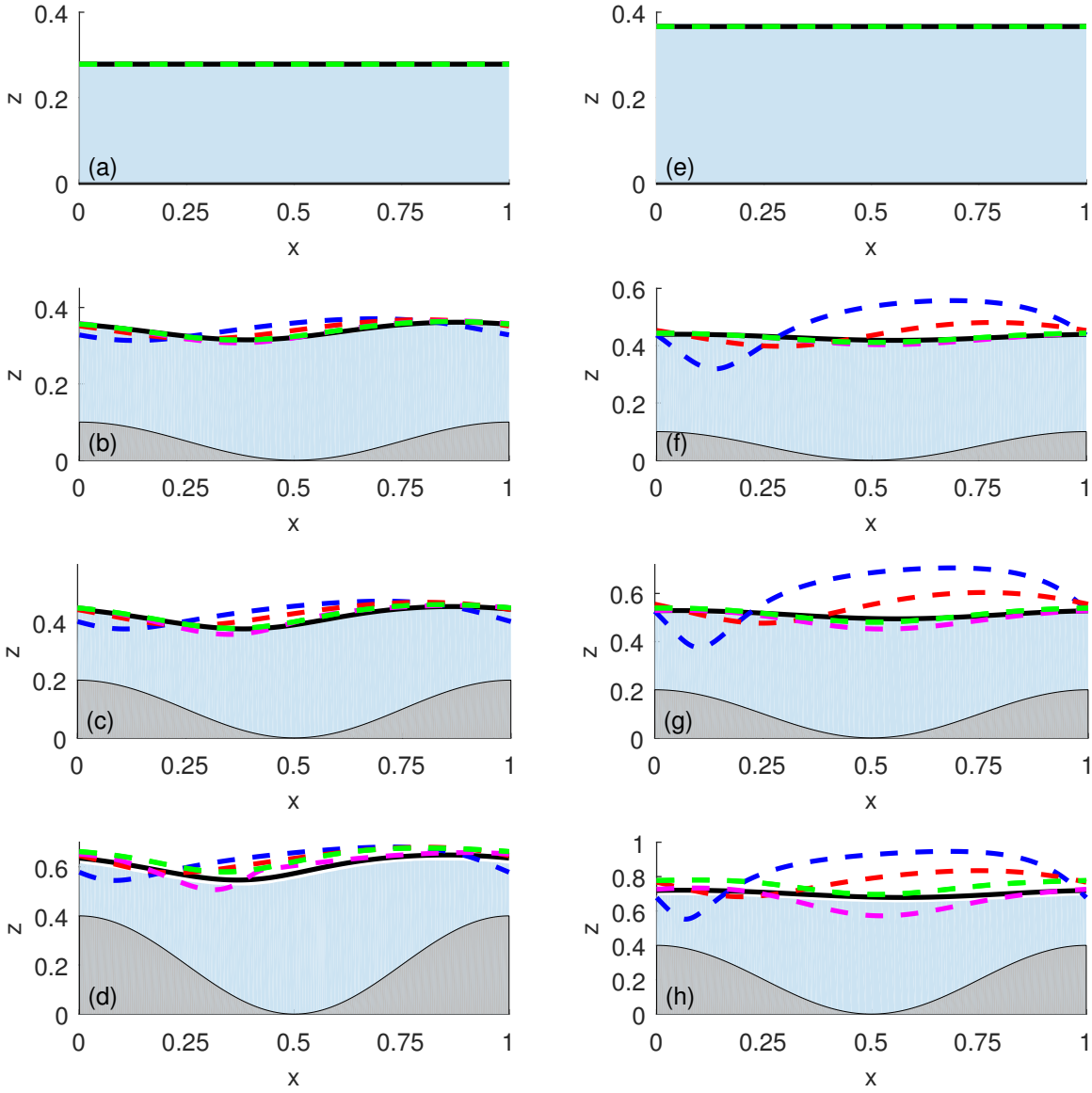

Figure 6.1: Steady-state free-surface profile predictions obtained utilising $RAM[\epsilon^n/\hat{z}^2]$ for $n = 1$ [dashed blue curve], $n = 2$ [dashed red curve], $n = 3$ [dashed magenta curve] and $n = 4$ [dashed green curve] compared for film flow over sinusoidally varying substrate for the case $Ka = 1.069$, $L/L_c = 13.741$, $\beta = 10°$, (a-d) $Re = 7.0$ and (e-h) $Re = 16.0$ for (top-to-bottom) $A/L = 0.0, 0.1, 0.2, 0.4$. The corresponding *N-SE* solution is shown as a solid black curve and experimental data from figure 8 of Schörner et al. [2016] is depicted by the shaded blue area.

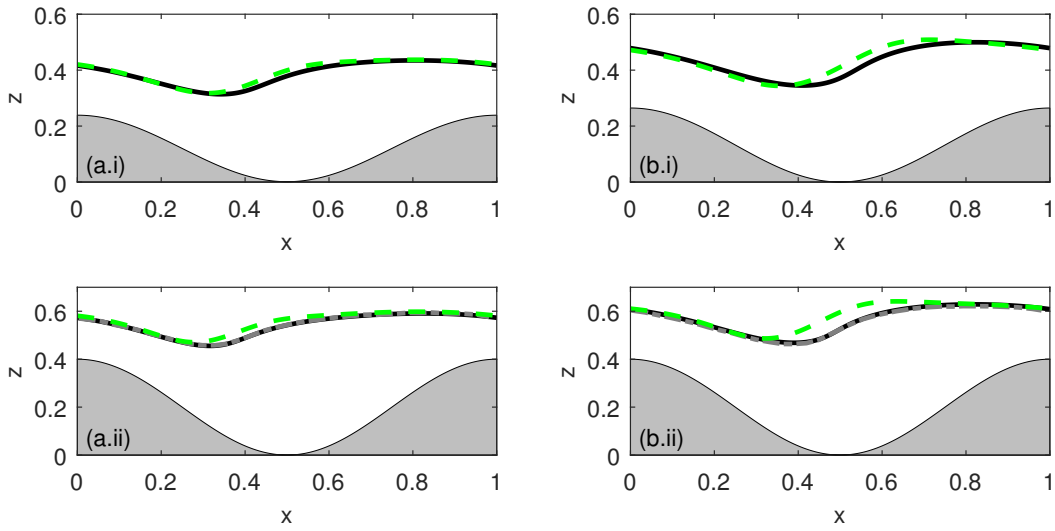

Figure 6.2: Steady-state free-surface profile predictions obtained utilising $RAM[\epsilon^4/\hat{z}^2]$ [dashed green curve] compared for film flow over sinusoidally varying substrate for the case Ka = 1.434, L/L_c = 13.746, β = 10°, (a) Re = 12.75 with (i) A/L = 0.24 and (ii) A/L = 0.4 and (b) Re = 17.55 with (i) A/L = 0.26 and (ii) A/L = 0.4. The corresponding N-SE solution is shown as a solid black curve and NS data from figure 9 of Trifonov [2014b] is plotted as a dot-dashed grey curve.

(n = 4) in the long-wave expansion that consistently good agreement is found with the full *N-SE* solutions, with the fourth-order formalism performing exceptionally well up to a substrate amplitude of A/L = 0.2. The necessity of incorporating vertical inertia ($\epsilon^3 Re$) and viscosity (ϵ^4) into the RAM formulation in order to achieve agreement with the *N-SE* solutions when $A/L > 0$ indicates that the presence of surface topography creates a significant component of the flow velocity in the $\hat{z}$-direction and that this component varies enough along the x-domain that its inclusion is key to modelling gravity-driven film flow down wavy substrate. Previous modelling attempts have frequently excluded the effects of vertical inertia and viscosity on the grounds that they are either negligible to the film dynamics or even potentially detrimental to the modelling approach as moving such terms ahead of their formal order in the long-wave expansion will imbalance the long-wave expansion; whilst the first point is often true for the case of A/L = 0.0, the second point neglects that the power series method is an expansion of the fluid velocity with respect to the $\hat{z}$-coordinate and thus accurately resolving the film dynamics relies upon deriving accurate descriptions for the degrees of freedom with respect to $\hat{z}$. To this effect, including higher-order derivatives with respect to (x, t) is rarely detrimental to the modelling approach because such terms improve the description of the degrees of freedom with respect to $\hat{z}$ and thus improve the overall performance of the model in question.

Figure 6.2 focuses upon the performance of the $RAM[\epsilon^4/\hat{z}^2]$ formalism which was

seen to offer the best free-surface predictions amongst the four reduced asymptotic models possessing two degrees of freedom with respect to $\hat{z}$ considered in figure 6.1 – for further justification see Veremieiev and Wacks [2019]. The NS data [dot-dashed magenta curves] included in figures 6.2(a.ii) and 6.2(b.ii) is taken from Trifonov [2014b] and serves to validate the in-house *N-SE* solutions. Comparing the RAM prediction with the *N-SE* solutions in figure 6.2, the $RAM[\epsilon^4/\hat{z}^2]$ prediction is seen to match better with *N-SE* solutions and NS data at the lower Reynolds number of Re = 12.75 in figure 6.2(a) than when at a larger Reynolds number of Re = 17.55 in figure 6.2(b); Veremieiev and Wacks [2019] attributed this discrepancy at larger Re to an increased stretching of the long-wave approximation since, for constant Ka and L/L_c, the shallowness parameter scales with the Reynolds number, namely $\epsilon = (2Re/sin\beta)^{1/3}/(Ka^{11/6}L/L_c)$, but this reasoning is misplaced and betrays a lack of understanding about the modelling approach on their part – a consequence of relying upon the weighted-residual technique to derive the asymptotic models in their paper. Indeed, one should expect any finite-order RAM formalism to diverge from the true Navier-Stokes solution in the limit of $\epsilon \to \infty$, however, one must also appreciate that the RAM methodology is primarily an expansion with respect to the powers of $\hat{z}$ and therefore it is when the expansion of the fluid velocity is not extended to high enough powers of $\hat{z}$ that these models diverge from the full equation set. Inertia is the mechanism demanding a ever greater extension of the fluid velocity expansion to higher powers of $\hat{z}$; this is because the non-linear inertial terms generated by lower powers of $\hat{z}$ are balanced against higher powers of $\hat{z}$, in contrast, viscous terms only ever need to balanced by equivalent or lesser powers of $\hat{z}$ – see section 3.4.1. $RAM[\epsilon^4/\hat{z}^2]$ only incorporates the full (x,t)-dependence of the first two gradients of the velocity field with respect to $\hat{z}$; their evolution across the x-domain is then balanced against higher-order $\hat{z}$-gradients whose own (x,t)-dependence is assumed to be negligible. Howbeit, at greater Re, the evolution of higher-order $\hat{z}$-gradients ceases to be negligible and thus even higher-order $\hat{z}$-gradients are required to balance their evolution; with this understanding, the reduction in performance of $RAM[\epsilon^4/\hat{z}^2]$ at greater Re can be attributed squarely to the increase in Re alone and not to a stretching of the long-wave approximation. An important feature of the RAM methodology is that the long-wave expansion is secondary to the power series expansion with respect to $\hat{z}$ – see section 3.34.

Figure 6.3 details the improved performance of $RAM[\epsilon^4/\hat{z}^2]$ over the fourth-order weighted residual model (WIBL4) presented in Veremieiev and Wacks [2019]; whilst both models are based upon a power series expansion of the fluid velocity with respect to $\hat{z}$ and possess the same number of degrees of freedom, each utilises an algebraically distinct expression to describe the pressure distribution through the film – the expression for the fluid pressure used presently was derived in section 2.7. Whilst algebraically distinct, the expressions used to describe the fluid pressure in Veremieiev and Wacks [2019] and in the present monograph are asymptotically equivalent in the long-wave limit; indeed, this feature is demonstrated by figures 6.3(a-c) where both models are seen to perform exceptionally well, being not only in perfect agreement with one another (the $RAM[\epsilon^4/\hat{z}^2]$ prediction lies directly atop the WIBL4 prediction) but also in near-perfect

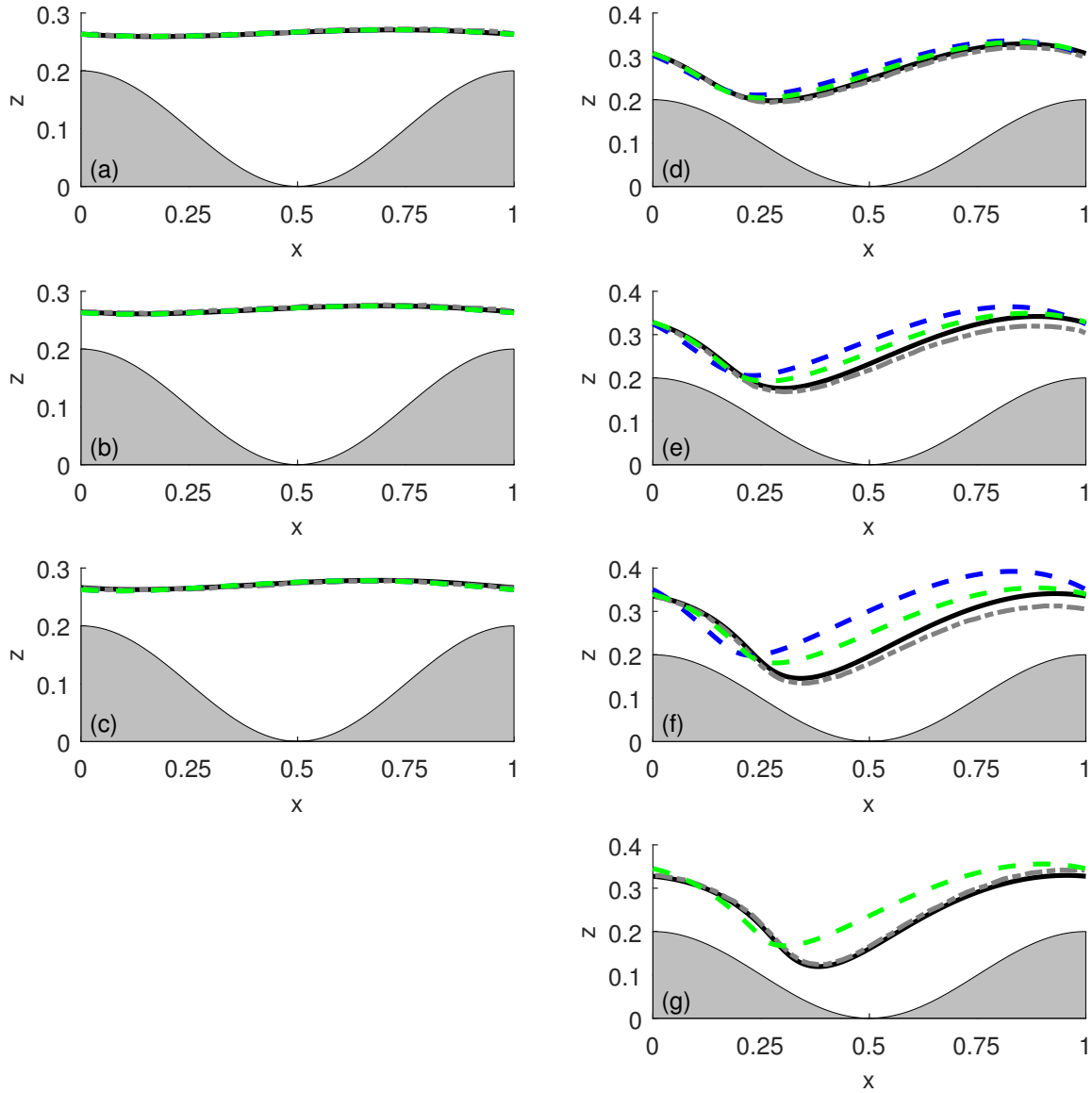

Figure 6.3: Steady-state free-surface profile predictions obtained utilising $RAM[\epsilon^4/\hat{z}^2]$ [dashed green curve] and WIBL4 [dashed blue curve] of Veremieiev and Wacks [2019] compared for film flow over sinusoidally varying substrate for the case $\beta = 45°$, $A/L = 0.2$, (a-c) $L/L_c = 1.057$, $Re = 7.5, 15, 22.5$, $Ka = 5.937, 6.735, 7.250$, and (d-g) $L/L_c = 3.342$, $Re = 15, 22.5, 30, 37.5$, $Ka = 3.594, 3.869, 4.077, 4.246$. The corresponding N-SE solution is shown as a solid black curve and NS data from (left-column) figure 5 and (right-column) figure 6 of Nguyen and Bontozoglou [2011] is plotted as a dot-dashed grey curve. There is no prediction from WIBL4 in figure 6.3(g) as the model in question failed to converge to a stable solution when surface curvature is retained, $g = (\partial f/\partial x)^2$.

agreement with the corresponding *N-SE* solutions – the latter detail confirms that the long-wave approximation is a strong conjecture within this parameter space. The validity of the long-wave approximation in this parameter space is likely due to the effect of surface tension extending across the entire x-domain, $L/L_c = 1.057 \approx 1$, and thus the pressure distribution throughout the film will be characterised by the capillary pressure term; accordingly, one should expect exceptional performance from both $RAM[\epsilon^4/\hat{z}^2]$ and WIBL4 in this parameter space because the capillary pressure term remains a strong form term in each respective formalism[1]. The influence of surface tension is weaker in figures 6.3(d-g) with the corrugation wavelength being more than three times the capillary length, $L/L_c = 3.342$, and this results in larger deformations of the free-surface as the liquid film flows down the corrugated substrate; the fluid pressure is no longer dominated by the capillary term in this parameter space and thus the accuracy of each model increasingly relies upon how well-approximated the other pressure terms are in their respective formalisms. As the Reynolds number is increased through 6.3(d-g), $RAM[\epsilon^4/\hat{z}^2]$ is seen to out-perform WIBL4 from Veremieiev and Wacks [2019]; this can be attributed to the fact that the derivation of the fluid pressure in section 2.7 utilises the Leibniz integral rule and shear stress boundary condition to minimise the degree of approximation in the fluid pressure expression and thus one can say that equation (2.40) is a more robust and accurate representation of the fluid pressure then its counterpart featured in the work of Veremieiev and Wacks [2019]. Indeed, one key advantage granted by using equation (2.40) to model the fluid pressure is that, with the exception of the capillary pressure term, surface curvature is absent from this expression; surface curvature is frequently omitted from asymptotic models by setting $g = 0$ because if it is not well-handled then its inclusion can lead to numerical difficulties and rapid divergence of the model under scrutiny – the reason why there is no data available for WIBL4 in figure 6.3(g) is because the model diverges when $g = (\partial f/\partial x)^2$. However, accurate implementation of surface curvature into any asymptotic model leads to improved performance as demonstrated by $RAM[\epsilon^4/\hat{z}^2]$; $RAM[\epsilon^4/\hat{z}^2]$ is able to accommodate $g = (\partial f/\partial x)^2$ because the dangerous surface curvature terms in the fluid pressure which could cause divergence have been exchanged with asymptotically equivalent terms which are more well-behaved; in consequence, the RAM formalism is able to push past the point at which previous models have diverged due to a mishandling of the surface curvature terms and extend the parameter space within which the model is applicable.

6.2 Uniformly heated substrate

Turning attention to the problem of steady film flow down uniformly heated substrate, a key comparison to be made is between a reduced asymptotic model (RAM) which assumes the leading temperature expansion to be linear and the one which allows the leading temperature expansion to be quadratic. As outlined in section 3.4, the RAM

[1] In any asymptotic model, terms which retain their algebraic form from the original equation set (2.23 – 2.31) are said to be of strong form; in contrast, weak form terms are those which have been approximated and are thus only valid within a given parameter space.

methodology expands the velocity and temperature fields with respect to the powers of $\hat{z}$ but in order to form a closed-form solution, the spatial and temporal evolution of only a finite number of degrees of freedom are considered and this is justified through a long-wave expansion. The leading velocity and temperature expansions refer to those degrees of freedom which appear at leading-order in the long-wave expansion: in the case of the flow velocity, it is well-known that the leading velocity profile is parabolic and thus the leading velocity expansion is quadratic; however, in the case of the fluid temperature, a long-standing assumption has been that the leading temperature expansion must be linear because the temperature field reduces to the Nusselt linear temperature distribution in the long-wave limit. Despite this fact, studies have repeatedly shown that heat transfer models based upon a linear temperature ansatz rapidly diverge from the solution to the full governing equation set [Trevelyan et al., 2007, Chhay et al., 2017, Thompson et al., 2019, Cellier and Ruyer-Quil, 2020]. The derivation of the reduced asymptotic model for the heated film case presented in section 3.4.3 shows that the leading temperature expansion requires a minimum of two degrees of freedom: (i) the first is needed to describe the evolution of the free-surface temperature (ϑ); whilst (ii) the second describes the evolution of the heat flux through the free-surface ($-Bi\vartheta$). Models derived from a linear temperature ansatz only model the evolution of one of these quantities, the only exception being Thompson et al. [2019] who proposed a model based on a linear temperature ansatz which incorporated both the free-surface temperature and heat flux but at the expense of excluding the substrate temperature which means the temperature expansion is not properly bounded from above. Despite the fluid temperature possessing two distinct degrees of freedom at leading order, the energy residual belonging to any RAM formalism based solely upon the leading temperature expansion can be reduced to a single evolution in terms of ϑ because the free-surface temperature and heat flux through the free-surface are linearly proportional to one another and so the original set of two energy residuals can be collapsed down to one.

To demonstrate the improved performance of the quadratic leading temperature expansion over the linear one, a series of reduced asymptotic models based on both a linear and a quadratic temperature ansatz are compared in this section: RAM formalisms derived from a linear leading temperature expansion are referred to as $RAM[\epsilon^n/\hat{z}^m]-\theta_{lin}$ for a given long-wave order n and number of degrees of freedom m; whereas those derived from a quadratic leading temperature expansion, such as those derived in section (3.4.3), are referred to as $RAM[\epsilon^n/\hat{z}^m]-\theta_{para}$ in the following section. The $RAM[\epsilon^n/\hat{z}^m]-\theta_{lin}$ formulation utilises the exact same mass – equation (3.149) – and momentum – equation (3.150) – residuals as $RAM[\epsilon^n/\hat{z}^m]-\theta_{para}$, the only change is that $RAM[\epsilon^n/\hat{z}^m]-\theta_{lin}$ assumes the leading temperature expansion to be linear, stipulating that $b_2 \sim \mathcal{O}(\epsilon)$; this yields a distinct energy residual in which higher-order temperature terms are approximated by the following linear temperature profile:

$$\theta_{lin} = 1 + \frac{(\vartheta - 1)}{h}\hat{z}, \tag{6.2}$$

which models the evolution of the free-surface temperature (ϑ) but neglects the evolution

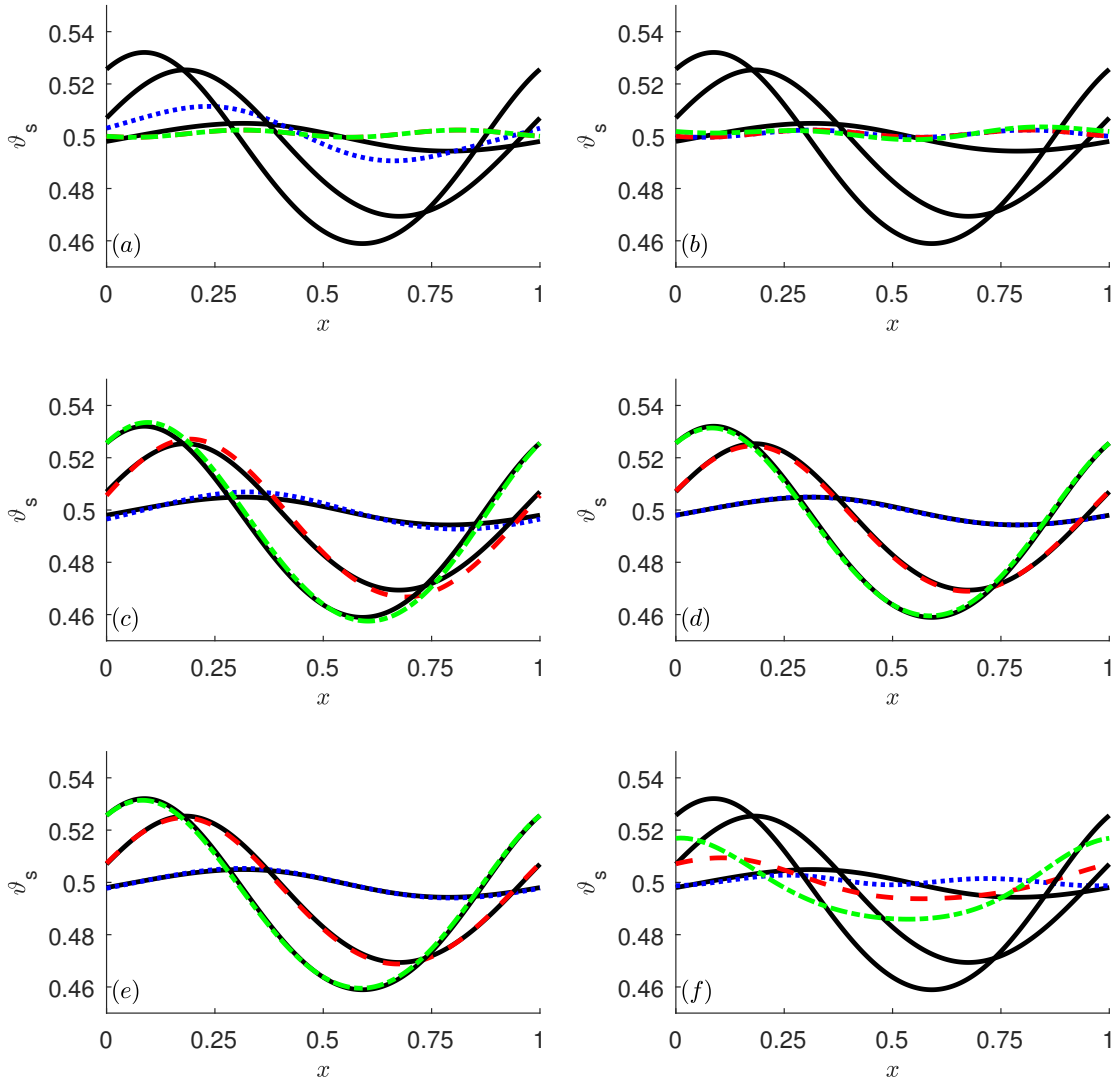

Figure 6.4: Steady-state free-surface temperature predictions obtained utilising (a) BE, (b) RBE, (c) $RAM[\epsilon^4/\hat{z}^2] - \theta_{lin}$, (d) $RAM[\epsilon^2/\hat{z}^2] - \theta_{para}$, (e) $RAM[\epsilon^4/\hat{z}^2] - \theta_{para}$ and (f) $RAM[\epsilon^2/\hat{z}^6] - \theta_{para}$ for film flow over sinusoidally varying substrate for the case $Re = 0.75$, $\beta = 63.4349°$, $Pr = 7.0$, $Bi = 1.0$ and $A/L = 0.04$ when $Ka = 1.2249$ $(L/L_c = 8.19,\ Ma = 0.1)$ [dashed blue curve], $Ka = 2.2953$ $(L/L_c = 2.59,\ Ma = 0.01)$ [dashed red curve] and $Ka = 3.5602$ $(L/L_c = 1.158,\ Ma = 0.002)$ [dashed green curve]. The corresponding N-SE solution is shown as a solid black curve.

of the heat flux through the free-surface ($-Bi\vartheta$); equation (6.2) is compared against equation (3.90) which is the quadratic leading temperature expansion and is capable of modelling the evolution of both the free-surface temperature (ϑ) and heat flux ($-Bi\vartheta$):

$$\theta_{para} = 1 + \frac{(\vartheta - 1)}{h}\hat{z} + \frac{(\vartheta - 1 + Bih\vartheta)}{h^2}\left(h\hat{z} - \hat{z}^2\right), \tag{6.3}$$

In the case of the $RAM[\epsilon^n/\hat{z}^2] - \theta_{lin}$ where $n \geq 2$, the linear temperature ansatz – equation (6.2) – yields the following energy residual:

$$\begin{aligned}
\epsilon RePr\left[\frac{4}{5}\frac{\partial\vartheta}{\partial t} + \frac{27}{25}\frac{q}{h}\frac{\partial\vartheta}{\partial x} + \frac{7}{50}\frac{(\vartheta-1)}{h}\frac{\partial q}{\partial x}\right] + \frac{12}{5h^2}\left[\vartheta - 1 + \frac{Bih\vartheta}{\sqrt{1+\epsilon^2 g}}\right] \\
+\epsilon^2\Bigg[\frac{4}{5}\frac{(\vartheta-1)}{h}\frac{\partial^2 h}{\partial x^2} - \frac{12}{5}\frac{(\vartheta-1)}{h^2}\frac{\partial h}{\partial x}\frac{ds}{dx} + \frac{6}{5}\frac{(\vartheta-1)}{h}\frac{d^2 s}{dx^2} + \frac{8}{5h}\frac{\partial h}{\partial x}\frac{\partial\vartheta}{\partial x} \\
+\frac{12}{5h}\frac{ds}{dx}\frac{\partial\vartheta}{\partial x} - \frac{8}{5}\frac{(\vartheta-1)}{h^2}\left(\frac{\partial h}{\partial x}\right)^2 - \frac{4}{5}\frac{\partial^2\vartheta}{\partial x^2} - \frac{12}{5h}\frac{\frac{\partial f}{\partial x}\frac{\partial\vartheta}{\partial x}}{1+\epsilon^2 g}\Bigg] = 0.
\end{aligned} \tag{6.4}$$

The results in figures 6.4 and 6.5 show the free-surface temperature, ϑ_s, and profile, $f_s(x)$, predictions, respectively, for three different values of Ka and relate to the parameter set of Figures 3 and 4 from D'Alessio et al. [2010]. The predictions in figures 6.4 and 6.5 were obtained from: (a) the Benney equation (BE) – equation (3.21); (b) the regularised Benney equation (RBE) – equation (3.21); (c) $RAM[\epsilon^4/\hat{z}^2] - \theta_{lin}$; (d) $RAM[\epsilon^4/\hat{z}^2] - \theta_{para}$; (e) $RAM[\epsilon^2/\hat{z}^2] - \theta_{para}$; (f) $RAM[\epsilon^2/\hat{z}^6] - \theta_{para}$. Note that solving BE and RBE returns a solution for the film thickness, h, and so the free-surface temperature predictions were obtained by evaluating $\theta = \theta_{\mathbb{N}} + \theta_1 + \mathcal{O}(\epsilon^2)$ at $\hat{z} = h$ where $\theta_{\mathbb{N}}$ is the Nusselt linear temperature distribution seen in equation (3.7) and θ_1 is the first-order correction given by equation (3.19). Beginning with the free-surface temperature predictions of the Benney equation (BE) and its regularised form (RBE) in figures 6.4(a,b), it is immediately clear that neither is capable of capturing the thermodynamics at play in gravity-driven film flow down wavy substrate; the main feature of these predictions is a drastic under-estimation of how much the temperature fluctuates across the free-surface, however, this appears to be a consequence of these models failing to capture the true deformation of the free-surface due to substrate topography, instead the film thickness prediction of these models remains almost uniform across the entire domain, $h \approx 1 \ \forall x$ – see figures 6.5(a,b). In contrast, all the RAM formalisms offer respectable agreement with *N-SE* solutions with the major exception being the free-surface temperature prediction of $RAM[\epsilon^2/\hat{z}^6] - \theta_{para}$ – figure 6.4(f); the reason behind the poor behaviour of $RAM[\epsilon^2/\hat{z}^6] - \theta_{para}$ is not entirely clear but it stems from the introduction of higher-order free-surface gradients as new variables to the modelling approach, naturally these predictions are disappointing and indicate that there is some inconsistency in the present attempt to extend the RAM methodology to higher-orders in the long-wave expansion. The free-surface temperature predictions of (c) $RAM[\epsilon^4/\hat{z}^2] - \theta_{lin}$, (d)

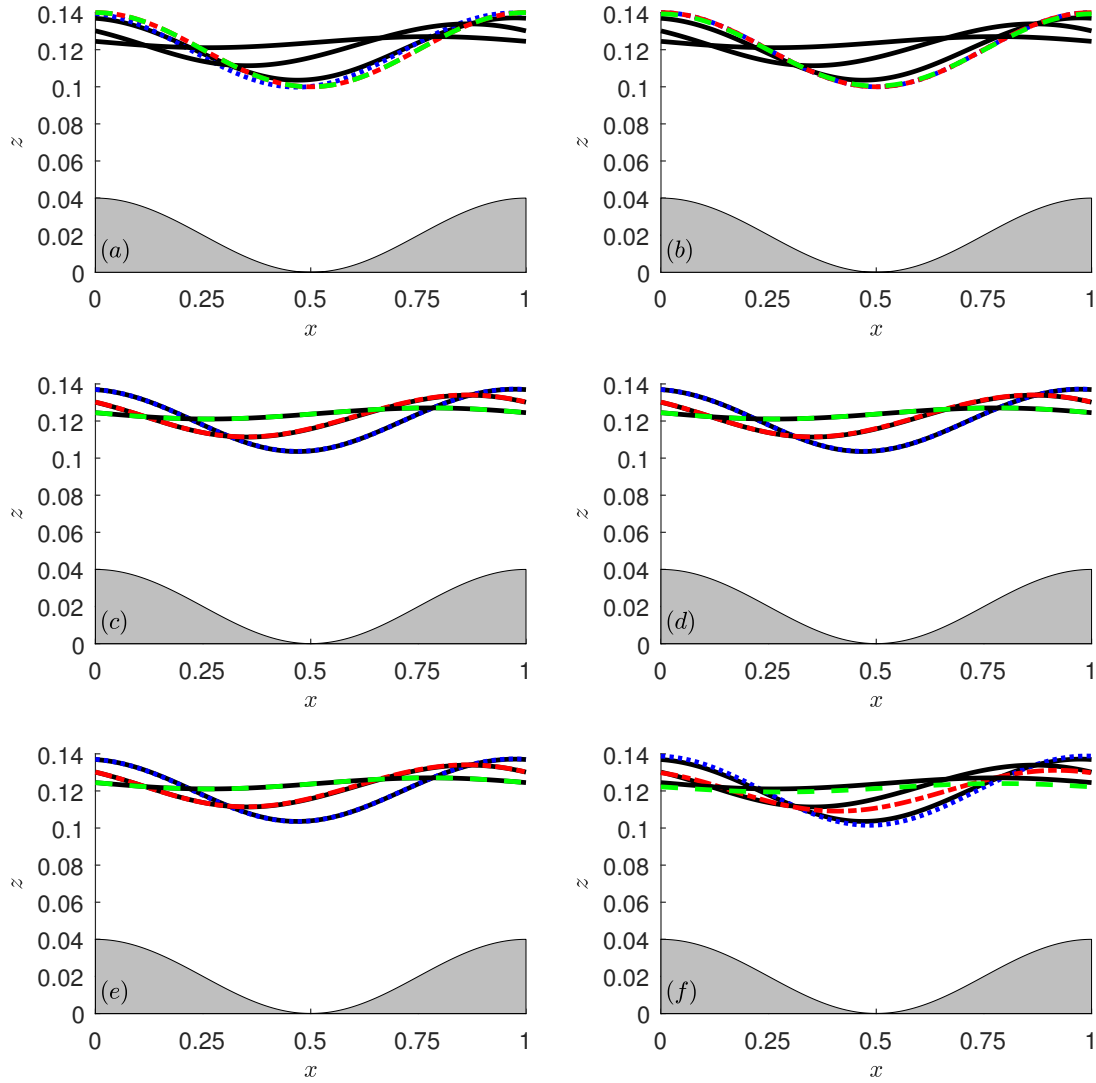

Figure 6.5: Steady-state free-surface profile predictions obtained utilising (a) BE, (b) RBE, (c) $RAM[\epsilon^4/\hat{z}^2]$ – θ_{lin}, (d) $RAM[\epsilon^2/\hat{z}^2]$ – θ_{para}, (e) $RAM[\epsilon^4/\hat{z}^2]$ – θ_{para} and (f) $RAM[\epsilon^2/\hat{z}^6]$ – θ_{para} for film flow over sinusoidally varying substrate for the case Re = 0.75, β = 63.4349°, Pr = 7.0, Bi = 1.0 and A/L = 0.04 when Ka = 1.2249 (L/L_c = 8.19, Ma = 0.1) [dashed blue curve], Ka = 2.2953 (L/L_c = 2.59, Ma = 0.01) [dashed red curve] and Ka = 3.5602 (L/L_c = 1.158, Ma = 0.002) [dashed green curve]. The corresponding N-SE solution is shown as a solid black curve.

$RAM[\epsilon^4/\hat{z}^2]-\theta_{para}$ and (e) $RAM[\epsilon^2/\hat{z}^2]-\theta_{para}$ are all very good; nevertheless, it can be seen that those models based on a quadratic temperature ansatz perform better than $RAM[\epsilon^4/\hat{z}^2]-\theta_{lin}$ in every case and achieve almost perfect agreement with the corresponding *N-SE* solutions. Indeed, it can be seen the $RAM[\epsilon^4/\hat{z}^2]-\theta_{lin}$ predictions tends to over-estimate the variation in ϑ_s. This is attributable to θ_{lin} assuming the evolution of the heat flux through the film with respect to (x,t) is negligible and primarily constant in the z-direction, as in the flat-film case, whereas θ_{para} affords a degree of freedom to the heat flux inside the film. Accordingly, $RAM[\epsilon^4/\hat{z}^2]-\theta_{lin}$ under-estimates the dissipation of heat within the film and consequently over-emphasises the dependence of ϑ_s on the film thickness, in contrast to $RAM[\epsilon^n/\hat{z}^2]-\theta_{para}$ for $n=2,4$ which correctly predicts how thermal conduction seeks to dissipate heat throughout the film and minimise temperature fluctuations at the free-surface. Kalliadasis et al. [2003a] assumed having the energy residual satisfy Newton's law of cooling, even if the assumed linear temperature profile did not, would be sufficient to describe the fluid temperature across the free-surface. However, temperature deviations stem entirely from the fluid convection and stream-wise conduction, therefore it is the reduction in dimensionality of these terms which is critical to achieving accurate free-surface temperature predictions beyond the flat-film case. The linear temperature approximation – equation (6.2) – is unable to ensure an accurate transformation of these terms because it fails to satisfy Newton's law of cooling; thus, decreasing the accuracy of $RAM[\epsilon^4/\hat{z}^2]-\theta_{lin}$. In contrast, θ_{para} achieves a reduction in dimensionality of both the convection and stream-wise conduction terms, explaining its superior predictive capability.

The accompanying free-surface profiles are shown in figure 6.5 and show how the film thickness (h) predictions of the BE and RBE remain close to the long-wave solution of $h=1$; meanwhile, the four RAM formalisms all achieve perfect agreement with the corresponding *N-SE* solutions with the notable exception of (f) $RAM[\epsilon^2/\hat{z}^6]-\theta_{para}$ which diverges slightly; in general, for small Reynolds number, $Re<1$, and substrate amplitude, $A/L\ll 0.2$, one would expect good agreement with *N-SE* solutions. The predictions of (c) $RAM[\epsilon^4/\hat{z}^2]-\theta_{lin}$, (d) $RAM[\epsilon^4/\hat{z}^2]-\theta_{para}$ and (e) $RAM[\epsilon^2/\hat{z}^2]-\theta_{para}$ all agree because these models all share the same momentum residual; in addition, the Marangoni effect is not large enough in this case for any differences in the steady free-surface temperature predictions to modify the film thickness predictions. Once again, it is not clear what has caused a divergence in the $RAM[\epsilon^2/\hat{z}^6]-\theta_{para}$ prediction, merely that there is an underlying issue with the derivation of this model. A final feature to point out in figure 6.5 is that there is no discrepancy between $RAM[\epsilon^4/\hat{z}^2]-\theta_{para}$ and $RAM[\epsilon^2/\hat{z}^2]-\theta_{para}$, this indicates that both vertical inertia and viscosity are negligible and that the second-order approximation is sufficient to describe the film dynamics within this parameter space.

Herein, the focus of the steady-state results is on the improvement offered by θ_{para} over θ_{lin}. Figure 6.6 explores how $RAM[\epsilon^4/\hat{z}^2]-\theta_{lin}$ and $RAM[\epsilon^4/\hat{z}^2]-\theta_{para}$ perform with increasing Pr, and A/L; the top three rows contain free-surface temperature predictions for $Pr=14,\ 28,\ 56$ whilst the bottom row contains free-surface profile predictions for $Pr=14$. As in the previous set of steady-state results, the analysis was carried out

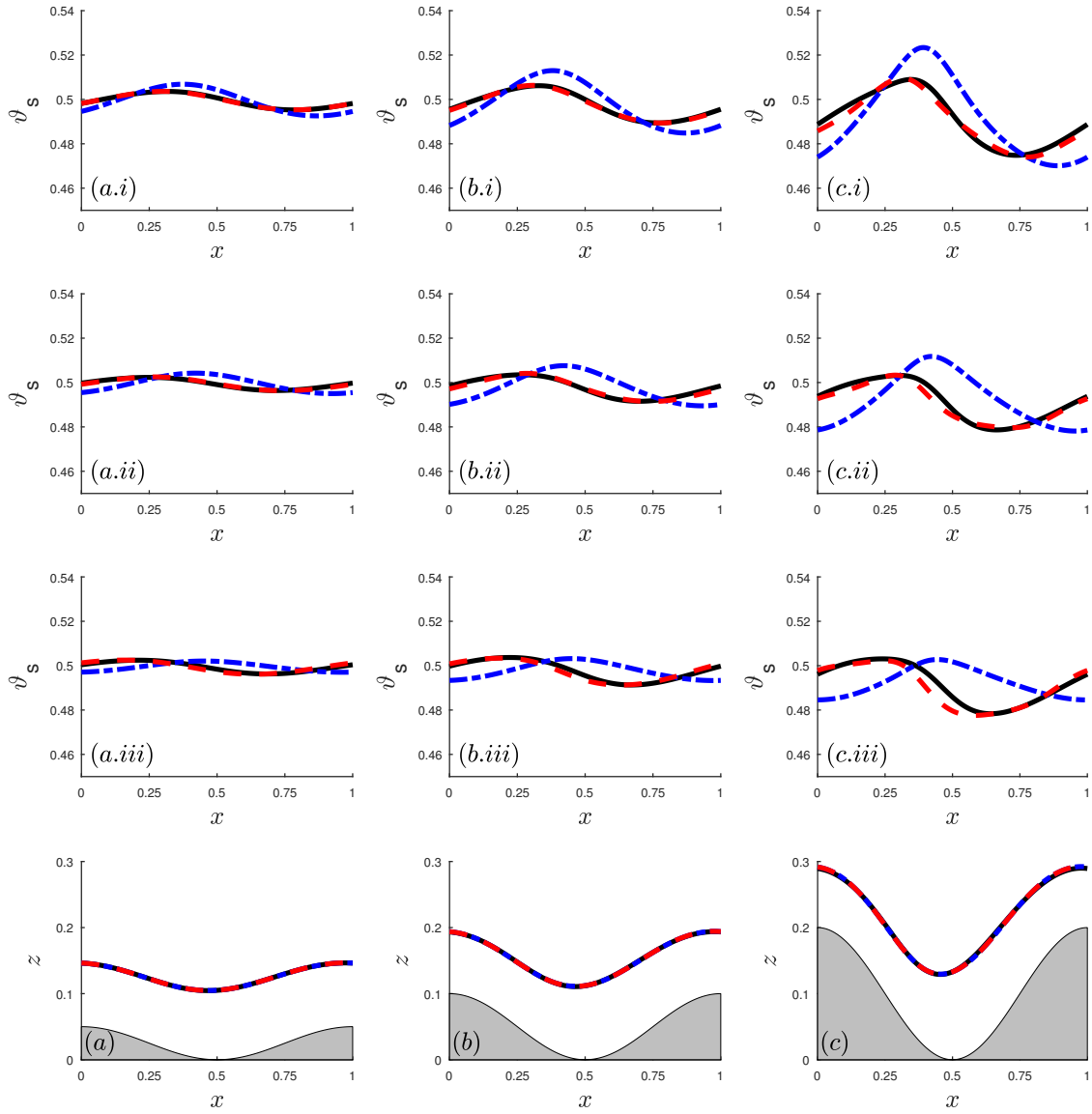

Figure 6.6: Steady-state free-surface temperature predictions (top three rows) for film flow over sinusoidally varying substrate obtained for (a–c) $A/L = 0.05,\ 0.1,\ 0.2$ and (i–iii) $Pr = 14,\ 28,\ 56$; with $Re = 0.75$, $\beta = 63.4349°$, $L/L_c = 8.19$, $Ka = 1.2249$, $Ma = 0.1$ and $Bi = 1.0$. $RAM[\epsilon^4/\hat{z}^2] - \theta_{lin}$ predictions [dot-dashed blue curve]; $RAM[\epsilon^4/\hat{z}^2] - \theta_{para}$ predictions [dashed red curve]; corresponding *N-SE* solutions [solid black curve]. The free-surface disturbance predictions (bottom row) relate to the case $Pr = 14$ only; the predictions for $Pr = 28,\ 56$ are not included because the smallness of Ma means the variation of Pr has no noticeable effect on the shape of the free-surface.

for creeping flow, $Re < 1$; it is shown in later figures that neither leading temperature expansion is sufficient for describing the temperature distribution inside films flowing down wavy inclines when $Re > 1$. $RAM[\epsilon^4/\hat{z}^2] - \theta_{para}$ attains quantitatively accurate results for heated film flow up to $A/L = 0.2$. This limit may be a consequence of modelling the velocity and temperature fields as power series; Scholle et al. [2004] found that, for thick films $H \sim L$, an infinite series describing the velocity field failed to converge in the troughs of the substrate corrugations when $A/L > 0.2$. Turning now to the effect of increasing Pr, denoted (i-iii) in figure 6.6, the $RAM[\epsilon^4/\hat{z}^2] - \theta_{para}$ free-surface temperature predictions are very encouraging particularly when compared against those from $RAM[\epsilon^4/\hat{z}^2] - \theta_{lin}$. The top row in Figure 6.6 corresponds to $Pr = 14$, which is twice that of water ($Pr_{water} = 7$); in subsequent rows Pr is double the value of the row above. The inaccuracy of the $RAM[\epsilon^4/\hat{z}^2] - \theta_{lin}$ free-surface temperature prediction is evident and increases with increasing Pr to the point where not even weak agreement persists with the corresponding *N-SE* solutions. The $RAM[\epsilon^4/\hat{z}^2] - \theta_{para}$ predictions on the other hand, demonstrate excellent agreement with the corresponding *N-SE* solutions up to $Pr = 56$ and $A/L = 0.1$. The results in figure 6.6 lend significant credence to θ_{para} because the RAM methodology laid out in section 3.4.3 should be asymptotically equivalent to first-order and therefore asymptotically accurate at moderate values of Pr.

To further reinforce that the leading temperature expansion needs to be non-linear, the temperature expansions according to $RAM[\epsilon^4/\hat{z}^2] - \theta_{para}$ and $RAM[\epsilon^4/\hat{z}^2] - \theta_{lin}$ – which include first-order contributions – are plotted against corresponding *N-SE* solutions in figure 6.7a at two locations along the x-axis ($x = 0$ and $x = 0.5$) for the case $Pr = 14$ and $A/L = 0.1$. Expanding the fluid temperature – as per equation (3.64) – with $\{b_j\}$ given by the recurrence relations (3.45); the $RAM[\epsilon^4/\hat{z}^2] - \theta_{para}$ result was generated from the expressions obtained by substituting θ_{para} into the recurrence relations and computing via the $RAM[\epsilon^4/\hat{z}^2] - \theta_{lin}$ solutions for $h_s(x)$ and $\vartheta_s(x)$ from Figures 6.6b and 6.6($b.i$), respectively; $RAM[\epsilon^4/\hat{z}^2] - \theta_{para}$ prediction was generated from the expressions for $\{b_j\}$ obtained by substituting θ_{lin} into the recurrence relations and computing via the RAM–θ_{lin} solutions for $h_s(x)$ and $\vartheta_s(x)$ from Figures 6.6b and 6.6($b.i$), respectively. The non-linear behaviour is modest but contrasting the *N-SE* solutions [solid black curves] against solutions according to the Nusselt linear temperature distribution [dotted grey lines] – equation (3.7) – clearly show the temperature profile possesses a significant curve. The temperature expansion based upon θ_{para} [the red and green dashed curves] replicates the temperature field inside the film very well, whereas the linear approximation θ_{lin} [the blue and magenta dot-dashed curves] is not as good. The error associated with the RAM temperature predictions relative to corresponding *N-SE* solutions through the film is plotted in figure 6.7b, revealing the temperature expansion based on θ_{para} is around five times more accurate than the one based on θ_{lin} in the two cases considered. Note the dimensionless error in Figure 6.7(b) is equal to the % of Θ_Δ, where $\Theta_\Delta = \Theta_s - \Theta_a$ is the temperature difference between the substrate and ambient gas.

The error associated with $RAM[\epsilon^4/\hat{z}^2] - \theta_{para}$ and $RAM[\epsilon^4/\hat{z}^2] - \theta_{lin}$ across the entire flow domain, is assessed in terms of the mean squared error (MSE) through the

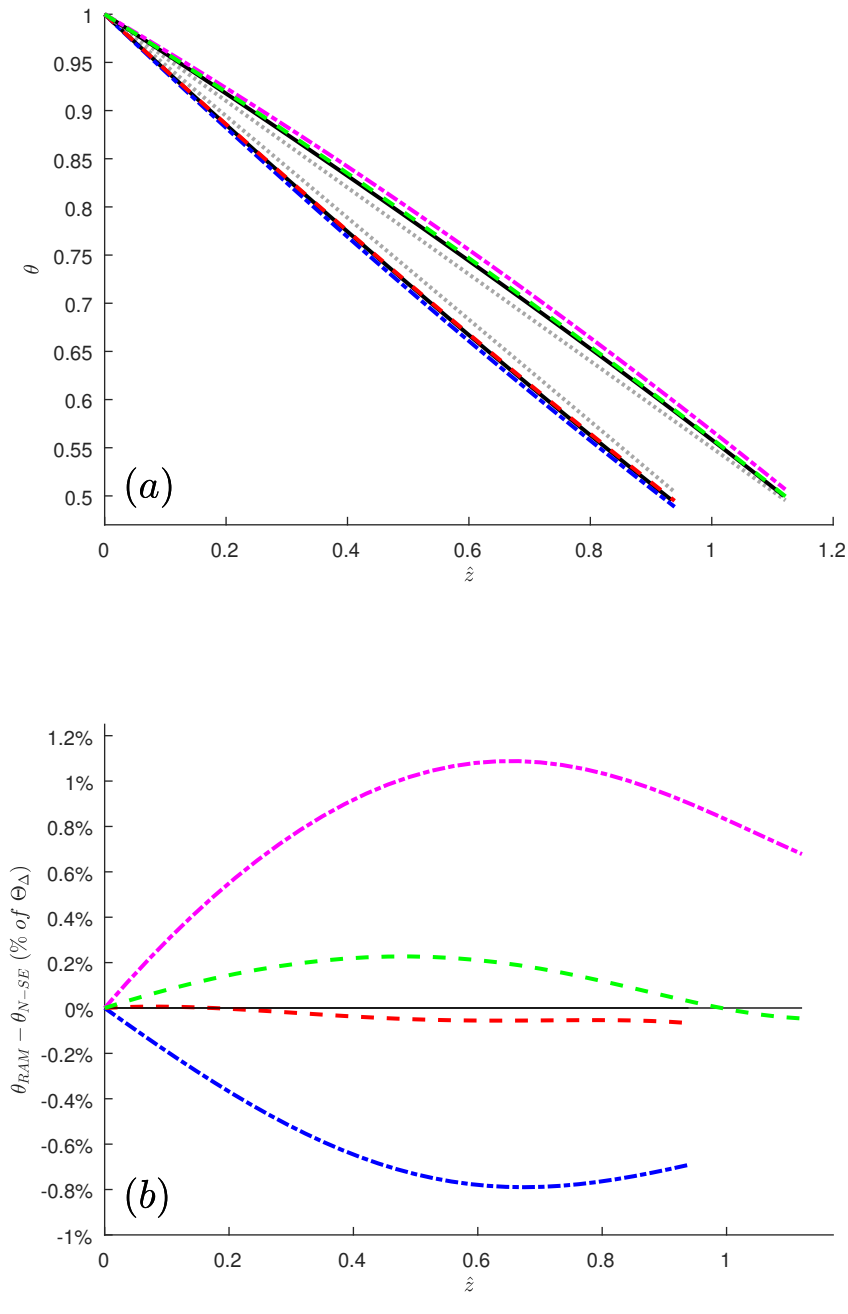

Figure 6.7: (a) Plots of the predicted temperature profile through the film, for film flow over sinusoidally varying substrate, where $\hat{z} = z - s(x)$, obtained for $Re = 0.75$, $\beta = 63.4349°$, $L/L_c = 8.19$, $Bi = 1.0$, $Ka = 1.2249$, $Ma = 0.1$, $Pr = 14$ and $A/L = 0.1$; the θ_{lin}. Two x-locations are considered: $x = 0$ [red dashed, θ_{para}, and blue dot-dashed, θ_{lin}, curves] and $x = 0.5$ [green dashed, θ_{para}, and magenta dot-dashed, θ_{lin}, curves]. The corresponding *N-SE* solutions and Nusselt linear temperature distributions – equation $(3.7b)$ – are given by the solid black curves and dotted grey lines, respectively. (b) Plot of the predictive error associated with θ_{para} and θ_{lin} relative to the *N-SE* solution.

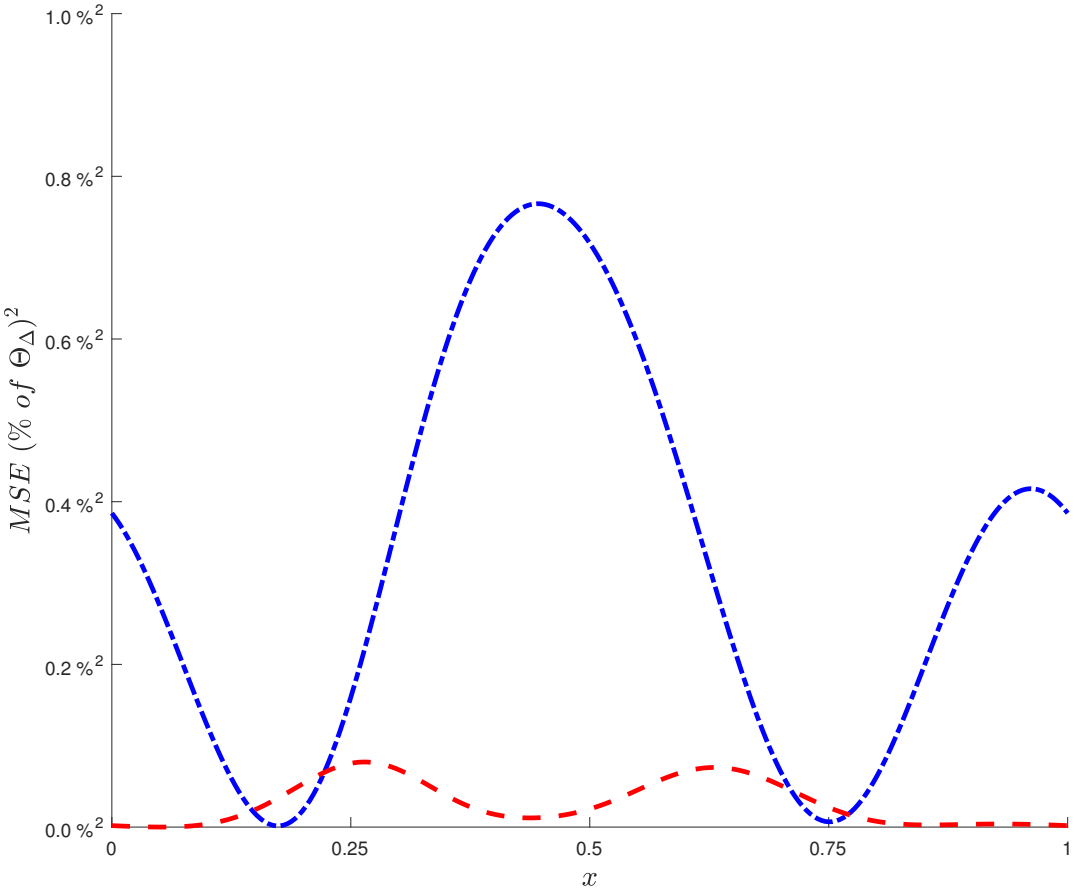

Figure 6.8: Plot of the MSE (= $(1/N_{\hat{z}})\sum_{i=1}^{N_{\hat{z}}}[\theta_{RAM,i} - \theta_{N\text{-}SE,i}]^2$) vs. x for a temperature dependence based on θ_{para} [dashed red curve] and θ_{lin} [dot-dashed blue curve], respectively, within films flowing over sinusoidally varying substrate. Obtained for Re = 0.75, β = 63.4349°, L/L_c = 8.19, Bi = 1.0, Ka = 1.2249, Ma = 0.1, Pr = 14 and A/L = 0.1.

film relative to the corresponding *N-SE* solutions, such that at any given point along the x-axis, $MSE = (1/N_{\hat{z}}) \sum_{i=1}^{N_{\hat{z}}} [\theta_{RAM,i} - \theta_{N\text{-}SE,i}]^2$; with $N_{\hat{z}}$ being the number of mesh points along the $\hat{z}$-axis. Figure 6.8 shows the temperature expansion based on θ_{para} exhibits far less error and variance than the one based on θ_{lin}. The error associated with θ_{para} is largest in the transition regions between the peaks and the troughs of the corrugated substrate; in these regions, the concavity of the temperature field changes sign. The increased error in these regions can be attributed to θ_{para} failing to predict the change in concavity at the correct position along the x-axis. In contrast, the largest source of error associated with θ_{lin} is in over-estimating the concavity of the temperature field – see Figure 6.7*a* – which is a consequence of assuming $b_2 \sim \mathcal{O}(\epsilon)$. In the present analysis, the parabolic temperature coefficient b_2 is associated with the dissipation of heat throughout the film; in restricting the entry of b_2 to first-order in the *long-wave* expansion and not ascribing a degree of freedom to model the evolution of the heat flux through the free-surface, $RAM[\epsilon^4/\hat{z}^2] - \theta_{lin}$ under-estimates how much heat is being dissipated within the film and leads to an over-estimation of the temperature field's concavity. The MSE shows there are two points where θ_{lin} attains better agreement with *N-SE* solutions than θ_{para} but overall it is far worse.

The final set of steady-state solutions for the film thickness and free-surface temperature are presented in figure 6.9 and examine the performance of the RAM model at moderate Reynolds number, $Re > 1$. The inclination angle of the substrate, β, was reduced so the estimated Re_{crit} was comparable to the Re values considered; equation (5.30) yields $Re_{crit.}^{flat} = \{7.00, 6.94\}$ for $Ka = \{1.664, 1.8878\}$ when $\beta = 10°$, $Ma = 0.1$ and $Bi = 1.0$. These results were specifically chosen to examine whether a moderate increase in the fluid inertia has an effect on the accuracy of the predictions of $RAM[\epsilon^4/\hat{z}^2] - \theta_{lin}$ and $RAM[\epsilon^4/\hat{z}^2] - \theta_{para}$. Accordingly, the parameter sets for Figure 6.9 were chosen so only the coefficient in front of the stream-wise and vertical inertia increased; Pr was decreased so the Péclet number, $Pe = RePr$ remained constant. The predictions further reveal how $RAM[\epsilon^4/\hat{z}^2] - \theta_{para}$ outperforms $RAM[\epsilon^4/\hat{z}^2] - \theta_{lin}$ and achieves good agreement with the corresponding *N-SE* solution to the full problem. However, the results do highlight the sensitivity of the RAM free-surface temperature prediction to changes in the independent parameters. In order to achieve reasonable agreement with *N-S* solutions for the free-surface temperature, the film thickness prediction must be in excellent agreement with its *N-S* counterpart. This can be attributed to the fact that the leading-order flow rate and free-surface temperature solutions – see equation (3.7) – are functions of the film thickness and whilst additional degrees of freedom are introduced at first-order, the dynamics of the film are still chiefly governed by the film thickness. Good agreement is achieved between the $RAM[\epsilon^4/\hat{z}^2] - \theta_{para}$ and *N-SE* solutions for moderate Pr and small Re in Figure 6.6 because the film thickness h_s remains mostly uniform. At moderate Re and small Pr, the free-surface shape deviates significantly from the flat-film solution leading to a poorer prediction of the free-surface temperature. This is unsurprising since the leading temperature expansion is only a relaxation of the trivial case. Given most functional fluids have moderate to large Pr values, future models may benefit from energy residuals which are asymptotically equivalent at higher-order, al-

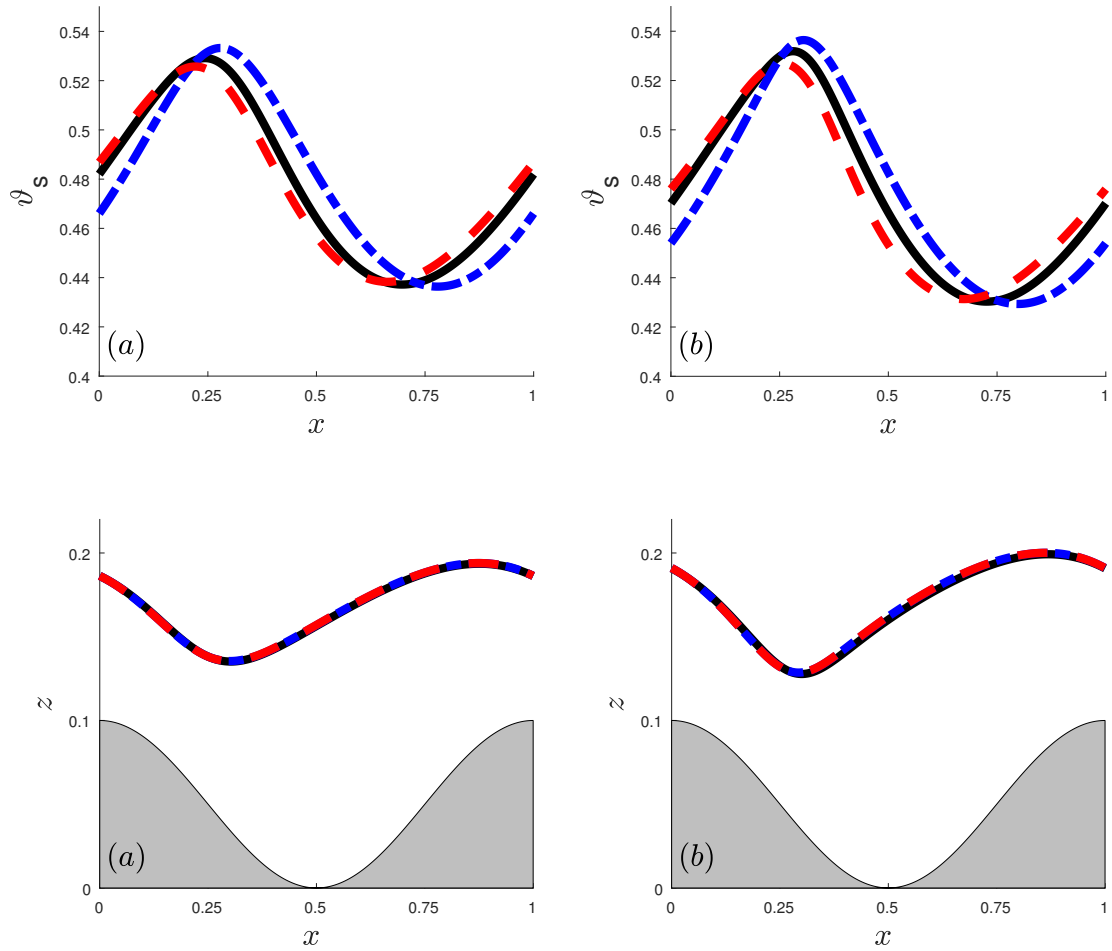

Figure 6.9: Steady-state free-surface temperature (top row) and profile (bottom row) predictions for film flow over sinusoidally varying substrate, obtained for: (a) Re = 5.0, Ka = 1.664, Pr = 3; (b) Re = 10.0, Ka = 1.8878, Pr = 1.5; with β = 10°, L/L_c = 15.17, A/L = 0.1, Ma = 0.1, Bi = 1.0. $RAM[\epsilon^4/\hat{z}^2] - \theta_{lin}$ predictions [dot-dashed blue curve], $RAM[\epsilon^4/\hat{z}^2] - \theta_{para}$ predictions [dashed red curve], corresponding *N-SE* solutions [solid black curve].

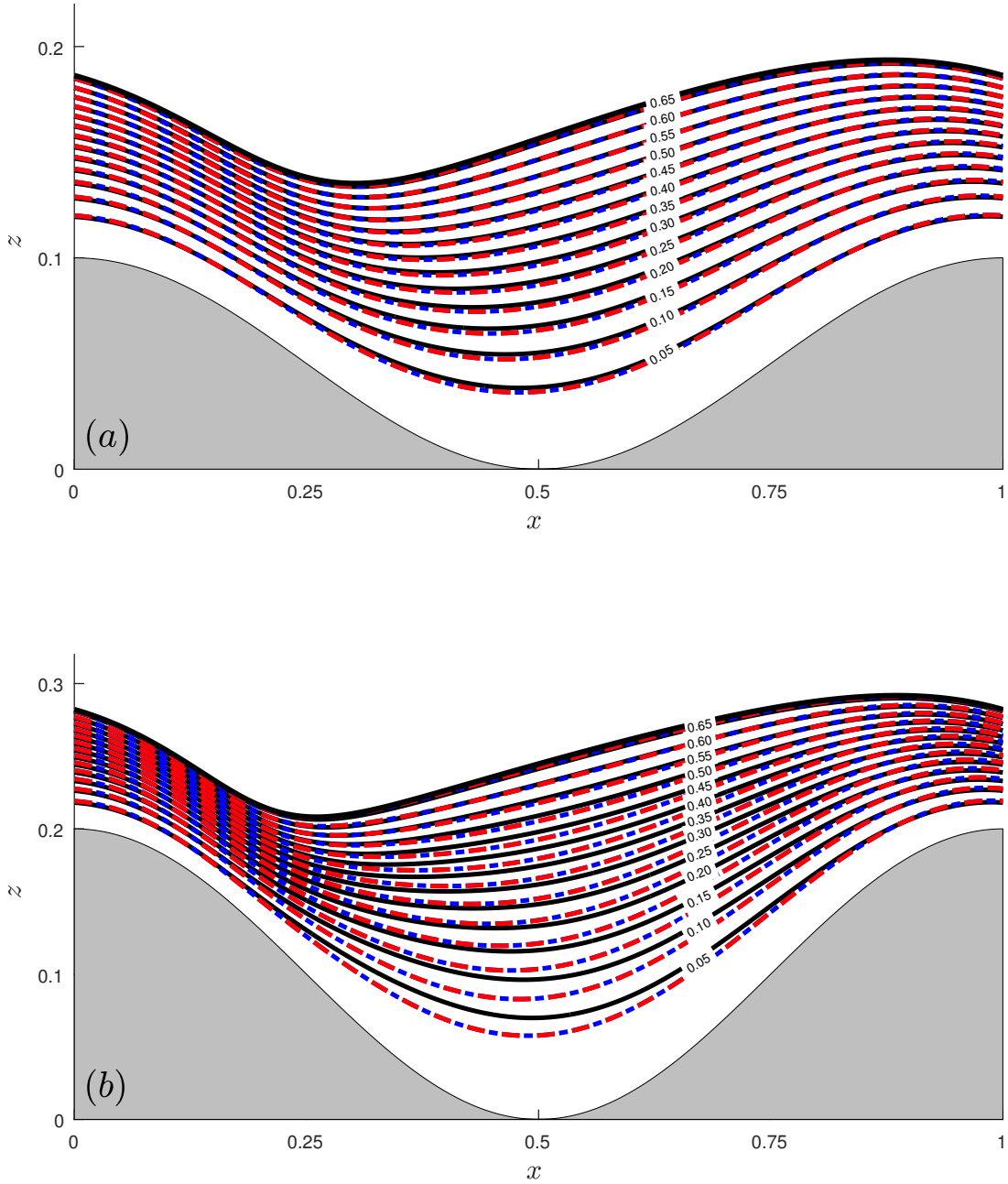

Figure 6.10: Steady-state stream-function contours, ψ, for film flow over sinusoidally varying substrate: obtained for (a) $A/L = 0.1$ and (b) $A/L = 0.2$; with $Re = 5.0$, $\beta = 10°$, $L/L_c = 15.17$, $Ka = 1.664$, $Ma = 0.1$, $Pr = 3$, $Bi = 1.0$. *N-SE* solution [solid black curves], $RAM[\epsilon^4/\hat{z}^2] - \theta_{para}$ prediction [dashed red curves], $RAM[\epsilon^4/\hat{z}^2] - \theta_{lin}$ prediction [dot-dashed blue curves]. Note that the $RAM[\epsilon^4/\hat{z}^2]-\theta_{para}$ and $RAM[\epsilon^4/\hat{z}^2]-\theta_{lin}$ predictions are indistinguishable as they lay one on top of the other. The flow is from left-to-right.

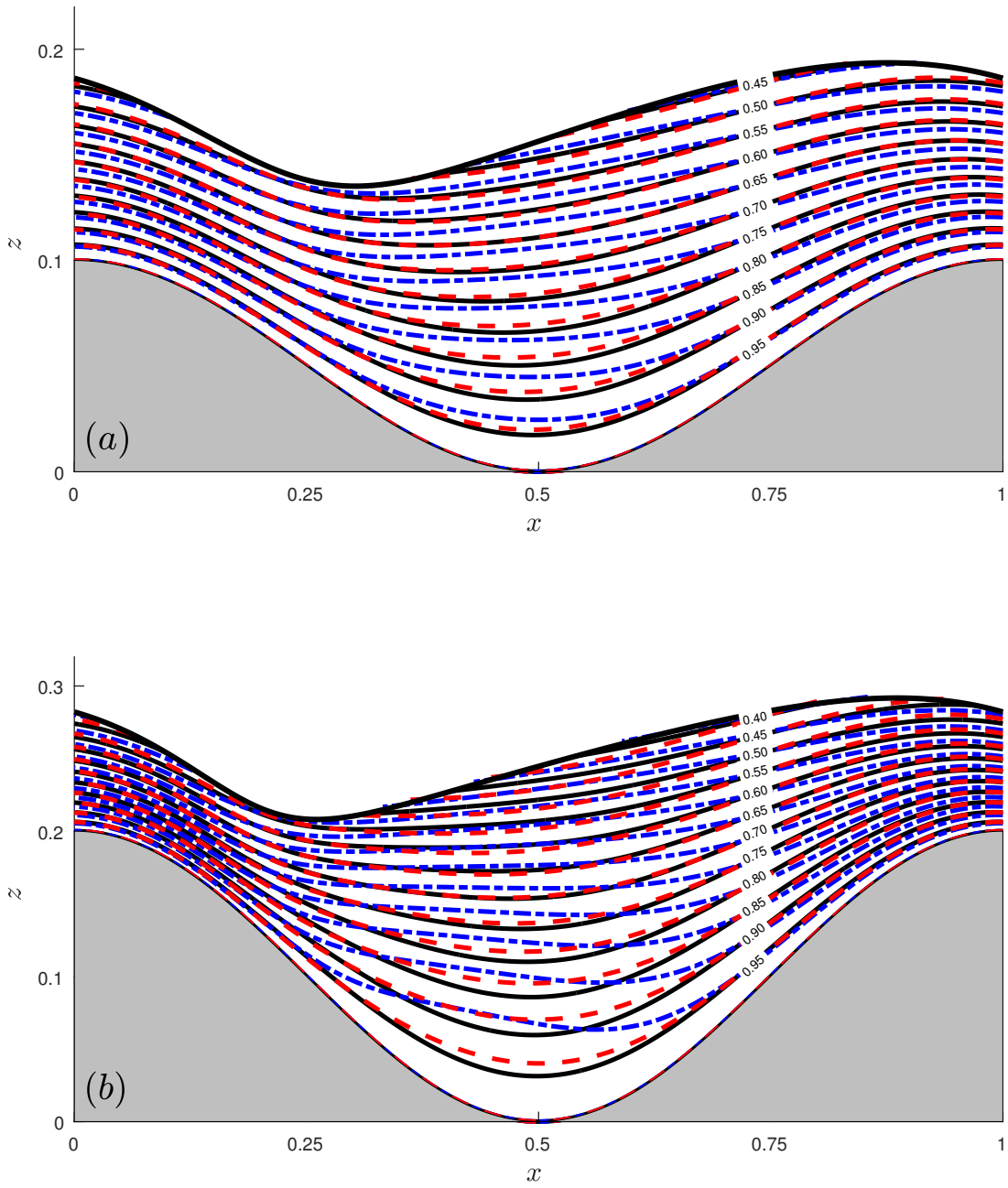

Figure 6.11: Steady-state temperature contours, θ, for film flow over sinusoidally varying substrate: obtained for (a) A/L = 0.1 and (b) A/L = 0.2; with Re = 5.0, β = 10°, L/L_c = 15.17, Ka = 1.664, Ma = 0.1, Pr = 3, Bi = 1.0. *N-SE* solution [solid black curves], $RAM[\epsilon^4/\hat{z}^2]$–$\theta_{para}$ prediction [dashed red curves], $RAM[\epsilon^4/\hat{z}^2]$–$\theta_{lin}$ prediction [dot-dashed blue curves]. Note that, unlike the stream-function contours of Figure 6.10, the $RAM[\epsilon^4/\hat{z}^2] - \theta_{para}$ and $RAM[\epsilon^4/\hat{z}^2] - \theta_{lin}$ predictions are easily distinguishable, especially so in the trough region. The flow is from left-to-right.

lowing accurate predictions to be achieved even when the flow has deviated significantly from the flat-film solution.

The stream-lines inside the flow according to the *N-SE* solutions (solid black curves), and as predicted by $RAM[\epsilon^4/\hat{z}^2] - \theta_{para}$ (dashed red curves) and $RAM[\epsilon^4/\hat{z}^2] - \theta_{lin}$ (dot-dashed blue curves), are plotted together in figure 6.10: for (a) $A/L = 0.1$ and (b) $A/L = 0.2$. The RAM stream-function predictions were generated using the velocity expansions – equation (3.43) with the expressions for $\{a_j\}$ given by the recurrence relations (3.45), the corresponding steady-state solutions for the film thickness, h_s, and free-surface temperature, ϑ_s, and the stream-function equation, $\psi = \int_s^z u \, dz$. Both RAM predictions show remarkably good agreement with the *N-SE* solution for the case of $A/L = 0.1$; the agreement is weaker for the case of $A/L = 0.2$, particularly in the trough of the substrate corrugation.

The RAM predicted temperature contours inside the film for the same parameter set as figure 6.10 were generated using the temperature expansions based on θ_{para} and θ_{lin}, respectively; these are plotted in figure 6.11 together with corresponding *N-SE* solutions. The results display the shift in concavity of the temperature field inside the film. In the fluid above the peaks of the substrate corrugation the spacing between isotherms starts small, becoming larger when moving towards the free-surface; while in the corrugation troughs the opposite occurs with the spacing between isotherms being largest in the trough and smallest at the free-surface. This occurs because fluid in the trough is being heated from the sides, as well as from below, and so the fluid remains hotter in this region. Above the corrugation peaks, the fluid is flanked by cooler fluid on either side, accelerating the cooling process in these regions. Agreement between the *N-SE* solutions and the corresponding $RAM[\epsilon^4/\hat{z}^2] - \theta_{para}$ prediction for $A/L = 0.1$ is very good. Agreement is weaker for $A/L = 0.2$ but $RAM[\epsilon^4/\hat{z}^2] - \theta_{para}$ nevertheless retains the qualitative behaviour of the temperature field inside the film. In contrast, the $RAM[\epsilon^4/\hat{z}^2] - \theta_{lin}$ prediction features noticeable errors for the case of $A/L = 0.1$ and diverges significantly in the trough of the substrate corrugation for the case of $A/L = 0.2$. The results in figure 6.11*b* clearly illustrate how starting the gradient expansion with an inadequate temperature assumption, *i.e.* θ_{lin}, leads to irrecoverable errors at higher-order. The accuracy of $RAM[\epsilon^4/\hat{z}^2] - \theta_{lin}$ is impeded by its assumption that $b_2 \sim \mathcal{O}(\epsilon)$; this imbalances the gradient expansion and it is unlikely this defect can be overcome by increasing the number of variables in the temperature field. Regardless, extending $RAM[\epsilon^4/\hat{z}^2] - \theta_{lin}$ to higher-order with a greater number of variables would be redundant since θ_{para} already offers improved accuracy without the need of additional variables; the better option would be to extend $RAM[\epsilon^4/\hat{z}^2] - \theta_{para}$ to higher-order which was attempted with $RAM[\epsilon^2/\hat{z}^2] - \theta_{para}$ but unfortunately the resulting formulation was found to produce inadequate predictions and requires revision.

Chapter 7

Results II: Linear Stability

This chapter explores the numerical solutions obtained from the linear stability analysis of gravity-driven liquid film flow, the theory of which was laid out in chapter 4. Within the present study, the linear stability is separated into two sections: (i) the first is concerned with the stability of falling films down planar substrate; whilst (ii) the second extends the analysis to wavy substrate. In both scenarios, the effect of heated/cooled substrate on the stability characteristics is considered concurrently.

7.1 Planar substrate

Figure 7.1 shows the curves of neutral stability for glycerin-water films (50%-by-weight) flowing down a flat plate inclined at an angle of $\beta = 5.6^\circ$ to the horizontal; the glycerin-water is at a constant temperature ($Ma = 0$) and possesses a fluid density of $\rho = 1.13 \times 10^3 kgm^{-3}$, a kinematic viscosity of $\nu = 5.02e \times 10^{-6} m^2 s^{-1}$, and a surface tension of $\sigma_0 = 69 \times 10^{-3} Nm^{-1}$, resulting in a Kapitza number of $Ka = 4.87$. An experimental determination of the stability boundary is given by the solid black curve which has been fitted to experimental measurements taken by Liu et al. [1993]; meanwhile, a theoretical prediction of the stability boundary is offered by the solutions to the Orr-Sommerfeld equation and its associated boundary conditions. The experimental neutral stability curve in figure 7.1 offers a critical Reynolds number of $Re_{crit}^{exp} = 12.2$ which is slightly less than the value of $Re_{crit}^{exp} = 12.4 \pm 0.1$ given by Liu et al. [1993]; this discrepancy stems from a difference in how the line of best fit is computed. In Liu et al. [1993], the frequency cut-off measurements [black boxes] were fitted to a square root function, namely:

$$f_\omega = a \left(Re - Re_{crit} \right)^{1/2}, \tag{7.1}$$

in which f_ω is the dimensional frequency with a and Re_{crit} being fitting parameters – the subscript in the dimensional frequency is used to distinguish it from the free-surface position ($f = s + h$). The square root function – equation (7.1) – stems from

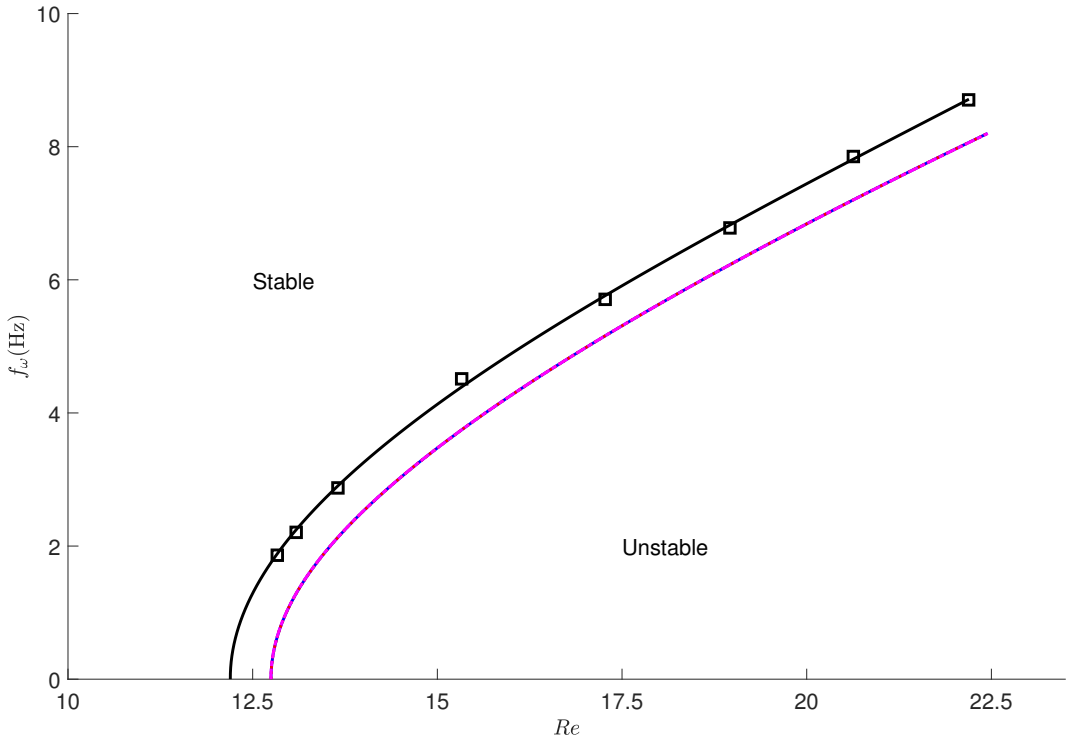

Figure 7.1: Curves of neutral stability in the frequency domain $(Re, f_\omega(\text{Hz}))$ for isothermal gravity-driven film flow down planar substrate obtained for β = 5.6° and Ka = 4.87. Experiments measurements taken by Liu et al. [1993] for glycerin-water films (50%-by-weight) are marked by the black boxes and accompanied by a line of best fit [solid black curve] which gives an experimental determination of Re_{crit}^{exp} = 12.2. Solutions to the Orr-Sommerfeld equation obtained via a power series expansion [blue solid curve], Chebyshev polynomials [dotted red curve], and a central difference scheme [dot-dashed magenta curve] are included and predict a theoretic value of Re_{crit}^{theory} = 12.7. Labels have been added to denote the stable and unstable regions of the domain.

an approximate expression for the curve of neutral stability obtained by Gjevik [1970a] through analysis of the Benney equation (BE); however, this means equation (7.1) is only strictly valid in the long-wave limit, *i.e.* $f_\omega \to 0$. In the present analysis, the line of best fit was fitted to the frequency cut-off values [black boxes] using a least squares method, a cubic polynomial in f_ω, and a boundary condition along the Re-axis requiring $dRe/df_\omega|_{f_\omega=0} = 0$ which can be derived directly from equation (7.1).

A theoretical prediction of the stability boundary in figure 7.1 was obtained by solving the Orr-Sommerfeld system of equations; this prediction was acquired through three separate methods, namely: (i) a power series expansion of the perturbation stream-function [solid blue curve] – section 5.3.2; (ii) an expansion of the perturbation stream-function in terms of the Chebyshev polynomials [dotted red curve] – section 5.3.3; and (iii) a discretisation of the perturbation stream-function via a central difference scheme [dot-dashed magenta curve] – section 5.3.4. In each case, the Orr-Sommerfeld system equation was solved for the case of temporal stability, $\omega \in \mathbb{C}$ and $\tilde{Q} \in \mathbb{R}$ where ω is the dimensionless angular frequency and $\tilde{Q}$ is the reduced wave-number; however, because ω and $\tilde{Q}$ are both wholly real along the curve of neutral stability, the stability boundary sought through temporal stability analysis is identical to the one found through spatial stability analysis in which $\omega \in \mathbb{R}$ and $\tilde{Q} \in \mathbb{C}$. Thus, when $(\omega, \tilde{Q}) \in \mathbb{R}$, one can use the identity $\epsilon\omega = c\tilde{Q}$ to exchange the reduced wave-number $\tilde{Q}$ with the angular frequency ω, where c is the phase velocity. The dimensional frequency f_ω is then connected to the dimensionless angular frequency ω through $f_\omega(\mathrm{Hz}) = (U_0/L_0) \cdot (\omega/2\pi)$ where (U_0/L_0) is the time scale of the problem and the units of the dimensional frequency are Hertz (Hz). Using these two expressions, one can then express the dimensional frequency in terms of the phase velocity and reduced wave-number like so:

$$f_\omega(\mathrm{Hz}) = \left(\frac{U_0}{H_0}\right)\frac{c\tilde{Q}}{2\pi}, \tag{7.2}$$

in which $(U_0/H_0) = (\bar{g}\sin\beta/2)^{2/3} \cdot (\rho Re/\mu)^{1/3}$ – the velocity scale U_0 and Nusselt film thickness H_0 were introduced in chapter 2.

It can be seen from figure 7.1 that all three methods used to solve the Orr-Sommerfeld equation for the isothermal case ($Ma = 0$) are in perfect agreement with one another; despite this, they are only in qualitative agreement with experiment. Indeed, the curves of neutral stability obtained from the Orr-Sommerfeld equation share the exact same shape as the experimental line of best fit but they do under-estimate the instability in gravity-driven liquid film flow with the theoretic curves lying to the right of the experimental one. Furthermore, the theoretical predictions return a critical Reynolds number of $Re_{crit} = 12.7$ which matches identically with the long-wave instability threshold of $Re_{crit} = (5/4)\cot\beta$ found by Benjamin [1957] but is nevertheless larger than the experimental estimates of $Re_{crit} = 12.2$ and $Re_{crit} = 12.4$, respectively.

Whilst not being a perfect description of reality, the Orr-Sommerfeld solutions provide a benchmark from which the accuracy of the linear stability predictions of the asymptotic models derived in chapter 3 can be measured. Accordingly, figure 7.2 includes the curves

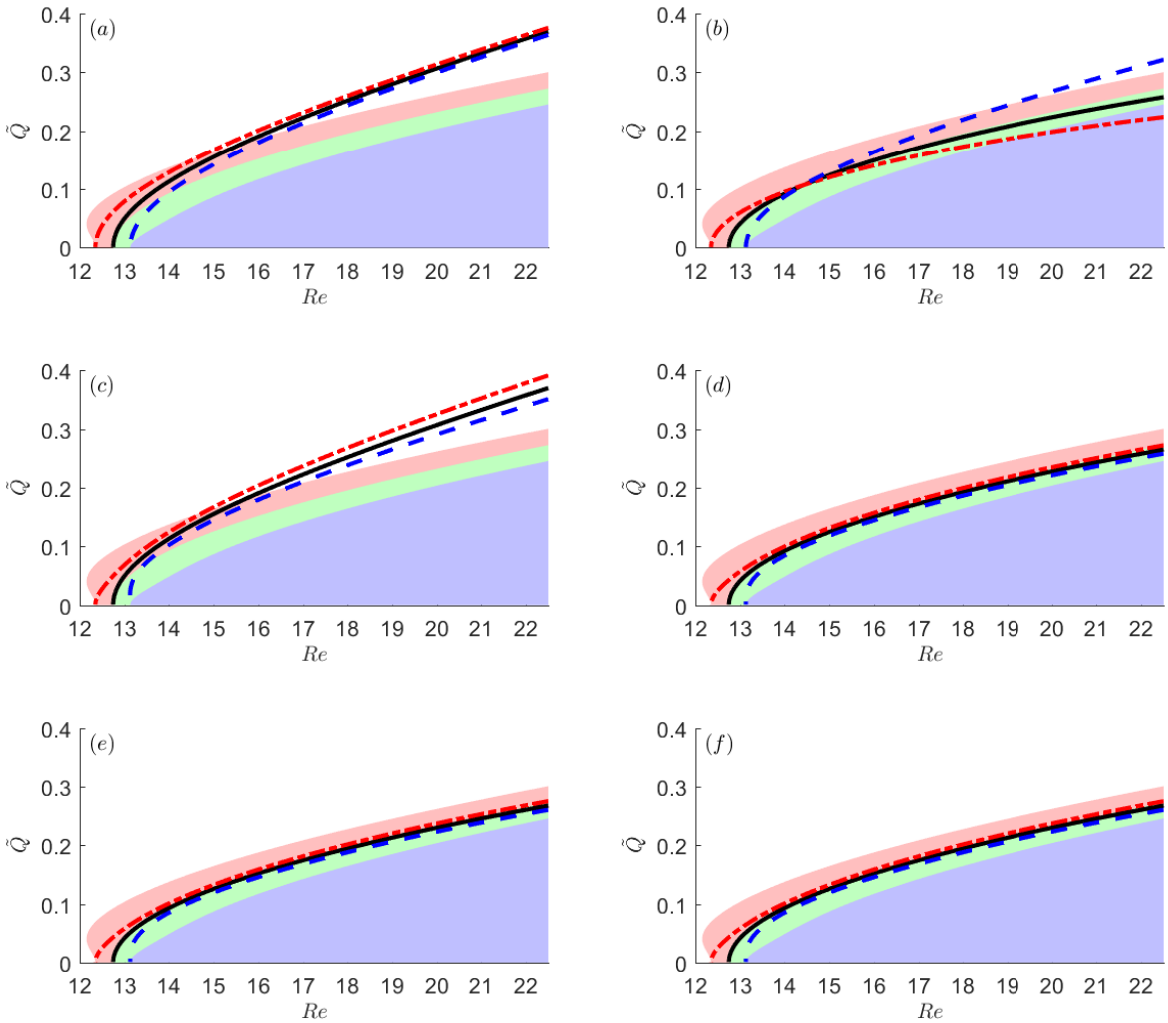

Figure 7.2: Curves of neutral stability in the Floquet domain $(Re, \tilde{Q})$ for gravity-driven film flow down planar substrate obtained for β = 5.6°, Ka = 4.87, Pr = 7.0, Bi = 1.0 when Ma = −0.01 [dashed blue curve], Ma = 0.0 [solid black curve], Ma = 0.01 [dot-dashed red curve]; as predicted by (a) the Benney equation (BE), (b) the regularised Benney equation (RBE), (c) $RAM[\epsilon^1/\hat{z}^2]$, (d) $RAM[\epsilon^3/\hat{z}^2]$, (e) $RAM[\epsilon^3/\hat{z}^2]$, and (d) $RAM[\epsilon^4/\hat{z}^2]$ – all RAM formalisms utilise θ_{para} as the leading temperature expansion. The unstable region of the domain according to the Orr-Sommerfeld equation (solved via Chebyshev polynomials) is given for Ma = −0.01 by the blue shaded area, Ma = 0.0 by the green & blue shaded areas, and Ma = 0.01 by the red, green & blue shaded areas.

of neutral stability as predicted by: (a) the Benney equation (BE); (b) the regularised Benney equation (RBE); (c) $RAM[\epsilon^1/\hat{z}^2]$; (d) $RAM[\epsilon^3/\hat{z}^2]$; (e) $RAM[\epsilon^3/\hat{z}^2]$; and (d) $RAM[\epsilon^1/\hat{z}^2]$; for the parameter space which was considered above in figure 7.1. The parameter space is extended to include heating ($Ma = 0.01$) and cooling ($Ma = -0.01$) with $Pr = 7$ and $Bi = 1.0$; additionally, the curves of neutral stability are plotted within the Floquet domain $(Re, \tilde{Q})$. The results in figure 7.2(a) show the well-known deficiency of the Benney equation which is only valid in the long-wave limit, $\tilde{Q} \to 0$; the solution to the linearised Benney equation is indistinguishable from the perturbation series solution to the Orr-Sommerfeld and so the defect which limits the former is the same one which limits the latter – this defect is detailed in section 5.3.1. Interestingly, the regularisation procedure of Takeshi [1999] significantly improves the performance of the Benney equation for the isothermal problem with the regularised Benney equation (RBE) achieving good agreement with the Orr-Sommerfeld solution in figure 7.2(b) for the case of $Ma = 0.0$; unfortunately, the RBE exhibits catastrophic behaviour for the heated/cooled problem with the curves of neutral stability for $Ma = -0.01$ and $Ma = 0.01$ incepting beyond the point of criticality – this is not predicted by the Orr-Sommerfeld equation and there is no precedent in the literature for a film undergoing cooling to be less stable than its heated counterpart. Moving onto the RAM formalisms, figures 7.2(c-f), it can be seen the greatest increase in performance is achieved when moving from $RAM[\epsilon^1/\hat{z}^2]$ to $RAM[\epsilon^2/\hat{z}^2]$ – as a matter of fact, the isothermal prediction from the first-order RAM formulation is identical to the BE prediction; the improvement in performance at second-order is due to the viscous dissipation terms entering into the RAM formalism, these terms dissipate inertia throughout the film, decrease the phase velocity of disturbances and stabilise the free-surface leading to more accurate predictions – the improved performance of the RBE over the BE is likewise due to the latter taking viscous dissipation into account. There is a slight increase in performance moving from $RAM[\epsilon^2/\hat{z}^2]$ to $RAM[\epsilon^3/\hat{z}^2]$, however, at the present resolution, it is almost imperceptible; this is noteworthy because the established consensus of the research field is that vertical inertia is negligible to the problem of film flow down planar substrate, and whilst the improvement here is slight, one must be aware that linear stability analysis is only capable of describing the initial development of instabilities and this suggests that vertical inertia may play a significant role in the evolution of nonlinear disturbances. Stepping from $RAM[\epsilon^3/\hat{z}^2]$ to $RAM[\epsilon^3/\hat{z}^2]$, there is no perceivable change in the predicted curve of neutral stability. Overall, the predicted curves of neutral stability for the case of $Ma = 0.0$ from the second- to fourth-order RAM formulations are excellent in figures 7.2(d-f); contrarily, the non-isothermal predictions are abysmal, as the Orr-Sommerfeld solutions predict a short-wave thermo-capillary instability in the case of $Ma = 0.01$ and a much greater stabilisation of the film when $Ma = -0.01$, despite the Marangoni effect being small in each case, none of the RAM formalisms are able to capture these features. At this moment, it would be apt to acknowledge that neither the heated nor cooled parameter spaces are entirely realistic from an experimental standpoint because the Biot number remains constant across the entire domain, $Bi = 1.0 \; \forall Re$; in practice, an experimental study would control the Reynolds numbers by increasing

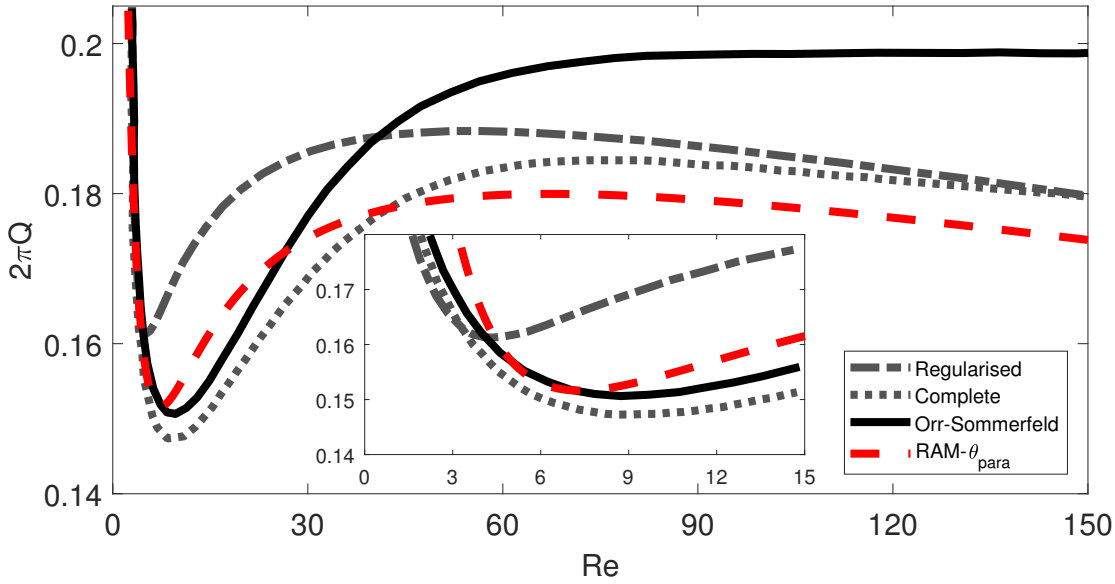

Figure 7.3: Curves of neutral stability in the Floquet domain (Re, Q) for film flow down a vertical flat plate: obtained for $\beta = 90°$, $L/L_c = 0.063$, $Ka = 4.508$, $Ma = 0.2$, $Pr = 7$, and $Bi = (2Re)^{1/3}$. $RAM[\epsilon^2/\hat{z}^2] - \theta_{para}$ prediction [dashed red curve], accompanied by the regularised model [dot-dashed grey curve], the complete model [dotted grey curve] and the Orr-Sommerfeld solution [solid black curve] from figure 1 of Scheid et al. [2005].

and decreasing the film thickness, this is achieved by varying the volume flux at the top of inclined plate, since the Biot number is a function of the Nusselt film thickness, $Bi = \alpha H_0/\kappa$, this implies that the Biot number would increase as Re increases, an increased Biot number would mean greater heat flux through the free-surface and thus a lower the free-surface temperature which would result in a weaker Marangoni effect across the free-surface. Suffice to say, the short-wave thermo-capillary mode seen in figure 7.2 may not be physical for a single-fluid setup. Despite this, the Orr-Sommerfeld results for the heated/cooled problem showcase a severe deficiency in the RAM methodology as the associated formalisms should be asymptotically equivalent to the governing equation set at small wave-numbers regardless of whether the parameter space is physical or not. It can be seen that the RAM formalisms correctly predict the critical Reynolds number, given by equation (5.30), and thereby agree with the Orr-Sommerfeld equation in the long-wave limit ($\tilde{Q} \to 0$) but in the case of finite wave-numbers, $\tilde{Q} > 0$, there is no agreement between the asymptotic models and the linear stability of the governing equations, at best there is a weak qualitative agreement between the RAM formalisms and the Orr-Sommerfeld equation. The results in figure 7.2 are revealing, they suggest that the RAM methodology may not be as accurate at predicting the thermodynamics at play in gravity-driven film flow as has been previously believed; in any event, further development of the thermal models is critical.

The stability of film flow down a uniformly heated, vertically aligned ($\beta = 90°$) flat

plate is considered in figure 7.3; the curve of neutral stability as predicted by RAM–θ_{para} is compared with corresponding predictions from the *complete* and *regularised* second-order weighted-residual models, and the Orr-Sommerfeld (O-S) solution obtained by Scheid et al. [2005]. The parameter space in this figure is more representative of an experimental setup with the Biot number being dependent upon the Reynolds number. The models derived by Scheid et al. [2005] and plotted in figure 7.3 assumed the leading temperature expansion through the film to be linear: in their *complete* model the fluid velocity and temperature were expanded to second-order; in contrast, their *regularised* model arose from truncating the temperature expansion at first-order and applying a Padé-like approximant to the velocity expansion, as such the energy residual of the regularised model is asymptotically equivalent to equation (6.4). The flow in Figure 7.3 depicts a transition from the thermo-capillary instability mode to the hydrodynamic instability mode and is unstable for all Reynolds numbers; the range of unstable wave-numbers (Q) explodes to infinity in the limit of $Re \to 0$ because the destabilising thermo-capillary stress is inversely proportional to the fluid inertia in this parameter space, *i.e.* $Ma \propto Re^{-1}$, accordingly, the Marangoni number becomes infinitely large as the Reynolds number approaches zero. Good agreement with the O-S solution is achieved by all the asymptotic models at small Reynolds numbers when the thermo-capillary mode characterises the stability. This is clear from the expanded view for $Re \in [0, 15]$. However, none of the asymptotic models offer accurate predictions at large values of Re when inertia becomes the dominant mechanism. $RAM[\epsilon^4/\hat{z}^2] - \theta_{para}$ diverges from the complete and regularised models at large Re because its description of inertia is only asymptotically equivalent to first-order; the models of Ruyer-Quil et al. [2005] feature second-order momentum residuals. Having said that, $RAM[\epsilon^4/\hat{z}^2] - \theta_{para}$ offers the best estimation of the minimum wave-number/Floquet parameter (Q) on the curve of neutral stability; this is the point at which the stability transitions from the thermo-capillary to the *hydrodynamic* mode. This could be attributed to the energy residual of $RAM[\epsilon^4/\hat{z}^2] - \theta_{para}$ offering an improved description of the *thermo-capillary* mode in this region. However, it is important to acknowledge the models on display in figure 7.3 differ in more ways than just their choice of temperature ansatz, *e.g. fluid pressure expression, algebraic form of Newton's cooling law, momentum residual, etc.*

Figure 7.4 focuses upon the linear damping rate of the temperature field in response to an infinitesimal disturbance with a wave-number of $\tilde{Q}$; the predictions of several competing models from the literature are compared against the linear damping rate of the governing energy equation – equation (2.26). The solutions to each asymptotic model were obtained by considering an infinitesimal disturbance to the temperature field of a laminar film flowing down planar incline, such that $\vartheta = \vartheta_{\mathbb{N}} + \breve{\vartheta}(\hat{z}) \exp(i(kx - \omega t))$ whilst $h = 1$ and $q = 2/3$. Discarding all non-linear in $\breve{\vartheta}$, one obtains an expression for the linear damping rate according to each asymptotic model, namely:

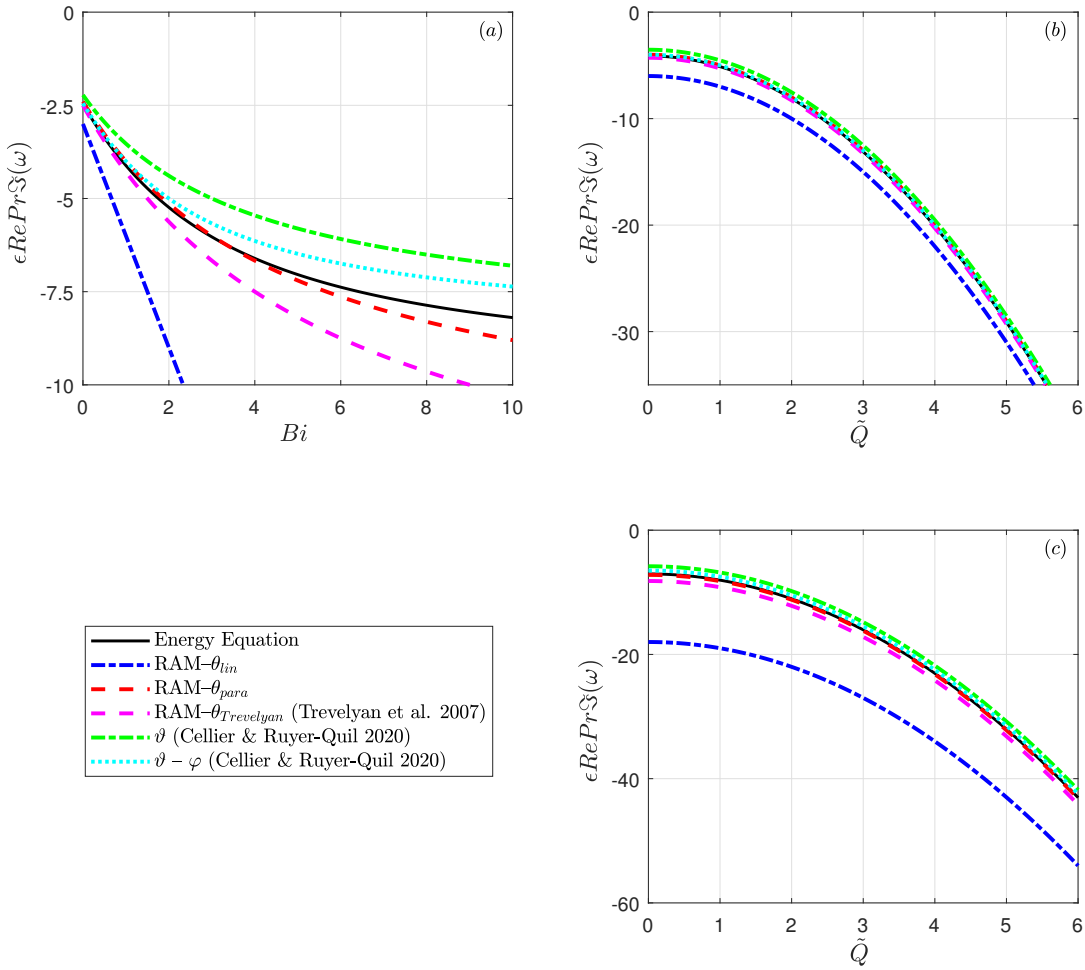

Figure 7.4: Imaginary part of the eigenvalue (*i.e.* the linear damping rate) corresponding to a perturbation of the temperature field for a uniform laminar flow when (a) $\tilde{Q} = 0$, (b) $Bi = 1.0$, and (c) $Bi = 5.0$. The linear damping rates as predicted by various models are compared against the linear damping rate of the governing energy equation (2.26).

$$\theta_{lin} : \epsilon RePr\mathfrak{I}(\omega) = -3\,(1+Bih) - \tilde{Q}^2, \quad \theta_{para} : \epsilon RePr\mathfrak{I}(\omega) = -\frac{12\,(1+Bih)}{5+Bih} - \tilde{Q}^2, \tag{7.3}$$

$$\theta_{Trev} : \epsilon RePr\mathfrak{I}(\omega) = -\frac{15\,(1+Bih)}{6+Bih} - \tilde{Q}^2, \quad \vartheta : \epsilon RePr\mathfrak{I}(\omega) = -\frac{60\,(1+Bih)}{27+7Bih} - \tilde{Q}^2, \tag{7.4}$$

$$\vartheta - \varphi : \epsilon RePr\mathfrak{I}(\omega) = -27/2 - \frac{(7+Bih)}{2} + \frac{\sqrt{49Bi^2h^2 + 138Bih + 489}}{2} - \tilde{Q}^2, \tag{7.5}$$

where $\mathfrak{I}(\omega)$ is the imaginary part of the angular frequency, *i.e.* the linear damping rate. In contrast, the linear damping rate of the governing equation in the long-wave limit ($\tilde{Q} \to 0$) is given by the solutions to [Cellier and Ruyer-Quil, 2020]:

$$\sqrt{i\epsilon RePr\mathfrak{I}(\omega)} \cdot \cot\left(\sqrt{i\epsilon RePr\mathfrak{I}(\omega)}\right) + Bih = 0. \tag{7.6}$$

The plots of the linear damping rate in figure 7.4 illustrate the poor predictive strength of the linear temperature ansatz (θ_{lin}) which clearly performs the worst out of the five competing models due to the fact that it does not satisfy Newton's law of cooling at the free-surface. Of the remaining four: θ_{para}, $\theta_{trevelyan}$, ϑ, and $\vartheta - \varphi$; all offer reasonable predictions for the linear damping rate when compared against the corresponding solutions of the energy equation (2.26); this is of no great surprise because in each of these models, the temperature ansatz is made to satisfy all of the boundary conditions. Scrutinising the results reveals the $\theta_{trevelyan}$ and ϑ models perform worse than the θ_{para} and $\vartheta - \varphi$ models; this can be attributed to the former models imposing a degree of constraint on the quadratic component of the temperature field which means their predictions do not follow the asymptotic behaviour of the energy equation quite as well as the latter models which place no such constraint on the temperature expansion. This supports the hypothesis that the quadratic temperature component must be included as its own degree of freedom in all asymptotic modelling approaches.

7.2 Wavy substrate

Curves of neutral stability generated by $RAM[\epsilon^4/\hat{z}^2] - \theta_{para}$ for gravity-driven film flow over smoothly corrugated, uniformly heated substrate are plotted in figures 7.5 and 7.6. The parameter set is based upon Figure 15 of D'Alessio et al. [2010] with Figure 7.5*a* being an exact match; however, only half the wave-number interval is considered here due to the symmetry of the system, $c_n(\frac{1}{2} + Q) = c_n^*(\frac{1}{2} - Q)$. The results in figure 7.5a, $Pr = 7$, show the same qualitative behaviour seen in D'Alessio et al. [2010]; increasing A/L stabilises the flow dynamics and leads to a short-wave instability whilst increasing Ma destabilises the film. The destabilisation effect of thermo-capillarity is independent of the fluid inertia in this part of the parameter space; the coefficient Ma/Ca in front of the thermo-capillary terms remains constant across all values of Re for a given value

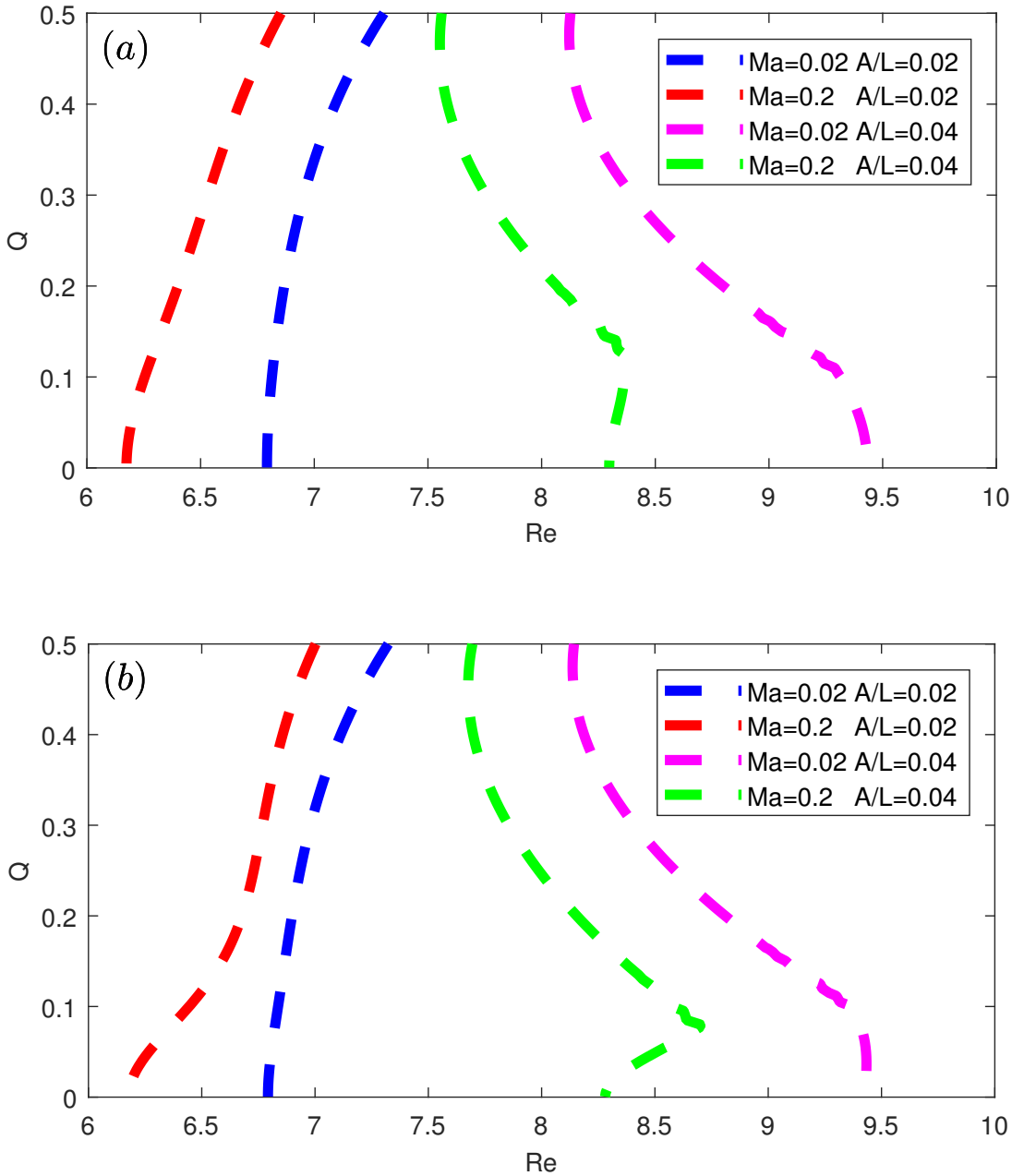

Figure 7.5: $RAM[\epsilon^4/\hat{z}^2] - \theta_{para}$ generated curves of neutral disturbance in the Floquet domain (Re, Q) for film flow over sinusoidally varying substrate, obtained for (a) $Pr = 7$ and (b) $Pr = 14$; with $\beta = 11.3099°$, $L/L_c = 60/\sqrt{2Re}$, $Ka = \left(800Re^5/729\right)^{1/11}$, $Bi = 1.0$, $Ma = 0.02,\ 0.2$ and $A/L = 0.02,\ 0.04$.

of Ma. Despite this, the destabilisation effect of thermo-capillarity is clearly affected by A/L with the same value of Ma leading to a greater reduction in the critical Reynolds number when A/L = 0.04 than when A/L = 0.02. Furthermore, increasing A/L leads to an overall stabilisation of the film. Having said that, the results in figure 7.2 for the case of planar substrate showed the RAM methodology under-estimating the effect on heating/cooling of the stability characteristics; if this deficiency translates over to the wavy substrate case then the RAM formalism will be understating the Marangoni effect within this parameter space and it would follow that the destabilisation effect of thermo-capillarity is much greater than the predicted curves of neutral stability suggest. The Prandtl number is doubled to Pr = 14 in figure 7.5b to investigate its effect on the stability criteria: for small Ma, the change is negligible due to the Marangoni effect being too small to effect a change in the curve of neutral stability; for larger Ma, the increase in Pr does not lead to any significant change in the critical stability criteria BUT it does cause a selection of wave-numbers to become stable points within the domain. This can be attributed to the higher Pr leading to less variation in the free-surface temperature as was seen in Figure 6.6, this in turn leads to a smaller Marangoni effect and less destabilisation of the film.

To further explore the dependency of the thermo-capillary mode on substrate amplitude, the problem is extended to large A/L in figure 7.6 with all curves of neutral stability now exhibiting a short-wave mode. The results illustrate how the relative destabilisation effect of thermo-capillarity becomes greater as A/L is increased. The curves of neutral stability furthest to the left in the figures represent the most unstable cases; these correspond to Ma = 0.2 in figure 7.6 when A/L is large, whereas in figure 7.5 when A/L was small they corresponded to A/L = 0.02. The increased destabilisation effect of thermo-capillarity at large A/L is likely a result of the free-surface temperature variation being greater in film flow over large A/L, resulting in larger thermo-capillary stress across the fluid's surface. Similar to the small A/L case, increasing Pr for large A/L – figure 7.6b – has a noticeable effect only when Ma is large. Increasing Pr tends to reduce free-surface temperature variation and consequently the Marangoni effect, leading some wave-numbers (Q) to become stable; however, overall there is less change in the neutral stability predictions than was seen in the small A/L case. This suggests the effect of Pr and fluid convection on the flow stability is lessened at large A/L.

The effect of heating and cooling is considered in Figure 7.7 for when the thermo-capillary stress does depend on the fluid inertia. $RAM[\epsilon^4/\hat{z}^2] - \theta_{para}$ generated curves of neutral stability for different Marangoni numbers are plotted together with digitised N-S generated data for the isothermal flow case taken from Trifonov [2014b]. The isothermal RAM is accurate at small A/L and Re but its accuracy against the N-S data decreases as these parameters are increased. Since the N-S data plotted is only for the isothermal flow case, the thermal $RAM[\epsilon^4/\hat{z}^2] - \theta_{para}$ predictions are speculative. Introducing heating to the problem reduces the film stability and shifts the curve of neutral stability to the left, which is in agreement with the principle understanding of the thermo-capillary instability mode [Goussis and Kelly, 1991]. Cooling on the other hand, indicated by a negative value for Ma, stabilises the film and shifts the curve to the right. However,

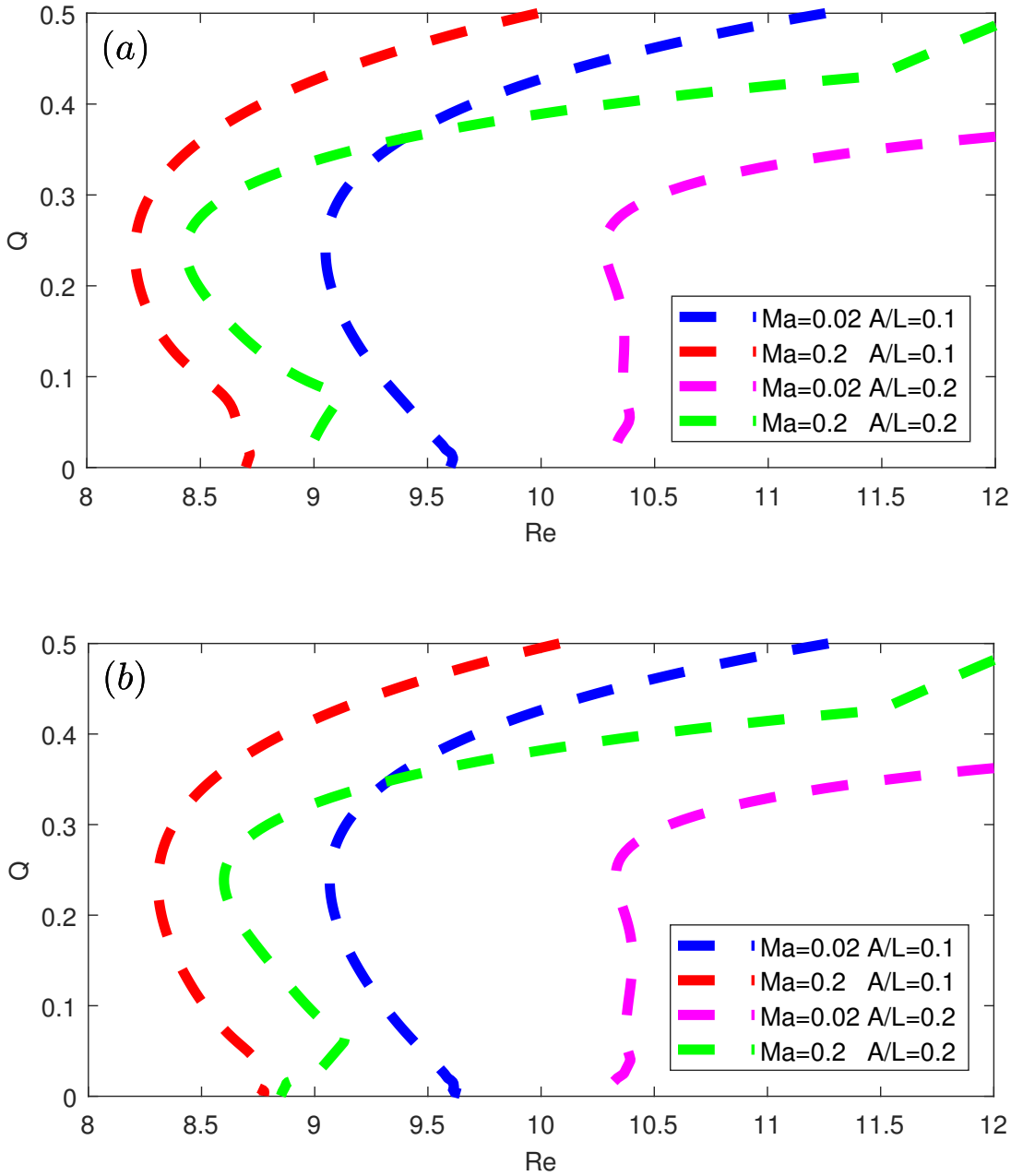

Figure 7.6: $RAM[\epsilon^4/\hat{z}^2] - \theta_{para}$ generated curves of neutral disturbance in the Floquet domain (Re, Q) for film flow over sinusoidally varying substrate, obtained for (a) $Pr = 7$ and (b) $Pr = 14$; with $\beta = 11.3099°$, $L/L_c = 60/\sqrt{2Re}$, $Ka = \left(800Re^5/729\right)^{1/11}$, $Bi = 1.0$, $Ma = 0.02,\ 0.2$ and $A/L = 0.1,\ 0.2$.

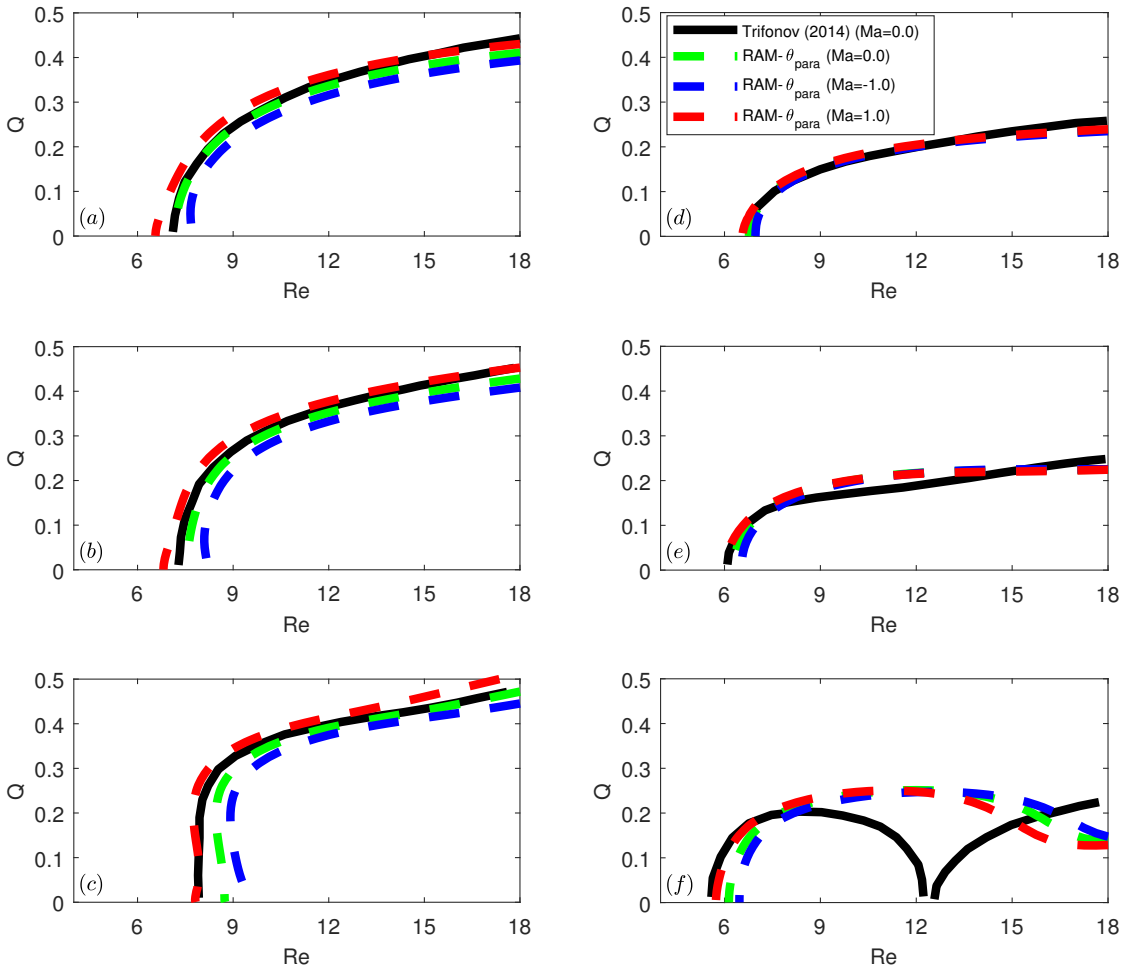

Figure 7.7: $RAM[\epsilon^4/\hat{z}^2] - \theta_{para}$ generated curves of neutral disturbance in the Floquet domain (Re, Q) for film flow over sinusoidally varying substrate, obtained for (a-c) β = 10°, L/L_c = 13.746, Ka = 1.434, Pr = 7, A/L = 0.02, 0.05, 0.1, Bi = 1.0, and (d-f) β = 10°, L/L_c = 13.741, Ka = 1.069, Pr = 7, A/L = 0.05, 0.1, 0.2, Bi = 1.0. $RAM[\epsilon^4/\hat{z}^2] - \theta_{para}$ predictions [dashed green, blue and red curves] for Ma = 0.0, −1.0, 1.0 are compared with N-S data [solid black curve] taken from figures 3(a)[(a)–(d)] and 3(a')[(e)–(h)] of Trifonov [2014b] for the case of Ma = 0.0.

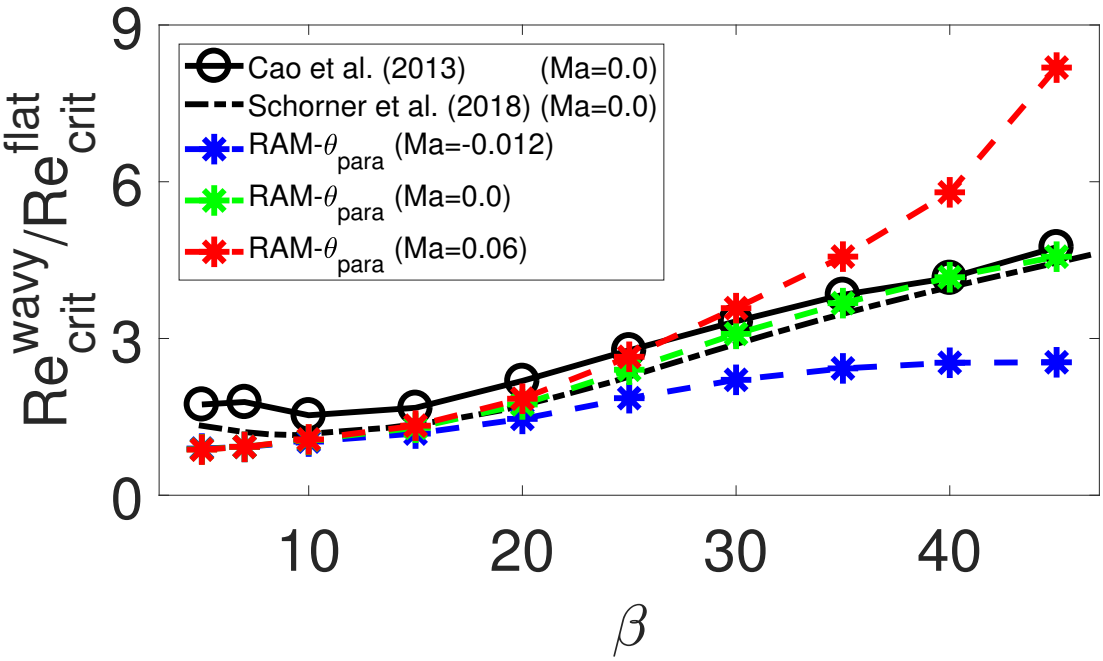

Figure 7.8: Normalised critical Reynolds number versus angle of inclination, β, for film flow over sinusoidally varying substrate, obtained for $Ka = 3.604$, $L/L_c = 4.982$, $Pr = 7$, $A/L = 0.167$, $Bi = 1.0$. $RAM[\epsilon^4/\hat{z}^2] - \theta_{para}$ predictions [dashed blue, green and red curves] and are compared with experimental data from figure 12 of Cao et al. [2013] and the *N-S* solutions from figure 8(d) Variant 1b of Schörner et al. [2018]. The critical Reynolds number is normalised *with respect to* the critical Reynolds number for a heated flat incline, the latter was computed from eqn. (5.30).

large values of $Ma = \Theta_\Delta\,(-\partial\sigma/\partial\Theta)$ are required to produce any meaningful change in the stability charts. It is important to remember the present formulation only models how thermo-capillarity causes the flow dynamics to deviate from the primary parabolic flow, it does not model the interaction between inertia and thermo-capillarity and how this might cause deviations to evolve; furthermore, the results in figure 7.2 for the heated/cooled planar substrate case suggest that the RAM methodology may drastically under-estimate the Marangoni effect in gravity-driven film flow. Since the thermo-capillary and hydrodynamic instability modes reinforce one another, it is possible smaller values of Ma could cause significant shifts in the stability behaviour, such as those seen in figure 7.2, depending upon how thermo-capillarity and inertia interact. However, based upon the accuracy of $RAM[\epsilon^4/\hat{z}^2] - \theta_{para}$ for the steady-state problem, it can be argued the qualitative behaviour predicted by the reduced asymptotic model is correct in a weak fashion. Overall, the stability results suggest that substrate topography is more important to film stability than thermo-capillarity, however, this could just be an artefact of the RAM methodology failing to capture the complete dynamics of thermo-capillarity.

Finally, figure 7.8 considers the effect of the substrate inclination angle, β, on the normalised critical Reynolds number for film flow down corrugated substrate; the critical Reynolds number, Re_{crit}^{wavy}, is normalised with respect to the corresponding value for a flat plate, Re_{crit}^{flat}, given by equation (5.30). The isothermal prediction ($Ma = 0.0$) is compared with experimental data from Cao et al. [2013] and *N-S* solutions from Schörner et al. [2018]. This result shows how the stabilising effect of the substrate undulations becomes greater as β increases. The $RAM[\epsilon^4/\hat{z}^2] - \theta_{para}$ isothermal prediction shows good agreement with the *N-S* solutions and only underestimates the stability criteria when $\beta < 10°$. When a temperature gradient is introduced across the liquid film, $RAM[\epsilon^4/\hat{z}^2] - \theta_{para}$ predicts a significant shift in the relationship between the critical Reynolds number and β. In the heated case ($Ma = 0.06$), the relative stabilisation effect of substrate undulations increases for larger β, while in the case of cooling ($Ma = -0.012$), the effect of topography is less important at large β. In either case, it can be seen that the presence of topography has a minimal effect on stability at small inclination angles, $\beta < 10°$. The results reveal how heating/cooling characterises the stability at low angles of inclination when the critical Reynolds number is given approximately by equation (5.30), while topography is implied to be the defining factor governing stability at large angles of inclination. It is well-understood from experiment that substrate topography plays a major role in determining the stability of isothermal gravity-driven film flow down smoothly corrugated inclined substrate [Schörner and Aksel, 2018b]; however, since there have been no analogous experiments exploring the heated problem, it is difficult to establish the role of thermo-capillarity in gravity-driven film flow down corrugated substrate. The present theoretical results suggest that thermo-capillarity plays a secondary role to substrate topography and yet there is evidence that the adopted modelling approach under-estimates the Marangoni effect, inevitably it is impossible at this stage to disentangle the deficiency of the modelling approach from the true physics at play and thus further investigation is warranted.

Chapter 8

Conclusions

Conclusions are drawn in this chapter with the major outcomes of the research being detailed in the discussion section whilst pathways for further research are laid out in the future work section.

8.1 Discussion

The present monograph has explored the stability and morphology of gravity-driven film flow down functional surfaces in order to understand the combined effect of substrate topography and substrate heating/cooling on the film dynamics. This has been achieved through a theoretical and computational analysis of the problem, with the overarching goal of the research being to identify which physical mechanisms play the most important roles in falling film dynamics and implement these mechanisms into a series of asymptotic modelling approaches such that behaviour of gravity-driven film flow can be described accurately and efficiently through the use of simplified mathematical models.

The asymptotic modelling approaches under consideration were laid out in chapter 3 and were separated into a perturbation series solution [Benney, 1966a] and a power series solution [Ruyer-Quil and Manneville, 1998] of the governing equation set (2.23 – 2.31), both of which were carried out within the framework of a long-wave expansion. Naturally, the limitation of the perturbation approach proposed by Benney [1966a] is it is only valid close to the exactly solvable problem, however, it is also argued here that the catastrophic behaviour of the Benney equation stems from the flawed assumption upon which the model is derived, namely that powers of ϵ are linearly independent because this requires $h \neq h(\epsilon)$ but the film thickness is in fact a function of the shallowness parameter, $h = h(\epsilon)$. A superior approach to modelling gravity-driven film dynamics is offered by the power series method; either through the Tau method of Lanczos [1938] outlined in section 3.4.1 or the reduced asymptotic model (RAM) methodology of section 3.4.3 which was was used presently. The RAM methodology stems from the modelling approach of Ruyer-Quil and Manneville [2000] which was originally developed as a relaxation of the perturbation approach; indeed, one the contributions of this monograph is to clearly show that the RAM methodology is a special case of the Tau method, and

that the perturbation series is a special case of the RAM methodology. In divergence with previous work, the present derivation of the RAM formalism for the heated film case embodies a quadratic leading temperature expansion though the film, in contrast to the far more widely used linear leading temperature expansion. It was shown in section 3.4.3 that the leading temperature expansion must be quadratic in order to afford a degree of freedom to both the free-surface temperature but also the heat flux through the free-surface – the linear temperature ansatz only possesses one degree of freedom. Whilst there are a handful of existing heat transfer models capable of modelling the evolution of both the free-surface temperature and the heat flux through the free-surface [Trevelyan et al., 2007, Thompson et al., 2019, Cellier and Ruyer-Quil, 2020], the present formulation based on a quadratic temperature ansatz is the first to be strictly consistent with the long-wave expansion. An unsuccessful attempt was made to extend the RAM methodology fully to second-order in the long-wave expansion, this required introducing additional degrees of freedom to velocity and temperature expansions; in spite of disappointing results of the resulting second-order formulation, it serves as a reference point from which future attempts can be made.

The asymptotic models were tested through a series of steady-state solutions. For the case of steady isothermal film flow over wavy substrate, the results confirm that mixed-order RAM formalisms, with respect to the long-wave expansion, extend the validity of the model to large amplitude, whilst a fresh treatment of the fluid pressure allows for the implementation of surface curvature. The cases explored for steady film flow over heated, corrugated substrate showed the Benney equation (BE) and its regularised form (RBE) are incapable of accurately resolving the film dynamics outside of the flat-film case; furthermore, the steady-state results for the heated problem confirm that a degree of freedom must be afforded to the heat flux through the film when approximating higher-order terms, to ensure Newton's law of cooling at the free-surface (2.31) is satisfied and allow for the inter-facial temperature to be captured accurately. Comparison of the reconstructed internal flow structure, in terms of streamlines and isotherms, compared with corresponding $N-SE$ solutions of the governing equations – continuity, momentum and energy – and attendant boundary conditions, reveals explicitly that the steady-state heat flux becomes non-uniform when the film thickness is no longer synonymous with a flat-film solution. The non-linear behaviour of the temperature field in these cases stems from thermal conduction and the diffusion of heat across the film; the quadratic component of the temperature expansion enters at leading-order in the long-wave expansion prior to the entry of fluid convection or conductive dissipation. Nevertheless, the improved description of thermal conduction results in a superior prediction of the convective heat transfer, illustrated by the good agreement shown with corresponding $N-SE$ solutions for moderate Prandtl (and Péclet) number; conversely, an assumed linear temperature ansatz is shown to perform poorly over a range of parameters.

The flow stability of gravity-driven film flow has been explored through linear stability analysis, chiefly via curves of neutral stability. The Orr-Sommerfeld equation and its attendant boundary conditions were solved for the case of heated/cooled film flow down planar incline; these results provided a benchmark with which the linear stability of

the asymptotic models could be checked. Comparison against the Orr-Sommerfeld solutions showed the Benney equation (BE) and first-order RAM formalism yield inadequate descriptions of the flow stability outside of the long-wave limit – in line with previous studies; the regularised Benney equation (RBE) and higher-order RAM formalisms were seen to perform very well in the isothermal flow case, however, upon the introduction of substrate heating/cooling, the RBE exhibits catastrophic behaviour whilst the RAM formalisms fail to accurately capture the effect of thermo-capillarity on the flow stability. The reason for the poor performance of the RAM methodology in the thermal stability problem is not readily apparent; indeed, the thermal steady-state results show that the RAM methodology is perfectly capable of predicting the temperature along the free-surface, provided the heat flux through the free-surface is afforded it own degree of freedom; nevertheless, the modelling approach as it stands appears to be unable to accurately predict the linear evolution of the thermo-capillary mode in gravity-driven film flow except in the long-wave limit. For film flow down a vertically aligned plate, when the steady-state is given by the flat-film solution, the parabolic temperature profile was able to achieve good agreement with the Orr-Sommerfeld solution and, as to be expected, with the regularised and complete second-order models derived by Ruyer-Quil et al. [2005], Scheid et al. [2005] centred on the linear temperature approximation; however, this is because, within this part of the parameter space, the thermo-capillary dominates the flow stability as the Reynolds number goes to zero – outside of this limit, none of the reduced asymptotic models achieved agreement with the Orr-Sommerfeld equation. Stability results for film flow down smoothly corrugated, uniformly heated inclined substrate are found to be in agreement with the qualitative behaviour of the thermo-capillarity mode as described by Goussis and Kelly [1991], and with stability results from D'Alessio et al. [2010]. Those considering the stabilisation/destabilisation merit of topography and thermo-capillarity are affected considerably by the choice of parameter space. When the Marangoni effect is independent of the fluid inertia, the stability results suggest that topography is the deciding factor at small values of A/L; at larger values of A/L, when short-waves are the most unstable modes, thermo-capillary effects appear to play a much greater role in determining the stability of the system. In contrast, when the Marangoni effect depends in the fluid inertia, the destabilising effect of thermo-capillarity is weaker overall for moderate surface tension, $Ka \sim \mathcal{O}(1)$. However, the lack of existing numerical and experimental data leaves doubt surrounding the quantitative and even qualitative accuracy of these results. Although showing good agreement with experimental and $N-S$ data for the case of isothermal film flow ($Ma = 0$), all that can be safely attributed to the RAM-generated stability results is that substrate topography plays the greater role in determining the stability of film flow over wavy substrate, in contrast, thermo-capillarity appears to play a secondary role when substrate corrugations and heating/cooling are present, the only exception would be when a particularly large temperature difference is considered.

8.2 Future Work

At the outset, the desire was to try and incorporate the interplay of substrate topography with heating into a single simplified asymptotic model, such that their combined effect on the film dynamics could be studied. The present monograph has revealed this task to be much larger than original thought, which is at the very least a positive from the standpoint of future research. The methodology of the reduced asymptotic model (RAM) is first and foremost a power series expansion with respect to the powers $\hat{z}$ and so extension of the modelling approach to new parameter spaces relies upon the introduction of new degrees of freedom into the power series; whilst the present work has done its part in unifying the power series expansion with the long-wave expansion by showing that the leading temperature expansion must be quadratic in order for the asymptotic behaviour of the governing equations to be emulated, it is clear that the modelling approach requires further development. In particular, linear stability analysis of film flow down a heated incline has revealed that the reduced asymptotic methodology to be incapable of accurately modelling the thermo-capillary instability mode even in the absence of substrate topography; accordingly, it might be best for future efforts to return to the problem of film flow down planar substrate and focus on amending this defect in the modelling approach. Indeed, accurate modelling of thermo-capillarity is no trivial task, when attempting to extend the RAM formalism to second-order in the long-wave expansion, the present work introduced the shear stress at the free-surface as its own degree of freedom in an effort to try and capture the full dynamics of the Marangoni effect; however, as detailed above, the complete second-order model yields unsatisfactory results, but be that as it may, the ideas included its in derivation may yet bear fruit. Beyond the derivation of higher-order formulations, another noteworthy task would be to study the non-linear behaviour of the existing RAM formalisms, either through the Stuart-Landau equation or by exploring travelling wave solutions; presently, because of the complexity of the system of interest, only non-linear steady solutions and linearised non-steady solutions were considered, and so it unclear whether the non-linear predictions of the asymptotic models derived presently are sufficiently better than those given by existing models in the literature.

In closing, the recommendation for future work would be to simplify the underlying problem to contain just substrate topography or substrate heating/cooling, and then to focus on the improving the modelling approach in each respective area. Of the two, the more lucrative option would appear to be the problem of isothermal film flow over substrate topography; recent studies have shown the existing methodology is capable of predicting the qualitative behaviour of liquid film flow over substrate topography. Of particular interest would be an investigation into whether a reduced asymptotic model is able to model the eddies which form in the troughs of large substrate corrugations; however, it is unlikely that the RAM methodology will ever be able to capture this phenomenon without significant revision because in its current form the method attempts to model the flow dynamics as a single polynomial across the entire liquid layer and thus treats the whole liquid film as a single flow regime. If an eddy was to form in the trough

of a corrugation then the problem would involve two distinguishable flows: the primary flow and the eddy; a potential route to overcoming this issue would be develop a reduced asymptotic model which models the liquid film as a two-layer system, in effect, separating the z-domain into one part containing the eddy and one part containing the primary flow, however, there would now exist a free boundary between the upper and lower layers, in addition to the one already present at the free surface. The alternative path is to explore gravity-driven film flow down uniformly heated/cooled planar substrate; this may be more difficult to make ground in because the deviations to the temperature field away from the Nusselt linear distribution appear to be much more complex than the deviations to the velocity field away from the Nusselt parabolic profile – as showcased by the leading temperature expansion needing to be quadratic. In addition, asymptotic models are known to yield non-physical negative free-surface temperatures in finite-time simulations, with the cause for this catastrophic behaviour still being unknown; and one has the difficulty of accurately modelling the Marangoni effect which present models typically restrict to an infinitesimal layer just below the free-surface, in reality the thermo-capillary effect needs to penetrate down into the film. Having said that, recently published experimental data on the heated film problem offers a new avenue of research – see Collignon et al. [2021, 2022]; whilst the present formalisms are not comparable with the aforementioned experiments due to a difference in boundary conditions, a perfectly viable route of research would be to re-formulate the problem to include the appropriate boundary conditions and then derive the corresponding reduced asymptotic model so that its accuracy can be tested against the experimental data. In any event, the work contained within this monograph provides a strong foundation for new investigations and new models, providing clarity about the strengths and weaknesses of the existing methodologies and giving insight into how one might extend these techniques to fresh pastures.

Appendix A

The Nusselt Theory of Laminar Film Dynamics

Nusselt [1916] marks the earliest work on gravity-driven film flow; his theory on laminar film dynamics was part of his research on the condensation of vapours on solid surfaces. In his original paper, Nusselt considered five fundamental cases:

1. Vapour condensing on a smooth plane at an angle β to the horizontal; the vapour is assumed to be pure and saturated, and stationary relative to the condensate.
2. Vapour condensing on the outside of a horizontal tube under the above conditions.
3. Vapour condensing on surface as in 1. but with appreciable vapour velocity.
4. Super heated vapour condensing on any surface.
5. Impure vapour condensing on any surface.

Within the context of the present monograph, it is only pertinent to re-visit Case 1. In order to simplify the mathematical treatment of the problem, Nusselt made several assumptions – some of which can be proved; these were:

1. The film of condensate is so thin that the temperature gradient through it is a straight line.
2. The heat is all carried to the metal surface by pure conduction in the direction perpendicular to the surface.
3. Physical properties of the condensate may be taken at the mean film temperature.
4. The surface is relatively smooth and clean.
5. The film of condensate always moves in viscous motion.

6. The curvature of the film may be neglected.

7. The temperature of the solid surface is constant.

Case 1.
Nusselt considered a vapour, at a temperature Θ_a, condensing on a smooth wall which is inclined at an angle β to the horizontal and kept at a constant, uniform temperature, Θ_s. Nusselt realised that, for a condensate film of uniform thickness, surface tension has no effect on the film thickness and that the thickness can be calculated from hydrodynamical considerations alone.

Given enough time, a condensate film of thickness H_0 will form on the wall and begin to flow downward under the action of gravity. Assuming the flow of the condensate film is governed entirely by the law of viscous motion, the shear stress at any point inside the film, $\mathbb{S}$, and its variation, $d\mathbb{S}$, will depend on: the viscosity of the fluid μ, the variation of fluid velocity dU, and the distance from the wall dZ; in the following fashion:

$$\mathbb{S} = \mu \frac{dU}{dZ}, \qquad d\mathbb{S} = \mu \frac{d^2U}{dZ^2} dZ. \tag{A.1}$$

The coordinate system employed above is the same one used in Chapter 2; the X-axis lies in the direction parallel to the wall and the Z-axis is in the direction normal to it. For gravity-driven film flow, the variation in the shear stress from one point to another, $d\mathbb{S}$, will be counterbalanced by the change in weight of the condensate film, like so:

$$d\mathbb{S} + \rho g \sin\beta dZ = 0, \qquad \frac{d^2U}{dZ^2} = -\frac{\rho g \sin\beta}{\mu}. \tag{A.2}$$

Integrating the above yields:

$$U = -\frac{g \sin\beta}{2\nu} Z^2 + C_1 Z + C_2, \tag{A.3}$$

where $\nu = \mu/\rho$ is the kinematic viscosity, and $\{C_1, C_2\}$ are constants of integration. Assuming a no-slip condition at the wall, $U = 0$ at $Z = S$, and that the stationary vapour exhibits no force on the condensate film, $dU/dZ = 0$ at $Z = S + H_0$, leads to:

$$U = \frac{g \sin\beta}{2\nu} \left(S + 2H_0 - Z\right)\left(Z - S\right). \tag{A.4}$$

Equation (A.4) is called the Nusselt parabolic velocity profile and is only strictly valid

when the wall is perfectly smooth, $S = 0$, and the film thickness H_0 is uniform across the entire domain. Substituting equation (A.4) into the continuity equation (2.3) reveals the component of the velocity normal to the wall becomes finite whenever there is any variation in the wall profile or film thickness; Nusselt [1916] was aware of this but assumed this effect to be negligible on the basis of assumptions 4 and 6 from the above.

The volumetric flow rate per cross-sectional unit width, according to equation (A.4), at any point down the wall X is given by:

$$\mathbb{Q}_0 = \int_S^{S+H_0} U\,dZ = \frac{H_0^3 g \sin\beta}{3\nu}, \tag{A.5}$$

and the free-surface velocity, $U_0 = U(Z = S + H)$, by:

$$U_0 = \frac{H_0^2 g \sin\beta}{2\nu}, \tag{A.6}$$

thus, $U_0 = 3\mathbb{Q}_0/2H_0$. Expressions (A.5 – A.6) define the vertical length and velocity scales utilised in Chapter 2.

Nusselt also considered the thermodynamics of the condensate. In the absence of convection and radiation, the rate at which an infinitesimal column of the condensate film accumulates heat can be described by Fourier's law of thermal conduction like so:

$$\phi_q = -\kappa \frac{\Theta(Z = S + H_0) - \Theta_s}{H_0}, \tag{A.7}$$

where ϕ_q is the heat flux density, κ is the thermal conductivity and Θ is the temperature inside the condensate film. In a similar fashion, the rate of heat transfer from the condensate film to the vapour, $\hat{\phi}_q$, can be described by Newton's law of cooling:

$$\hat{\phi}_q = \alpha\left(\Theta(Z = S + H_0) - \Theta_a\right), \tag{A.8}$$

where α is the heat transfer coefficient.

For the case of conductive heat transfer, an expression for the temperature distribution inside the film is readily derived from equations (A.7 – A.8); to begin, an expression for $\Theta(Z = S + H_0)$ is found. The temperature of the surface and the temperature of the vapour are assumed to be fixed and to be both below the boiling point of the condensate; therefore, the effects of condensation/vaporisation can be neglected and the heat transfer inside the fully developed film will tend toward a steady-state in which the heat flux into the film is equal to the heat flux out of it, or put mathematically $\phi_q = \hat{\phi}_q$. This allows equations (A.7 – A.8) to be equated, which leads to the following expression:

$$\Theta(Z = S + H_0) = \frac{\Theta_s + \frac{\alpha H_0}{\kappa}\Theta_a}{1 + \frac{\alpha H_0}{\kappa}}. \tag{A.9}$$

To find an expression for the temperature distribution throughout the film, equation (A.7) must be generalised to an infinitesimal column of arbitrary height dZ such that:

$$\phi_q = -\kappa \frac{\Theta - \Theta_s}{dZ}. \tag{A.10}$$

The same steady-state principle applies allowing $\phi_q = \hat{\phi}_q$; this leads to:

$$\Theta = \Theta_s - \frac{\alpha}{\kappa}\Big(\Theta(Z = S + H_0) - \Theta_a\Big)dZ, \tag{A.11}$$

which can be integrated once, with the requirement that $\Theta(Z = S) = \Theta_s$, to find:

$$\Theta = \Theta_s - \frac{\alpha}{\kappa}\left(\frac{\Theta_s - \Theta_a}{1 + \frac{\alpha H_0}{\kappa}}\right)(Z - S), \tag{A.12}$$

which is the Nusselt linear temperature distribution and confirms assumption 1 – provided the heat transfer through the film is purely conductive and the film thickness is uniform across the whole domain. If the film thickness is not uniform then there will be component of the velocity toward/away from the wall which arises because of the continuity of mass, this flow will convect heat toward/away from the wall; thus, breaking the assumption that the heat transfer is purely conductive.

Appendix B

Tau method: recurrence relations

Substituting the power series (3.43) into the equations (3.37 – 3.38) yields the following expressions in terms of the expansion coefficients $\{a_j, b_j\}$, the film thickness $h(x,t)$, and substrate position $s(x)$. The laminar viscosity/conduction terms are given by:

$$\frac{\partial^2 u}{\partial \hat{z}^2} = \sum_{j=1}^{N} j\,(j-1)\,a_j \hat{z}^{j-2} = \sum_{j=0}^{N-2} (j+2)\,(j+1)\,a_{j+2}\hat{z}^j, \tag{B.1}$$

$$\frac{\partial^2 \theta}{\partial \hat{z}^2} = \sum_{j=1}^{N} j\,(j-1)\,b_j \hat{z}^{j-2} = \sum_{j=0}^{N-2} (j+2)\,(j+1)\,b_{j+2}\hat{z}^j. \tag{B.2}$$

The stream-wise inertia/convection terms are given by:

$$\frac{\partial u}{\partial t} = \sum_{j=1}^{N} \frac{\partial a_j}{\partial t}\hat{z}^j, \qquad u\frac{\partial u}{\partial x} + w\frac{\partial w}{\partial \hat{z}} = \sum_{i=1}^{N}\sum_{j=1}^{N}\left\{a_i\frac{\partial a_j}{\partial x} - \frac{i}{(j+1)}a_i\frac{\partial a_j}{\partial x}\right\}\hat{z}^{i+j}, \tag{B.3}$$

$$= \sum_{j=2}^{2N}\sum_{i=1}^{j-1}\left\{\frac{(j-2i+1)}{(j-i+1)}a_i\frac{\partial a_{j-i}}{\partial x}\right\}\hat{z}^j,$$

$$\frac{\partial \theta}{\partial t} = \sum_{j=1}^{N} \frac{\partial b_j}{\partial t}\hat{z}^j, \qquad u\frac{\partial \theta}{\partial x} + w\frac{\partial \theta}{\partial \hat{z}} = \sum_{i=1}^{N}\sum_{j=1}^{N}\left\{a_i\frac{\partial b_j}{\partial x} - \frac{j}{(i+1)}b_j\frac{\partial a_i}{\partial x}\right\}\hat{z}^{i+j}, \tag{B.4}$$

$$= \sum_{j=2}^{2N}\sum_{i=1}^{j-1}\left\{a_i\frac{\partial b_{j-i}}{\partial x} - \frac{(j-i)}{(i+1)}b_{j-i}\frac{\partial a_i}{\partial x}\right\}\hat{z}^j, \tag{B.5}$$

in which the summations concerning the nonlinear inertia/convection terms have been re-arranged to be terms of the coefficients of $\hat{z}^j$, as oppose to $\hat{z}^{i+j}$; note that for $j > N$, $a_j = 0$ and $b_j = 0$ due to the truncation of the power series.

The viscous/conductive dissipation terms are given by:

$$\frac{\partial^2 u}{\partial x^2} = \sum_{j=1}^{N} \left\{ \frac{\partial^2 a_j}{\partial x^2} \hat{z}^j - j \left(2 \frac{\partial a_j}{\partial x} \frac{ds}{dx} + a_j \frac{d^2 s}{dx^2} \right) \hat{z}^{j-1} + j\,(j-1)\, a_j \hat{z}^{j-2} \left(\frac{ds}{dx} \right)^2 \right\} \tag{B.6}$$

$$= \sum_{j=0}^{N} \left\{ \frac{\partial^2 a_j}{\partial x^2} - (j+1) \left(2 \frac{\partial a_{j+1}}{\partial x} \frac{ds}{dx} + a_{j+1} \frac{d^2 s}{dx^2} \right) + (j+2)\,(j+1)\, a_{j+2} \left(\frac{ds}{dx} \right)^2 \right\} \hat{z}^j,$$

$$\frac{\partial^2 \theta}{\partial x^2} = \sum_{j=1}^{N} \left\{ \frac{\partial^2 b_j}{\partial x^2} \hat{z}^j - j \left(2 \frac{\partial b_j}{\partial x} \frac{ds}{dx} + b_j \frac{d^2 s}{dx^2} \right) \hat{z}^{j-1} + j\,(j-1)\, b_j \hat{z}^{j-2} \left(\frac{ds}{dx} \right)^2 \right\} \tag{B.7}$$

$$= \sum_{j=0}^{N} \left\{ \frac{\partial^2 b_j}{\partial x^2} - (j+1) \left(2 \frac{\partial b_{j+1}}{\partial x} \frac{ds}{dx} + b_{j+1} \frac{d^2 s}{dx^2} \right) + (j+2)\,(j+1)\, b_{j+2} \left(\frac{ds}{dx} \right)^2 \right\} \hat{z}^j. \tag{B.8}$$

The time-dependent vertical inertia terms are given by:

$$\frac{\partial}{\partial x} \int_{\hat{z}}^{h} \frac{\partial w}{\partial t} d\hat{z} = \frac{\partial}{\partial x} \sum_{j=1}^{N} \left\{ \frac{\partial a_j}{\partial t} \frac{ds}{dx} \frac{h^{j+1} - \hat{z}^{j+1}}{(j+1)} - \frac{\partial^2 a_j}{\partial x \partial t} \frac{h^{j+2} - \hat{z}^{j+2}}{(j+1)\,(j+2)} \right\}$$

$$= \frac{\partial}{\partial x} \sum_{j=1}^{N} \left\{ \frac{\partial a_j}{\partial t} \frac{ds}{dx} - \frac{h}{(j+2)} \frac{\partial^2 a_j}{\partial x \partial t} \right\} \frac{h^{j+1}}{(j+1)}$$

$$+ \sum_{j=1}^{N} \left\{ \frac{\partial^3 a_j}{\partial x^2 \partial t} \frac{\hat{z}^{j+2}}{(j+1)\,(j+2)} - \left(\frac{\partial a_j}{\partial t} \frac{d^2 s}{dx^2} + 2 \frac{\partial^2 a_j}{\partial x \partial t} \frac{ds}{dx} \right) \frac{\hat{z}^{j+1}}{(j+1)} + \frac{\partial a_j}{\partial t} \left(\frac{ds}{dx} \right)^2 \hat{z}^j \right\},$$

$$= \frac{\partial}{\partial x} \sum_{j=1}^{N} \left\{ \frac{\partial a_j}{\partial t} \frac{ds}{dx} - \frac{h}{(j+2)} \frac{\partial^2 a_j}{\partial x \partial t} \right\} \frac{h^{j+1}}{(j+1)}$$

$$+ \sum_{j=1}^{N} \left\{ \frac{1}{j} \left(\frac{\frac{\partial^3 a_{j-2}}{\partial x^2 \partial t}}{(j-1)} - \frac{\partial a_{j-1}}{\partial t} \frac{d^2 s}{dx^2} - 2 \frac{\partial^2 a_{j-1}}{\partial x \partial t} \frac{ds}{dx} \right) + \frac{\partial a_j}{\partial t} \left(\frac{ds}{dx} \right)^2 \right\} \hat{z}^j. \tag{B.9}$$

The nonlinear vertical inertia terms are given by:

$$
\begin{aligned}
\frac{\partial}{\partial x}\int_{\hat{z}}^{h}\left(u\frac{\partial w}{\partial x}+w\frac{\partial w}{\partial \hat{z}}\right)d\hat{z} &= \frac{\partial}{\partial x}\sum_{i=1}^{N}\sum_{j=1}^{N}\left\{\left(\frac{(j+1)}{(i+1)}\frac{\partial a_i}{\partial x}\frac{\partial a_j}{\partial x}-a_i\frac{\partial^2 a_j}{\partial x^2}\right)\frac{h^{i+j+2}-\hat{z}^{i+j+2}}{(j+1)(i+j+2)}\right.\\
&\qquad\left.+\left(a_i a_j\frac{d^2 s}{dx^2}+a_i\frac{\partial a_j}{\partial x}\frac{ds}{dx}-\frac{j}{(i+1)}a_j\frac{\partial a_i}{\partial x}\frac{ds}{dx}\right)\frac{h^{i+j+1}-\hat{z}^{i+j+1}}{(i+j+1)}\right\}\\
&= \frac{\partial}{\partial x}\sum_{i=1}^{N}\sum_{j=1}^{N}\left\{\left(\frac{\frac{\partial a_i}{\partial x}\frac{\partial a_j}{\partial x}}{(i+1)}-\frac{a_i\frac{\partial^2 a_j}{\partial x^2}}{(j+1)}\right)\frac{h^{i+j+2}}{(i+j+2)}+\left(a_i\frac{\partial}{\partial x}\left[a_j\frac{ds}{dx}\right]-\frac{j a_j\frac{\partial a_i}{\partial x}\frac{ds}{dx}}{(i+1)}\right)\frac{h^{i+j+1}}{(i+j+1)}\right\}\\
&\quad+\sum_{i=1}^{N}\sum_{j=1}^{N}\left\{\left(a_i\frac{\partial^3 a_j}{\partial x^3}+\frac{(i-j)}{(i+1)}\frac{\partial a_i}{\partial x}\frac{\partial^2 a_j}{\partial x^2}-\frac{(j+1)}{(i+1)}\frac{\partial a_j}{\partial x}\frac{\partial^2 a_i}{\partial x^2}\right)\frac{\hat{z}^{i+j+2}}{(j+1)(i+j+2)}\right.\\
&\qquad-\left(\frac{i+2j+2}{(j+1)}a_i\frac{\partial^2 a_j}{\partial x^2}\frac{ds}{dx}-\frac{j}{(i+1)}\left(a_j\frac{\partial^2 a_i}{\partial x^2}+2\frac{\partial a_i}{\partial x}\frac{\partial a_j}{\partial x}\right)\frac{ds}{dx}\right.\\
&\qquad\quad+\left(2a_i\frac{\partial a_j}{\partial x}+\frac{i-j+1}{(i+1)}a_j\frac{\partial a_i}{\partial x}\right)\frac{d^2 s}{dx^2}+a_i a_j\frac{d^3 s}{dx^3}\Big)\frac{\hat{z}^{i+j+1}}{(i+j+1)}\\
&\qquad\quad\left.+\left(a_i\frac{\partial a_j}{\partial x}\left(\frac{ds}{dx}\right)^2-\frac{j}{(i+1)}a_j\frac{\partial a_i}{\partial x}\left(\frac{ds}{dx}\right)^2+a_i a_j\frac{ds}{dx}\frac{d^2 s}{dx^2}\right)\hat{z}^{i+j}\right\},\\
&= \frac{\partial}{\partial x}\sum_{i=1}^{N}\sum_{j=1}^{N}\left\{\left(\frac{\frac{\partial a_i}{\partial x}\frac{\partial a_j}{\partial x}}{(i+1)}-\frac{a_i\frac{\partial^2 a_j}{\partial x^2}}{(j+1)}\right)\frac{h^{i+j+2}}{(i+j+2)}+\left(a_i\frac{\partial}{\partial x}\left[a_j\frac{ds}{dx}\right]-\frac{j a_j\frac{\partial a_i}{\partial x}\frac{ds}{dx}}{(i+1)}\right)\frac{h^{i+j+1}}{(i+j+1)}\right\}\\
&\quad+\sum_{j=2}^{2N}\sum_{i=1}^{j-1}\left\{\frac{1}{j(j-i-1)}\left(a_i\frac{\partial^3 a_{j-i-2}}{\partial x^3}+\frac{(2i-j+2)}{(i+1)}\frac{\partial a_i}{\partial x}\frac{\partial^2 a_{j-i-2}}{\partial x^2}+\frac{(i-j+1)}{(i+1)}\frac{\partial a_{j-i-2}}{\partial x}\frac{\partial^2 a_i}{\partial x^2}\right)\right.\\
&\qquad-\frac{1}{j}\left(\frac{2j-i}{(j-i)}a_i\frac{\partial^2 a_{j-i-1}}{\partial x^2}\frac{ds}{dx}-\frac{(j-i-1)}{(i+1)}\left(a_{j-i-1}\frac{\partial^2 a_i}{\partial x^2}+2\frac{\partial a_i}{\partial x}\frac{\partial a_{j-i-1}}{\partial x}\right)\frac{ds}{dx}\right.\\
&\qquad\quad+\left(2a_i\frac{\partial a_{j-i-1}}{\partial x}+\frac{(2i-j+2)}{(i+1)}a_{j-i-1}\frac{\partial a_i}{\partial x}\right)\frac{d^2 s}{dx^2}+a_i a_{j-i-1}\frac{d^3 s}{dx^3}\Big)\\
&\qquad\quad\left.+\left(a_i\frac{\partial a_{j-i}}{\partial x}-\frac{(j-i)}{(i+1)}a_{j-i}\frac{\partial a_i}{\partial x}\right)\left(\frac{ds}{dx}\right)^2+a_i a_{j-i}\frac{ds}{dx}\frac{d^2 s}{dx^2}\right\}\hat{z}^{j}. \qquad \text{(B.10)}
\end{aligned}
$$

The vertical viscosity terms are given by:

$$
\begin{aligned}
\frac{\partial^2}{\partial x^2}\int_{\hat{z}}^{h}\frac{\partial w}{\partial x}d\hat{z} &= \frac{\partial^2}{\partial x^2}\int_{\hat{z}}^{h}\sum_{j=1}^{N}\left\{-\frac{\partial^2 a_j}{\partial x^2}\frac{\hat{z}^{j+1}}{(j+1)}+\left(2\frac{\partial a_j}{\partial x}\frac{ds}{dx}+a_j\frac{d^2s}{dx^2}\right)\hat{z}^j-a_j\left(\frac{ds}{dx}\right)^2 j\hat{z}^{j-1}\right\}d\hat{z}\\
&= \frac{\partial^2}{\partial x^2}\sum_{j=1}^{N}\left\{-\frac{\partial^2 a_j}{\partial x^2}\frac{h^{j+2}}{(j+1)(j+2)}+\left(a_j\frac{d^2s}{dx^2}+2\frac{\partial a_j}{\partial x}\frac{ds}{dx}\right)\frac{h^{j+1}}{(j+1)}-a_j\left(\frac{ds}{dx}\right)^2 h^j\right\}\\
&\quad-\frac{\partial^2}{\partial x^2}\sum_{j=1}^{N}\left\{-\frac{\partial^2 a_j}{\partial x^2}\frac{\hat{z}^{j+2}}{(j+1)(j+2)}+\left(a_j\frac{d^2s}{dx^2}+2\frac{\partial a_j}{\partial x}\frac{ds}{dx}\right)\frac{\hat{z}^{j+1}}{(j+1)}-a_j\left(\frac{ds}{dx}\right)^2\hat{z}^j\right\}\\
&= \frac{\partial^2}{\partial x^2}\sum_{j=1}^{N}\left\{-\frac{\partial^2 a_j}{\partial x^2}\frac{h^{j+2}}{(j+1)(j+2)}+\left(a_j\frac{d^2s}{dx^2}+2\frac{\partial a_j}{\partial x}\frac{ds}{dx}\right)\frac{h^{j+1}}{(j+1)}-a_j\left(\frac{ds}{dx}\right)^2 h^j\right\}\\
&\quad+\sum_{j=1}^{N}\left\{\frac{\partial^4 a_j}{\partial x^4}\frac{\hat{z}^{j+2}}{(j+1)(j+2)}-\left(4\frac{\partial^3 a_j}{\partial x^3}\frac{ds}{dx}+6\frac{\partial^2 a_j}{\partial x^2}\frac{d^2s}{dx^2}+4\frac{\partial a_j}{\partial x}\frac{d^3s}{dx^3}+a_j\frac{d^4s}{dx^4}\right)\frac{\hat{z}^{j+1}}{(j+1)}\right.\\
&\qquad+\left(6\frac{\partial^2 a_j}{\partial x^2}\left(\frac{ds}{dx}\right)^2+12\frac{\partial a_j}{\partial x}\frac{ds}{dx}\frac{d^2s}{dx^2}+3a_j\left(\frac{d^2s}{dx^2}\right)^2+4a_j\frac{ds}{dx}\frac{d^3s}{dx^3}\right)\hat{z}^j\\
&\qquad\left.-\left(4\frac{\partial a_j}{\partial x}\left(\frac{ds}{dx}\right)^3+6a_j\left(\frac{ds}{dx}\right)^2\frac{d^2s}{dx^2}\right)j\hat{z}^{j-1}+a_j\left(\frac{ds}{dx}\right)^4 j(j-1)\hat{z}^{j-2}\right\}\\
&= \frac{\partial^2}{\partial x^2}\sum_{j=1}^{N}\left\{-\frac{\partial^2 a_j}{\partial x^2}\frac{h^{j+2}}{(j+1)(j+2)}+\left(a_j\frac{d^2s}{dx^2}+2\frac{\partial a_j}{\partial x}\frac{ds}{dx}\right)\frac{h^{j+1}}{(j+1)}-a_j\left(\frac{ds}{dx}\right)^2 h^j\right\}\\
&\quad+\sum_{j=0}^{N}\left\{\frac{1}{j(j-1)}\frac{\partial^4 a_{j-2}}{\partial x^4}-\frac{1}{j}\left(4\frac{\partial^3 a_{j-1}}{\partial x^3}\frac{ds}{dx}+6\frac{\partial^2 a_{j-1}}{\partial x^2}\frac{d^2s}{dx^2}+4\frac{\partial a_{j-1}}{\partial x}\frac{d^3s}{dx^3}+a_{j-1}\frac{d^4s}{dx^4}\right)\right.\\
&\qquad+6\frac{\partial^2 a_j}{\partial x^2}\left(\frac{ds}{dx}\right)^2+12\frac{\partial a_j}{\partial x}\frac{ds}{dx}\frac{d^2s}{dx^2}+3a_j\left(\frac{d^2s}{dx^2}\right)^2+4a_j\frac{ds}{dx}\frac{d^3s}{dx^3}\\
&\qquad-(j+1)\left(4\frac{\partial a_{j+1}}{\partial x}\frac{ds}{dx}+6a_{j+1}\frac{d^2s}{dx^2}\right)\left(\frac{ds}{dx}\right)^2\\
&\qquad\left.+(j+2)(j+1)a_{j+2}\left(\frac{ds}{dx}\right)^4\right\}\hat{z}^j, \qquad \text{(B.11)}
\end{aligned}
$$

Isolating the contributions to the coefficients of $\hat{z}^{j-2}$, and re-arranging to find $\{a_j, b_j\}$ yields the following recurrence relations:

$$a_j = \frac{\mathbb{M}^*_{j-2}\left(\{a_i\}\right)}{|\ell_s|^4 j\,(j-1)}, \qquad\qquad b_j = \frac{\mathbb{E}^*_{j-2}\left(\{a_i, b_i\}\right)}{|\ell_s|^2 j\,(j-1)}, \tag{B.12}$$

for $j \geq 3$ where $i < j$; in which $\{\mathbb{M}^*_j, \mathbb{M}^*_j\}$ are given by:

$$\begin{aligned}
\mathbb{M}^*_j =& \epsilon Re\,|\ell_s|^2 \left\{ \frac{\partial a_j}{\partial t} + \sum_{i=1}^{j-1} \frac{(j-2i+1)}{(j-i+1)} a_i \frac{\partial a_{j-i}}{\partial x} \right\} - \epsilon^2 |\ell_s|^2 \left\{ \frac{\partial^2 a_j}{\partial x^2} - \frac{(j+1)}{a_{j+1}} \frac{\partial}{\partial x}\left[a^2_{j+1} \frac{ds}{dx} \right] \right\} \\
&+ \epsilon^3 Re \left\{ \frac{\frac{\partial^3 a_{j-2}}{\partial x^2 \partial t}}{j\,(j-1)} - \frac{1}{j}\left(2 \frac{\partial^2 a_{j-1}}{\partial x \partial t} \frac{ds}{dx} + \frac{\partial a_{j-1}}{\partial t} \frac{d^2 s}{dx^2} \right) \right\} \\
&+ \epsilon^3 Re \sum_{i=1}^{j-1} \left\{ \frac{1}{j\,(j-i-1)} \left(a_i \frac{\partial^3 a_{j-i-2}}{\partial x^3} - \frac{\partial a_{j-i-2}}{\partial x} \frac{\partial^2 a_i}{\partial x^2} \right) + a_i a_{j-i} \frac{ds}{dx} \frac{d^2 s}{dx^2} \right. \\
&\qquad - \frac{2a_{j-i-1}}{(i+1)} \frac{\partial^2 a_i}{\partial x^2} \frac{ds}{dx} - \frac{1}{j} \left(\frac{2i}{(j-i)} \frac{\partial a_{j-i-1}}{\partial x} \frac{\partial a_i}{\partial x} \frac{ds}{dx} \right. \\
&\qquad\qquad \left. \left. + \frac{(3j-4i)}{(j-i)} a_i \frac{\partial a_{j-i-1}}{\partial x} \frac{d^2 s}{dx^2} + a_i a_{j-i-1} \frac{d^3 s}{dx^3} \right) \right\} \\
&- \epsilon^4 \left\{ \frac{1}{j\,(j-1)} \frac{\partial^4 a_{j-2}}{\partial x^4} - \frac{1}{j} \left(4 \frac{\partial^3 a_{j-1}}{\partial x^3} \frac{ds}{dx} + 6 \frac{\partial^2 a_{j-1}}{\partial x^2} \frac{d^2 s}{dx^2} + 4 \frac{\partial a_{j-1}}{\partial x} \frac{d^3 s}{dx^3} + a_{j-1} \frac{d^4 s}{dx^4} \right) \right. \\
&\qquad + 5 \frac{\partial^2 a_j}{\partial x^2} \left(\frac{ds}{dx} \right)^2 + 12 \frac{\partial a_j}{\partial x} \frac{ds}{dx} \frac{d^2 s}{dx^2} + 3 a_j \left(\frac{d^2 s}{dx^2} \right)^2 + 4 a_j \frac{ds}{dx} \frac{d^3 s}{dx^3} \\
&\qquad \left. - \frac{(j+1)}{a_{j+1}} \left(\frac{\partial}{\partial x}\left[a^2_{j+1} \frac{ds}{dx} \right] + 4 a^2_{j+1} \frac{d^2 s}{dx^2} \right) \left(\frac{ds}{dx} \right)^2 \right\},
\end{aligned} \tag{B.13}$$

$$\mathbb{E}^*_j = \epsilon RePr \left\{ \frac{\partial b_j}{\partial t} + \sum_{i=1}^{j-1} \left(a_i \frac{\partial b_{j-i}}{\partial x} - \frac{(j-i)}{(i+1)} b_{j-i} \frac{\partial a_i}{\partial x} \right) \right\} - \epsilon^2 \left\{ \frac{\partial^2 b_j}{\partial x^2} - \frac{(j+1)}{b_{j+1}} \frac{\partial}{\partial x}\left[b^2_{j+1} \frac{ds}{dx} \right] \right\}, \tag{B.14}$$

Bibliography

S. V. Alekseenko, V. E. Nakoryakov, and B. G. Pokusaev. Wave formation on vertical falling liquid films. *Int. J. Multiphase Flow*, 11(5):607–627, 1985a.

S. V. Alekseenko, V. E. Nakoryakov, and B. G. Pokusaev. Wave formation on a vertical falling liquid film. *A. I. C. H. E. Journal*, 31(9):1445–1460, 1985b.

K. Argyriadi, M. Vlachogiannis, and V. Bontozoglou. Experimental study of inclined film flow along periodic corrugations: The effect of wall steepness. *Phys. Fluids*, 18: 012102, 2006.

W. L. Badger and C. G. Monrad. The condensation of vapors. *Ind. End. Chem.*, 22(11): 1103–1112, 1930.

G. Baker and P. Graves-Morris. *Padé Approximants*. Cambridge University Press, 2nd ed., encyclopedia of mathematics and its applications edition, 1996.

S. G. Bankoff. Stability of liquid flow down a heated inclined plane. *International Journal of Heat and Mass Transfer*, 14(3):377–385, 1971.

H. Bateman. Some recent researches on the motion of fluids. *Monthly Weather Review*, 43(4):163–170, 1915.

T. B. Benjamin. Wave formation in laminar flow down an inclined plane. *J. Fluid Mech.*, 2(6):554–573, 1957.

D. J. Benney. Long waves on liquid films. *J. Math. and Phys.*, 45(1-4):150–155, 1966a.

D. J. Benney. Long non-linear waves in fluid flows. *J. Math. and Phys.*, 45(1-4):52–63, 1966b.

A. M. Binnie. Experiments on the onset of wave formation on a film of water flowing down a vertical plane. *J. Fluid Mech.*, 2(6):551–553, 1957.

A. M. Binnie. Instability in a slightly inclined water channel. *J. Fluid Mech.*, 5(4): 561–570, 1959.

M. G. Blyth and A. P. Bassom. Flow of a liquid layer over heated topography. *Proc. R. Soc. A*, 468:4067–4087, 2012.

V. Bontozoglou. Laminar film flow along a periodic wall. *CMES*, 1(2):133–142, 2000.

V. Bontozoglou and G. Papapolymerou. Laminar film flow down a wavy incline. *International Journal of Multiphase Flow*, 23(1):69–79, 1997.

A. V. Bunov, E. A. Demekhin, and V. Y. Shkadov. On the non-uniqueness. of non-linear wave solutions in a viscous layer. *Journal of Applied Mathematics and Mechanics*, 48(4):495–499, 1984.

J. M. Burgers. A mathematical model illustrating the theory of turbulence. *Advances in Applied Mechanics*, 1:171–199, 1948.

Z. Cao, M. Vlachogiannis, and V. Bontozoglou. Experimental evidence for a short-wave global mode in film flow along periodic corrugations. *J. Fluid Mech.*, 718:304–320, 2013.

N. Cellier and C. Ruyer-Quil. A new family of reduced models for non-isothermal falling films. *International Journal of Heat and Mass Transfer*, 154:119700, 2020.

H. C. Chang. Wave evolution on a falling film. *Annu. Rev. Fluid Mech.*, 26:103–136, 1994.

M. Chhay, D. Dutykh, M. Gisclon, and C. Ruyer-Quil. Asymptotic heat transfer model in thin liquid films. *HAL*, 01224182v1, 2015.

M. Chhay, D. Dutykh, M. Gisclon, and C. Ruyer-Quil. New asymptotic heat transfer model in thin liquid films. *Applied Mathematical Modelling*, 48:844–859, 2017.

C. Chicone. *Ordinary Differential Equations with Applications*. Springer, 2 edition, 1999.

R. Collignon, O. Caballina, F. Lemoine, and G. Castanet. Temperature distribution in the cross section of wavy and falling thin liquid films. *Exp Fluids*, 62:115, 2021.

R. Collignon, O. Caballina, F. Lemoine, and G. Castanet. Simultaneous temperature and thickness measurements of falling liquid films by laser-induced fluorescence. *Exp Fluids*, 63(4):1–13, 2022.

J. B. Conway. *Functions of one complex variable I*. Springer Science & Business Media, 1978.

J. B. Conway. *Functions of one complex variable II*. Springer Science & Business Media, 1995.

C. M. Cooper, T. B. Drew, and W. H. McAdams. Isothermal flow of liquid layers. *Ind. Eng. Chem.*, 26:425–428, 1934.

V. Cornish. *Ocean Waves and Kindred Geophysical Phenomena*. Cambridge University Press, 2 edition, 1934.

R. V. Craster and O. K. Matar. Dynamics and stability of thin liquid films. *Rev. Mod. Phys.*, 81:1131, 2009.

S. J. D. D'Alessio, J. P. Pascal, and H. A. Jasmine. Instability in gravity-driven flow over uneven surfaces. *Phys. Fluids*, 21:062105, 2009.

S. J. D. D'Alessio, J. P. Pascal, H. A. Jasmine, and K. A. Ogden. Film flow over heated wavy inclined surfaces. *J. Fluid Mech.*, 665:418–456, 2010.

G. R. Daly, P. H. Gaskell, and S. Veremieiev. Gravity-driven film flow down a uniformly heated smoothly corrugated rigid substrate. *J. Fluid Mech.*, 930:A23, 2022.

L. A. Dávalos-Orozco. Instabilities of thin film flowing down flat and smoothly deformed walls. *Microgravity Sci. Technol*, 20:225–229, 2008.

L. A. Dávalos-Orozco. The effect of the thermal conductivity and thickness of the wall on the nonlinear instability of a thin film flowing down an incline. *Int. Journal of Non-Linear Mechanics*, 47:1–7, 2012.

E. A. Demekhin and V. Y. Shkadov. Nonstationary waves in a film of viscous liquid. *Izv. AN SSSR. Mekh. Zhidk. i Gaza*, 3:151–154, 1979.

E. A. Demekhin and V. Y. Shkadov. Three-dimensional waves in a liquid flowing down a wall. *Izv. AN SSSR. Mekh. Zhidk. i Gaza*, 19:689–695, 1984.

E. A. Demekhin, I. A. Demkhin, and V. Y. Shkadov. Solitons in viscous films flowing down a vertical wall. *Izv. AN SSSR. Mekh. Zhidk. i Gaza*, 4:9–16, 1983.

E. A. Demekhin, M. A. Kaplan, and V. Y. Shkadov. Two-dimensional waves in a thin layer of a viscous liquid. *Izv. AN SSSR. Mekh. Zhidk. i Gaza*, 3:63–67, 1985.

E. A. Demekhin, M. A. Kaplan, and V. Y. Shkadov. Mathematical models of the theory of viscous liquid films. *Fluid Dynamics*, 22(6):885–893, 1987.

A. E. Dukler and O. P. Bergelin. Characteristics of flow in falling liquid films. *Chem. Eng. Prog.*, 48(11):557–563, 1952.

N. Esmail and V. Y. Shkadov. Nonlinear theory of waves in a viscous liquid layer. *Izv. AN SSSR. Mekh. Zhidk. i Gaza*, 4:54–59, 1971.

R. Fallah, T. G. Hunter, and A. W. Nash. The application of physico-chemical principles to the design of liquid±liquid contact equipment. part iii. isothermal flow in liquid wetted-wall systems. *Journal of the Society of Chemical Industry*, 53:369–379, 1934.

G. Floquet. Sur les équations différentielles linéaires à coefficients périodiques. *Annales scientifiques de l'É.N.S. 2^e série*, 12:47–88, 1883.

L. S. Friedman and C. O. Miller. Liquid films in the viscous flow region. *Ind. Eng. Chem.*, 33(7):885–891, 1941.

P. H. Gaskell, P. K. Jimack, M. Sellier, H. M. Thompson, and M. C. T. Wilson. Gravity-driven flow of continuous thin liquid films on non-porous substrates with topography. *J. Fluid Mech.*, 509:253–280, 2004.

B. Gjevik. Occurrence of finite-amplitude surface waves on falling liquid films. *Phys. Fluids.*, 13(8):1918–1925, 1970a.

B. Gjevik. Spatially varying finite-amplitude wave trains on falling liquid films. *Preprint series. Mechanics and Applied Mathematics*, 1970b.

B. Gjevik. On the non-linear stability of a liquid film flowing down an inclined plane. *Preprint series. Mechanics and Applied Mathematics*, 1971.

P. Glendinning. *Stability, instability and chaos: an introduction to the theory of nonlinear differential equations*. Cambridge university press, 1994.

D. A. Goussis and R. E. Kelly. Effects of viscosity variation on the stability of film flow down heated or cooled inclined surfaces: Long-wavelength analysis. *Phys. Fluids*, 28(11):3207–3214, 1985.

D. A. Goussis and R. E. Kelly. On the thermocapillary instabilities in a liquid layer heated from below. *Int. J. Heat Mass Transfer*, 33(10):2237–2243, 1990.

D. A. Goussis and R. E. Kelly. Surface wave and thermocapillary instabilities in a liquid film flow. *J. Fluid Mech.*, 223:25–45, 1991.

S. S. Grimley. Liquid flow condition in packed towers. *Trans. Inst. Chem. Engrs*, 23: 228, 1945.

C. Heining and N. Aksel. Bottom reconstruction in thin-film flow over topography: Steady solution and linear stability. *Phys. Fluids*, 21:083605, 2009.

A. P. Hooper and R. Grimshaw. Nonlinear instability at the interface between two viscous fluids. *Phys. Fluids*, 28(1):37–45, 1985.

L. Hopf. Turbulenz bei einem flusse. *Ann. Physik*, 337(4):777–808, 1910.

J. M. Hyman, B. Nicolaenko, and S. Zaleski. Order and complexity in the kuramoto-sivashinsky model of weakly turbulent interfaces. *Physica D*, 23:265–292, 1986.

P. A. Iyer and R. E. Kelly. The stability of the laminar free convection flow induced by a heated inclined plate. *Int. J. Heat Mass Transfer*, 17(4):517–525, 1974.

H. Jeffreys. Lxxxiv. the flow of water in an inclined channel of rectangular section. *Phil. Mag. S. 6.*, 49(293):793–807, 1925.

S. W. Joo, S. H. Davis, and S. G. Bankoff. Long-wave instabilities of heated falling films: two-dimensional theory of uniform layers. *J. Fluid Mech.*, 230:117–146, 1991a.

S. W. Joo, S. H. Davis, and S. G. Bankoff. On falling film instabilities and wave breaking. *Phys. Fluids.*, A 3:231–232, 1991b.

S. Kalliadasis and G. M. Homsy. Stability of free-surface thin-film flows over topography. *J. Fluid Mech.*, 448:387–410, 2001.

S. Kalliadasis, C. Bielarz, and G. M. Homsy. Steady free-surface thin film flows over topography. *Phys. Fluids*, 12:1889, 2000.

S. Kalliadasis, E. A. Demekhin, C. Ruyer-Quil, and M. G. Velarde. Thermocapillary instability and wave formation on a film falling down a uniformly heated plane. *J. Fluid Mech.*, 492:303–338, 2003a.

S. Kalliadasis, A. Kiyashko, and E. A. Demekhin. Marangoni instability of a thin liquid film heated from below by a local heat source. *J. Fluid Mech.*, 475:377–408, 2003b.

P. L. Kapitza. Wave flow of thin layers of a viscous fluid: I. free flow. II. fluid flow in the presence of continuous gas flow and heat transfer. *J. Exp. Theor. Phys*, 18(1):3–28, 1948.

P. L. Kapitza and S. P. Kapitza. Wave flow of thin layers of a viscous fluid: III. experimental study of undulatory flow conditions. *J. Exp. Theor. Phys*, 19(2):105–120, 1949.

R. E. Kelly, S. H. Davis, and D. A. Goussis. On the instability of heated film flow with variable surface tension. *Heat Transfer*, pages 1937–1942, 1986.

L. Kelvin. *Mathematical and Physical Papers*, page 321. Cambridge University Press, 4 edition, 1887.

C. G. Kirkbride. Heat transfer by condensing vapor on vertical tubes. *Ind. Eng. Chem.*, 26:425–428, 1934.

W. B. Krantz and S. L. Goren. Finite-amplitude, long waves on liquid films flowing down a plane. *Ind. Eng. Chem. Fundam.*, 9(1):107–113, 1970.

M. V. G. Krishna and S. P. Lin. Nonlinear stability of a viscous film with respect to three-dimensional side-band disturbances. *Phys. Fluids.*, 20(7):1039–1044, 1977.

C. Lanczos. Trigonometric interpolation of empirical and analytic functions. *J. Math. and Physics*, 17:123–199, 1938.

L. D. Landau. On the problem of turbulence. *In Dokl. Akad. Nauk SSSR*, 44(8):339–349, 1944.

J. W. Lee. Kapitza's method of film flow description. *Chemical Engineering Science*, 24(8):1309–1319, 1969.

S. P. Lin. Instability of a liquid film flowing down an inclined plane. *Phys. Fluids.*, 10(2):308–313, 1967.

S. P. Lin. Finite-amplitude stability of a parallel flow with a free surface. *J. Fluid Mech.*, 36(1):113–126, 1969.

S. P. Lin. Roles of surface tension and reynolds stresses on the finite amplitude stability of a parallel flow with a free surface. *J. Fluid Mech.*, 40(2):307–314, 1970a.

S. P. Lin. Stabilizing effects of surface-active agents on a film flow. *A. I. C. H. E. Journal*, 16:375–379, 1970b.

S. P. Lin. Profile and speed of finite amplitude waves in a falling liquid layer. *Phys. Fluids.*, 14(2):263–268, 1971.

S. P. Lin. Finite-amplitude side-band stability of a viscous film. *J. Fluid Mech.*, 63(3): 417–429, 1974.

S. P. Lin. Stability of liquid flow down a heated inclined plane. *Letters in Heat and Mass Transfer*, 2(5):361–369, 1975.

S. P. Lin and M. V. G. Krishna. Stability of a liquid film with respect to initially finite three-dimensional disturbances. *Phys. Fluids.*, 20(12):2005–2011, 1977.

J. Liu and J. P. Gollub. Solitary wave dynamics of film flows. *Phys. Fluids*, 6:1702 – 1712, 1994.

J. Liu, J. D. Paul, and J. P. Gollub. Measurements of the primary instabilities of film flows. *J. Fluid Mech.*, 250:69–101, 1993.

N. A. Malamataris and V. Bontozoglou. Computer aided analysis of viscous film flow along an inclined wavy wall. *Journal of Computational Physics*, 154:372–392, 1999.

A. Mazouchi and G. M. Homsy. Free surface stokes flow over topography. *Phys. Fluids*, 13(10):2751–2761, 2001.

C. C. Mei. Nonlinear gravity waves in a thin sheet of viscous fluid. *Journal Math. Phys.*, 45(3):266–288, 1966.

E. Mogilevskiy and V. Y. Shkadov. Stability analysis of a thin film flow on a weakly wavy wall. *International Journal of Multiphase Flow*, 114:168–179, 2019.

S. Mukhopadhyay and A. Mukhopadhyay. Hydrodynamics and instabilities of falling liquid film over a non-uniformly heated inclined wavy bottom. *Phys. Fluids*, 32: 074103, 2020.

C. Nakaya. Long waves on a thin fluid layer flowing down an inclined plane. *Phys. Fluids.*, 18:11:1407–1412, 1975.

C. Nakaya and R. Takaki. Non-linear stability of liquid flow down an inclined plane. *Journal of the Physical Society of Japan*, 23(3):638–645, 1967.

V. Nakoryakov and l. R. Shreiber. Waves at the surface of a thin layer of viscous liquid. *Zh. Prikl. Mekh. Tekh. Fiz.*, 2, 1973.

P. K. Nguyen and V. Bontozoglou. Steady solutions of inertial film flow along strongly undulated substrates. *Phys. Fluids*, 23(5):052103, 2011.

W. Nusselt. Die oberfl´achenkondensation des wasserdampfes. *VDI-Zs*, 60:541 – 546, 569 – 575, 1916.

K. A. Ogden, S. J. D. D'Alessio, and J. P. Pascal. Gravity-driven flow over heated, porous, wavy surfaces. *Phys. Fluids*, 23:122102, 2011.

A. Oron and C. Henining. Weighted-residual integral boundary-layer model for the nonlinear dynamics of thin liquid films falling on an undulating vertical wall. *Phys. Fluids*, 20:082102, 2008.

A. Oron and P. Rosenau. Nonlinear evolution and breaking of interfacial rayleigh-taylor waves. *Phys. Fluids A*, 1:1155, 1989a.

A. Oron and P. Rosenau. Evolution and breaking of liquid film flowing on a vertical cylinder. *Phys. Fluids A*, 1:1763, 1989b.

A. Oron and P. Rosenau. Formation of patterns by thermocapillarity and gravity. *J. Phys. II France*, 2:131–146, 1992.

W. M. F. Orr. The stability or instability of the steady motions of a perfect liquid and of a viscous liquid. part i: A perfect liquid. *Proceedings of the Royal Irish Academy. Section A: Mathematical and Physical*, 27:9–68, 1907a.

W. M. F. Orr. The stability or instability of the steady motions of a perfect liquid and of a viscous liquid. part ii: A viscous liquid. *Proceedings of the Royal Irish Academy. Section A: Mathematical and Physical*, 27:69–138, 1907b.

M. K. R. Panga and V. Balakotaiah. Low-dimensional models for vertically falling viscous films. *Phys. Rev. Lett.*, 90(15):154501, 2003.

J. P. Pascal, S. J. D. D'Alessio, and M. Hasan. Instability of gravity-driven flow of a heated power-law fluid with temperature dependent consistency. *AIP Advances*, 8(10):105215, 2018.

L. M. Peurrung and D. B. Graves. Spin coating over topography. *IEEE Transactions on semiconductor manufacturing*, 6(1):72–76, 1993.

C. Pozrikidis. The flow of a liquid film along a periodic wall. *J. Fluid Mech.*, 188: 275–300, 1988.

A. Pumir, P. Manneville, and Y. Pomeau. On solitary waves running down inclined planes. *J. Fluid Mech.*, 135:27–50, 1983.

O. Reynolds. Xxix. an experimental investigation of the circumstances which determine whether the motion of water shall be direct or sinuous, and of the law of resistance in parallel channels. *Phil. Trans. R. Soc.*, 174:935–982, 1883.

O. Reynolds. Iv. on the dynamical theory of incompressible viscous fluids and the determination of the criterion. *Phil. Trans. R. Soc. (a.)*, 186:123–164, 1895.

W. C. Reynolds and M. C. Potter. Finite-amplitude instability of parallel shear flows. *J. Fluid Mech.*, 27(3):465–492, 1967.

A. J. Roberts. Low-dimensional models of thin film fluid dynamics. *Phys. Lett. A*, 212: 63 – 71, 1996.

P. Rosenau and A. Oron. Bounded and unbounded patterns of the benney equation. *Phys. Fluids A: Fluid Dynamics*, 4:1102, 1992.

G. J. Roskes. Three-dimensional long waves on a liquid film. *Phys. Fluids.*, 13(6): 1440–1445, 1970.

C. Ruyer-Quil and P. Manneville. Modeling film flows down inclined planes. *Eur. Phys. J. B.*, 6:277–292, 1998.

C. Ruyer-Quil and P. Manneville. Improved modeling of flows down inclined planes. *Eur. Phys. J. B.*, 15:357–369, 2000.

C. Ruyer-Quil and P. Manneville. Further accuracy and convergence results on the modeling of flows down inclined planes by weighted-residual approximations. *Phys. Fluids*, 14(1):170–183, 2002.

C. Ruyer-Quil, B. Scheid, S. Kalliadasis, M. G. Velarde, and R. K. Zeytounian. Thermocapillary long waves in a liquid film flow. part 1. low-dimensional formulation. *J. Fluid Mech.*, 538:199–222, 2005.

T. R. Salamon, R. C. Armstrong, and R. A. Brown. Traveling waves on vertical films: Numerical analysis using the finite element method. *Phys. Fluids*, 6:2202 – 2220, 1994.

S. Saprykin, P. M. J. Trevelyan, R. J. Koopmans, and S. Kalliadasis. Free-surface thin-film flows over uniformly heated topography. *Physical Review E*, 75:026306, 2007.

B. Scheid, C. Ruyer-Quil, S. Kalliadasis, M. G. Velarde, and R. K. Zeytounian. Thermocapillary long waves in a liquid film flow. part 2. linear stability and nonlinear waves. *J. Fluid Mech.*, 538:223–244, 2005.

B. Scheid, C. Ruyer-Quil, and P. Manneville. Wave patterns in film flows: Modelling and three-dimensional waves. *J. Fluid Mech.*, 562:183–222, 2006.

B. Scheid, S. Kalliadasis, C. Ruyer-Quil, and P. Colinet. Interaction of three-dimensional hydrodynamic and thermocapillary instabilities in film flows. *Physical Review E*, 78: 066311, 2008.

M. Scholle, A. Wierschem, and N. Aksel. Creeping newtonian film flow down an inclined wavy plane. part i. *Z. Angew. Math. Mech.*, 81:487–488, 2001a.

M. Scholle, A. Wierschem, and N. Aksel. Creeping newtonian film flow down an inclined wavy plane. part ii. *Z. Angew. Math. Mech.*, 81:493–494, 2001b.

M. Scholle, A. Wierschem, and N. Aksel. Creeping films with vortices over strongly undulated bottoms. *Acta Mechanica*, 168(3-4):167–193, 2004.

M. Scholle, A. Haas, N. Aksel, M. C. T. Wilson, H. M. Thompson, and P. H. Gaskell. Competing geometric and inertial effects on local flow structure in thick gravity-driven fluid films. *Phys. Fluids*, 20:123101, 2008.

M. Schörner and N. Aksel. The stability cycle - a universal pathway for the stability of films over topography. *Phys. Fluids*, 30:012105, 2018a.

M. Schörner and N. Aksel. Films over topography: from creeping flow to linear stability, theory, and experiments, a review. *Acta Mech*, 229:1453–1482, 2018b.

M. Schörner, D. Reck, and N. Aksel. Does topography's specific shape matter in general for the stability of film flows? *Phys. Fluids*, 27:042103, 2015.

M. Schörner, D. Reck, and N. Aksel. Stability phenomena far beyond the nusselt flow - revealed by experimental asymptotics. *Phys. Fluids*, 28:022102, 2016.

M. Schörner, D. Reck, N. Aksel, and Y. Trifonov. Switching between different types of stability isles in films over topographies. *Acta Mech*, 229:423–436, 2018.

S. Shetty and R. L. Cerro. Flow of a thin fiom over a periodic surface. *International Journal of Multiphase Flow*, 19:1013–1027, 1993.

V. Y. Shkadov. Wave flow regimes of a thin layer of viscous fluid subject to gravity. *Izv. AN SSSR. Mekh. Zhidk. i Gaza*, 2(1):43–51, 1967.

V. Y. Shkadov. Theory of wave flow of a thin layer of a viscous liquid. *Izv. AN SSSR. Mekh. Zhidk. i Gaza*, 3(2):20–25, 1968.

V. Y. Shkadov. The nonlinear development of perturbations in a plane-parallel poiseuille flow. *Izv. AN SSSR. Mekh. Zhidk. i Gaza*, 2:49–57, 1973.

V. Y. Shkadov. Solitary waves in a layer of viscous liquid. *Izv. AN SSSR. Mekh. Zhidk. i Gaza*, 1:63–66, 1977.

G. I. Sivashinsky and D. M. Michelson. On irregular wavy flow down a vertical plane. *Prog. Theor. Phys.*, 63(6):2112–2114, 1980.

M. K. Smith. The mechanism for the long-wave instability in thin liquid films. *J. Fluid Mech.*, 217:469–485, 1990.

A. Sommerfeld. Über die ausbreitung der wellen in der drahtlosen telegraphie. *Annalen der Physik*, 333(4):665–736, 1908.

S. Sreenivasan and S. P. Lin. Surface tension driven instability of a liquid film flow down a heated incline. *International Journal of Heat and Mass Transfer*, 21(12):1517–1526, 1978.

E. Sterman-Cohen and A. Oron. Dynamics of nonisothermal two-thinfluid-layer systems subjected to harmonic tangential forcing under rayleigh–taylor instability conditions. *Phys. Fluids*, 32:082113, 2020.

L. E. Stillwagon and R. G. Larson. Fundamentals of topographic substrate leveling. *Journal of Applied Physics*, 63:5251, 1988.

L. E. Stillwagon and R. G. Larson. Leveling of thin films over uneven substrates during spin coating. *Phys. Fluids A*, 2(11):1937–1944, 1990.

L. E. Stillwagon and R. G. Larson. Planarization during spin coating. *Phys. Fluids A: Fluid Dynamics*, 4(5):895–903, 1992.

L. E. Stillwagon, R. G. Larson, and G. N. Taylor. Planarization of substrate topography by spin coating. *J. Electrochem. Soc.*, 134:2030, 1987a.

L. E. Stillwagon, R. G. Larson, and G. N. Taylor. Spin coating and planarization. *Proc. SPIE 0771, Advances in Resist Technology and Processing IV*, 1987b.

J. T. Stuart. On the non-linear mechanics of hydrodynamic stability. *J. Fluid Mech.*, 4(1):1–21, 1958.

J. T. Stuart. On the non-linear mechanics of wave disturbances in stable and unstable parallel flows part 1. the basic behaviour in plane poiseuille flow. *J. Fluid Mech.*, 9(3): 353–370, 1960.

S. R. Tailby and S. Portalski. The determination of the wavelength on a vertical film of liquid flowing down a hydrodynamically smooth plate. *Trans. Inst. Chem. Eng.*, 40: 114–122, 1962.

O. Takeshi. Surface equation of falling film flows with moderate reynolds number and large but finite weber number. *Phys. Fluids*, 11:3247–3269, 1999.

A. Thompson, S. Gomes, F. Denner, M. Dallaston, and S. Kalliadasis. Robust low-dimensional modelling of falling liquid films subject to variable wall heating. *J, Fluid Mech.*, 877:844–881, 2019.

H. Tougou. Long waves on a film flow of a viscous fluid down an inclined uneven wall. *J. Phys Soc. Jpn.*, 44:1014–1019, 1978.

P. M. J. Trevelyan, S. Kalliadasis, J. H. Merkin, and S. K. Scott. Dynamics of a vertically falling film in the presence of a first-order chemical reaction. *Phys. Fluids*, 14:2402, 2002.

P. M. J. Trevelyan, B. Scheid, C. Ruyer-Quil, and S. Kalliadasis. Heating falling films. *J. Fluid Mech.*, 592:295–334, 2007.

Y. Trifonov. Stability of the wavy film falling down a vertical plate: The dns computations and floquet theory. *Int. J. Multiphase Flow*, 61:73–82, 2014a.

Y. Trifonov. Stability of a film flowing down an inclined corrugated plate: The direct navier-stokes computations and floquet theory. *Phys. Fluids*, 26:114101, 2014b.

Y. Y. Trifonov. Viscous liquid film flows over a periodic surface. *Int. J. Multiphase Flow*, 24:1139–1161, 1998.

Y. Y. Trifonov. Stability and nonlinear wavy regimes in downward film flows on a corrugated surface. *J. Appl. Mech. and Tech. Phys.*, 48:91–100, 2007.

D. Tseluiko, M. Blyth, and D. Papageorgiou. Stability of film flow over inclined topography based on a long-wave nonlinear model. *J. Fluid Mech.*, 729:638–671, 2013.

S. Veremieiev. Gravity-driven continuous thin film flow over topography. *PhD. Thesis, University of Leeds*, 2011.

S. Veremieiev and D. H. Wacks. Modelling gravity-driven film flow on inclined corrugated substrate using a high fidelity weighted residual integral boundary-layer method. *Phys. Fluids*, 31:2:022101, 2019.

S. Veremieiev, H. M. Thompson, and P. H. Gaskell. Free-surface film flow over topography: Full three-dimensional finite element solutions. *Computers & Fluids*, 122: 66–82, 2015.

M. Vlachogiannis and V. Bontozoglou. Experiments on laminar film flow along a periodic wall. *J. Fluid Mech.*, 457:133–156, 2002.

C. Y. Wang. Liquid film flowing slowly down a wavy incline. *AIChE*, 27.2:207–212, 1981.

C. Y. Wang. Thin film flowing down a curved surface. *ZAMP*, 35:532–544, 1984.

A. Wierschem and N. Aksel. Instability of a liquid film flowing down an inclined wavy plane. *Physica D*, 186:221–237, 2003.

A. Wierschem and N. Aksel. Influence of inertia on eddies created in films creeping over strongly undulated substrates. *Phys. Fluids*, 16(12):4566–4574, 2004.

A. Wierschem, M. Scholle, and N. Aksel. Comparison of different theoretical approaches to experiments on film flow down an inclined wavy channel. *Experiments in Fluids*, 33:429–442, 2002.

A. Wierschem, M. Scholle, and N. Aksel. Vortices in film flow over strongly undulated bottom profiles at low reynolds numbers. *Phy. Fluids*, 15(2):426–435, 2003.

A. Wierschem, C. Lepski, and N. Aksel. Effect of long undulated bottoms on thin gravity-driven films. *Acta Mechanica*, 179:41–66, 2005.

A. Wierschem, T. Pollak, C. Heining, and N. Aksel. Suppression of eddies in films over topography. *Phys. Fluids*, 22:113603, 2010.

C. Yih. Stability of liquid flow down an inclined plane. *Phys. Fluids.*, 6(3):321–334, 1963.

C. S. Yih. Stability of parallel laminar flow with a free surface. *Proc. 2nd U.S. Natl. Congress Applied Mechanics, ASME*, page 623, 1954.

L. Zhao and R. L. Cerro. Experimental characterization of viscous film flow over complex surfaces. *International Journal of Multiphase Flow*, 18(4):495–516, 1992.